The Determination of Drying Kinetics and Equilibrium Characterisation at Low Moisture Contents

Andrew M. Keech

A thesis presented in fulfilment of the requirement for the degree of
Doctor of Philosophy
in
Chemical and Process Engineering
at the
University of Canterbury,
Christchurch, New Zealand.

14 August 1997

CONTENTS

ABSTRACT xiii

ACKNOWLEDGEMENTS xv

NOMENCLATURE xvii

CHAPTER 1 INTRODUCTION 1
1.1 General 1
1.2 This Work 2

CHAPTER 2 PREVIOUS WORK 9
2.1 Moisture Bonding and Sorption 9
2.1.1 Scope 9
2.1.2 Equilibrium in sorption 10
2.1.3 Thermodynamic equilibrium between two phases 11
2.1.3.1 General 11
2.1.3.2 Binding energy 12
2.1.4 Classification of sorption isotherms 14
2.1.5 Classification of porous materials 15
2.1.5.1 Macropores 15
2.1.5.2 Mesopores 15
2.1.5.3 Micropores 16
2.1.6 Micropore sorption and volume filling 17
2.1.6.1 Thermodynamics of sorption in micropores 17
2.1.6.2 Thermal equation of sorption in micropores 18
2.1.7 Layerwise sorption in pores 19
2.1.7.1 Surface adsorption 19
2.1.7.2 Multilayer formation - traditional models 21
2.1.7.3 Other multilayer models 23
2.1.7.4 Capillary condensation and hysteresis 25
2.1.8 Empirical relationships 26
2.2 Moisture Binding Mechanisms at Low Moisture Contents 29
2.2.1 Water - how it is held in solids 29
2.2.2 Enthalpic-driven effects 29

2.2.3 Entropic-driven effects 30
2.2.3.1 Hydrophobic hydration 30
2.2.3.2 Micropore volume filling 30
2.2.3.3 Water in crystalline hydrates 30
2.2.3.4 Water in inert rigid solids 31
2.2.3.5 Water in polymer-based solids 31
2.3 Drying Kinetics 33
2.3.1 Drying history of a material 33
2.4 The Mechanisms of Moisture Flow Through a Cylindrical Pore 35
2.4.1 Diffusion in the gas phase 37
2.4.2 Boundary layer for mass transfer at low concentration gradients 38
2.4.3 Capillarity 39
2.5 Drying of Materials Wet With Water/Solvent Mixtures 39
2.5.1 Krishna's approach (1990a) 39
2.5.2 Schlünder's approach (Thurner and Schlünder, 1986) 41
2.5.2.1 Evaporation of a binary solution from a free liquid surface 41
2.5.2.2 Drying of porous materials containing binary mixtures 43
2.6 Theories of Drying 43
2.6.1 Earlier work 43
2.6.2 Mechanistic models 47
2.6.2.1 Wetted-surface model (Peck and Kauh, 1969) 48
2.6.2.2 Receding evaporative interface model (Keey, 1978) 48
2.6.2.3 Diffusion model (Sherwood, 1929a, 1929b, 1936) 48
2.6.2.4 Surface diffusion model (Suzuki, 1988) 48
2.6.3 Surface diffusion 49
2.6.3.1 General 49
2.6.3.2 Random walk concept 50
2.6.3.3 Site-hopping model 51
2.6.3.4 Effect of surface coverage 52
2.6.3.5 Surface flow induced by a surface pressure gradient - hydrodynamic or Poiseuille flow 53
2.6.4 Short-cut methods 54
2.6.4.1 Schoeber's or Thijssen's method (Liou and Bruin, 1982, and Thijssen and Coumanns, 1984) 55
2.6.4.2 van Meel's method (1958) 56

2.6.5 Method of obtaining characteristic drying curves 63
2.6.6 Calculating a particle's critical moisture content 70
2.7 Moisture Movement Near Dryness 74
2.8 Theory of Drying Discrete Particles to Particles in Layers 75
2.8.1 Using suspended isolated vermiculite particles, from Keey (1992) 75
2.8.2 Using Canterbury thin layer apparatus, Keech (1992) 77
2.9 Analytical Methods Used to Characterise Sorption 77
2.9.1 Thermogravimetric analysis and differential scanning calorimetry 77
2.9.2 Description of thermal methods for moisture characterisation 81
2.9.2.1 Thermal methods of analysis (Manley, 1989) 81
2.9.2.2 Thermogravimetric analysis 81
2.9.2.3 Differential scanning calorimetry 82
2.9.3 Comments on thermal analysis methods 82
2.9.3.1 Disadvantages of using TG equipment 83
2.9.3.2 Direct methods of evolved gas analysis 84
2.9.3.3 Indirect methods of evolved gas analysis 86
2.9.3.4 Comment 86
2.9.3.5 Present technology to determine drying behaviour 87
2.9.3.6 Equipment investigated for low moisture drying 88
2.9.4 Variations in amounts of heat required to dry solids 89
2.9.4.1 Effect of particle size 89
2.9.4.2 Non-swelling solids 89
2.9.4.3 Swelling solids 90
2.9.5 Calculating the heats of wetting of particulate/powdery material at low moisture contents 92
2.10 Literature Survey on Physical Properties of Materials 95
2.10.1 Silica gel 95
2.10.1.1 Silica gel preparation 95
2.10.1.2 Types of silica gel 95
2.10.1.3 Physisorbed and chemisorbed water on silica gel 96
2.10.2 Crude terephthalic acid 105
2.10.3 Adipic acid (fine chemical) 106
2.10.4 Comments on the Variations in the Types of Materials Used in this Work 109

CHAPTER 3 APPLYING EXISTING MODELS TO LOW MOISTURE CONTENT DRYING 111
3.1 Introduction 111

3.2 Physio-chemical Drying Kinetics 112
3.3 Surface Diffusion Model for Bound Moisture 114
3.4 Water Clustering at Low Moisture Contents (< 1%) 116
3.5 Conductive Heat Drying Models at Low Moisture Contents 119
3.6 Discussion 126

CHAPTER 4 PRELIMINARY SORPTION AND DRYING KINETICS 129
4.1 Calibration of equipment 129
4.1.1 Pressure gauges 129
4.1.2 Thermometers 129
4.2 Sorption Studies at Harwell 130
4.2.1 Static method used to find isotherms 130
4.2.1.1 Equilibrium moisture isotherms using SPS dynamic (Figure 4.2) equilibrium moisture content (emc) rig and possible alterations to rig 130
4.2.1.2 Results of static sorption studies 130
4.2.2 The importance of minimising the experimental scatter in isotherms 131
4.2.3 The emc apparatus and isotherm experiments at Harwell 132
4.2.3.1 Alterations to sample section 133
4.2.3.2 Connecting a line from the emc rig to the inlet gas section of the thermogravimetric (TG) unit 133
4.2.4 Nitrogen sorption by single point BET (AEA intec) 134
4.2.4.1 Using the TG unit for equilibrium isotherms 134
4.3 Thermogravimetric analysis 137
4.3.1 Thermogravimetric analysis (TGA) of silica gel from 25 to 1000$degC$ 137
4.3.1.1 Advantages of TGA 137
4.3.1.2 Disadvantages of TGA 138
4.3.2 Sorption studies by thermogravimetric analysis (TGA) 138
4.3.3 Experimental test conditions for TGA/DSC work at Harwell 140
4.3.3.1 Sample preparation for TGA and DSC tests 141
4.3.4 TGA/DSC Results 141
4.3.4.1 Effect of varying scan rate in DSC tests 141
4.4 Drying kinetics studies 144
4.4.1 Apparatus for experiments 144
4.4.2 Types of experiments performed 145

4.4.2.1 Single particle drying experiments 145
4.4.2.2 Single layer drying 145
4.4.2.3 Multiple layer drying 145
4.4.3 Constructing drying kinetics curves 146
4.4.3.1 Filtering of data, Raw data → drying kinetics curves 146
4.4.3.2 The first-derivative drying rate curves 146
4.4.4 Test Conditions for Harwell and Canterbury Drying Kinetics Experiments 147
4.4.4.1 Harwell experiments - isolated particles and single particle agglomerate trials 147
4.4.4.2 Canterbury experiments - isolated particles and single particle agglomerate trials 149
4.4.5 Results of drying kinetics studies 149
4.4.5.1 Vacuum drying of silica gel (preliminary vacuum drying experiments) 149
4.4.5.2 Single Particle - Multiple Particle Drying Kinetics 155
4.4.5.3 Comparison of Harwell TG results with Canterbury thin-layer results 156
4.4.5.4 Comparison of Harwell with Canterbury Results 156
4.4.5.5 Single Particle - Multiple Particle Drying Kinetics 158
4.4.5.6 The effect of structural variations in a bed on the shape of the characteristic drying curve 160
4.4.6 Discussion of preliminary drying kinetics studies 161
4.4.6.1 Primary comments 161
4.4.6.2 Secondary comments 162

CHAPTER 5 EXPERIMENTAL 167
5.1 Development of Low Moisture Content Kinetics Rig 167
5.1.1 Preliminary design of new drying kinetics rig 167
5.1.1.1 Preliminary design ideas 167
5.1.1.2 Determining whether infrared hygrometry or Karl Fisher titrimetry would be sensitive enough to record profiles of low humidity air 167
5.1.2 Design of drying kinetics apparatus 171
5.1.2.1 Overall design 171
5.2 Test Conditions for Drying Tunnel Sorption Studies 181
5.2.1 Equipment 181
5.2.1.1 General 181

5.2.1.2 Procedure for sorption experiments at Canterbury 181
5.2.1.3 Test conditions 182
5.2.1.4 Material investigated 182
5.2.2 Experimental 183
5.2.2.1 Measurement of sorption isotherms and binding energy 183
5.3 Test Conditions for Drying Kinetics Experiments Under Vacuum 183
5.4 Test Conditions for Drying Kinetics Experiments at Low Moisture Contents of Alumina Containing a Binary Solution of Water and Isopropyl Alcohol 184

CHAPTER 6 RESULTS 185
6.1 Accuracy of the new drying kinetics apparatus 185
6.1.1 Drying using a through flow of air 185
6.1.1.1 Drying alumina - raw data 185
6.1.1.2 Conclusion 186
6.1.2 Drying using vacuum conditions 188
6.1.2.1 Drying alumina - raw data 188
6.1.2.2 Conclusion 189
6.2 Testing the Low-moisture Content Models 189
6.2.1 Testing the surface diffusion model on the materials at low-moisture contents 190
6.2.1.1 Alumina 190
6.2.1.2 Iron sand 191
6.2.1.3 Pure terephthalic acid 191
6.2.1.4 Pre-dried terephthalic acid 191
6.2.1.5 Copolymer III 192
6.2.2 Conductive heat drying models - testing Okazaki conductive heat drying model 192
6.3 Solids Characterisation 192
6.3.1 Using microscopic photographs to observe particle's surface before and after drying 192
6.3.2 Variations in the types of materials used in this work 194
6.3.3 Physical appearances 194
6.3.3.1 Silica gel 194
6.3.3.2 Alumina 196
6.3.3.3 Pre-dried terephthalic acid (before drying) (fine chemical) 196
6.3.3.4 Adipic acid (fine chemical) 198
6.3.3.5 Styrene-butadiene copolymer (I) 198
6.3.3.6 Styrene-butadiene co-polymer (II) 198

6.3.3.7 Styrene-butadiene co-polymer (III) 200
6.3.3.8 Titaniferous iron sand 200
6.3.4 Heat of vaporisation + wetting against moisture content at low moisture contents 200
6.4 Drying Tunnel Sorption Studies - graphs of sorption isotherms 207
6.5 Experimental Programme With New Drying Kinetics Rig 211
6.6 Drying Kinetics of Selected Material at Low-moisture Contents Using the New Apparatus 214
6.6.1 Comparisons between Harwell's drying kinetics rig with new apparatus - characteristic drying curves 214
6.6.1.1 Effect of changing bed configurations under a laminar through-flow of air 214
6.6.1.2 Effect of changing external flow conditions under a laminar through-flow of air 216
6.6.2 Determining the critical moisture content of the copolymer - I 216
6.6.3 Determining the drying kinetics of selected materials at low moisture content 218
6.6.4 Vacuum drying 219
6.6.4.1 Single particle tests 219
6.6.4.2 Vacuum drying tests of silica gel 124 and alumina 220
6.6.5 Drying kinetics at low-moisture contents of alumina containing a binary solution of water and isopropyl alcohol 220

CHAPTER 7 DISCUSSION 227
7.1 Sorption studies 227
7.2 Comparison of Harwell with Canterbury Results 228
7.3 Single Particle - Multiple Particle Drying Kinetics 230
7.4 Equilibrium Moisture Isotherms Using SPS Equilibrium Moisture Content (EMC) Rig and Possible Alterations to Rig 232
7.5 Thermogravimeteric Analysis and Differential Scanning Calorimetry 233
7.6 Constructing Drying Kinetics Curves 235
7.7 Limits of Accuracy on Measuring the Drying Kinetics of Particulate Material 239
7.8 Answers to the main objectives of this PhD work 240
7.8.1 Do isolated particles dry differently from particles in layers, both cross and through-circulated? 240
7.8.2 Is it possible to use existing equipment to investigate drying kinetics at low moisture contents, or will a new design concept be required? 241

7.8.3 Is the drying selective at low moisture contents when organic volatiles are present? 241
7.8.4 Do the drying kinetics differ when moisture is held by volume filling and/or strongly adsorbed on pore surfaces at low moisture contents, compared with vapour diffusion and capillary action at higher moisture contents? 242
7.9 Moisture Equilibrium Characteristics of Materials 242
7.10 General Fitting Characteristics of Correlations 243
7.11 Testing Low-moisture Content Models 245
7.11.1 Physio-chemical kinetics drying model 245
7.11.2 Testing the surface diffusion model on the materials 245
7.11.3 Fickian diffusion at low-moisture contents? 246
7.11.4 Testing Fick's laws of diffusion to drying at low moisture contents 247
7.11.5 Conductive heat drying models at low moisture contents 248
7.11.5.1 Okazaki's drying model (Okazaki *et al.*, 1981) 248
7.11.5.2 Thurner and Schlünder's (1986) heat transfer drying model at low moisture contents 249
7.11.5.3 Comparison of models 250
7.11.6 Drying selectivity of a binary mixture at low moisture contents 252
7.12 Characteristic Drying Curves of Selected Materials at Low-moisture Contents 253

CHAPTER 8 CONCLUSIONS 255

APPENDIX A PRELIMINARY DRYING KINETICS STUDIES AT HARWELL 259
A.1 Smoothing Raw Data Drying Curves 259
A.2 Raw Data of Outlet Gas Humidity vs. Time Using an Infrared Gas Analyser from Keech (1992) 260
A.3 Moisture Content vs. Time Experiments 260
A.3.1 Group A moisture content with time profiles 261
A.3.2 Group B moisture content with time profiles 262
A.4 Fitting Drying Rate Curves with Time 262
A.4.1 Group A experiments 262
A.4.2 Group B experiments 262
A.5 Fitting Drying Rate Curves with Normalised Drying Rate 263
A.5.1 Group A experiments 263
A.5.2 Group B experiments 263

A.6 Characteristic Drying Rate Curves with Normalised Drying Rate 264
A.6.1 Group A experiments 264
A.6.2 Group B experiments 264

APPENDIX B THE NTH ORDER FORWARD DIFFERENCE DERIVATION 269

APPENDIX C RAW DATA OF DRYING KINETICS WORK AT LOW-MOISTURE CONTENTS 271
C.1 Comparison of Harwell Drying Kinetics Results with New Apparatus 271
C.2 Low-moisture Content Drying Kinetics Experiments 271

APPENDIX D OPERATING INSTRUCTIONS FOR NEW DRYING KINETICS APPARATUS 277
D.1 Operating Instructions 277
D.1.1 Important points to note before proceeding to respective operating method 277
D.1.2 Sample preparation 278
D.1.3 Operating microbalance 278
D.1.4 Operating mass spectrometer 279
D.1.5 Operating Dew-All 911 281
D.1.6 Thermocouple data acquisition program 281
D.1.7 Microbalance initialisation routine 282
D.2 Operating Procedures for Drying Samples 283
D.2.1 Operating procedure number 1 for drying of a single particle under a through-flow in sample section #1 283
D.2.1.1 Hardware configuration 283
D.2.1.2 Software, instrumentation configuration 283
D.2.1.3 Sample insertion 284
D.2.2 Operating procedure number 2 for drying of layer/s (d_p=50 *mm*) under a through-flow in sample section #1 284
D.2.2.1 Hardware configuration 284
D.2.2.2 Software, instrumentation configuration 284
D.2.2.3 Sample insertion 285
D.2.3 Operating procedure number 3 for drying of layer/s (d_p=100 *mm*) under a through-flow in sample section #1 285
D.2.3.1 Hardware configuration 285
D.2.3.2 Software, instrumentation configuration 285
D.2.3.3 Sample insertion 285

D.2.4 Operating procedure number 4 for drying of a single particle under a vacuum in sample section #1 286
D.2.4.1 Hardware configuration 286
D.2.4.2 Software, instrumentation configuration 286
D.2.4.3 Sample insertion 286
D.2.5 Operating procedure number 5 for drying of a particle layer under a vacuum in sample section #1 287
D.2.5.1 Hardware configuration 287
D.2.5.2 Software, instrumentation configuration 287
D.2.5.3 Sample insertion 287
D.2.6 Operating procedure number 6 for drying of particle layer/s (1-4 layers) under a vacuum in sample section #2 288
D.2.6.1 Hardware configuration 288
D.2.6.2 Software, instrumentation configuration 288
D.2.6.3 Sample insertion 288
D.2.7 Operating procedure number 7 for drying of particle bed (<4 layers) under a vacuum in sample section #2 289
D.2.7.1 Hardware configuration 289
D.2.7.2 Software, instrumentation configuration 289
D.2.7.3 Sample insertion 289

APPENDIX E MOISTURE EQUILIBRIUM CHARACTERISTICS OF MATERIALS 291
E.1 Silica Gel 291
E.2 Alumina 292
E.3 Iron sand 293
E.4 Adipic Acid 295
E.5 Pure Terephthalic acid 298
E.6 Non-dried Terephthalic Acid 299
E.7 Polystyrene-Butadiene Copolymer I 300
E.8 Polystyrene-Butadiene Copolymer II 301
E.9 Polystyrene-Butadiene Copolymer III 302
E.10 Heat-treated silica gel 304

APPENDIX F RAW DATA FOR CHARACTERISTIC DRYING RATE CURVES 307

APPENDIX G SOFTWARE PROGRAM FOR OPERATION OF NEW DRYING KINETICS APPARATUS 309

REFERENCES 311

ABSTRACT

Recently there has been focus on determining the drying behaviour of particulate material at low moisture contents ($< 1\%$), as a result of increased energy costs and purity requirements for dried products. As little is known about the drying behaviour of particulate material at these low moisture levels, driers have been oversized by including large safety factors in the sizing calculations, thus incurring unnecessary capital expenditure. A research programme was formulated in an attempt to provide a greater understanding of the moisture movement processes occurring at these low moisture levels. The results of this work indicate the significant effects that influence the drying behaviour of particulate material, which may be implemented into drier sizing calculations. Most particulate materials require a significant amount of energy to remove residual amounts of moisture, particularly from microporous media or from strongly hydrophilic surfaces. Quantifying the energy required to remove this bound moisture is possible from a knowledge of heats of wetting as a function of moisture content. These can be calculated from isotherms under controlled conditions using the Clausius-Claperyon equation. As part of a research programme to look at this type of drying behaviour, a novel apparatus was designed and constructed. The function of this apparatus was to record drying profiles of particulate material under various drying conditions and sample sizes. The sensitivity and reproducibility of the drying profiles were the overiding parameters in the design of such an apparatus.

Moisture movement at low moisture levels in thin layers and single particulate arrangements can be described by two mechanisms. Solute bound to hydrophilic and/or active pore surfaces requires a normally distributed activation energy to be overcome, for surface diffusion to occur. Solute held in "water clusters" by hydrophobic media, such as polymeric, some plastic and generally swelling solids, can be described by Fickian movement similar to the familiar transport processes known to occur at higher moisture contents. Thus, it is possible to extrapolate the drying kinetics at higher moisture contents to lower-moisture contents in this instance, but not for the surface diffusion process which takes place only at lower moisture levels. For the drying of thicker layers and beds of particles, accurate overall diffusion coefficients need to include a gas phase diffusion term for gaseous movement through the particulate bed.

The studies here have extended the understanding of the drying kinetics dissimilar-

ities between drying single isolated particles, single particle agglomerates, thin layers and beds of particulate material. In sizing calculations of drying units, preliminary kinetics tests on the material to be dried need to be performed under similar bed geometries to that in the full-scale drying unit. For example, thin-layer experiments appear to provide accurate drying kinetic data for the design of cascade rotary driers. The thickness of the thin layer in the drying kinetic tests is determined by the observed thickness of the falling film of material during operation of the cascade rotary drier. Higher gas velocities in a fluidised bed, or flash driers, may be best modelled by drying kinetics studies on single particles or single particle agglomerates. However, at lower gas velocities, thin-layer tests may be more suitable because the drying material in the fluidised bed may dry in a bubbling motion.

The final section of this work looked at selective drying of various isopropyl alcohol/water mixtures at low moisture levels. Selective drying at higher moisture contents is generally well understood, by applying azeotropic principles to describe liquid-phase moisture removal from porous matrices. Two-component bound moisture in a porous particulate resides in a solid phase. It is not possible for a binary mixture bound directly to the solid to form an azeotropic mixture. Modelling the removal of this binary bound moisture was shown to fit a surface diffusion model, in which each of the two solvents was treated as a separate entity. In short, selective drying is prevalent at low moisture contents but can be described by two distinct surface diffusion models working independently on each binary species.

ACKNOWLEDGEMENTS

This work was financially supported by AEA Technology Ltd. (contract no. TH10715TK) which provided a fellowship, travel expenses and equipment costs.

The author would like to express his gratitude to Professor Roger Keey for his guidance as supervisor throughout the three-year term. Without his support and wisdom this contract and thesis would not have been possible. The author is grateful for the support given by Ian Kemp, assistant supervisor, research colleague, flatmate and friend. He provided an invaluable link between this work and the SPS member companies.

During the author's year at Harwell, Oxfordshire, he is appreciative of the support given by the Industrial Technology section. Particular thanks are extended to Dr. Ollie Okeke, Dr. Chris Price, Nick Hallis, Dr. Richard Bahu, Humphrey Pasley and Dr. Peter Cains.

The remaining two years spent in New Zealand was supported by the staff of the Department of Chemical and Process Engineering, University of Canterbury. The author acknowledges specifically the support given by Neville Foot, Senior Technical Officer, for his time spent constructing the new drying kinetics apparatus. The Department's competent electrical technicians, Bob Gordon, Warwick Earl and Tony Allen, also deserve particular mention.

NOMENCLATURE

a	surface to volume ratio	[m^{-1}]
a	radius of a spherical particle, Equations 3.17, 3.16	[m]
A	Gibbs free energy given in Equation 2.17	[kJ kg^{-1}]
A	empirical constant in Table 2.2 constant	[mol kg^{-1}]
B	constant in Equation 2.33	[-]
B	empirical constant in Table 2.2 constant	[mol kg^{-1}]
C	concentration	[kg m^{-3}]
C_B	ratio of internal partition functions of bound and liquid water	[-]
C_o	constant surface concentration of the spherical particles	[kg m^{-3}]
C_1	initial uniform concentration of the spherical particles	[kg m^{-3}]
C_{ps}	specific heat capacity of material	[J kg^{-1} K^{-1}]
C_{pw}	specific heat capacity of water	[J kg^{-1} K^{-1}]
D	diffusion coefficient	[m^2s^{-1}]
D_{eff}	effective vapour diffusion coefficient	[m^2s^{-1}]
D_k	Knudsen diffusion coefficient	[m^2s^{-1}]
D_s	surface diffusion	[m^2s^{-1}]
D_*	surface diffusion constant	[m^2s^{-1}]
D_v	vapour diffusion coefficent	[m^2s^{-1}]
d	particle diameter	[m]
E	characteristic free energy for test material	[kJ kg^{-1}]
E_a	activation energy	[kJ kg^{-1}]
E_o	characteristic free energy of adsorption of standard	[kJ kg^{-1}]
f	fugacity	[Pa]
f	fraction of molecules that undergo reflection at the pore wall	[-]
f	relative drying rate at the critical moisture content	[-]
g	reduced relative drying rate content	[-]
h	Plank's constant (6.6218*10-34)	[J s]
h_b	heat of wetting	[kJ kg^{-1}]
h	initial relative drying rate (where $X_o < X_{cr}$)	[-]
k	frequency that a molecule will jump to a vacant site	[s^{-1}]

k	Boltsmann constant ($1.381*10^{-23}$)	[J K^{-1}]
k_a	equilibrium constant for adsorption	[-]
k_d	equilibrium constant for desorption	[-]
k_H	Henrys equilibrium constant for adsorption	[-]
k_F	Freundlich equilibrium constant for desorption	[-]
K	adsorption equilibrium constant	[-]
K_s	moisture permeability	[-]
K_p	temperature coefficient of saturated vapour pressure of water	[-]
J	flux	[m^2 s^{-1}]
l	modified free path of the gas molecules	[m]
L	depth of particulate bed	[m]
M	molecular weight of water	[kg mol^{-1}]
n	number of moles	[-]
$\ddot{n}$	drying flux	[kg $m^{-2} s^{-1}$]
$\tilde{n}$	drying flux	[kg $m^{-2} s^{-1}$]
$\tilde{n}_{max}$	maximum drying rate	[kg $m^{-2} s^{-1}$]
n_F	Freundlich constant in Equation 2.25	[-]
N	relative drying rate	[kg $kg^{-1} s^{-1}$]
NTU	number of transfer units	[-]
p	pressure	[Pa]
p_o	saturated pressure of water vapour	[Pa]
p_s	saturated pressure of water vapour	[Pa]
P_A	Partial pressure of A outside the mass transfer boundary layer	[Pa]
q_{sat}	total saturation concentration of adsorbed species	[mol kg^{-1}]
Q_m	content of the gas product m released in the temp. range	[kg]
r	sub-radial distance within a spherical particle	[m]
R	universal gas constant	[J $mol^{-1} K^{-1}$]
R_p	pore radius	[m]
s	fractional saturation of the pores	[-]
s_1	evaporative selectivity	[-]
S	cross-sectional area	[m^2]
S_1	position of evaporative front	[m]
t	time	[s]
t_c	contact time	[s]
T	temperature	[K]
T_b	boiling temperature	[K]
T_b	temperature at the base of a particulate bed	[K]
T_H	temperature of the submerged surface	[K]
T_S	temperature of the particulate material	[K]

T_1	temperature at s_1	[K]
T_v	temperature of the saturated state of water vapour	[K]
u	interaction energy in Eqution 2.23	[-]
v_1	jump frequency	[-]
V_m	mean molecular velocity	[m s^{-1}]
V_L	specific volume of liquid	[-]
W_s	mass of dry material	[kg]
X	moisture content	[kg H_2O/kg dry solid]
x	fraction of moisture loading, X, from 2.8	[m]
x	sub-radial distance within spherical particle	[m]
x_1	mole fraction of more volatile component in the liquid phase	[mol kg^{-1}]
X_g	geometric parameter at the moisture-gas interface	[kg kg^{-1}]
X_i	moisture content at the beginning of the falling-rate period	[-]
X_v	moisture content (volumetric saturation of water based on void space of material)	[kg H_2O/kg dry solid]
Y	humidity	[kg kg^{-1}]
z	rate of desorption constant	[kg H_2O/kg dry solid]
z_1	molar selectivity of first species	[-]
Greek		
α_{ws}	surface-to-particle heat transfer coefficient	[W $m^{-2}K^{-1}$]
α	heat transfer coefficient	[W $m^{-2}K^{-1}$]
β	initial relative moisture content (where $X_o < X_{cr}$)	[-]
α_{12}	relative volatility of first species relative to the other	[-]
β	constant in Equation 2.18	[-]
δ	roughness of the particle	[-]
δ_e	effective diffusivity of water vapour	[m^2s^{-1}]
ΔH_d	heat of desolvation	[kJ kg^{-1}]
ΔH_{dis}	heat of dissociation	[kJ kg^{-1}]
ΔH_f	heat of fusion	[kJ kg^{-1}]
ΔH_t	heat of transition	[kJ kg^{-1}]
ΔH_v	heat of vaporisation	[kJ kg^{-1}]
ΔH_w	heat of wetting	[kJ kg^{-1}]
ΔG	Gibb's differential free energy	[kJ kg^{-1}]
ΔG_o^*	molar free energy of activation	[kJ kg^{-1}]
ΔS_h^o	entropy of hydration	[-]
ΔU_v	internal energy of vaporisation	[kJ kg^{-1}]
ϵ	voidage	[-]
γ	activity or accommodation coefficient	[-]
Γ	reduced relative moisture content	[-]
λ	shrinkage coefficient	[m]

λ_e	eff. thermal cond. without the enthalphy transfer effect	[W m^{-1}K^{-1}]
λ_{ed}	eff. thermal cond. dried up zone	[W m^{-1}K^{-1}]
λ_{ew}	eff. thermal cond. wet zone	[W m^{-1}K^{-1}]
λ_g	heat conductivity of the continuum gas	[W m^{-1}K^{-1}]
Λ	mean free path of the gas molecules	[-]
ρ_b	bulk density of the dry material	[kg m^{-3}]
ρ_w	mass density of water	[kg m^{-3}]
Φ	relative moisture content at the critical moisture content	[-]
Ψ	void fraction	[-]
σ_v	contact angle	[-]
τ_s	torosity factor	[-]
θ	contact angle in Equation 2.153	[-]
θ	fraction of surface loading	[-]
φ	relative humidity	[-]
μ	chemical potential	[J mol^{-1}]

Subscripts

a	ambient
b	bound phase
cr	critical
E	equilibrium
g	gas phase
gi	inlet gas phase
I	induction
l	liquid
L	liquid
M	monolayer
v	vapour
w	wetting W / wet-bulb

Chapter 1

INTRODUCTION

1.1 GENERAL

A material containing moisture/s, in a liquid or bound form of an organic solvent and/or water, in excess or in equilibrium with its surroundings can be subjected to a change in conditions favourable for the removal of moisture, i.e. an increase in temperature or air velocity or a decrease in humidity or pressure. Such a step change will inevitably result in the material losing moisture to re-establish equilibrium with its surroundings. This change is called "drying", an important separation process which has been extensively studied over the past 60 years.

Recently, greater attention than hitherto has been to focus on the drying limits of materials, because drying to states close to these limits is generally expensive. By investigating how a material dries, the expenses of drying can be minimised, especially as a rapid rise in energy costs has been witnessed over the last three decades. Also, there are demands to improve product purity in the pharmaceutical and health industries, as traces of solvent residues can cause additional health problems to patients. As removing these traces of solvents to an acceptable level is difficult, a knowledge of the drying process is important.

Drying is both energy and capital intensive, and plays an integral part in the manufacture of a wide range of materials. Presently drying processes in the UK consume as much as 20% of all industrial energy (I Kemp, unpublished). The energy involved is of the order of 150 PJ per annum. This energy loading corresponds to $2 * 10^{10}$ litres of evaporated water, which is equivalent to approximately $4.4*10^{9}$ flushes of a toilet.

Efficient use of energy has become more significant in company accounting. Process optimisation and a drop in production have resulted in a 20-30% decrease in energy demand in the UK since the early 1980s. Many older energy-intensive driers have been replaced by more modern units. Since the recent development of more specialised products, as in the pharmaceutical industry, there has been a swing back from continuous to batch drying units for these specialised products. Even more recently, as these fine chemicals are now being produced in greater quantities, continuous operation of driers

is required to divert operations from the costly batch drying units.

Considerable research efforts have ensured an increase in the overall understanding of the drying process, as evidenced by publications such as "Advances in Drying, 1 - 5", "Drying Volumes 80, 82, 86, 91, 92, 94, 96" (some proceedings from IDS), further publications from the biennial International Drying Symposia (IDS)(since 1978) not incorporated in the "Drying Volumes", and the specialist journal "Drying Technology".

1.2 THIS WORK

The objectives of this contract were subdivided into two principal industrial objectives and several secondary academic aims. The first principal objective was to develop drying kinetics and equilibrium determination procedures for individual particles based on a thin-layer technique to generate the necessary data to model various industrial driers. A thin-layer apparatus was built at the University of Canterbury to investigate the drying kinetics of thin-layers. T Langrish supervised this earlier work which was completed at the end of 1994. The second part of the project (this PhD programme) required the determination of the drying kinetics and equilibrium characterisation of selected porous particulate materials at low moisture contents. Initial feedback from industrial sources indicated that an area of interest involved the drying of organic particles of diameter 10-500μg with moisture contents in the range 0.01-1%.

The fundamentals and kinetics of drying at moisture contents above 1% have been extensively investigated this century. However, at lower levels of moisture in a solid, the fundamental drying kinetics have generally been believed to follow an exponential heat of wetting relationship between solid, and bound moisture. This may help model removing bound moisture from an inhomogeneous surface, but would fail to predict drying behaviour from homogeneous or hydrophobic surfaces at moisture contents less that 1%. Drying profiles of various particulate solids were used to investigate suitable drying models at low-moisture contents. Possible variations in drying behaviour would be specific to that type of solid. A possible insight into variations in drying behaviour was predicted by determining equilibrium characterisation on each particulate solid. The development of an experimental method for equilibrium sorption of solids with moisture contents less than 1% was necessary.

A number of secondary academic aims were identified to help understand the mechanisms responsible for low moisture content drying. Do isolated particles dry differently from particles in layers? This question was an extension of work carried out on the thin-layer apparatus. As the determination of the drying kinetics of discrete particles was not possible using the thin-layer apparatus, a thermogravimetric unit was used to obtain desorption profiles of individual particles. The thermogravimetric unit also provided an insight to the usefulness of using an electronic microbalance for possible future gravimetric weight loss measurements. How does moisture move and ad/desorb?

An equilibrium characterisation of each material provides an insight to the internal pore structure by using a number of analytical methods such as single-point nitrogen sorption and sorption isotherm determination. Sorption isotherms also quantify the strengths of the bound moisture at or near the pore surface. A number of relevant drying models can be used or modified to simulate such drying processes. These are described later. Do volatiles dry selectively, as is normally the case at higher moisture contents? Are the same mechanisms of selective drying applicable to residual moisture levels? These questions are the initial ideas that needed to be understood at the end of this work. Are existing test rigs, which traditionally use evolved gas analysis methods, sensitive enough to resolve the low drying rates of low moisture content drying? These are the questions that which were to be resolved to help provide a good understanding of the desorption processes occurring at low moisture levels ($< 1\%$).

Why investigate drying at low moisture contents:

- To reach a better understanding of the transport properties in drying to low-moisture contents.
- To estimate precisely the extensive time of drying to low moisture contents.
- To determine the effect of small amounts of moisture on product purity and/or product performance.
- To enable the design of equipment to handle low moisture products to be improved, with lower capital investment.
- To predict the accurate monitoring of drier exhausts for emission levels to meet discharge quality consents.

In the falling-rate period, drying rates decrease rapidly as the moisture content decreases. The lower the desired final moisture content, the larger is the overall volume of the drier/s. Achieving a better understanding of the mechanisms present in drying at these moisture levels would benefit not only the design of the equipment, but also provide process optimisation with an easier task. Thus, by observing the drying kinetics at low moisture contents, we are better able to optimise drier performance and minimise drier size. Previously the drying behaviour of material has been investigated at relatively high moisture contents, where the kinetics of most types of materials are generally well understood. Models of drying processes, such as receding evaporative fronts, hydrodynamic flow by capillary action and gas diffusion, are generally valid ways of describing drying processes at higher moisture contents. However, once moisture is removed from places at or near the particle's surface (especially if the surface is strongly hydrophilic), the strength of the moisture bonds becomes the limiting factor in the drying rates. Some materials are very microporous, where moisture is held in a

volume-filling arrangement of the pores which may be comparable in size with individual moisture molecules. In this case, an activation energy is still required to "dislodge" the moisture molecules. Other factors then affect the desorption of moisture from a particle's surface. Often, as no free pathway for moisture to the particle surface may exist, moisture is trapped permanently in the particle's lattice. This makes it very difficult or impossible to remove moisture from the infrastructure of the particle. This situation occurs especially in fine chemicals or particulate polymer crystals, where moisture of condensation is a by-product of a chemical reaction process. This condensed moisture is often trapped in the crystallising lattice of the solidifying particle matrix.

It is of commercial concern to know how the moisture near dryness moves through the pores to the particle's surface. When either a porous or a fibrous material has almost dried out, moisture can move only by unhindered vapour diffusion through the pore or surface diffusion along the pore surface. At higher moisture contents, moisture may condense at the waists in each capillary, but moisture still travels mainly in the vapour phase.

The development of specialised products over the past few years, particularly in the pharmaceutical industry, has induced a concern for an understanding of the drying nature of these materials at low moisture contents. Product purity in the pharmaceutical industry is of paramount importance. Trace solvents or "organic residues" may limit the effectiveness of the product. Further removal of these residues to an "acceptable level" is difficult as removing all moisture is impossible. On a quantitative basis, probably the most important issue is the production of pharmaceutical tablets, for which the material is usually produced as a granulated powder from which the moisture in either the aqueous or the organic solvent must be removed. Large scale productions of crystalline chemicals, whether for the removal of surface free moisture or for the removal of a degree of chemically bound moisture, can be successfully dealt with in pneumatic driers. Bulk quantities of some products are also dried in steam-heated continuous rotary driers whereas whilst smaller quantities are conveniently handled in agitated pan driers. The removal of all physisorbed moisture without disrupting the chemically adsorbed moisture, as in the drying of adipic acid, is an optimisation process, as sometimes a narrow buffer region (if any) exists between these two types of bonding. Separations of this nature are very specific to the particle topology, the type of condensed vapour/solid bonds and the strengths of bound moisture.

Establishing the drying behaviour is a function of two things. First, the chemical composition of the material may influence drying limits, i.e. many organic compounds or polymers are able to fragment at moderately high temperatures and condensation of water molecules may be possible; therefore desorption of condensed water, not physisorbed water, is recorded. Second, working at low levels of moisture/solvent residues, the sensitivity of the equipment becomes very important. One problem experienced in this area of research is determining exactly the amount of moisture/solvent in the

particle. What is the exact reference point for determining the moisture content of a material? This is usually interpreted as the lowest attainable moisture content, which depends on the type of drying equipment that has been used. Sazanov (1989) recorded the condensation of water molecules from a furan polymer, using a mass spectrometer in the range from 200 to $1200 degC$, as a result of the molecules of the furan polymer undergoing degradation and structural deformation, with the carbonised residue as the final product. Thus, in an attempt to remove all physisorbed moisture, a drying temperature should be used such that the disruption of the material by condensing water molecules is not possible. Equipment such as differential scanning calorimeters and thermogravimetric units were used in this work to find a suitable drying temperature.

There are additional benefits as a result of drying to low moisture levels. First, product storage may dictate many materials to have a maximum moisture content at which they may be stored without degradation occurring. Second, other materials have their handling properties enhanced by maintaining a strict specification on the final product moisture content. Third, a much lower moisture content may be desired because of a reduction in transport costs of some bulk materials by transporting them in a moisture-reduced form. Finally, removing toxic organic residues from materials promotes possible financial incentives for companies and reduces environmental concerns.

Many contact drying units in industry yield products that reach final moisture contents of 0.01-0.5% and even lower. This "extreme drying" is normally performed under high vacuum contact drying, and has been possible due to the development of high performance equipment. Some companies prefer to purge the vacuum chamber with inert gases or nitrogen before applying a vacuum, to dry the chamber and create a lower partial pressure than with a reduced air atmosphere containing oxygen.

Extreme drying is also possible for through-flow, cross-circulation or fluidised beds, if the dew point of the air is very low and the bed temperature is increased along the length of the drier in step with glass transition temperatures. Different synthetic and natural sorbents, such as silica gel, active aluminium oxide, P_2O_5, synthetic zeolites, bauxite, some salts, CaO, MgO, and other hydrophilic chemical adsorbents on a porous base, are used in the industrial drying of air and other gases. The degree of drying by these different desiccants are limited by their respective pore topologies and/or chemical compositions. Some desiccants, with their drying ability, are reported in Table 1.1.

Regeneration temperatures are approached in a stepwise fashion to prevent scalding of the desiccant, and the desiccant is then held at this temperature for up to $24h$. The frost points are maximum attainable values. The most effective method of producing a dry gas flow is to use a flow of dry nitrogen directly. Industrial-grade nitrogen usually contains between 1 and $2 ppm$ water, which corresponds to frost (dew) points of -79 and -71 $degC$ respectively. This suggests that it is possible to use the regenerated adsorbers in

Table 1.1 Desiccants for gases (from Fedorov *et al.*, 1990)

Desiccant	Moisture content [mg litre^{-}1]	Frost point [*degC*]	Regeneration temperature [*degC*]
$CaCl_2$ (Good moisture capacity)	0.2	-33	
$CaSO_4$	0.065	-63	250
Silica gel	0.02	-70	300
Al_2O_3	0.0008	-75	500 (in vacuum) or 700 (in air)
Molecular sieves, zeolites	0.0008	-75	350 (in vacuum)

Table 1.1 instead of expensive through-flow compressed nitrogen gas. As noted before, large scale operations now use continuous units, such as cascade rotary driers with an enhanced temperature profile along the drier. As a result, this work concentrated more on drying by an air flow rather than drying under vacuum conditions

Provided moisture is not trapped in micropores or a path for moisture transport to the surface exists, extreme drying is possible. Such is the case for non-porous particles. However, heating the material can disrupt the alignment of the molecules and further desorption can occur more freely. Entrapped solvent is evolved only during melting of the host material. The amount of entrapped solvent can be determined by thermogravimetric analysis together with differential scanning calorimetry and/or mass spectrometry.

Porous materials with low moisture levels may contain traces of unbound moisture such as liquid, or bound moisture on the surface in layers, clusters or constrained by volume filling of any micropores slightly larger than the adsorbate molecule. Some of this water may be removed only after the structure of the material has been altered, for example in the transition from the crystalline to the amorphous state, and even after melting. If there is no free path for this moisture to travel from the micropores to the surface, then only melting or softening the material will promote the removal of the final traces of water.

Evaluation of the final moisture content of porous materials can be achieved with certainly only by pyrolysing it and using an evolved gas analysis (i.e. mass spectrometry or hygrometry) or by Karl Fischer titration to record fragment profiles against temperature until siliceous or carbon products remain at a very high temperature. Determining accurately the amount of water held in most fine organic chemicals is widely done using a suitable solvent to dissolve the solid and performing Karl Fischer analysis on the newly created solution. This is the most accurate method of determining the moisture content of these materials. However, as not all solids are soluble in a given solvent, less accurate pyrolysis methods are employed. This technique has limited value in determining the drying behaviour of material, as most drying is performed without

disrupting the physical structure of the material. Therefore moisture that is of interest, such as free water or water molecules bound to the surface, can be removed by drying at a temperature below the solid's melting or glass transition points. Moisture that is stable in the structure is not driven off. Such retained moisture may provide major problems with later processing and use of the dried product, and may interfere with post-drying processes such as extrusion. This problem is not easy to resolve. The present way of combating this problem is to attempt to produce high grade crystalline products with a low porosity by drying under ultra-high vacuum conditions.

Once final moisture levels have been reached, it may be necessary to vacuum seal the product or store under nitrogen to prevent re-adsorption of vapours from the atmosphere.

Because of recent environmental concerns, tighter controls are required on drier exhausts. Selective or preferential desorption of binary mixtures (Thurner and Schlünder, 1986) and more recently ternary mixtures (Riede *et al.*, 1988) has been extensively studied over the past 25 years. Selective desorption at higher moisture contents (>1%) is dependent on a number of factors (Schlünder, 1984). Krishna (1990a, 1990b, 1992, 1993a, 1993b) has been successful in describing selective desorption in the monolayer region by applying the Maxwell-Stefan equations to this type of work. Generally the more volatile component is removed preferentially, when the drying rate is low, as would be the case at low moisture levels. At sufficiently high drying rates, the moisture always evaporates with constant composition; the drying is non-selective. Non-selective drying is also obtained when the moisture has a pseudo-azeotropic composition; however at initial compositions above this, the less volatile component may be removed preferentially.

There appear to be a number of questions to be resolved.

- Do isolated particles dry differently from particles in layers, both cross and through circulated?
- Do the drying kinetics differ when moisture is held by volume filling and/or strongly adsorbed on pore surfaces at low moisture contents, compared with vapour diffusion and capillary action at higher moisture contents?
- Is it possible to use existing equipment to investigate drying kinetics at low moisture contents, or will a new design concept be required?
- Is the drying selective at low moisture contents when organic volatiles are present?

Chapter 2

PREVIOUS WORK

2.1 MOISTURE BONDING AND SORPTION

2.1.1 Scope

Adsorption on to solids is the selective transfer of one or more vapours from a gas, or from a liquid, to a solid which may or may not swell as a result. The selectivity of an adsorbent between adsorbate and carrier gas, or between different adsorbates, makes it possible to separate certain adsorbates from the carrier gas or from one another. Similarly a reverse operation, desorption, will often bring about separations of species initially in the solid. The preferential removal of one component is called "selective drying". Schlünder (1976, 1978) pioneered selective desorption studies of sorbent mixtures from porous materials over the past 20 years using "drying curves" and "composition curves". A drying curve basically is the relationship between the drying rate and the moisture (normally refers to H_2O only) content and is useful in estimating the drying time to reach particular moisture contents. In the drying of materials containing mixtures, it is also important to know the composition of the moisture as a function of the moisture content; this is called a composition curve.

Adsorption involves, in general, the accumulation of solute molecules at a solid interface. The accumulation per unit area is small: thus highly porous solids with very large internal areas per unit volume are required for good adsorbents. The surfaces are usually irregular, and the bonding energies (primarily from van der Waals' forces, as in vapour condensation) vary widely from one site to another. However, with "molecular sieves", the adsorptive surfaces are provided by channels or cavities within a microcrystalline structure; the sieves exhibit high uniformity of adsorptive surface with practically constant binding energy.

Adsorbents are natural or synthetic materials of amorphous or microcrystalline structure; those used on a large scale include activated carbon, activated alumina, silica gel, fuller's earth, other clays and molecular sieves. At room temperatures, adsorption is usually caused by intermolecular forces rather than by the formation of new chemical bonds; it is then called "physical adsorption" or physisorption. At higher temperatures

(above $100 degC$), the activation energy is normally available to make or break chemical bonds, and, if such a mechanism prevails, the adsorption is called "chemisorption" or "activated adsorption".

As all microporous and mesoporous materials (defined as pores less than 100-200nm) readily adsorb moisture, virtually all physically adsorbed moisture can be removed by exposing these materials to an atmosphere or a vacuum devoid of any water vapour. Porous materials adsorbing moisture that is partially bound to the host material are described as hygroscopic, and it is this affinity for water that frustrates efforts to dry them. The extent to which hygroscopic materials contain water is dependent upon the moisture content of the surrounding air; when a sample of a porous material is exposed to air of constant humidity, adsorption or desorption will take place depending upon the material's original condition. Eventually, the total mass of the sample then achieves dynamic equilibrium with the surrounding air.

2.1.2 Equilibrium in sorption

The relationship between an adsorbent and an adsorbate at equilibrium can be described using sorption isotherms. These are used to relate the loading or moisture content X of the adsorbent (equilibrium loading) as a function of the vapour pressure p or relative humidity ($\varphi = p/p_o$) at temperature T= constant, where p_o is the saturation vapour pressure; see Figure 2.1.

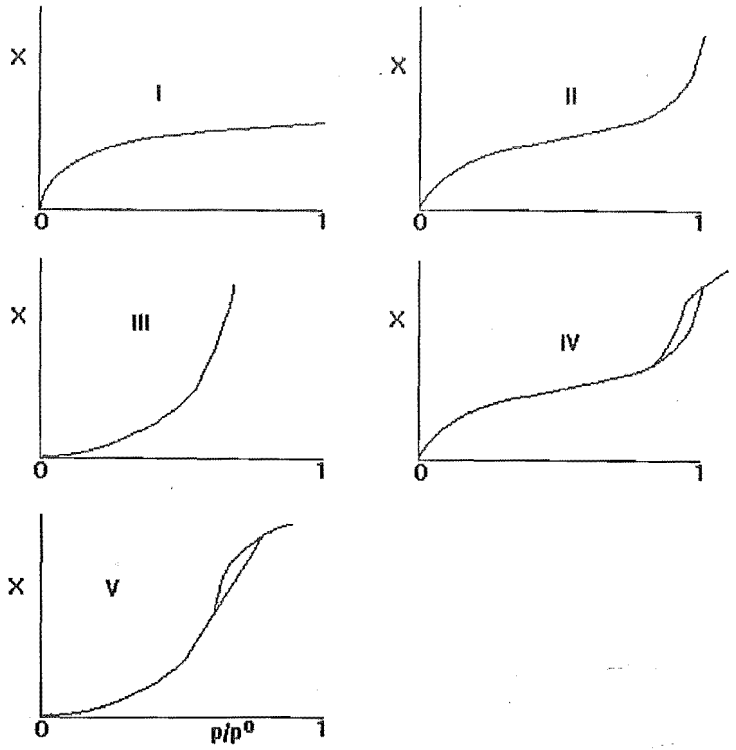

Figure 2.1 Types of sorption isotherms

Each of the three differently shaped isotherms represents a different sorptive behaviour. Curve "III" demonstrates capillary condensation as the vapour loading is increased. Curve "II" is explained by the formation of multilayers on the adsorbent surface. Curve "I" indicates the occupation of a single layer only on the host material.

2.1.3 Thermodynamic equilibrium between two phases

2.1.3.1 General

The most general condition for thermodynamic equilibrium between two phases under isothermal conditions is that the partial molar free energy (μ), commonly called the chemical potential, must be the same in both phases. For the vapour component in the gas phase (μ_g) and the bound phase at the adsorbent surface (μ_b), Kast and Jokisch (1972) stated that:

$$\mu_g = \mu_b \tag{2.1}$$

Because of the relation between the chemical potential (μ) and the fugacity (f), the above equation can be rewritten as:

$$f_g = f_b \tag{2.2}$$

If we assume ideal behaviour of the vapour in the gas, the fugacity becomes identical to the vapour pressure of the component in the gas:

$$f_g = p_g \tag{2.3}$$

For the sorbed phase, the activity (f_b) may be related to the vapour pressure (p_b) of this phase:

$$f_b = \gamma p_b \tag{2.4}$$

The activity coefficient γ and the partial molar binding energy (h_b) (equivalent to the differential heat of wetting) are related by:

$$h_b = RTln\gamma \tag{2.5}$$

where $\gamma = f_b/p_b = f_g/p_b = e^{-h_b/RT}$. Plots of the partial molar binding energy against moisture content give an indication of the strengths of binding between moisture and adsorbent. Moisture held beyond the monolayer tends to be more easily removed than moisture held at the surface, and as non-homogeneous adsorbent surfaces also have stronger adsorption sites, further increases in binding energy can be observed.

If h_b is positive, as it is for adsorbents, the fugacity (f_b) of the pure component becomes less than the vapour pressure; consequently, there is a drop in vapour pressure of the adsorbate. Cases can occur where h_b can be zero or negative for the adsorbent, for example gels and plastics; this involves a rise in vapour pressure.

For the equilibrium condition, for the relative humidity φ, Equation 2.5 can be written:

$$\varphi = \frac{p_g}{p_s} = \frac{f_g}{p_b}\frac{p_b}{p_s} = xexp(-\frac{h_b}{RT}) \tag{2.6}$$

where x is the fraction corresponding to the loading X as actually measured, and φ is known as the relative humidity. It should be possible to describe the sorption isotherm by this relation if we know the dependence of the binding energy on the loading, $h_b = h_b(x)$, and if it is possible to convert the fraction x of the moisture content X as actually measured.

We know that the binding energy can be found from the sorption isotherms through the derived expression:

$$\left(\frac{\partial ln\varphi}{\partial(\frac{1}{T})}\right)_{x=constant} = -\frac{h_b}{R} \tag{2.7}$$

To relate these quantities, a proportionality is normally assumed:

$$x \approx \frac{X}{cX_{max}}, X \leq X_{max} \tag{2.8}$$

in the region of low loading, where c is a coefficient and X_{max} is the maximum hygroscopic moisture content. It follows that, apart from the inner surface area and the pore distribution, the binding energy will be the determining thermodynamic quantity in the analysis of sorption isotherms.

2.1.3.2 Binding energy

The binding energy and its dependence on loading can be given for two important cases of adsorption in monomolecular Langmuir loading (Figure 2.1, *Type I*) (Langmuir,

1918). The sorption isotherm is given by the equation

$$\varphi = \frac{cx}{b(1-cx)} = \frac{X}{b(X_{max}-X)} \tag{2.9}$$

The resulting binding energy as a function of loading is given by

$$h_b(x) = RTln(\frac{b}{c})(1-cx) \tag{2.10}$$

In this Langmuir region, the heat of sorption is determined by this equation as a function of loading x or moisture content X.

At higher loadings, when in accordance with BET theory (Brunauer, Emmett and Teller, 1938) the adsorbent surface is uniformly covered with several molecular layers, the binding energy must, according to Polanyi (1932) , supply the work of compressing the vapour from its vapour pressure p_g in the gas phase to its vapour pressure p_b in the bound phase:

$$h_b(x) = RT\int_{p_g}^{p_s}\left[\frac{dp}{p}\right]_{X=constant} = RTln\left(\frac{1}{p_g/p_{s[x=1]}}\right)_{X=constant} \tag{2.11}$$

$$= RTln\left(\frac{1}{\varphi}\right)_{X=constant} \tag{2.12}$$

where x is constant. For curve plotting, we have to find $y_x = f(X)$ from the sorption isotherm; at low loading ($y \approx 0$), this function would make h_b infinite. This would contradict the Langmuir behaviour which is to be expected in this region for the majority of porous adsorbents. In many respects however, present day conceptions have departed so greatly from Polanyi's view that the connection with this theory has been almost completely discounted. In certain aspects of modern theory it is non-existent (Bering *et al.*, 1971)

In the other extreme case, with capillary condensation in the pores of the adsorbent, Kelvin's relation, as cited by Quenard and Bentz (1992), yields the decrease of vapour pressure in the pores:

$$\varphi = \frac{p_g}{p_s} = \frac{exp(-2\sigma_v)}{rRT} \tag{2.13}$$

The binding energy for this process is:

$$h_b = \frac{2\sigma_v}{r} = RTln\left[\frac{1}{\varphi}\right]_{X=constant} \tag{2.14}$$

and this gives h_b identical to that of Equation 2.12. Thus, multilayer coating and capillary condensation are two thermodynamically equivalent and indistinguishable processes, but do not accurately predict the bonding energy of multilayers on active surfaces. However, in the monomolecular region the binding energy as given by Equation 2.7 is often observed to be lower than that obtained from Equation 2.12. This may be the case where adsorption occurs at locally preferred sites on the surface with reducing energy potential, on the lines of heterogeneous nucleation. This is typical of non-uniform adsorbent surfaces, but less predominant for molecule-specific adsorbents such as molecular sieves.

2.1.4 Classification of sorption isotherms

Here, typical isotherms are discussed and equations for several that can be used easily for prediction and design are included. Unless the form of the isotherm is known, extrapolation of data over a limited range can be misleading.

Once equilibrium isotherms have been obtained, empirical algebraic expressions may then be fitted to the data and usually selected for generality and simplicity of calculation use. Representative isotherms are shown in Figure 2.1.

The majority of physisorption isotherms may be grouped into the four main types shown in Figure 2.1. In most cases, at sufficiently low surface coverage, the isotherm reduces to a linear form of Equation 2.21, which is often referred to as Henry's law region. On heterogeneous surfaces, this region may fall below the lowest experimentally measurable pressure. However, various authors have investigated the shapes of isotherms at very low pressures (Dubinin *et al.*, 1970; and Hobson and Chapman (1972).

The reversible *type I* isotherm (or Langmuir isotherm) is convex upwards throughout the relative humidity φ range and the curve approaches a limiting value as φ approaches 1.0. The *type I* isotherm is further discussed below.

The reversible *type II* isotherm is the normal form of isotherm obtained with a non porous or microporous adsorbent. The *type II* isotherm represents unrestricted monolayer-multilayer adsorption and can be correlated well with the BET isotherm (Equation 2.29, Equation 2.30). The beginning of the almost linear middle section of the isotherm is often taken to indicate the stage at which monolayer coverage is complete and multilayer adsorption is about to begin.

The reversible *type III* isotherm is concave upwards to the relative humidity axis over its entire range and therefore does not exhibit any inflection points. Isotherms of

this type are not common; the best known are found with water vapour adsorption on pure non porous carbon.

Characteristic features of *type IV* isotherms are their "hysteresis loops", which are associated with capillary condensation taking place in mesopores, and the limiting uptake over a range of high relative humidity. *Type IV* isotherms are obtained for many mesoporous industrial adsorbents.

Two other kinds of isotherm have been identified. The *type V* isotherm is uncommon; it is related to the *type III* isotherm in that the adsorbent-adsorbate interaction is weak, but is obtained with certain porous adsorbents.

2.1.5 Classification of porous materials

A classification of pores given by Dubinin (1968) is based on the difference in the mechanisms of sorption and the capillary phenomena taking place in them.

2.1.5.1 Macropores

The effective radii of the largest adsorbent pores known as macropores exceed 0.1-0.2μm (1000-2000 $\dot{A}$) and their specific surface area ranges between 0.5 and 2 $m^2 g^{-1}$. Adsorption on the surface of macropores is usually unimportant and capillary condensation does not take place. Therefore, the macropores provide channels for moisture transport and are rarely rate determining.

2.1.5.2 Mesopores

The effective radii of a smaller variety of adsorbent pores - intermediate (mesopores) greatly exceed the sizes of the molecules adsorbed. On the surface of intermediate pores there occurs monolayer and multilayer adsorption occur: i.e. the formation of successive adsorption layers leads to the volume filling of this variety of pores by capillary condensation. The effective radii of intermediate pores range from 18-20 to 2000 $\dot{A}$ (2 to 200 nm). The lower boundary, which corresponds to meniscus curvature radii of 15-16 $\dot{A}$ (1.5-1.6 nm), corresponds, in the pores of indicated dimensions, to the limit of applicability of the Kelvin equation. Depending on the development of the volume of intermediate pores and their predominant radii, the specific surface areas of intermediate pores may range from 10 to 400 $m^2\ g^{-1}$. On the whole, for non-porous, macroporous and intermediate-pore adsorbents of the same chemical nature, the quantitative difference in vapour adsorption is basically due to the different specific surface areas, because the surface curvature (prior to capillary condensation) in practice exerts only a slight effect on adsorption. In all these cases, the concept of adsorbent surface has a clear-cut physical meaning, and vapour adsorption amounts to the formation of successive adsorption layers. Note, in intermediate pores when the relative pressures

are sufficiently high, adsorption in layers on the surface turns into volume filling by capillary condensation.

2.1.5.3 Micropores

The effective radii of the smallest micropores are substantially below the lower boundary of sizes of intermediate pores. The total volume per unit mass of adsorbent does not exceed 0.5 $cm^3 g^{-1}$ to any degree. The volume of these micropores corresponds to effective radii from 5 to 16 $\dot{A}$ (0.5-1.6nm). This volume has been described by a two-term volume distribution. Dubinin (1968) coined the micropore terminology, micropores (i.e., pores of width, $x<$ 6-7 $\dot{A}$(0.6 – 0.7nm)) and supermicropores (i.e. 6-7 $< x <$15-16 $\dot{A}$ (0.6-1.6nm)). Although these limits have not been accepted by IUPAC, Everett and Powl (1976) also suggested a two-term micropore distribution as a result of a detailed mathematical analysis of the potential energy of adsorption of inert gas molecules by microporous carbons. Also Pendleton and Zettlemoyer (1984) further applied this two-term micropore distribution to the adsorption of water and various solvents on silica. They commented that, at very low pressures ($p/p_o = 10^{-6}$), the bulk of the adsorption occurs in the micropores. As the relative pressure increases, some of the molecules also adsorb in the supermicropores until at sufficiently high relative pressures, the bulk of the adsorption occurs in the supermicropores.

The micropores are commensurate with the sizes (steric nature) of the molecules adsorbed. In particular, this range includes the sizes of zeolite voids and microporous silica gel. Adsorption follows the mechanism of volume filling of the adsorption space rather than the mechanism of surface coverage, i.e. formation of successive layers. The entire volume of micropores represents a space where an adsorption field exists. At any point within this space, adsorption potentials set up by "the walls of the pores" and the fields are superimposed on each other. For this reason, the substance adsorbed in micropores cannot be regarded as a single phase. However, the existence of an adsorption field in micropores is dependent on the size of the micropores, and the size of the adsorbate molecules. The theory of the potential energy for adsorption given by Gurfein *et al.* (1970), for cylindrical pores, and by Everett and Powl (1976), for slit-shaped pores, implies that micropore filling depends upon the ratio of the pore to the adsorbate diameter. For example, if the neck of the pore or the pore itself is smaller than the absorbate molecule, then the molecule cannot enter the pore. Conversely, if the pore is too large, then surface adsorption may occur. Also, if the adsorbed molecule is very small compared with the micropore, e.g. water has a cross-sectional area per molecule of 10.5 $\dot{A}^2$ (Bassett *et al.*, 1968) from density calculations at 25$degC$, then surface adsorption occurs rather than volume filling of micropores. Thus, selectivity of adsorption in micropores can be interpreted as a molecular sieve effect and has been seen to apply to a number of adsorbates on silica gel by Pendleton and Zettlemoyer

(1984).

2.1.6 Micropore sorption and volume filling

2.1.6.1 Thermodynamics of sorption in micropores

From a thermodynamic standpoint, the whole diversity of the "physical adsorption phenomena" (caused mainly by van der Waals' and electrostatic forces) lies between two limiting cases of sorption on non-porous, homogeneous surfaces and sorption in micropores. All real cases of sorption represent a more or less complex superposition of these two sorption phenomena. In sorption on non-porous material, and also on wide-pore material, a pictorial molecular model is the coverage of the adsorbent surfaces with the formation of successive adsorption layers. The most important parameter that characterises sorption equilibrium is the surface area of the material. One particular molecular model of adsorption in micropores is "volume filling". The process of volume filling porous solids by sorption or condensation of vapours (the filling of pores by adsorbate of density, no lower than 50-60% of the density of the liquid), as shown by Brunauer (1943), consists of two quite distinguishable mechanisms: capillary condensation and micropore filling (Dubinin, 1972). With the first mechanism, the presence of the menisci and the possibility of hysteresis in the adsorption/desorption isotherm are characteristic. In the second mechanism, first considered by Eucken (1914) and Polanyi (1916), a force field exists, enhanced especially in micropores with closely spaced opposite walls because of the additive nature of the van der Waals' dispersion forces. This is the reason for the presence of sorption vapours, firstly in a compressed gaseous phase and thereafter, at higher pressures, in the dense adsorbed/condensed phase. Goldmann and Polyani (1928) have shown, for relative pressures near to one, that the material in the field of force is found in a strongly compressed state. This sorption mechanism is the consequence of the relative smallness of the sizes of the micropores in whose entire space a sorption field is set up. A pictorial molecular model of sorption in micropores is not layer-by-layer coverage of the surface, but volume filling of the micropores, whose size does not allow us to regard the sorbate in them as a separate phase.

Bering *et al.* (1971) gave a clear explanation, in rigorous thermodynamic language, of the fundamental principles underlying the two limiting cases - sorption on non porous (large-pore) surfaces and sorption in micropores. It was shown that, from the thermodynamic point of view, the first limiting case applies to a non porous, inert (non-swelling and non-dissolving) sorbent, with a constant chemical potential, and can be described by the well-known Gibbs equation; the second case describes sorption in micropores and is the Gibbs-Duhem equation. In other words, from the thermodynamic viewpoint, sorption in micropores is a process similar to the formation of a sort of solution resulting in a change in the chemical potentials of both components of the system. Also, Bering *et al.* (1971) suggested that the concept of spreading pressure as

applied to microporous adsorbents is devoid of any physical meaning, as is the concept of the surface area.

In the design of drying equipment, it is advisable to have an equilibrium equation that would be able to fit to experimental data over a wide range of relative humidities, but with a limited number of constants. Accurate fitting of the isotherms by various model/s then helps characterise the solid.

2.1.6.2 Thermal equation of sorption in micropores

The concepts of volume filling of micropores in physical sorption make it possible to formulate a thermal equation of sorption, i.e. a function of surface coverage θ, partial pressure p and temperature T:

$$F(\theta, p, T) = 0 \tag{2.15}$$

from which one can obtain directly the adsorption/desorption isotherm equation by the substitution *T=constant*.

It has been shown by Dubinin *et al.* (1970), that the function F in Equation 2.15 is of the form

$$\theta = exp\left(-\frac{\Delta G}{E}\right)^n \tag{2.16}$$

This gives an indication of the extent of micropore fractional filling. In this equation, θ is the normalised amount adsorbed, E is numerically equal to the Gibb's differential molar free energy ΔG at a point for which the degree of filling of the sorption space θ is equal to e^{-1}, and can also be called the characteristic free energy. At n=1, Equation 2.16 becomes an ordinary Freundlich's equation. For microporous sorbents, this case is evidently never realised. At n=2, Equation 2.16 transforms into the so-called Dubinin-Radushkevich equation, which describes vapour sorption on active carbons particularly well and is a specialised case of the Dubinin-Astakov equation, Equation 2.17 below. Higher values of n have proved to be applicable in some cases to sorption on especially fine porous Saran active carbon, n=3, and on microporous silica gel as described by Pendleton and Zettlemoyer (1984) .

The generalised Dubinin-Astakov equation can be written (Bering *et al,*, 1971):

$$\theta = exp\left(-\frac{A}{\beta E_o}\right)^n \tag{2.17}$$

where E_o is the characteristic free energy of adsorption of a standard material, and β is the ratio between the characteristic free energy of adsorption for the test (E) and the standard free energy (E_o). Differentiation of Equation 2.17 with respect to A gives the probability density distribution of fractional filling of the total micropore volume, i.e. an indication of the probability of the fractional filling of the micropores as a function of the relative humidity p/p_s (A=$RT\ ln\ p_o/p$):

$$-\frac{d\theta}{dA} = \frac{nA^{n-1}}{(\beta E_o)^n} exp - \left(-\frac{A}{\beta E_o}\right)^n \tag{2.18}$$

A plot of θ against free energy A indicates an approximate adsorption site energy distribution. It can be used to investigate whether a relation exists between the parameters of Equation 2.17 and the distribution of micropore sizes with sorbate width (Stoecki *et al.*, 1982).

The above arguments apply to systems of narrow micropore size distribution, but can be easily extended to systems exhibiting a wide micropore size distribution (Pendleton and Zettlemoyer, 1984).

2.1.7 Layerwise sorption in pores

2.1.7.1 Surface adsorption

The simplest model of adsorption on a surface is that in which localised adsorption takes place on an energetically uniform surface without any interaction between adsorbed molecules (Suzuki, 1988). At constant temperature, the adsorption rate is expressed as $k_a p(1-q)$, on assuming first-order kinetics, with the desorption rate given as $k_d q$, where q is a ratio of the amount adsorbed at pressure p to the amount absorbed at the saturation pressure. When the adsorption and desorption rates are equal:

$$\theta = \frac{Kp}{1+Kp} \tag{2.19}$$

and

$$p = \frac{1}{K}\left(\frac{\theta}{1-\theta}\right) \tag{2.20}$$

Here K=k_a/k_d is called the adsorption equilibrium constant. The above equation is called the Langmuir isotherm and can be employed to fit isotherms of *type I* in Figure 2.1. *Type I* isotherms are given by microporous solids having relatively small external surfaces (e.g. activated carbon, molecular sieves), the limiting uptake being governed by the accessible micropore volume rather than by the internal surface area.

When the amount adsorbed, q, is far smaller than the adsorption capacity of the adsorbent, q_s, Equation 2.19 reduces to the Henry-type equation:

$$\theta = Kp \tag{2.21}$$

Further, when the concentration is high enough, $p >> 1/K$, then the adsorption sites are saturated and

$$\theta = 1 \tag{2.22}$$

Suzuki (1988) notes that Equation 2.20 is modified when interaction between adsorbing molecules is taken into account. For example Fowler and Guggenheim (1939) gave

$$p = \frac{1}{K}\left(\frac{\theta}{1-\theta}\right) exp\left(\frac{2u\theta}{kT}\right) \tag{2.23}$$

where $2u$ represents the pair interaction energy (positive for repulsion and negative for attraction) and k is the Boltzmann constant.

When adsorbed molecules are free to move on the adsorbent surface (mobile adsorption) the Langmuir equation is modified to (Suzuki, 1988)

$$p = \frac{1}{K}\left(\frac{\theta}{1-\theta}\right) exp\left(\frac{\theta}{1-\theta}\right) \tag{2.24}$$

Another typical example of the isotherms that is frequently employed is the Freundlich equation (1926):

$$q = k_F p^{1/n_F} \tag{2.25}$$

where $n_F = E/RT$ and E is the characteristic energy of adsorption.

This equation is often considered to be an empirical equation and corresponds to an exponential distribution of heats of adsorption. At low coverages of the adsorbent, the Freundlich isotherm implies the existence of sites with a very high heat of adsorption. This form of the isotherm can also be related to the generalised Dubinin-Astakov equation, Equation 2.17, which was derived for adsorption of the micropore filling type

by Bering *et al.* (1971) . Intermediate conditions between the Langmuir and Freundlich assumptions are more realistic, and this concept leads to the equation:

$$q = \frac{1}{\left[\frac{1}{\frac{K_L p}{1+K_L p}} + \frac{1}{k_F p^{1/n_F}}\right]} \tag{2.26}$$

The Freundlich equation does not satisfy the conditions given by Equations 2.21 and 2.24 because it gives no limit of adsorption capacity, making the amount adsorbed go to infinity when the concentration increases. It is applicable only below the saturation vapour pressure where condensation or crystallisation occurs and adsorption phenomena are no longer significant. Sholakhov *et al.* (1970) showed that the equilibrium adsorption of water vapour on silica gel KSM-5 at $25 degC$ and at low surface coverages can be described by the Freundlich expression, Equation 2.25, and that the high heat of sorption (6592 kJ kg^{-1}) can be accounted for by the low surface coverages ($< 0.1 kgwater/kgdrysolid$).

At extremely low concentrations of adsorbate, the Henry-type equation, Equation 2.21, usually becomes valid. Radke and Prausnitz (1972) formulated the following equation, which combines the Freundlich equation with the Henry-type equation:

$$q = \frac{1}{\left[\frac{1}{K_H p} + \frac{1}{k_F p^{1/n_F}}\right]} \tag{2.27}$$

This equation contains three empirical constants and is useful in correlating isotherm data obtained over a wide range of adsorbate concentrations.

2.1.7.2 Multilayer formation - traditional models

At low relative humidities, below about 0.35, water is adsorbed monomolecularly by many natural fibres. The equilibrium moisture content X_E then relates to the fraction of available sites taken up, that is

$$X_E = \theta X_m \tag{2.28}$$

where X_m is the moisture content corresponding to a fully completed monomolecular layer (not to be confused with the maximum hygroscopic moisture content) and q is the fraction of surface coverage.

Monolayer adsorption is formed in the same way as the Langmuir-type adsorption whereas adsorption above monolayers is equivalent to condensation of the adsorbate

molecules. These considerations give rise to the two-parameter BET equation:

$$\theta = \frac{X_E}{X_M} = \frac{C_B\varphi}{(1-\varphi)(1-\varphi+C_B\varphi)} \tag{2.29}$$

where φ is the relative humidity or relative vapour pressure and C_B is the ratio of the internal partition functions of the bound and liquid water. A BET plot of fitting isothermal data is shown in Figure 2.2 :

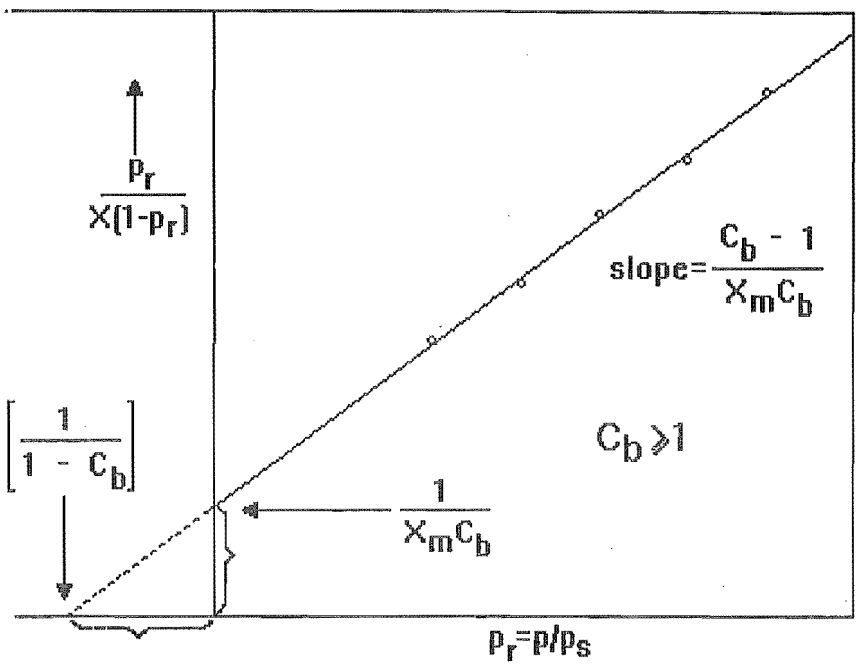

Figure 2.2 BET plot of gas-phase adsorption isotherm

The BET isotherm is used effectively to estimate the internal surface area once the sectional area per molecule of adsorbate is known.

In contrast to the assumed bulk liquid properties of the multilayer molecules of the BET model, compare this with the GAB model (*Guggenheim* (1966), *Anderson* (1946), *DeBoer* (1953)) of sorption which includes an additional parameter K. K is related to the equilibrium loading of sorbate on the surface. This isotherm equation was derived independently by the three authors. It was first proposed by Anderson, later derived kinetically by DeBoer and statistically by Guggenheim. These investigators worked independently on this form of isotherm and therefore the acronym GAB has been adopted for it.

$$\frac{X}{X_m} = \frac{C_B K\varphi}{(1-K\varphi)(1-K\varphi+C_B K\varphi)} \tag{2.30}$$

The GAB model of sorption can be regarded as a more general expression for which the BET model is just a limiting case when K is unity.

More recently, Jaafar and Michalwski (1990) created a similar modified BET equation by assuming that moisture adsorption occurs at randomly located, equal-sized active sites and that there is no interaction between adsorbate entities. This analysis results in a three-parameter BET-like equation

$$\frac{X}{X_m} = \frac{C_B \varphi}{(1-k\varphi)(1+(C_B-k)\varphi)} \tag{2.31}$$

For $k=0$, Equation 2.31 is transformed into Equation 2.19, which is Langmuir's relationship. For $0 < k < 1$, it describes material for which $\varphi=1$ reaches a finite maximum hygroscopic moisture content. The condition $k=1$ corresponds to the BET equation whereas $k \geq 1$ refers to the materials at which φ approaches an asymptotic moisture content.

This modified BET isotherm, Equation 2.31, presents a good fitting equation to a wide range of isotherm shapes. This equation incorporates a third parameter which forces an improved fitting to the traditional BET isotherm which assumes an infinite maximum hygroscopic moisture content. Isotherms of *type III* (concave-upward isotherms) can be fitted.

From the adsorption of liquid nitrogen, the surface area of the adsorbent is determined by relating the maximum moisture content X_M to the surface area. In most cases, X_M is obtained from the BET plot of the adsorption data. A plot of $p_r/X(1-p_r)$ against p_r often gives a straight line at lower relative humidities; X_M is readily determined from the gradient, as shown in Figure 2.2. Then by associating the surface area of nitrogen with X_M, the specific surface area of the adsorbent based on nitrogen adsorption is calculated.

2.1.7.3 Other multilayer models

There are a number of variants on the above multilayer equations, which have been formulated from characterising some foods and polymers (van den Berg, 1985); see Table 2.1. Variants on the more common BET and GAB isotherm equations give rise to several other formulations, such as those listed in Table 2.1.

The parameters C, K and E contain the contributions of the energy of sorbate-sorbent and sorbate-sorbate interactions respectively. The parameters C and K theo-

Table 2.1 Various isotherm equations and parameters (from van den Berg, 1985)

Acronym	Adjustable parameters	Isotherm equation
BET	W_m, C_B	$\frac{X}{X_m} = \frac{C_B \varphi}{(1-k\varphi)(1+(C_B-k)\varphi)}$
GAB	W_m, C_G, K	$\frac{X}{X_m} = \frac{C_B K \varphi}{(1-K\varphi)(1-K\varphi+C_B K\varphi)}$
NBET	W_m, C_B, n	$\frac{X}{X_M} = \frac{C_B \varphi(1-(n+1)\varphi^n+n\varphi^{n+1})}{(1-\varphi)(1-\varphi+C_B\varphi-C_B\varphi^{n+1})}$
PIR	W_m, C_B, n	$\frac{X}{X_M} = \frac{C_B \varphi(1-\varphi^n)}{(1-\varphi)(1-\varphi+C_B\varphi)}$
TLBET	W_m, C_B, C_{TB}	$\frac{X}{X_M} = \frac{C_B \varphi(1-2\varphi+\varphi^2+2C_{TB}\varphi-C_{TB}\varphi^2)}{(1-\varphi)(1-\varphi+C_B\varphi^2-C_{TB}\varphi^2+C_B C_{TB}\varphi^2)}$
SVBET	W_m, C_B, S	$\frac{X}{X_M} = \frac{C_B \varphi(1-\varphi+(S+1)C_B\varphi)}{(1-\varphi)(1-\varphi+C_B\varphi)^2}$
NGAB	W_m, C_G, K, n	$\frac{X}{X_M} = \frac{C_G K\varphi(1-(n+1)(K\varphi)^n+n(K\varphi)^{n+1})}{(1-K\varphi)(1-K\varphi+C_G K\varphi-C_G(K\varphi)^{n+1})}$
PIRGAB	W_m, C_G, K, n	$\frac{X}{X_M} = \frac{C_G K\varphi(1-(K\varphi)^n)}{(1-K\varphi)(1-K\varphi+C_G K\varphi)}$
TLGAB	W_m, C_G, C_{TG}, K	$\frac{X}{X_M} = \frac{C_G K\varphi(1-2K\varphi+(K\varphi)^2+2C_{TG}K\varphi-C_{TG}(K\varphi)^2)}{(1-K\varphi)(1-K\varphi+C_G K\varphi-C_G(K\varphi)^2+C_G C_{TG}(K\varphi)^2)}$
TLNBET	W_m, C_G, C_{TB}, n	$\frac{X}{X_M} = \frac{C_B\varphi(1-2\varphi+\varphi^2+C_{TB}\varphi(2-\varphi-(n+1)\varphi^{n+1}+n\varphi^n))}{(1-\varphi)(1-\varphi+C_B\varphi(1-\varphi+C_{TB}\varphi-C_{TB}\varphi^2))}$
SVGAB	W_m, C_G, K, S	$\frac{X}{X_M} = \frac{C_G K\varphi(1-K\varphi+(S+1)C_G K\varphi)}{(1-K\varphi)(1-K\varphi+C_G K\varphi)^2}$
LBGAB	W_m, C_G, K', E	$\frac{X}{X_M} = \frac{(C_G-1+E)K'\varphi}{(1-EK'\varphi)(1-K'\varphi+C_G K'\varphi)}$

retically have meaning of a ratio of reduced partition functions times the exponential net enthalpy of sorption, e.g. $z \exp(\Delta H/RT)$.

The NBET equation was derived by Brunauer *et al.* (1938) for food systems that are usually composed of strong swelling and soluble materials when there is little justification for restricting the sorbed layers to a finite number, which is typical of a BET-type equation. The same comment holds for the NGAB equation, which contains an additional parameter K, similar to the improvement in the GAB equation over the BET equation. The PIR equation is a variation of the NBET equation, proposed by Pickett (1946) and Rounsley (1961). It proceeds from a minor simplification in the mathematical derivation. Rounsley claimed that this equation is superior to the NBET equation in describing practical isotherms for foods and other biological materials

The TLBET equation is described briefly by Steele (1956). Presumably, the surface forces decay according to some function of distance. Therefore it is arbitrary to divide sorbed molecules into those that are affected by the sorbent surface and those that are not. The TLBET model assumes that not only the first molecule on a site deviates in behaviour from average multilayer molecules, but also the second and subsequent molecules deviate. Likewise, the TLGAB and TLNBET equations are based on their GAB and NBET counterparts.

The SVBET and SVGAB equations emerge from the assumption of an increasing number of active sites during the sorption process due to swelling. During the solvent swelling of polymers, the number of interactions between polymer chains decreases in favour of solvent-chain interactions.

The LBGAB equation follows from the splitting of sorbate-sorbate interactions into an entropic part and an enthalpic part. This divides the parameter K of the GAB

model into two parameters, E and K_E.

When adsorption takes place in multiple layers, adsorption on the adsorbent surface and above the adsorbed molecules is considered to be based on different attractive forces. Anderson and Wickersheim (1964), using near-infrared spectroscopy, identified at least two types of adsorbed water and two types of surface hydroxyl groups. They inferred, from the different infrared absorption bands (stretching fundamentals) of adsorbed water and hydroxyl groups, that, even at low water contents (below complete monolayer formation), the existence of water in a multilayer was noticeable for the tested materials. Conversely, high levels of hydration (equivalent to multilayer adsorption) suggest a "patchiness" of dry zones on the internal pore surfaces, rather than the formation of complete molecular layers.

2.1.7.4 Capillary condensation and hysteresis

The sorption of water vapour in a porous medium is a complex phenomenon which can be explained by two basic mechanisms operating either simultaneously or successively:

- monolayer and multi layer adsorption of molecules;
- capillary condensation.

All hygroscopic porous materials (pore size $< 1 - 2$ mm) exhibit "hysteresis" of some form over a limited range of relative humidity: that is, the adsorption and desorption isotherms are often not congruent, with the equilibrium moisture content being less on adsorption than on desorption. Hysteresis may have two origins: one at the pore level due to local effects, and one at the pore-space level due to the topology of the pore network. On desorption, part of the pore network is filled with the condensed phase at a given humidity, whereas a lesser quantity of vapour will saturate the system on starting from an essentially sorbate-free system. Surface tension of the condensed phase aides in lowering the local equilibrium gas phase partial pressure near the liquid surface. Quenard and Bentz (1992), using 2-D image analysis, showed that the adsorption-desorption behaviour depends critically on the structure of the pore space and not simply on the total porosity. Yoshiyuki and Nakajima (1988) measured sorption isotherms for a polyelectrolyte complex (poly(acrylic acid)/poly(4-vinylpyridine)) + water vapour system. They concluded that the appearance of sorption hysteresis is due to the depression mobility of polymer chains resulting from cross-links between carboxyl groups and pyridine rings.

Whereas adsorption equilibrium can be described in terms of thermodynamics, desorption from mesoporous solids is a percolation process and the extent of sorption hysteresis is related to the connectivity of the pore network. Mason and Malinaushas (1983) and Mason (1988) presented an analysis to describe the interconnections in a

network of pores using adsorption-desorption hysteresis. Lui *et al.* (1992) presented an analysis method based on a percolation theory which allows a measure of the topology, the mean co-ordination number of the pore network, to be determined from sorption measurements; for example, by nitrogen sorption and mercury porosimetry methods. This recent work is applicable to hysteresis loops (IUPAC) types H1 and H2 (Figure 2.3). In a related analysis, Seaton (1991) found an upper bound to the mean co-ordination number of solids having type H3 hysteresis loops.

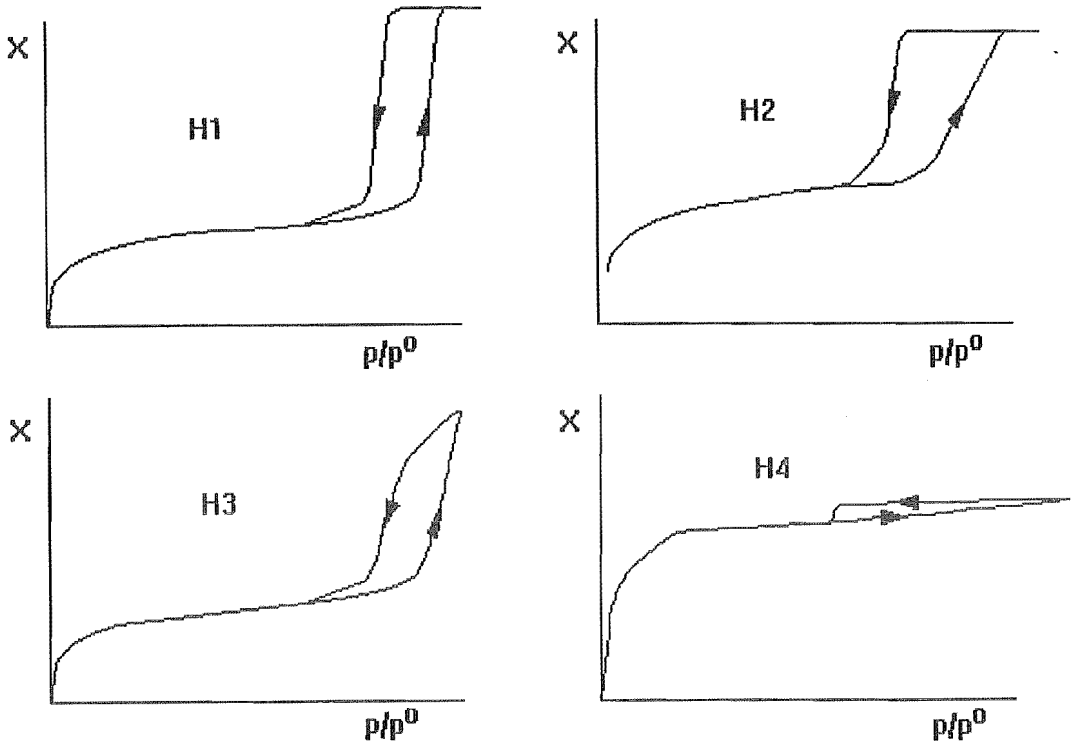

Figure 2.3 The IUPAC hysteresis loop classification (from Seaton, 1991)

Capillary condensation and its associated hysteresis play an important role in the wetting and drying of microporous-media-like soils, cement-based materials, gels or woods. This phenomenon may be associated with numerous disorders including shrinkage and micro-cracking during drying-wetting cycles and can strongly alter transfer coefficients, such as thermal conductivity or moisture diffusivity.

2.1.8 Empirical relationships

The phase equilibrium for one or several transferable components (adsorbates) between a carrier gas and an adsorbent depends on the adsorbate concentration and on temperature. In the simplest systems, a single curve can be drawn to show the adsorbate concentration in the solid in relation to the solid concentration or partial pressure in

the fluid. Any such curve may apply only at one temperature, and is known as an "isotherm". Plotting isotherms at other temperatures gives the associated heats of wetting, which are essentially enthalpy differences between the bound moisture and the free moisture at the same temperature. This may be estimated from a form of the Clausius-Clapeyron equation:

$$\left(\frac{\partial ln\varphi}{\partial T}\right)_{X=constant} = -\frac{\Delta H_{w,v}}{RT^2} \tag{2.32}$$

which assumes that the moisture vapour behaves as an ideal gas and that the condensed moisture has a negligible volume compared with its vapour. The application of Equation 2.32 is restricted to reversible processes that normally do not exhibit hysteresis, which may be found with irreversible structural changes. For materials that do exhibit hysteresis, the associated heats of wetting and heats of desorption are different. Note, the enthalpy difference associated with Equation 2.32 can have an exponential form as the relative humidity approaches zero, but the thermodynamics of drying below an equivalent monolayer are different than the thermodynamics of multilayer (or capillary condensation) drying. Thus, the sorption isotherm for Langmuir loading, Equation 2.9, represents the equilibrium behaviour in the monolayer.

Luikov (1966) correlated a large body of experimental data, mainly for building materials, by an expression of the form:

$$\frac{1}{X} = \frac{1}{X_M} - Bln\varphi \tag{2.33}$$

where X_M is the maximum hygroscopic moisture content, when the vapour pressure lowering is negligible, and B is an empirical coefficient. A plot of -*ln* φ against the reciprocal moisture content $1/X$ should yield a straight line with slope $1/B$ and an intercept on the abscissa of $1/BX_M$. This expression is probably limited to relative humidities in the normal ambient range.

Papadakis (1992) described the theoretical bases of various correlations, dividing these into two categories: those based on the Gibbs free energy change ΔG, Equation 2.32, or those based on a ratio of concentrations to surface energy change. The Gibbs free energy change for the condensation of a vapour at a surface is given by

$$\Delta G = -RTln\varphi = RTln\left(\frac{1}{\varphi}\right) \tag{2.34}$$

Equation 2.34 suggests that *ln* φ is a preferred correlating parameter to describe moisture sorption rather than the relative humidity φ itself. Papadakis (1992) altered

Equation 2.34 into an expression involving the equilibrium moisture content and two empirical coefficients A and B:

$$ln(X_E) = \frac{A + RTln\frac{1}{\varphi}}{B} \tag{2.35}$$

The relationships are listed in Table 2.2:

Table 2.2 Types of empirical equations used by Papadakis (1992)

Equation name	Form of equation
Henderson	$X_e = A\left(\frac{1}{T}ln\left(\frac{1}{1-\varphi}\right)\right)^B$
Modified Henderson	$X_e = A + B\left(\frac{1}{T}ln\left(\frac{1}{1-\varphi}\right)\right)$
Luikov	$X_e = \frac{A}{1+BTln\left(\frac{1}{\varphi}\right)}$
SPS	$X_e = Aexp^{-RTln(1/\varphi)}$
Keey	$X_e = \frac{A}{1+BT^3ln\left(\frac{1}{\varphi}\right)}$
Modified b	$X_e = \frac{A}{1+BT^2ln\left(\frac{1}{\varphi}\right)}$
Schuchmann *et al.* (1988)	$X_e = \frac{A(\frac{1}{T}ln(\frac{1}{1-\varphi}))}{B-(\frac{1}{T}ln(\frac{1}{1-\varphi}))}$
Halsey	$X_e = A\left(Tln\left(\frac{1}{\varphi}\right)\right)^{-B}$

He listed a number of useful empirical correlations, e.g. the Henderson equation and the modified Henderson equation for moisture sorption data and commented on their effectiveness with the materials investigated. Others are more specific to the type of material, i.e. Luikov's equation. R Keey (private communication, 1993) suggested that the equilibrium moisture content appears to be a strong function of temperature, as shown by his alteration of Equation 2.29. Like many empirical correlations, the two Henderson equations are derived from a rearrangement of parameters in Equation 2.30 given by Luikov and both have been very successful in correlating a large body of data. The modified Henderson equation is used when the maximum hygroscopic moisture content is ill-defined and X_M increases rapidly with relative humidity.

Other correlations that Papadakis listed are considered and fitted to the sorption isotherms from the materials tested in this work. These include: the SPS correlation, Keey, modified b, Schuchmann and the Halsey equation (Halsey, 1948).

2.2 MOISTURE BINDING MECHANISMS AT LOW MOISTURE CONTENTS

2.2.1 Water - how it is held in solids

This section classifies the types of bonds that solvents or water share with drying solids and includes a summary of chemical bonding with water and its association with solids.

2.2.2 Enthalpic-driven effects

A covalent bond is a result of equal *sharing of electrons*. As water is a polar molecule, an even sharing of electrons (a true covalent bond) is impossible. Partially covalent or ionic bonds are representative of intramolecular bonding in water molecules.

An ionic bond is a result of the *transfer of electrons* from unequal electronegative atoms, producing either a polar or an ionic molecule. Oxonium ions exist in low concentrations in "free" liquid water. The liquid state of water can also exist with isolated "non-free" water molecules held in micropores through van der Waals' forces to an extent that depends on the pH of solutions. Oxonium ions include H_3O^+, H_5O^{2+}, H^+, and have a higher molar conductivity than free water molecules. Thus the oxonium ions can induce deformations in the hydrogen-bond structure of liquid water.

Once hydrogen has attached itself to an electronegative element, for example oxygen and fluorine, a highly polarised bond results. If this bond is near another atom, *E*, with a lone pair of electrons, a weak bond, results; that is an *O-H-E* hydrogen bond. Water has a strong affinity to form hydrogen bonds in the free liquid state. Hydrogen-bonded free water in macropores ($r > 10^{-7}m$) has a heat of vaporisation equivalent to that of liquid water at the drying temperature. Smaller mesopores ($10^{-7} > r > 2 * 10^{-9}m$) also contain liquid water in its free state, but exhibit a higher heat of desorption at or near the pore surface with a higher surface area. In short, hydrophilic surfaces attract water molecules, thus increasing their heat of wetting. The silica gel surface artificially increases the heat of desorption of water for up to five layers of water molecules on its surface (Staszczuk, 1986). This is a result of the hydroxyl nature of the silica gel surface. However, for non-active porous solids, for example non-active alumina, the amount of strongly bonded water to its surface is less. Thus, the nature of the solid's surface has a strong effect on the energy required to dry to low moisture contents.

Van der Waals' forces exist between molecules because of their momentary attractive or repulsive nature. These forces include dipole/dipole, dipole/induced-dipole and induced-dipole/induced-dipole interactions ("London forces"). In the free liquid and gas states, these forces tend to approximately eliminate each other's effects. Bound liquids, such as water bound to solid surfaces, forbid this interaction.

2.2.3 Entropic-driven effects

2.2.3.1 Hydrophobic hydration

The above bonds derive from enthalpic-driven effects. Hydrophobic interactions are entropically unfavourable interactions of non polar molecules or residues in water. Hydrocarbons are sparingly soluble ("oil and water do not mix"). Such low solubilities are a result of entropic effects, and this behaviour distinguishes aqueous solutions from liquid mixtures where mutual solubility is influenced by enthalpic factors.

2.2.3.2 Micropore volume filling

Micropore volume filling was first considered by Eucken (1914) and Polanyi (1916). It describes the presence of a "force field" enhanced in micropores with closely spaced opposite walls because of the additive nature of the van der Waals' dispersive forces. For such pores, it is quite difficult to define the concept of "surface area", and an experimental method for measuring surface area is absent. Bering *et al.* (1971) distinguished the difference between surface adsorption and micropore filling thermodynamically. With micropores, where the potential of the intermolecular forces can acquire values of up to several kilojoules per mole, the micropore volume filling by most adsorbents takes place at relative humidities lower than 0.2.

2.2.3.3 Water in crystalline hydrates

Crystalline hydrates may be either *true hydrates* or *pseudohydrates.* In true hydrates, water is present as recognisable water molecules ("water of crystallisation"), whereas pseudohydrates contain water as hydroxyl or hydroxonium ions or as OH and H groups ("water of constitution"). The crystalline nature of a hydrate determines whether any of its water content is water of constitution or water of crystallisation and is reflected in its infrared spectrum.

Most water molecules in crystals are essentially asymmetric, but the distortion of the remaining symmetric water molecules have their OH bond lengths no more than 1% different from the asymmetric molecules. In other words, the water molecule is held very rigidly in crystalline lattices. Highly symmetrical arrangements of water molecules may be energetically unfavourable because of repulsions between H atoms or between the lone pairs of electrons. These arrangements would not be compatible with the overall lattice energy requirements for the hydrate crystal, thus promoting asymmetrically based configurations.

Infrared spectroscopy (particularly in the near infrared region) can often confirm the presence of water of constitution in a crystalline compound, and in favourable

circumstances can unambiguously distinguish between a true hydrate and a pseudohydrate. Absence of the water-bending band in the 1600-1700 cm^{-1} region is usually a clear proof of the absence of ordinary water of hydration (Anderson and Wickersheim, 1964). Broad bands near 1700 cm^{-1}(bending) and near 3000 cm^{-1}(stretching) show the presence of H_3O^+, H_5O^{2+} and higher oxonium ions. The presence of OH ions is invariably indicated by sharp OH stretching bands in the region of 3600 cm^{-1}. In the near infrared region, identifying water structures is easier due to little adsorption of organic fragments. The combination of the bending and stretching frequencies of the OH and H_2O ions, have their vibration adsorption bands falling at near infrared wavelengths of 2.3, 1.9 and 1.4 μm. This factor is useful in determining the amounts of "water of crystallisation" and "water of constitution" that are present.

Compared with water or aqueous solutions, the water molecule in a crystalline hydrate is considerably more constrained, both by the rigidity of the crystal structure and by the restriction imposed by crystallographic symmetry. However, this very fact facilitates the study of the interaction of the water molecule with its environment and of the changes the molecule undergoes as a consequence of being incorporated in the hydrate.

The internal geometry of the water molecule in crystals differs very little from that in the vapour. Most water molecules in crystalline hydrates have one of two clear-cut configurations: approximately planer trigonal, with a single electron acceptor, or approximately tetrahedral, with two electron acceptors (Franks, 1972). Large deviations from these limiting configurations appear to be rare. Unusual arrangements that involve three or even four electron acceptors occasionally occur.

2.2.3.4 Water in inert rigid solids

Heats of sorption strengths in a monolayer depend very much on the chemical composition of the solid and the crystal packing structure/s. Rigid (non-swelling) materials often contain elements such as Al, Si and transition metals, with an oxygen component. The electronegativity of these elements can most often induce partial hydrogen bond formation depending on the chemical composition and the steric hindrances on the water molecule's access to the more electronegative elements such as oxygen (Franks, 1972). The more exposed the electronegative atoms, the greater is hydrogen bond formation in the monolayer. This increased exposure produces possible strong bonding in the above multilayers.

2.2.3.5 Water in polymer-based solids

The water molecule is relatively small and in the liquid and solid states is strongly associated through hydrogen bond formation. This feature distinguishes it from the majority

of organic sorbed materials. Strong localised interactions may develop between the water molecule and strong polar groups of the polymer; on the other hand, in relatively non-polar materials or on hydrophobic sections along polymer chains, clustering or association of sorbed water is possible.

Polar groups present in the polymer matrix produce a higher sorptive affinity towards water. However, the accessibility of these groups, the degree of crystallinity of the matrix and the relative strength of water-water and water-polymer bonds are important in determining the overall moisture uptake. This variability tends to rule out a simple correlation between the number of polar groups and the solubility of the solid matrix.

A thermodynamic analysis of the temperature variation of the sorption isotherm is helpful in investigating the physical state of the sorbed water. The entropy of sorption is generally negative and follows the increase in enthalpy with moisture content. Any interpretation of ΔH and ΔS in terms of the physical state of the sorbed water is complicated by the perturbation of the polymer matrix that often accompanies the sorption process (Bettleheim and Volman, 1957).

Electronegative positions (double bonds, aromatic ring structures) along polymer chains and side groups encourage hydrogen bond formation (if accessible) by water molecules in an equivalent monolayer. Completion of this monolayer is by simultaneous hydrophobic hydration of the surrounding polymer chains and partial water clustering in multilayers above existing monolayer regions. The co-current processes of hydrophobic hydration and water clustering are apparent by their similar strengths of desorption (gradual increase while drying into the monolayer). For polystyrene and polyvinylchloride, the heat of desorption is significantly less than the heat of condensation, which is 42.6 $kJmol^{-1}$ (Day, 1963), indicating that initially the water has been partial sorbed before being more strongly attached with the formation of water-water contacts. With more polar plastics, the initial water-polymer interactions are stronger and prior water-water interactions have a less noticeable effect on the overall sorption.

Additionally, there is a noticeable effect of sorbed water on the mechanical properties of polymers. The presence of water may greatly accelerate stress relaxation and creep in these polymers where interchain hydrogen bond solvation can occur. Once water starts to be sorbed in multimolecular layers, the material becomes elastoplastic with greater values of ultimate strain.

Hydrophobic hydration extends to complex molecules, the only two requirements being substantial polar residues of water and a non-aqueous environment. Thus the reversible aggregation of molecules or ions with long non-polar chains or aromatic groups depends mainly on the phenomenon of hydrophobic association. In these ways, complex aggregates such as micelles, bimolecular layers and lamellar structures can exist, depending on the nature of the aggregating species. This formation of aggregates can then

provide a base for enthalpic-driven processes such as "water clustering" or hydrogen bonding to polar sections of the polymer chains. Aggregate formation increases the maximum hygroscopic moisture contents of polymer-based materials (Franks, 1972). Extensive clustering of water molecules is restricted by the limited flexibility of the polymer chain networks. However, entropic interactions between polar residues attached to a common polymeric backbone can promote conformation changes of a material that is not rigid enough to restrict deformations on itself; most protein-based products induce a population explosion of water clusters, and the material swells.

2.3 DRYING KINETICS

2.3.1 Drying history of a material

Drying may be divided into three periods:

1. an induction period,
2. the so-called constant rate period, and
3. the falling rate period or periods.

An induction period exists while the heat and mass transfer processes between the material and the surrounding atmosphere approach an initial steady state (Figure 2.4). The length of the induction period depends on whether the material is fed to the drier hot or cold, but is usually insignificant compared with the time spent by the material during the subsequent drying periods.

A constant drying rate is observed when the exposed surface is maintained effectively wet and is at or near the wet-bulb temperature. Here the gas-phase mass transfer resistance in the boundary layer of surrounding air dominates the process and the extent of the constant rate period depends on the material's ability to keep its surface wet enough for drying to be boundary layer controlled. It is therefore not surprising that a constant period of drying is not always observed. van Brakel (1980) discussed the various reasons why a constant-rate period may be seen in convective drying.

The third stage of drying in a body is the falling-rate period or periods. Essentially, this is the period when the removal of moisture from the solid is retarded by the material itself. The transition between the constant and falling rate drying periods is termed the critical point, and the average moisture content at this transition point is called the critical moisture content. Keey (1972) has proposed that two distinctive falling-rate periods can appear in the drying of a porous medium. Initially, the moisture will recede to a position in the material where evaporation takes place with moisture supplied by capillary-driven flows. Inevitably, the drying time of this first falling-rate period depends on the size and distribution of the pores in the particle i.e. many macropores

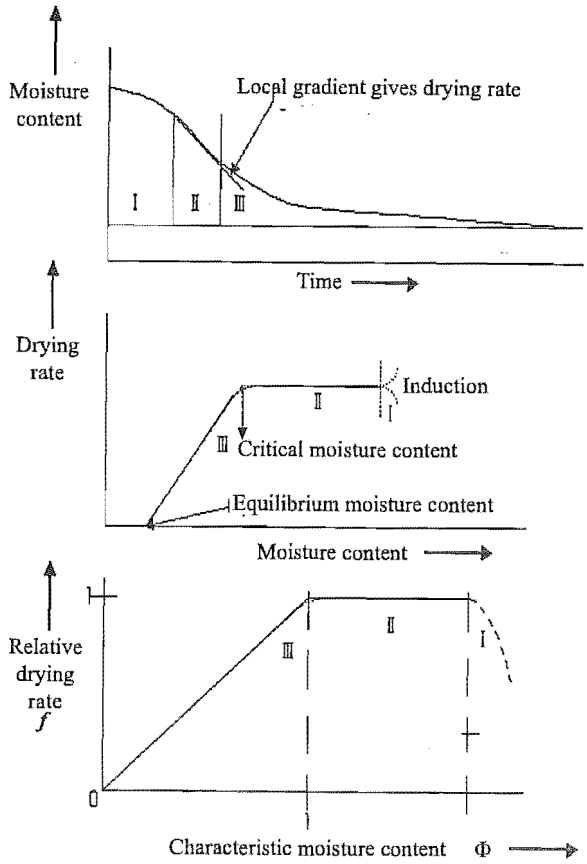

Figure 2.4 Transformation of drying curves

will extend this period of drying. When enough moisture has vaporised from the pores to allow the formation of "clusters" of vapour-filled pores so large that they span the microparticle, then a second falling-rate period is observed. This condition is also known as the "percolation transition".

This second falling-rate period of drying can be described by a progressive number of desorptive stages in the material. Firstly, in the mesopores or mesoporous solids, evaporation from capillaries induces a decrease in the drying rate; this transition into the second falling-rate period can sometimes be observed from drying rate curves if the mesopore size distribution is narrow. Chen and Schmidt (1988) indicated that the immediate onset of the second stage of drying corresponds to the propagation of a receding evaporative front in polymer particles. The initial moisture content in their tests was low ($< 10\%$), and no constant rate period was observed. The rapid initial rise in surface temperature (Figure 2.5), followed some time later by a rise in internal

temperature, indicates the transition between the first and second falling-rate periods. Secondly in micropores (pores of width $x < 1.5\text{-}2.0\ nm$), capillary condensation does not exist. Depending on the size of sorbate molecules, partially physisorbed molecules held in a potential field results in "volume filling" of the micropores. Removal of molecules from micropores is the most difficult type of moisture removal. Not only do physisorbed forces in the micropores have to be overcome, but also steric hindrances such as "pore-necking" make it sometimes difficult for molecules to pass through to escape to the exposed surface. These effects retard drying.

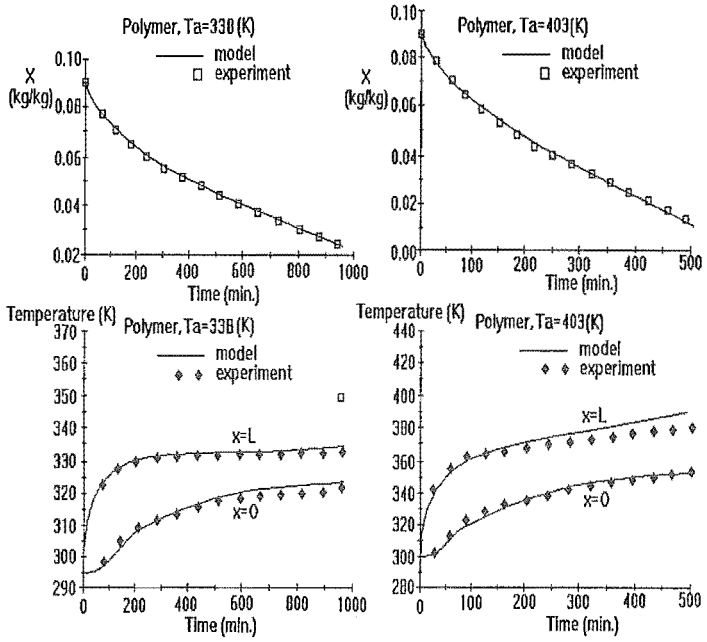

Figure 2.5 Results of drying polymer pellets at $65degC$ and $130degC$ (from Chen and Schmidt, 1988)

2.4 THE MECHANISMS OF MOISTURE FLOW THROUGH A CYLINDRICAL PORE

The mechanism of moisture transport through a single pore was been studied by Radjy (1974) . He analysed the steady flow of moisture in terms of three basic phenomena as follows:

- gas phase flow;
- surface flow;
- liquid flow.

A schematic presentation of these three flow mechanisms has been reproduced by Quenard and Bentz (1992), and is shown in Figure 2.6. A principal mechanism of moisture movement is by way of diffusion.

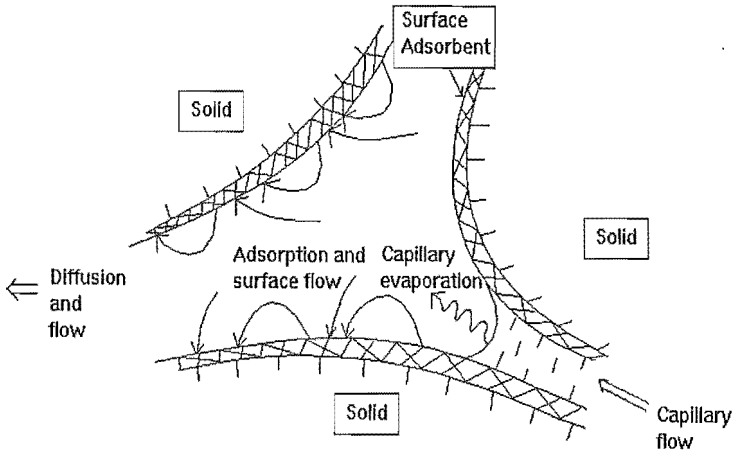

Figure 2.6 Physical model for moisture transfer in a porous medium (from Radjy, 1974)

Two types of diffusion through a porous particle exist.

1. Diffusion through macropores and mesopores consisting of a combination of:
   - molecular or bulk diffusion,
   - Knudsen diffusion,
   - surface/sorptive diffusion, with site hopping at low surface coverages, and
   - hydrodynamic or Poiseuille flow at higher surface coverages.
2. Diffusion through micropores.

Diffusion mechanisms are driven by a gradient of partial pressure or more fundamentally by a gradient of the chemical potential, which measures the combined effect of concentration and molecular velocity. In an ideal case, the driving force gradient reduces to one of concentration.

Diffusion may first be described for linear flow in one dimension by Fick's first law, Equation 2.36:

$$J = -D_o \frac{\partial \mu}{\partial c} \cdot \frac{\partial c}{\partial x} = -D(c) \frac{\partial c}{\partial x} \tag{2.36}$$

where J is the flux, D_o is a diffusion coefficient or diffusivity, μ is the chemical potential and x is the distance from the mid-plane. The partial derivative represents the gradient. In general, the diffusion coefficients $D(c)$ vary with concentration. Many authors have described the drying of a clay material. For example, Evans and Keey (1975) and Langrish (1988) described how diffusion coefficients may be defined to take into account shrinking of the linear dimension x by using distances based on constant mass.

Fick's first law is invariably used as the fundamental equation that can be applied whenever diffusion of gases through solids takes place. However, Babbitt (1950), examined the fundamental basis of the differential equations of diffusion and concluded that, where there is an interaction between the diffusing gas and the solid, as in adsorption, the use of Fick's law as the fundamental equation of diffusion is not valid. Fick's preliminary work on the limitations of his laws seems not to be considered. In his most significant series of experiments, Fick (1855) placed a concentrated salt solution beneath a layer of pure water. At specific intervals he withdrew small samples in order to determine the salt concentration at specific depths. He attempted to use these measurements to develop, from fundamental assumptions, laws governing diffusion. He concluded that diffusion is analogous to the conduction of heat in a solid, a process already described by Fourier (1755) in the heat equation

$$q = -k \frac{dT}{dx} \tag{2.37}$$

where T is temperature, t is time, x is a distance co-ordinate and k is the thermal conductivity.

Krishna in various publications (1990a, 1990b, 1993) , indicated the invalidity of Fick's laws for the diffusive behaviour of multicomponent mixtures and his work indicates the use equations formulated from the Maxwell-Stefan theory, developed by Maxwell (1867) and Stefan (1871), to help correct this type of multicomponent micropore diffusion.

2.4.1 Diffusion in the gas phase

Radjy (1974) showed the basic manner in which the three previous basic mechanisms interact with each other and pointed out the importance of both the surface effects in diffusion and the pore size. When the vapour pressure is close to the saturation

vapour pressure and the capillary radius is large, "molecular diffusion" predominates in the gas phase. This is controlled by collisions of molecules similar to that in the bulk gas. In pores of smaller dimensions or at low pressures, however, collisions between molecules and the pore wall become important. In collision with a wall, a molecule may be adsorbed for varying amounts of time. If the temperature of the surface is high enough, say high enough to break physisorbed bonds, then the time spent on the surface will be significantly shorter than would be the case for a cooler surface. A desorbed molecule will then "fly off" in a random direction dissimilar to molecular and surface-diffusive mechanisms. This process is called "Knudsen diffusion", after Knudsen who first investigated this type of behaviour for sorption in capillaries (Suzuki, 1988). The Knudsen diffusion coefficient is given by:

$$D_k = \frac{2}{3} R_p V_m \left(\frac{2-f}{f}\right) \tag{2.38}$$

where R_p is the pore radius, f is the fraction of molecules that undergo diffuse reflections at the walls, and is usually taken to be one, and V_m is the mean molecular velocity given by the kinetic theory of gases as:

$$V_m = \left(\frac{8RT}{\pi M}\right)^{1/2} \tag{2.39}$$

Thus the Knudsen diffusivity is independent of pressure, is proportional to $T^{1/2}$ and is inversely proportional to the square root of the molecular weight of the diffusing species.

2.4.2 Boundary layer for mass transfer at low concentration gradients

Eckert (1950) indicated that, if a small concentration gradient exists between a flowing fluid and a solid surface, the velocity and thermal boundary layers are unaffected by the small rate of mass transfer. A flux balance over the boundary layer gives

$$\frac{\partial}{\partial x}\int_0^l (P_{A1} - P_{A2}) u_y . dy = D\left(\frac{\partial P_A}{\partial y}\right)_{y=0} \tag{2.40}$$

where P_{A1} is the partial pressure of A at a distance y from the surface, P_{A2} is the value outside the mass transfer boundary layer and l is a distance in the normal (y) direction, greater than the thickness of any of the three boundary layers. Coulson and Richardson (1955) stated that it is not possible to obtain a simple relation connecting P_A and y, and a rigorous analytical solution cannot be found.

2.4.3 Capillarity

Capillarity is the movement of moisture through the inter/intraparticle structure due to the attractive forces between the liquid and the solid. The suction Ψ or pressure difference between the liquid and the gas at the curved interface is thought to be the driving force for capillary flow receding through a porous structure. The flux of capillary liquid flow is given by Buckingham (1907) in the form

$$J_L = -K_H \nabla \Psi \tag{2.41}$$

or

$$J_L = -K_H \frac{\partial \Psi}{\partial X} \nabla X \tag{2.42}$$

where $\partial \Psi / \partial X$ may be obtained from the gradient of the moisture isotherm. The coefficient K_H is the hydraulic conductivity, or $K_H = \rho_L K \text{where} \rho_L$ is the density of the liquid and K is the permeability.

2.5 DRYING OF MATERIALS WET WITH WATER/SOLVENT MIXTURES

2.5.1 Krishna's approach (1990a)

The application of Ficks laws to diffusion assumes that a concentration gradient must exist. However, it is known that diffusion can exist against a concentration gradient. Krishna, like some other authors mentioned previously, indicated flaws in Fick's laws of diffusion indicate that Fick's laws are not applicable for diffusion of a multicomponent mixture in a porous medium (Krishna, 1992). He modified the Maxwell-Stefan equations to cope with the diffusion of individual sorbed species in a multicomponent system. His success with this approach indicates the use of the Maxwell-Stefan equations to model the diffusion of individual components in a multicomponent system.

The bulk this work involves single component diffusion where the diffusive resistances are weighted strongly towards surface/sorptive diffusion, with minor diffusive resistances due to Knudsen and bulk diffusion, with these latter diffusive resistances dependent more on particle size and porosity of the layers and/or beds of particles. For example, experiments in this work indicate that very small particles ($< 200 \mu m$), at low initial moisture contents that are dried as isolated particle aggregates, can be modelled entirely by a surface diffusion model. However, in most industrial drying applications of these types of small particulate materials, drying of individual particles is influenced

by the close proximity of drying neighbouring particles; thus drying is controlled by other gas-flow diffusive resistances. This is why the drying of this type of material in a drier such as a cascade rotary drier is best modelled using a thin-layer approach rather than scale-up of single particle kinetics. Single-component diffusive fluxes can be calculated using the Maxwell-Stefan equations; however, for this type of diffusion, the Maxwell-Stefan equations reduce to a form similar to the surface diffusion equations of single-component diffusion. So the use of these equations is really limited to a multicomponent system. Investigating the use of the Maxwell-Stefan equations for the surface diffusion of a binary sorbed species in this work, was limited to using different molar concentrations of an organic solvent (isopropyl alcohol) with water. However, a more detailed look at applying the Maxwell-Stefan equations to low moisture selectrivity of drying is supplementary to the main body of this thesis.

The surface flux for a single diffusing species (N_1) is defined as

$$N_1 = \rho \epsilon q_{sat} \theta_1 v_1 \tag{2.43}$$

where ρ is the particle density, usually expressed in $kg\ m^{-3}$, ϵ is the porosity of the material, N_1 is the flux in $mol\ m^{-2}\, s^{-1}$, v_1 is the jump frequency of the diffusing component in s^{-1}, θ is the fractional surface coverage of the component, and q_{sat} is the total saturation concentration of the adsorbed species in $mol\ kg^{-1}$. This flux can be represented by a scalar expression, as shown by van den Broeke and Krishna (1995);

$$N_1 = -\rho \epsilon q_{sat} D_1' \Gamma \nabla \theta_1 \tag{2.44}$$

The coefficient D_1' is related to the surface diffusivity D_1 is by

$$D_1 \equiv D_1' \Gamma \tag{2.45}$$

where Γ is the so-called thermodynamic factor. For Langmuir adsorption isotherms, the thermodynamic factor Γ shows a strong dependence on surface coverage;

$$\Gamma = \frac{1}{1 - \theta_1} \tag{2.46}$$

Under these conditions, a single expression follows for single-component surface diffusion:

$$D_1 = \frac{D_1'}{(1-\theta_1)} \tag{2.47}$$

Binary diffusion involves two dimensional forms of Equations 2.45 and 2.46. These equations are presented and discussed in van den Broeke and Krishna (1995). Krishna took this approach to apply the Maxwell-Stefan equations to surface drying of binary solutions. Continuing from Equation 2.47:

For single file diffusion involving two components, they show a two dimensional form of Equation 2.49:

$$(N) = -\rho\epsilon_{sat}\begin{bmatrix} D_1^* & 0 \\ 0 & D_2^* \end{bmatrix}[\Gamma](\nabla\theta) \tag{2.48}$$

Using a Langmuir approximation for this binary mixture to calculate [Γ]:

$$(N) = -\rho\epsilon q_{sat}[D](\nabla\theta) \tag{2.49}$$

$$[D] = \frac{\begin{bmatrix} D_1^* & 0 \\ 0 & D_2^* \end{bmatrix}\begin{bmatrix} 1-\theta_2 & \theta_1 \\ \theta_2 & 1-\theta_1 \end{bmatrix}}{1-\theta_1-\theta_2} \tag{2.50}$$

where (N) is a 2*2 matrix of two Fick surface diffusivities $[D]$.

2.5.2 Schlünder's approach (Thurner and Schlünder, 1986)

2.5.2.1 Evaporation of a binary solution from a free liquid surface

Schlünder's (1984) initial work on selective evaporation involved work with the evaporation of binary solutions of isopropyl alcohol and water mixtures. Thurner and Schlünder (1986) described the arrangement used in the early tests; Figure 2.7

The composition of the freshly formed vapour is given by

$$z_1 = \frac{N_{v1}}{N_{v1}+N_{v2}} \tag{2.51}$$

where N_{v1} and N_{v2} are the respective molar vapour fluxes of the two components. If the mole fraction of the more volatile component in the liquid phase is x_1, then the

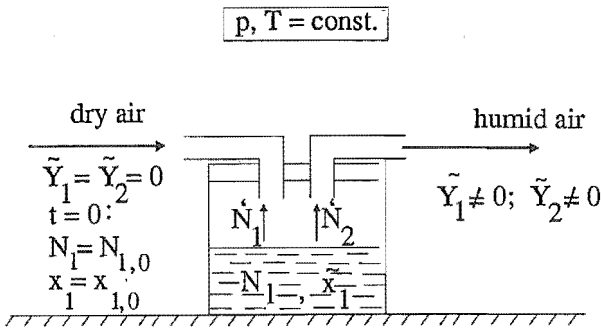

Figure 2.7 Evaporation of a binary mixture from a free liquid surface (Thurner and Schlünder, 1986)

evaporative selectivity is given by

$$s_1 = z_1 - x_1 \tag{2.52}$$

If $s_1 > 0$, then component 1 is removed preferentially; if $s_1 < 0$, then component 2 is removed preferentially. For $s_1 = 0$, neither of the components is removed preferentially; hence the composition of the liquid remains constant during the drying process. At low evaporation rates, selective evaporation is more likely to occur because vapour transport is controlling and there is equilibrium at the surface. In this case, Schlünder (1984) showed that

$$z_1 = \frac{x_1}{K_G/\alpha_{12} + (1 - K_G/\alpha_{12})x_1} \tag{2.53}$$

where α_{12} is the relative volatility of the two components and K_G is a relative vapour transfer coefficient. This parameter is related to the relative magnitude of the mass transfer coefficient for each species, and thus the relative magnitude of the diffusion coefficients:

$$K_G = \frac{\beta_2}{\beta_1} = \left(\frac{D_{13}}{D_{23}}\right)^m \tag{2.54}$$

In this expression the exponent m may be taken as $2/3$ from the Chilton-Colburn analogy (Thurner and Schlünder, 1986):

$$j_M \phi_M = \frac{\beta}{G_T} Sc^{2/3} \phi_M = j_H = \frac{\alpha}{C_P} Pr^{2/3} \tag{2.55}$$

where G_T is the total gas flow per unit cross section, Sc is the Schmidt number and Pr is the Prandtl number, and j_M and j_H are the so-called j-factors.

It follows from Equations 2.52 and 2.53 that the selectivity is given by

$$s_1 = \frac{x_1(1-x_1)(-K_G/\alpha_{12})}{K_G/\alpha_{12} + (1-K_G/\alpha_{12})x_1} \tag{2.56}$$

Thus the selectivity is dependent on the value of K_G/α_{12}. This means that

$$\begin{aligned} s_1 &> 0 \quad if \quad \frac{K_G}{\alpha_{12}} < 1 \\ s_1 &= 0 \quad if \quad \frac{K_G}{\alpha_{12}} = 1 \\ s_1 &< 0 \quad if \quad \frac{K_G}{\alpha_{12}} > 1 \end{aligned} \tag{2.57}$$

Thurner and Schlünder (1986) gave examples of evaporating a binary solution of isopropyl alcohol and water for cases of varying initial molar compositions. Cases for selective and non-selective evaporation arise depending on the initial concentrations.

2.5.2.2 Drying of porous materials containing binary mixtures

At a free liquid surface, the liquid-side mass transfer is due to either natural or forced convection. However, if the liquid is trapped in a porous matrix, the liquid-side mass transfer results from diffusion or natural convection (Luikov, 1966). Thurner and Schlünder (1986) modelled desorption from a porous matrix based on a model with straight capillaries perpendicular to the material's surface. They observed non-selective drying as a result of the liquid-side mass transfer being the dominant step, rather than the vapour-phase mass transfer. For the case of smaller microporous structures, for which the Kelvin equation does not apply, selectivity may be more likely to occur.

2.6 THEORIES OF DRYING

2.6.1 Earlier work

Keey (1992) provided an overview of the development of drying theory. The earliest description of drying put forward by Lewis (1921) implied that moisture from within

a particle diffuses to the particle's surface where evaporation takes place. This led to the conclusion that the drying was first-order, with a linear falling-rate period. For swelling materials, Lewis put forward a simple drying rate expression to describe the drying behaviour, Equation 2.60. The first-order rate expression for non-swelling materials

$$-\frac{dX'}{dt} = \frac{k'X'}{L} \tag{2.58}$$

was modified by including a functional relationship of the sample's length L with moisture content

$$L = L_o[1 + \lambda(X' - X'_s)] \tag{2.59}$$

Substitution of Equations 2.58 and 2.59 resulted in the expression

$$-\frac{dX'}{dt} = \frac{k'X'}{L_o[1 + \lambda(X' - X'_s)]} \tag{2.60}$$

which fits the experimental drying curve. When gravitational effects are neglected for samples with lower moisture contents, or the drying of single particles or thin-layers is considered, the effective vapour diffusion coefficient D_{eff} through the dried out region of the sample has been given by Audu and Jeffreys (1975):

$$D_{eff} = D_v \epsilon^{1.5} \tag{2.61}$$

where ϵ is the interparticle porosity of the sample, and D_v is the vapour diffusion coefficent.

Fick's equation for diffusion may be written as

$$\frac{\partial X}{\partial t} = \nabla(D_m \nabla X) \tag{2.62}$$

where c is the moisture concentration, and D_m is the moisture diffusion coefficient. As $c = \rho_s X$, Equation 2.62 can be written for an unshrinking solid as

$$\frac{\partial c}{\partial t} = \nabla(D_m \nabla c) \tag{2.63}$$

Crank (1970) gave numerous solutions to Equation 2.63 for constant or variable diffusion coefficients for first-order boundary conditions.

The concept of having liquid diffusion as the only mechanism for moisture movement has been criticised. Keey (1992) cited Hougen *et al.* (1940) who commented on the inability of such Fickian-type diffusion equations to predict accurately the moisture content profiles in the drying of many granular masses of materials. A more complete description of the drying process should take into account both the liquid capillarity in the wet zone and the vapour diffusion in the dried-out region. Chen and Whitaker (1986) obtained the constitutive relationships, Equation 2.64, on volume averaging the conditions in a three-phase, isothermal system of inert solids, moisture liquid and moisture vapour:

$$\frac{\partial s}{\partial t} = \nabla(K_s \nabla s - K_g \bar{g}) \tag{2.64}$$

where s is the fractional saturation of the pores, K_s is the moisture permeability, K_g is a coefficient and $\bar{g}$ is the gravitational vector. Equation 2.64 also indicates that for a porous bed of particles, a constant rate period occurs only when capillary and gravitational forces balance. When capillary forces dominate Equation 2.64 reduces to a Fickian-type equation which would represent the moisture movement under capillary flow conditions.

Other work by Krischer (1938) suggested that moisture movement to the particles surface was not entirely due to diffusion components, as initially described by Lewis (1921), and needs to involve a capillary component. He made two distinctive points. He ascribed vapour-phase movement to diffusion, and liquid motion to capillarity. To develop this idea further, Krischer (1942) presented a numerical expression to describe the simultaneous movement of moisture in both gaseous and liquid flow in a single direction thorough a body of uniform porosity:

$$\frac{\partial}{\partial z} = \left(K_s \frac{\partial s}{\partial z}\right) - \frac{\partial s}{\partial t} + \frac{D_v}{\mu_D}\frac{\partial^2 c_V}{\partial z^2} - \epsilon_G \frac{\partial c_V}{\partial t} = 0 \tag{2.65}$$

in which c_V is the moisture vapour concentration in the pores with voidage or fractional free space ϵ_G. The coefficient D_v is the moisture vapour diffusivity, and μ_D is the diffusion resistance coefficient, which takes into account the diminished cross-section for diffusion in a porous body and the tortuous flow paths that pass through the particle. Keey (1992) described how to calculate the various coefficients represented in Equation 2.65.

Whitaker (1977 , 1980 , 1984), and later working with Chen (Chen and Whitaker, 1986) (as described earlier), from a general theory of drying granular porous media, con-

structed a simplified theory that consists of a set of coupled, volume-averaged transport equations for the gas-phase convective transport and liquid movement under the action of a capillary pressure gradient (by making use of Darcy's law for moisture transport owing to capillary action), on the assumption of local thermal equilibrium. Using these volume-averaging equations, the relative permeability and capillary pressure have to be treated as adjustable functions to get good agreement with experimental data, with the permeability falling by many orders of magnitude at low pore saturation. Stanish *et al.* (1986) extended Whitaker's ideas to incorporate bound moisture diffusion through the solid matrix with coupled liquid and vapour diffusion through the drying matrix.

Luikov (1935, 1966) approached the fundamentals of the drying problem on the basis of using irreversible thermodynamics, from the initial ideas proposed (Equation 2.66) by Onsager (1931), Luikov noted that the fluxes J_i are linear combinations of the driving forces X_i:

$$J_i = \sum_k L_{ik} X_i; k = 1, 2, ..., n \tag{2.66}$$

which can decouple the vapour phase and the liquid phase transport equations. These now separate entities are functions of both the concentration gradient and the temperature gradient. These ideas led to the development of the following two equations.

The vapour flux:

$$J_V = -D_V \rho_s \nabla X - D_{VT} \rho_s \nabla T \tag{2.67}$$

The liquid flux:

$$J_L = -D_L \rho_s \nabla X - D_{LT} \rho_s \nabla T \tag{2.68}$$

where D_V, D_{VT}, D_L and D_{LT} are coefficients. If one assumes that the vapour and liquid motion of moisture through the particle during drying is Fickian, then Equations 2.67 and 2.68 can be transformed into

$$\frac{\partial X}{\partial t} = K_{11} \nabla^2 X + K_{12} \nabla^2 T \tag{2.69}$$

$$\frac{\partial T}{\partial t} = K_{21} \nabla^2 X + K_{22} \nabla^2 T \tag{2.70}$$

where

$$K_{11} = \delta \quad and \quad K_{22} = \kappa + \frac{\delta \Delta H_v}{C_B} K_m \zeta \tag{2.71}$$

$$K_{12} = K_{21} K_m = \frac{\delta \Delta H_v}{C_B} K_m \tag{2.72}$$

where K_m is a total moisture diffusivity, δ is the thermal gradient coefficient and ζ is the tortuosity factor for the capillary porous system. Various laboratory experiments on the porous material determine these coefficients, which are a complex superposition of both the moisture concentration and the temperature.

2.6.2 Mechanistic models

Models based on simple "pictures" of the moisture movement mechanisms include:

- wetted-surface models;
- receding evaporative interface models;
- Fickian models;
- surface diffusion models.

The wetted-surface model may apply well for the drying of porous materials in the initial stages of drying when the surface is well supplied with water, and for the entire drying period if the pore size is large or the sample is thin enough. Under these conditions, the characteristic drying curve concept (see van Meel's method which is described later) may hold well for all changes in air conditions (Langrish, 1984).

However, in the later stages of drying, a receding evaporative interface model or vapour diffusion model is appropriate. If a receding evaporative interface model is more suitable, the characteristic drying curve will hold well for changes in air temperature and velocity variations. The characteristic drying curve concept will not hold at all if a vapour diffusion model is appropriate in this region. For drying at very much lower moisture contents, i.e. into an equivalent monolayer region, a surface diffusion model may apply especially for the drying of materials with an active surface. Here the drying process and moisture transport are very much dependent on the air temperature especially for small samples or isolated particles. The characteristic drying curve is independent of air humidity and air velocity variations, but dependent on air temperature.

Often to simulate drying in the falling-rate period, a combination of the above models would be suitable for decreasing moisture contents during drying. For example, a combination of models may be suitable for solids with a varying pore size network which may be modelled using both a receding evaporative interface model and a Fickian model. For removing moisture close to the pore surface (especially if it is an active surface), a surface diffusion model may need to be incorporated.

2.6.2.1 Wetted-surface model (Peck and Kauh, 1969)

This model assumes that evaporation occurs only at the surface of the solid with liquid transport being redistributed throughout the solid by capillary action or other means. Concentration gradients are not present through the material. If there is a small resistance to moisture movement through the material, then this model should apply i.e. for macroporous and mesoporous structures that are relatively thin.

2.6.2.2 Receding evaporative interface model (Keey, 1978)

This model suggests that evaporation takes place at the surface of a shrinking wet core surrounded by a dry shell. Moisture movement is by vapour diffusion through the dry shell, and the liquid redistribution rate in the wet core is rapid compared with the evaporation rate.

2.6.2.3 Diffusion model (Sherwood, 1929a, 1929b, 1936)

This model assumes that evaporation takes place at the surface, with liquid diffusion-like movement through the solid. The rate of moisture movement is proportional to the moisture concentration gradient at each point. Boundary layer mass transfer resistance is negligible.

This model may be applicable to soaps, starches, food materials and polymer-based materials with hydrophobic surfaces. Diffusivities may decrease during drying as the materials shrink and relax.

The drying rate towards the end of drying should be almost independent of the gas velocity, as with the receding evaporative interface model.

2.6.2.4 Surface diffusion model (Suzuki, 1988)

This assumes that evaporation occurs close or near to the active pore surface, and to a lesser extent on a less active pore surface. Moisture transport occurs along the pore surface by sorbed molecules "hopping" along the pore wall to the particle's surface. At higher moisture contents, sorptive diffusion may occur by a shearing effect over

sorbed moisture layers at multilayer loadings. Boundary layer mass transfer resistance is negligible.

Generally a surface diffusion model is more applicable to drying at lower moisture contents at or near the pore surface. This model should be a physically realistic solution for the drying of rigid materials for mesoporous and microporous materials in the low-moisture content regions of monolayer loadings.

2.6.3 Surface diffusion

2.6.3.1 General

When there is a concentration gradient through a pore, there will also be a concentration gradient along the pore wall, resulting in parallel diffusion through the gas phase and lateral diffusion along the pore surface. Migration of the adsorbed species is determined by the relative magnitudes of the heat of sorption and the activation energy for migration. This process is called "surface diffusion". Developments in understanding surface diffusion have recently been reviewed by Kapoor and Young (1989).

Surface diffusion is more likely than total removal of moisture from the surface because of the lesser energy involved in the former process. The temperature dependence of the surface diffusivity can be expressed in terms of the Arrhenius law:

$$D_s = D_o e^{-\frac{E}{RT}} \tag{2.73}$$

where D_o is representative of the effective diffusion of moisture through the pores. It has been proposed by Sladek *et al.* (1974) that the effective diffusivity is related to the diffusivity D_G by

$$D_o = \frac{D_G \varepsilon}{\tau_s} \tag{2.74}$$

where the surface tortuosity factor τ_s is approximately equal to the ratio of the effective path length of a pore to the shortest distance from beginning to end of the pore. The surface diffusivity D_s is calculated according to Equation 2.73 by estimating the activation energy E to be 45% of the enthalpy of desorption.

Surface diffusion occurs by jumps between adjacent adsorption sites, sometimes called "mobile adsorption". The existence of mobile adsorption can be shown by fitting moisture isotherms to a modified Langmuir equation. Those molecules remaining in close proximity to the surface may have an activation barrier that is lower for surface diffusion than the desorption energy barrier, so "surface hopping" of adsorbed molecules

is possible. Although surface diffusivity (D_s) is a complex function of surface coverage θ, the observed dependence is:

$$\frac{D_s}{D_{so}} = \frac{1}{1-\theta} \tag{2.75}$$

where D_{so} is the counter-sorption or the Maxwell-Stefan surface diffusivities of the species through a monolayer (compare Equation 2.46).

As shown in Figure 2.8, when the energy barrier, E_a, existing between neighbouring sites is smaller than the heat of desorption, Q, then it is easier for a molecule to hop to the next site than to desorb into the bulk phase.

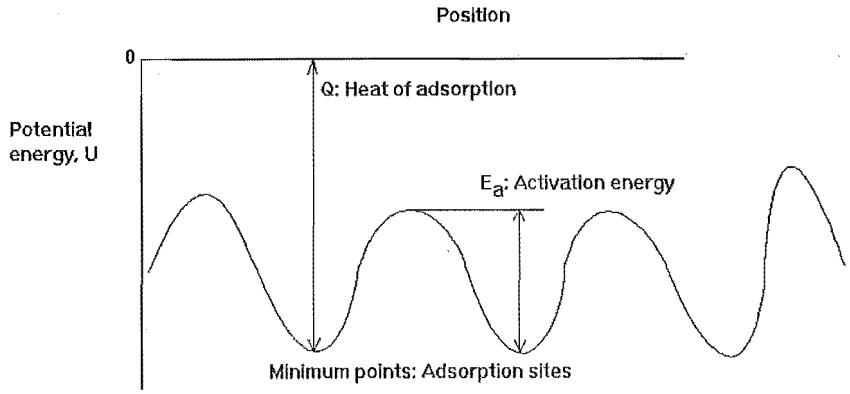

Figure 2.8 Cross-sectional view of potential energy distribution of adsorption on a solid surface

2.6.3.2 Random walk concept

Surface diffusion can be related to the random walking of adsorbed species in the direction of diffusion. Suppose a unit step is defined by a length, Δx, and time , Δt, as shown in Figure 2.9.

After n steps after an elapsed period $n\,\Delta t$, the variation in the position of x becomes $x = \pm\Delta x \pm \Delta x \pm ... \pm \Delta x$ (n *steps*) and the variance is given by

$$\bar{x^2} = n\bar{\Delta x^2} \tag{2.76}$$

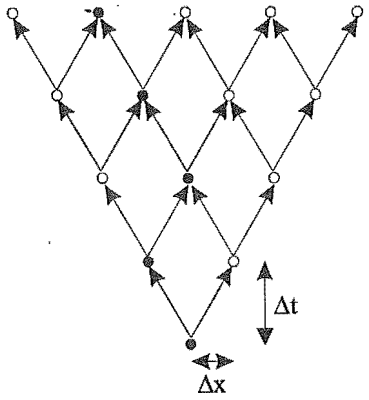

Figure 2.9 Concept of random walk model

For large n, the diffusion coefficient D is related to $\bar{x^2}$ by Einstein's equation (Suzuki, 1988)

$$\bar{x^2} = 2Dn\Delta t \tag{2.77}$$

Then D is given as

$$D = (1/2)(\bar{\Delta x^2}/\Delta t) \tag{2.78}$$

If $\bar{\Delta x}$ and Δt are determined by incorporating information about the pore topology and tortuosity factors, then surface diffusivity values can be determined.

2.6.3.3 Site-hopping model

When the energy barrier between neighbouring adsorption sites is not negligible, the hopping of an adsorbed molecule from one site to the nearest vacant site is considered to be a unit step of the random walk concept. If the hopping distance is taken from the lattice constants of the crystal, then the hopping frequency, $(1/\Delta t)$, is taken as the reciprocal of the residence time of the molecule at the site. Suzuki (1988) showed the hopping frequency to be

$$1/\Delta t = 2\upsilon_x exp(-E_s/RT) \tag{2.79}$$

where υ_x is the vibration of the adsorbed molecules and considered to be of the order of $10^{11} - 10^{13}\ s^{-1}$. E_s is the activation energy of hopping. Then D_s is given as

$$D_s = D_s^{'} exp(-E_s/RT) \tag{2.80}$$

where

$$D_s^{'} = (\Delta x)^2 \upsilon_x \tag{2.81}$$

2.6.3.4 Effect of surface coverage

At very low surface coverages, a random walk concept may be a best-fit model, because there is a ready supply of active sites available for receiving a molecule. However, when the surface is covered by a number of other molecules bound to these active sites, a molecule has to "hop over" other sorbed molecules to find these favoured positions on the pore surface. The expected number of hoppings is a function of surface coverage:

$$n(\theta) = \sum k(1-\theta)\theta^{k-1} = 1/(1-\theta) \tag{2.82}$$

which then results in the diffusion expression given in Equation 2.75. Several improvements to Equation 2.75 have been attempted by Yang *et al.* (1973) and Okazaki *et al.* (1981) to describe behaviour on silica glass and Vycor glass respectively. Yang *et al.* (1973) considered the effect of the residence time of the hopping molecule after it lands on the occupied site and before it starts the next hopping. They showed that the effective surface diffusion coefficient can be described as

$$D_s = D_{s0}\left[\frac{1}{1-\theta+\theta\frac{\upsilon_1}{\upsilon_2}exp(-(E_{s0}-E_{s1})/RT)}\right] \tag{2.83}$$

where E_{s0} and E_{s1} represent the activation energies of the diffusion molecules in the first layer and in the second layer respectively.

Active silica surfaces are well known to increase the sorptive strengths of water molecules in up to five layers away from the silica surface. The associated strengths of

each equivalent sorbate layer can be calculated from the fitting of multilayer sorption equations such as BET-type and GAB-type expressions.

Okazaki *et al.*(1981) developed this idea further by considering the effects of movement by molecules, not only in the first layer but also in the second and successive layers. For a homogeneous surface, the surface diffusion coefficient can be given by

$$D_s = D_{s0}\left(\frac{\theta_e}{\theta}\right)\left[\frac{exp\left(-\frac{E_{s0}}{RT}\right) - exp\left(-\frac{Q_{st}}{RT}\right)}{\left[1 - exp\left(-\frac{Q_{st}}{RT}\right)\right]\left[1 - \theta_e\left(1 - \frac{\tau_1}{\tau_0}\right)\right]}\right] \tag{2.84}$$

where θ_e is the fractional coverage of the surface effective to the surface diffusion, and τ_0 and τ_1 represent the residence time of the migrating molecule in the first and second layers, given by

$$\frac{\tau_1}{\tau_0} = \frac{\left[exp\left(-\frac{E_{s0}}{RT}\right) - exp\left(-\frac{Q_{st}}{RT}\right)\right]\left[1 - exp\left(-\frac{\lambda_{vap}}{RT}\right)\right]}{\left[exp\left(-\frac{E_{s1}}{RT}\right) - exp\left(-\frac{\lambda_{vap}}{RT}\right)\right]\left[1 - exp\left(-\frac{Q_{st}}{RT}\right)\right]} \tag{2.85}$$

Q_{st} and λ_{vap} are the heat of adsorption and the latent heat of vaporisation respectively, and E_{s0} and E_{s1} are the activation energies of transport at the first and at the second and successive layers. This model was further developed (Suzuki, 1988) to consider the effects of an energy distribution function over a homogenous surface. Further refinements may be considered to include energy distribution functions of the different sorptive layers, instead of assuming the same heats of vaporisation of the second and successive layers.

2.6.3.5 Surface flow induced by a surface pressure gradient - hydrodynamic or Poiseuille flow

Surface flow at higher coverages is induced by a surface pressure gradient. When there is a gradient of surface pressure, a two-dimensional flow is expected to occur. Suzuki (1988) derived the surface diffusion coefficient in this case as

$$D_s = \left(\frac{qRT}{SC_r}\right)\frac{dlnp}{dlnq} \tag{2.86}$$

where S is the surface area of the adsorbent (m^2g^{-1}), q is the amount adsorbed (*mg sorbate/mg sorbent*), C_r is the coefficient of friction between the adsorbed molecules and the adsorbent surface and p is the partial pressure in the gas phase.

An equivalent diffusivity due to Poiseuille flow depends on the pressure, viscosity and pore radius:

$$D_f = \frac{Pr^2}{8\mu} \tag{2.87}$$

Thus an effective overall pore diffusivity is the sum of the surface and equivalent flow diffusivities by the simple expression

$$\frac{1}{D_e} = \frac{a}{D_{liquidflow}} + \frac{b}{D_{gasflow}} + \frac{c}{D_{surface}} \tag{2.88}$$

This relationship can be represented by an electric analogue circuit (Figure 2.10 depicting the fluxes, with individual weights estimated on each of the diffusive forces depending on the pore topology and sorbate/sorbent interactions.

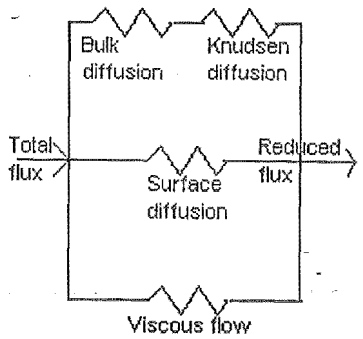

Figure 2.10 Electric analogue circuit depicting the flux of the diffusing species within a porous medium (after Mason and Malinaushas, 1983)

At low moisture contents, liquid-phase movement is negligible.

$$\frac{1}{D_e} = \frac{1}{D_{bulk+Knudsen}} + \frac{1}{D_{surface}} \tag{2.89}$$

2.6.4 Short-cut methods

Short-cut methods use laboratory data to develop drying curves which appear to be specific to that type of material and for the moisture content range of interest. This empirical approach to deciphering the drying behaviour is crude and involves more

experimental data gathering, but has been shown to be a suitable method to use to help size and design drying equipment. These short-cut methods must be treated as useful concepts and not as traditional drying models.

2.6.4.1 Schoeber's or Thijssen's method (Liou and Bruin, 1982, and Thijssen and Coumanns, 1984)

Schoeber's approach (cited by Keey, 1992) is presented by Liou and Bruin (1982) followed by an application of this method to a short-cut drying algorithm by Thijssen and Coumanns (1984). It is based on the observation that the drying process is independent of the starting conditions, once the penetration period has ended and a regular regime of concentration profiles is set up. The method is powerful and relatively rigorous, enabling moisture content profiles as the well as drying behaviour to be obtained for any shape of particle from two slab-drying experiments in the laboratory.

This procedure involves defining the drying parameters G and E, see Figure 2.11. These are defined as:

$$G = \frac{EF}{\upsilon + 1} \tag{2.90}$$

and

$$E = 1 - \bar{m} \tag{2.91}$$

where F is a dimensionless flux parameter given by

$$F = -D_r X_g \left(\frac{\partial m}{\partial \phi}\right)_i \tag{2.92}$$

with X_g being the value of the geometric parameter at the moisture-gas interface (where $\varphi = 1$) and thus

$$X_i = \upsilon + 1 \tag{2.93}$$

Here υ is a parameter that takes the value of 0, 1 or 2 for a slab, cylinder or sphere respectively. The relative diffusion coefficient D_r is assumed to be a simple algebraic function of the moisture content:

$$D_r = m^a \tag{2.94}$$

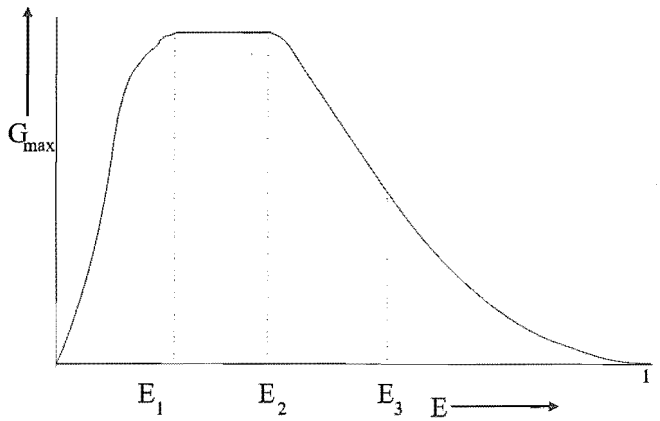

Figure 2.11 Transformed drying curve. E is the extent of moisture loss, from Keey (1992)

for which a is a constant.

The actual drying flux is found from F:

$$N_v = \left(\frac{\rho_L D_o}{R_o}\right) F \tag{2.95}$$

Keey (1992) described the process of constructing these drying rate curves, and provided a more complete picture of the theory.

Okazaki (1989) adapted this method to the drying of porous slab-form material for the modelling of a layer of cross-circulated particles. Keey (1992) commented that it is also confusing to employ a flux function that has a different form of moisture content dependence than the actual drying rate itself. The tests is also based upon the determination of an isothermal drying curve whereas most industrial driers are operated adiabatically.

2.6.4.2 van Meel's method (1958)

An effective but simple model to correlate drying kinetic behaviour has become known as the "concept of the characteristic drying curve". It implies that the shape of the drying rate curve for a given material is unique and independent of gas temperature,

humidity and velocity. van Meel also suggested that the relative ease of drying, as indicated by a normalised drying rate, is a simple function of the extent to which drying has occurred. A characteristic drying curve must be obtained from a laboratory drying test not only under constant external conditions but also with material of exactly the same form and size as that of interest in the industrial drier. A common method used to construct a characteristic drying curve is shown in Figure 2.4.

Keey (1978) examined the theoretical foundation of the concept by considering the drying of a porous, non-hydroscopic slab of infinite extent. He found that, under intensive drying conditions of the slab (when a drying front appears), the characteristic drying curve is a function of the relative intensity of drying, whereas, under less intensive drying conditions, it is not. It decouples the mass transfer from the transport of heat, and it separates internal from external resistances. From a practical point of view, it facilitates scale-down from laboratory-scale thin-layer tests to single particle drying kinetics, and enables single particle kinetics to be translated to the design of industrial-scale drying units (Tsotsas, 1992).

Adamson (1972), Ashworth and Carter (1980), Haertling and Schlünder (1980), and Hallström and Wimmerstedt (1983), Keey *et al.* (1985), Keey and Wu (1989), Nossar *et al.* (1974), Reay *et al.* (1982), Quenard *et al.* (1988), Schicketanz (1971), Schlünder (1976), Tubbs (1976), and Vaneék *et al.* (1966) and utilised this concept to model the drying processes of their materials.

Ashworth and Carter (1980) were some of the first workers to report the drying kinetics of thin layers of silica gel. Kravichik *et al.* (1988) took a different approach by investigating the adsorption kinetics of thin layers of silica gel. Langrish (1988) continued the work of Ashworth by using not only silica gel (non-shrinking) but also two ion-exchange resins (shrinking) to examine the drying kinetics behaviour of porous media as a basis for exploring the concept of the characteristic drying curve. The use of thin-layer through-flow methods to determine drying kinetics has a distinct advantage over other convective batch drying tests (contact or cross-circulation): with through-flow experiments, accurate drying kinetics data can be obtained directly by incorporating the concept of the characteristic drying curve; whereas, for other convective batch drying methods with larger samples, the large concentration profiles in a fixed bed make interpretation of the results more difficult.

The characteristic drying curve has been used extensively over the past two decades (Keey, 1992) in helping to size industrial drying equipment specific to that material, and has been extensively discussed in the previous section. It is a robust technique of obtaining the drying kinetics behaviour of selected materials.. The shape of the curves is independent of humidity, temperature and air velocity conditions. Recorded variations of these external conditions, by a number of authors (as cited by Keey, 1992), have resulted in insignificant effects on the shape of the curve. Significantly, no characteristic

drying curve is observed in the drying of large particles $\geq$ 20 *mm* in diameter (Haertling and Schlünder, 1980 and Schicketanz, 1971) [Schicketanz 1971]. With fibrous materials, scatter in the drying data may also be attributed to uncertainties in the measurement of the thin-layers of loose material (Keey and Wu, 1989). [Keey and Wu 1989] However, there are sufficient data available for particles less than 20 *mm* in diameter over a range of conditions that normally exist within a commercial-scale drier. T Langrish suggested that, for very small particles ($\leq$ 0.5 *mm*), the kinetics may vary to such an extent that different kinetics can be observed during drying. Work in this department by Zhang *et al.* (1992) showed the effect of varying the particle size on the shape of the characteristic drying curve.

Keey (1992) provided a review of known applications of the concept, and provided a simple understanding of the concept and evaluation of *f-curves*. Once a characteristic drying curve has been established, it would seem to be possible to estimate drying rates, and thus the time to dry between specific moisture levels, for any given set of process conditions. It provides a powerful conceptual tool in understanding commercial drying practice by separating the distinctive influences of the material (f), the operation of the drying equipment (k_o) and the humidity conditions, $\phi(Y_W - Y_G)$, where ϕ is the humidity potential coefficient. Keey and Suzuki (1974) examined the theoretical foundation for the concept by considering the drying of a porous, non-hygroscopic slab of infinite extent. They found that under intensive drying conditions when a drying front appears, the characteristic drying curve is a function of the relative drying intensity, whereas, under less intensive conditions, it is not. In the drying of thick, fairly impervious materials, a single linear characteristic drying curve appears.

The concept suggests that the drying kinetics can be represented by a local drying rate function, termed an *f-curve*, of the form:

$$f = f(\Phi) \tag{2.96}$$

where f is the drying rate normalised against the unhindered drying value in the first period of drying immediately before the beginning of the falling-rate period, and Φ is the normalised moisture content which is described by

$$\Phi = \frac{X - X_e}{X_{cr} - X_e} \tag{2.97}$$

where X is the moisture content, X_{cr} is the critical moisture content and X_e is the equilibrium value.

In terms of the concept of the characteristic drying curve, the drying kinetics can be represented by a local drying rate function shown by Equation **??**. For silica gel no

constant rate period is observed at any operating condition for silica gel humidified in a moist environment, so it is assumed that this material has a critical moisture content greater than the initail moisture content of the particles (X_o). If the characteristic drying curve is of simple geometric-form, then

$$f = \phi^A \qquad \phi > B \tag{2.98}$$

where A is some intermediate value of ϕ.

For the parameter-fitting process it is better to use a dual function relationship to model the curve below relative moisture content, $\phi = A$.

$$f = B^{A-C}\,\phi^C \qquad \phi < B \tag{2.99}$$

where A, B and C are constants for parameter fitting shown by Langish *et al.*, (1991). Generally, these three parameters indicate the variations in drying behaviour. For small values of B, there is a more linear appearance to the drying behaviour. The value of B determines where the drying kinetics becomes non-linear in behaviour. Below B the dual function relationship fits a non-linear relationship to the drying material. This approach of parameter fitting the characteristic drying curve has become successfully applied to swelling (Purolit) and non-swelling (silica gel) solids (Zhang *et al.*, 1992).

Ashworth (1972) and Keey (1978) used the concept to describe a number of drying operations. For example, the model yields a simple lumped-parameter model for the drying behaviour of a bed of material. A moisture balance and the rate expression give

$$\frac{\partial \Phi}{\partial \sigma} = \frac{\partial \Pi}{\partial \zeta} \tag{2.100}$$

The normalised moisture content (Φ) and the humidity potential (Π) are functions of the normalised position within the layer (ζ) that is less than the thickness of the layer (L), and the normalised drying time (σ) at the position ζ within the layer, whereas the normalised drying rate (f) is a function of the normalised drying time. Langrish *et al.* (1991), adjusted Equation 2.100 to Equation 2.101:

$$\frac{\partial \Phi}{\partial \sigma} = -\Pi f \tag{2.101}$$

Here Π is an air humidity potential, defined relative to the humidity potential at the air inlet to the layer:

$$\Pi = \frac{Y_w - Y_g}{Y_w - Y_{gi}} \tag{2.102}$$

where Y_w is the wet-bulb humidity, being the humidity of the gas adjacent to a fully wetted surface, $kg\ kg^{-1}$, Y_g is the humidity of the air in the layer, $kg\ kg^{-1}$, and Y_{gi} is the humidity of the inlet air, $kg\ kg^{-1}$.

A further theoretical explanation of the concept is described by Langrish *et al.* (1991). The construction of *f-curves*, as in Figure 2.12, requires knowledge of the critical moisture content.

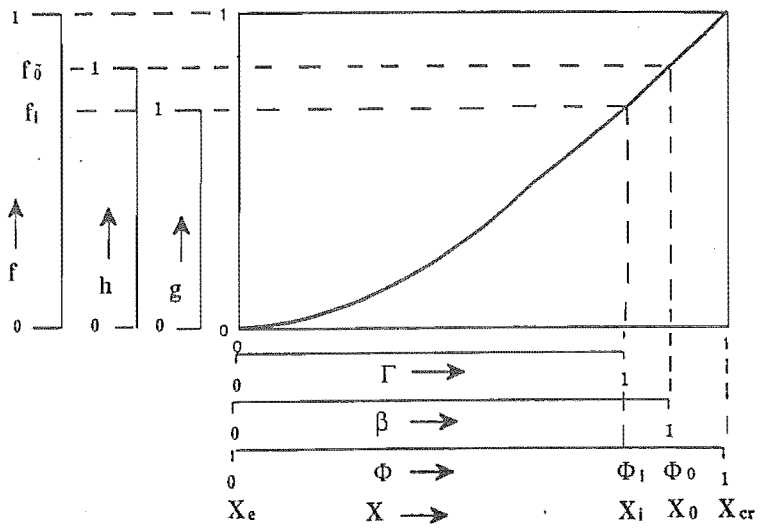

Figure 2.12 The form of the characteristic drying curve, $f - curve$, $h - curve$ and $g - curve$

However, the critical moisture content can be experimentally determined only after a constant rate period of drying has been observed. Often no constant rate period is observed at any operating condition, so extrapolation of the fundamental drying kinetics is necessary to remove the unknown critical point. To do this it is first necessary to construct a reduced form of the *f-curve*.

If the characteristic drying curve is of simple geometric form, $f = \Phi^n$, then we can define a new function, $h = h(\beta)$, as follows (Langrish *et al.*, 1991):

$$h = \frac{f}{f_o} \tag{2.103}$$

with a new relative moisture content β

$$\beta = \frac{\Phi}{\Phi_o} = \frac{X - X_e}{X_o - X_e} \tag{2.104}$$

with the following limiting values:

$$h = 1 \quad when \quad f = f_o \quad at \quad \Phi = \Phi_o \quad and \quad \beta = 1 \tag{2.105}$$

and

$$f = h = 0 at \Phi = \beta = 0 \tag{2.106}$$

Part of the drying behaviour of the falling rate period of drying is influenced by induction effects and part is not influenced; this period begins at a moisture content X_i rather than at X_o the initial value. It is difficult to extract the drying kinetics from the experimental data between X_o and X_i, suggesting that extrapolation of the critical moisture content from *h-curves* would be difficult. However, if we define a new function in terms of the moisture content which marks the start of the falling rate period (X_i) rather than the initial moisture content of the particles (X_o), then extrapolation of the drying kinetics *f-curves* can be made in the following way. Also, by way of definition, the critical moisture content (X_{cr}), cannot be defined at the start of the falling-rate period where no constant-rate period was observed.

If the characteristic drying curve is again of simple geometric form, $f = \Phi^n$, then we can define a new function, $g = g(\Gamma)$, say a *g-curve*, as shown in Figure 2.12. The new rate function is

$$g = \frac{f}{f_i} \tag{2.107}$$

and the corresponding moisture content is

$$\Gamma = \frac{\Phi}{\Phi_i} = \frac{X - X_e}{X_i - X_e} \tag{2.108}$$

These parameters take the limiting values:

$$\begin{aligned} g &= 1 \quad when \quad f = f_o \quad at \quad \Phi = \Phi_o \quad and \quad \Gamma = 1 \\ g &= h = f = 0 \quad at \quad \Gamma = \beta = \Phi = 0 \end{aligned} \tag{2.109}$$

where g is a dimensionless function of the reduced moisture content, Γ, based on the ostensible start of the falling rate period

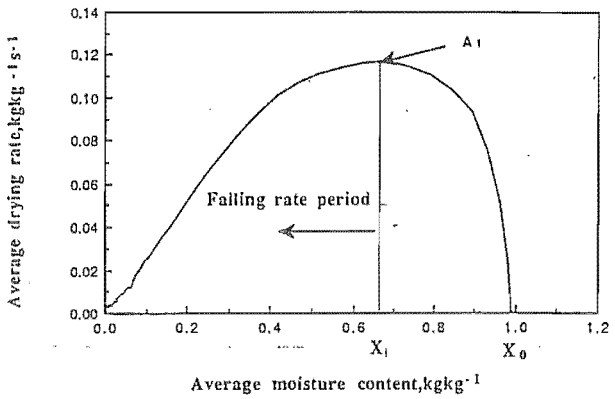

Figure 2.13 Simple drying rate curve with no constant rate period of drying

An exploration of the application of the characteristic drying curve concept was undertaken by Langrish (1988)and Langrish *et al.* (1991) with experiments on thin layers of particles. They found that the operating conditions (inlet temperature from $60 deg C$ to $150 deg C$, inlet humidity of 0.0025-0.015 $kg\ kg^{-1}$, layer thickness of 2-7 mm and air velocity of 3.5-7.0 $m\ s^{-1}$ had no significant effect on the fitted normalised drying rate curves and that, over moderate changes to these parameters, a characteristic drying curve appeared. However, the effect of the particle's initial moisture content on the characteristic drying curve was marked. For materials that have no constant rate function, such as Purolit and silica gel, the characteristic drying rate function at the falling-rate period could be expressed as follows:

$$f = B^{(A-C)}\Phi^C, \quad \Phi \leq B$$
$$f = \Phi^A, \quad \Phi \geq B \tag{2.110}$$

where the parameters A, B and C are constants that can be fitted from the experimental data.

Zhang *et al.* (1992) extended this study to particles of varying sizes (0.86-5 mm) and found a variation in the shapes of the characteristic drying curves. Keech (1992) also found a variation in the characteristic drying curve by extending the bed thickness from 2 to 16*mm*. This work attempts to extend the effect on the characteristic drying curve by using very small air velocities with particle Reynolds numbers between 4 and 70 for single particles while drying silica gel type-124 material.

2.6.5 Method of obtaining characteristic drying curves

When no constant rate drying period is observed, the initial drying rates are masked by the induction period of drying, so information about the initial stages of drying is lost. However, it is possible to extrapolate the fundamental drying kinetics back to the critical moisture. Secondly, once a critical moisture content for a material is known, the ratio of this moisture content to its maximum hygroscopic moisture content will give information about the nature of the external pore surface. At a material's critical moisture content, the moisture should act like a fully wetted surface and should exert its full vapour pressure at that temperature. At a material's maximum hygroscopic moisture content, only partial saturation of the external particle surface may exist. Thus, for X_{hyg}/X_{cr} ratios close to unity, a smooth external particle surface may exist; for ratios somewhat less than unity, a more uneven macroporous structure may exist. This difference may be helpful in the characterisation of the material. Thirdly, if an *f-curve* can be derived, then the rate of drying over a unit exposed surface (N_v) is given by

$$N_v = \frac{f_i K_o \phi (Y_w - Y_g) a}{\rho_s} \tag{2.111}$$

where f_i is the dimensionless function of the moisture content, somewhat less than unity if no constant-rate period is observed, and which takes account of the relative resistance to moisture movement within the solid. It may relate to the fractional area of the body covered by the capillary openings. Here a is the effective area of contact between particles and the gas per unit volume of drier. The relative drying rate (N_v) is expressed in $kg\ kg^{-1}\ s^{-1}$, and the overall mass transfer coefficient (K_o) based on the

humidity potential has units $kg\ m^3\ s^{-1}$, and ϕ is the humidity correction factor.

Calculation of the f-curves from the g-curves

One way of obtaining *f-curves* is to construct the various *g-curves* as a function of the particle diameter. First calculate the critical moisture content of the material to determine where to extrapolate the *g-curves*. Once this is performed, the *f-curves* can be calculated directly from these curves. The critical moisture content of a material can be calculated from Equation 2.97 and solved for X_{cr} (when $X_{cr} = X$) and Φ.

Equation 2.112 shows that X_i is a function of X_o:

$$X_i = kX_o \tag{2.112}$$

with $k=f(d_p)$ provided Equation 2.96 can be expressed as the simple relationship

$$f_i = \Phi_i^n \tag{2.113}$$

with $n = f(d_p)$. The initial moisture content Φ_i can be found experimentally using Equation 2.111.

For small particles, the critical moisture content approaches the maximum hygroscopic moisture content, so X_{cr} in this limit can be calculated from exposing the material to a saturated environment and obtaining a sorption isotherm point at approximately 100% relative humidity. For larger particles, the hygroscopic moisture content at the surface corresponds to the condition when the volume-averaged moisture content is equal to the critical moisture content for the particle (see Figure 2.14, provided

$$p_s \cong p_{vo} \tag{2.114}$$

where p_s is the vapour pressure at the particle surface and p_{vo} is the saturation vapour pressure of the surrounding air.

We can quantify the critical moisture content as

$$X_{cr} = \frac{1}{R} \sum_{X hyg^*}^{X_o} X dr \tag{2.115}$$

provided the moisture content of the particle can be described as a function of radial distance. Fick's second law may be written as:

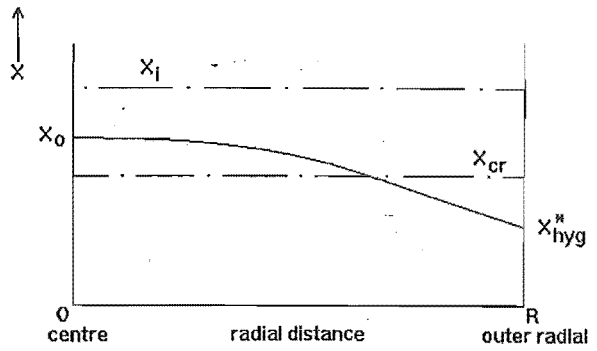

Figure 2.14 Moisture content profile through a spherical particle

$$\frac{\partial u}{\partial t} = D\frac{\partial^2 u}{\partial r} \tag{2.116}$$

where $u = \rho_s X r$. The appropriate boundary conditions are: $t = 0$ at $X = X_i$ for all r $[\partial X/\partial r]_{r=0} = 0$. The moisture content profile can be found after estimating an intraparticle diffusion coefficient.

The *f-curves* may be calculated from *g-curves* by using the number of transfer units to extrapolate the *f-curves*. From Equation 2.107, the *f-function* is a product of

$$f = g f_i \tag{2.117}$$

where

$$f_i = \frac{ln\left[\frac{Y_w - Y_{go(1)}}{Y_w - Y_{gi}}\right]}{NTU} \tag{2.118}$$

in which Y_w is the wet-bulb humidity, being the humidity of the gas adjacent to a fully wetted surface, $kg\ kg^{-1}$, $Y_{go(1)}$ is the outlet humidity at the transition point between the induction period and the falling-rate period, $kg\ kg^{-1}$, Y_{gi} is the inlet air humidity, $kg\ kg^{-1}$, and NTU is the number of transfer units.

Number of transfer units

General

The number of transfer units reflects the extent of humidification of the air as it passes through the layer. At the start of the first period of drying, at a material's critical point

$$\frac{Y_{go} - Y_{gi}}{Y_w - Y_{gi}} = 1 - exp(-NTU) \tag{2.119}$$

At any point in the falling-rate period, the NTU at the initial drying rate can be approximated from a reduced form of the relative drying intensity

$$\frac{Y_{go} - Y_{gi}}{Y_w - Y_{gi}} = 1 - exp(-fNTU) \tag{2.120}$$

The NTU can also be determined from the effective mass transfer coefficient, $fk_o\phi_m$

$$NTU = \frac{fk_o\phi az}{G} \tag{2.121}$$

where f_i is the initial relative drying rate, i.e. the maximum identifiable drying rate in the falling-rate period, k_o is the bed-averaged interparticle mass transfer coefficient, $kg\ m^{-2}s^{-1}$, a is the effective area of contact between particles and the gas per unit volume of drier, m^2m^{-3}, z is the distance through the layer in the direction of the air flow, m, G is the specific mass flowrate of dry air through the drier, $kg\ m^{-2}s^{-1}$, and ϕ is the humidity potential coefficient which accounts for the fact that the humidity difference $(Y_w - Y_{gi})$ is not a true driving force for mass transfer. The true driving force is given by $ln\frac{1-Y_w}{1-Y_{gi}}$, where Y_w and Y_{gi} are the mole fractions of moisture vapour in the gas.

Calculating the number of transfer units

Before the number of transfer units can be calculated directly, individual components of Equation 2.119 need to be determined.

Initial relative drying rate, f_i

As described above f_i is assumed to be close to unity and its corrected value can be determined from an iteration of Equations 2.120 and 2.121.

External mass transfer coefficient for particle aggregates, k_{oe}

The external mass transfer coefficient k_{oe} depends upon the particle's geometry and the air conditions. A number of methods are available to calculate this coefficient. By analogy with heat transfer, Krischer's universal heat transfer chart may be used (Keey, 1992, pg. 200). At small relative velocities between the particles and air ($Re_p < 100$),

Kothari's correlation (Coulson and Richardson, 1955) fits the behaviour of fixed and fluidised beds of particles:

$$Sh_p = 0.03 Re_p^{1.3}, \qquad Pr \approx Sc \tag{2.122}$$

At higher Reynolds numbers ($Re_p > 100$) for particle layers, then the Sherwood number may be calculated from a modification of the Frössling equation for the mass transfer for single spheres (Langrish, 1988):

$$Sh = (1 + \frac{3}{2}(1-\epsilon))(2 + 0.552\sqrt{Re}\sqrt[3]{Sc}) \tag{2.123}$$

where ϵ is the bed porosity.

The drying tests will yield the "internal" moisture diffusion coefficient only if the "external" transfer resistance is negligible. This is likely to be the case towards the end of drying at the low moisture transfer rates that are associated with low moisture levels.

Humidity potential coefficient, ϕ

Keey (1978) showed that the value of ϕ for air-water systems is given by:

$$\phi = \left[\frac{0.622}{0.622 + Y_w}\right]\left[\frac{(0.622 + Y_w) ln\left(1 + \frac{Y_w - Y_{gi}}{0.622 + Y_{gi}}\right)}{Y_w - Y_{gi}}\right] \tag{2.124}$$

A more readily estimated value for the effective area is that based on the bulk volume of the packing.

For spherical particles, Table 2.3 shows some typical values of sphericity for various materials:

Table 2.3 Data on sphericity, ϕ_s (Kunii and Levenspiel, 1969)

Material	high - low	
Sand	0.600	0.861
Iron Catalyst	0.578	0.579
Bituminous coal	0.624	0.626
Celite cylinders	0.861	0.863
Broken solids	0.61	0.63
Sand	0.534	0.628
Silica	0.534	0.628
Pulverised coal	0.696	0.697

The general surface per unit volume for a spherical particle is given by:

$$a_0 = \frac{n\pi d_p^2}{n\frac{\pi d_p^3}{6}} = \frac{6}{d_p} \tag{2.125}$$

If the particles are non-spherical, but are all the same shape and size and have volume equal to a sphere of size d_p, then

$$a_0 = \frac{6}{d_p \phi_s} \tag{2.126}$$

where d_p is the particle diameter and ϕ_s is the particle shape factor. The particle shape factor, or sphericity, can be defined as

$$\phi_s = \left(\frac{surface\quad of\quad sphere}{surface\quad of\quad particle}\right)_{both\quad of\quad same\quad volume} \tag{2.127}$$

With this definition, $\phi_s = 1$ for spheres, and $0 < \phi_s < 1$ for all other particle shapes. Kunii and Levenspiel (1969) list calculated sphericities of different solids (Table 2.4)

Table 2.4 Data on sphericity, ϕ_s (from Kunii and Levenspiel, 1969)

Material	ϕ_s high–low
Sand	0.600–0.861
Iron catalyst	0.578–0.579
Bituminous coal	0.624–0.626
Celite cylinders	0.861–0.863
Broken solids	0.61–0.63
Sand	0.534–0.628
Silica	0.534–0.628
Pulverised coal	0.696–0.697

The effective area of contact between the particles and the gas flow also depends on the bulk volume of the packing:

$$a_v = \frac{surface\quad of\quad packing}{bulk\quad volume\quad of\quad packing} \tag{2.128}$$

Multiplying the numerator and denominator by the volume of solids yields

$$a_v = a_o\left(\frac{volume\quad of\quad solids}{bulk\quad volume}\right) \tag{2.129}$$

$$= a_o(1-\epsilon) \tag{2.130}$$

$$= \frac{6(1-\epsilon)}{\phi_s d_p} \tag{2.131}$$

where ϵ is the mean voidage of the bed, which can be expressed as

$$\epsilon = \frac{volume\quad of\quad voids}{bulk\quad volume} = 1 - \frac{\rho_b}{\rho_p} \tag{2.132}$$

where ρ_b is the bulk density of the particulate bed and ρ_p is the particle density. On combining Equations 2.131 and 2.132 the resulting equation yields

$$a_v = \frac{6}{d_p\phi_s}\left(\frac{\rho_b}{\rho_p}\right) \tag{2.133}$$

Specific mass flowrate of dry air, G

This is a simple calculation from knowing the gas velocity and the volume of the drier.

As a result of combining these values in Equation 2.120, the number of transfer units can be calculated. This NTU value can then be used to extrapolate the drying kinetics of the *g-curves* to the *f-curves* from Equations 2.117 and 2.118. Under various test conditions, Equation 2.118 normalises the extent to which the material hinders the evaporative process during these separate experimental runs.

External mass transfer coefficient for single particles, k_{oi}

If the moisture transfer within the particle is diffusion based and isothermal, then approximately

$$ln\Phi = ln\frac{6}{\pi^2} - \left[\frac{Dt\pi^2}{a^2}\right] \tag{2.134}$$

Note that a is a radial distance and the Fourier number for mass transfer $F_o = Dt/a^2$ must be greater than 0.1 (Steinmetz *et al.*, 1991). For example, if the interparticle/intraparticle diffusion resistance of water vapour within the bed is approximately $10^{-8}\ m^2s^{-1}$, given that the diffusion of water vapour in air is $2*10^{-5}\ m^2s^{-1}$, and the particle diameter of the silica gel test material is $2*10^{-3}\ m$, then the time delay to apply this model from the start of drying is

$$t = \frac{0.1 * (2 * 10^{-3})}{10^{-8}} = 10s \tag{2.135}$$

A linear plot of Equation 2.134 provides a method of calculating the overall diffusion coefficient for single spherical particles. The external mass transfer coefficient can then be calculated from the Frössling equation

$$Sh = \frac{k_o d_p}{D} = 2 + 0.552\sqrt{Re}\sqrt[3]{Sc} \tag{2.136}$$

once the Reynolds and Schmidt numbers have been found.

2.6.6 Calculating a particle's critical moisture content

The effect of particle size and the characteristic drying functions

The fitted mean characteristic drying curves for all silica gel and Purolit materials are shown by Zhang *et al.* (1992), and are plotted in Figure 2.15. It can be seen that the relative drying rate decreases as the particle size increases. It is possible that the moisture vapour diffusion or surface diffusion process within the particle is the rate-determining step, and the internal resistance increases as the particle size increases. A clear trend can be seen for silica gel: drying rate decreases as particle size increases. This trend can be explained in terms of a receding evaporative interface model, assuming that drying is controlled by vapour diffusion from a wet core through the dry outer shell of the particle.

The general characteristic drying function of silica gel, as a function of particle size, is given by these workers as

$$\begin{aligned} g &= (0.76 - 0.11d_p)^{(0.47d_p - 0.89)}\Gamma^{1.32}; \qquad \Gamma \leq (0.76 - 0.11d_p) \\ g &= \Gamma^{(0.43 + 0.47d_p)}; \qquad \Gamma \geq (0.76 - 0.11d_p) \end{aligned} \tag{2.137}$$

in which d_p is the average particle diameter, *mm*. This equation is restricted to a range of particle sizes from 0.86 *mm* to 2.23 *mm*.

The general characteristic drying function of Purolit is given by

$$\begin{aligned} g &= 1.08\Gamma^{1.48}; \qquad \Gamma \leq 0.77 \\ g &= \Gamma^{1.17}; \qquad \Gamma \geq 0.77 \end{aligned} \tag{2.138}$$

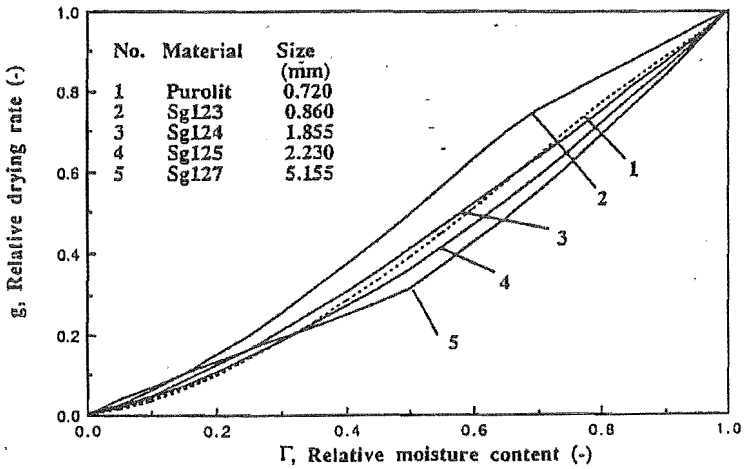

Figure 2.15 Fitted characteristic drying curves for all materials tested. $T_{gi} = 100 deg C, Y_{gi} = 0.052 kg kg^{-1}, X_o = 0.295 kg kg^{-1}$, 4 layers. Data of Zhang *et al.* (1992)

Equations 2.137 and 2.138 are based on the moisture content at the start of the falling-rate period (X_i) rather than the initial moisture content X_o in the experiments. On using the experimental data of all operating conditions for silica gel and Purolit, simple relationships between X_i, moisture content at the start of the falling-rate period, and X_o, the particle's initial moisture content, are found as follows:

for silica gel:

$$X_i = kX_o \tag{2.139}$$

with

$$k = 0.71 + 0.6d_p \tag{2.140}$$

for Purolit:

$$X_i = 0.73X_o \tag{2.141}$$

These relationships demonstrate that the difference between X_i and X_o cannot be

neglected even though the induction period is short relative to the total drying time, especially with high initial moisture contents. Nevertheless, the drying behaviour of the materials can be easily predicted from the particle's initial moisture content by using Equations 2.137 to 2.141.

It is claimed that the characteristic drying curve concept is a simple but powerful method to analysis the drying kinetics of particles (I Kemp, private communication). The critical moisture content of a material, which is used when normalising the relative free moisture level, is required beforehand. However, this is an unknown parameter for most materials and may not even be observed in a drying test. In this study, the relative free moisture content normalises using transition between the induction period and the falling-rate period. This value can be evaluated from a mass balance. When no constant-rate period is observed, one may assume that the material has a critical moisture content greater than the particle's initial moisture content. If it is also assumed that the geometrical forms of the relative drying rate curves at the range of moisture content from X_e to X_i and from X_e to X_{cr} are the same, then the critical moisture contents of the tested materials can be predicted from the fitted characteristic drying functions.

These functions in the range of moisture content from X_e to X_i for silica gel and Purolit are given by Equations 2.137 and 2.141. For silica gel, the function (Equation 2.137) is also a function of particle size. The relationships of normalised drying rates and normalised moisture contents between two ranges (from X_e to X_i and from X_e to X_{cr}) can be expressed as follows:

$$\begin{aligned} g &= \frac{f}{f_i} \\ \Gamma &= \frac{\Phi}{\Phi_i} \end{aligned} \tag{2.142}$$

and

$$f_i = \Phi_i^{(0.43+0.47d_p)} \tag{2.143}$$

where f_i is the fraction of the predicted maximum drying rate at the transitional moisture content. It can be calculated from the following equation, from a knowledge of the humidity change over the drying layer:

$$f_i = \frac{log\left[\frac{Y_w - Y_{go(i)}}{Y_w - Y_{gi}}\right]}{NTU} \tag{2.144}$$

in which Y_w is the wet-bulb humidity, being the humidity of the gas adjacent to

a fully wetted surface, $kg\ kg^{-1}$, $Y_{go(i)}$ is the outlet humidity at the transition point between the induction period and the falling-rate period, $kg\ kg^{-1}$, Y_{gi} is the inlet air humidity, $kg\ kg^{-1}$, and NTU is the number of transfer units calculated by solving the batch drying equations for the layer (Keey,1992).

The function f_i was correlated by Zhang *et al.* (1992) as the function of the particle size for silica gel, that is:

$$f_i = 0.283 d_p NTU \tag{2.145}$$

in which the correlation coefficient is 0.98 and d_p is the average particle diameter, mm.

The relationships between X_i and X_o have been given Equations 2.139 with 2.140 and Equation 2.141 for silica gel and Purolit respectively.

The previous equations give the critical moisture content for silica gel:

$$X_{cr} = (0.283 d_p)^{-1/(0.43+0.47 d_p)}[(0.71 + 0.06 d_p)X_o - X_e] + X_e \tag{2.146}$$

Now,

$$f_i = \Phi_i^{1.17} \tag{2.147}$$

and

$$X_{cr} = \frac{1}{\Phi_i}(X_i - X_e) + X_e \tag{2.148}$$

On combining Equations 2.146, 2.147 and 2.148, one gets

$$X_{cr} = 2.08(0.73 X_o - X_e) + X_e \tag{2.149}$$

From sorption isotherms, the equilibrium moisture content against relative humidity for silica gel is

$$X_e = 0.53 \varphi^{RT/187} \tag{2.150}$$

In all the experimental conditions used, the variation of equilibrium moisture content X_e is only from 0.002 $kg\,kg^{-1}$ to 0.04 $kg\,kg^{-1}$. As a first approximation, Equation 2.146 can be simplified with only a small error to:

$$\frac{X_{cr}}{X_o} = (0.71 + 0.06d_p)(0.283d_p)^{-1/(0.43+0.47d_p)} \tag{2.151}$$

with $0.86 < d_p/mm < 2.23$.

In the case of Purolit, the average value of f_i is about 0.424. A similar argument to that leading Equation 2.151 gives

$$\frac{X_{cr}}{X_o} = 1.52 \tag{2.152}$$

for Purolit.

Thus the critical moisture contents, which are a function of particle size and the particle's initial moisture content for silica gel, may now be predicted using Equations 2.151 and 2.152 respectively over the tested range of conditions. Equations 2.151 and 2.152 are restricted to the specific materials over the tested range of conditions. Their inclusion here is merely illustrative of the power of the thin-layer method in correlating drying kinetics behaviour.

2.7 MOISTURE MOVEMENT NEAR DRYNESS

In the past, theories on the drying behaviour of particulate masses have been almost exclusively analysed in terms of capillary flow and diffusion of gases and vapours in porous media, and at low moisture contents the moisture binding interactions at the pore surfaces have been considered mainly in terms of capillarity and diffusion from micropores. At sufficiently low moisture contents, when the moisture is bound to the solid skeleton, Keey (1978) noted that the pore saturation curve may be determined from the Kelvin equation, Equation 2.153, from which the vapour pressure of a liquid in a capillary can be calculated:

$$\frac{\Delta G}{RT} = ln\frac{p}{p_o} = \frac{2\sigma V_L cos\theta}{rRT} \tag{2.153}$$

where σ is the surface tension, V_L is the specific volume of liquid, θ is the contact angle, r is the radius of the capillary and T is the absolute temperature.

The removal of moisture at low concentrations depends on the vapour/solid interactions: more specifically, the strengths of the physisorbed bonds, activation ener-

gies for surface diffusion, or bond strengths between water/solid hydrated complexes. The kinetics of desorption at low moisture contents may become more dependent on physio-chemical kinetics between the moisture and the solid, rather than the moisture movement through the solid. The chemistry of porous granular solid with the solvent/moisture is an important factor in establishing the drying kinetics. At low moisture levels, the dried material cannot be regarded as an "inert" skeletal structure, but one with active pore walls.

Modelling the intraparticle diffusion of gases in porous media has been achieved by using the "dusty gas model". The basic concept for the formulation of this model was first put forward by Maxwell in 1860. In the last 30 years, various workers have developed, in stages, the dusty gas model from its original concept, including Evans (1961, 1962) , Krishna (1993), MacElroy *et al.*(1978), Mason (1963, 1967), and Warren (1983) , In the model, the walls of the porous adsorbent are depicted as giant dust molecules, and are regarded as pseudo species. Krishna (1993) developed the idea and described the intraparticle diffusion of multicomponent gaseous mixtures in macro- and microporous media. MacElroy *et al.* (1978) used a "dense dusty gas model" as an extension of the earlier "dusty" gas model proposed by Mason *et al.* (1967). The consideration of these gas/solid interactions in microporous media is relevant to low-moisture content drying, as moisture residues are often held in micropores. Although this approach to describe the drying process of microporous media appears to be effective, the use of empirical relationships specific for gas/solid interactions for drying kinetics at low moisture levels is easier to understand for the process engineer.

To observe the drying selectivity at low-moisture contents ($< 1\%$), it is important to determine:

- the types of moisture bound to the material from the varying strengths of the bonds;
- the amount of moisture bound to the material corresponding to these strengths.

Differential scanning calorimetry has been used successfully in the past to characterise the different strengths of water bound on to polymers, by reflecting a shift of the melting temperature of the water held in the polymers (Ohno *et al.*, 1983).

2.8 THEORY OF DRYING DISCRETE PARTICLES TO PARTICLES IN LAYERS

2.8.1 Using suspended isolated vermiculite particles, from Keey (1992)

Keey *et al.* (1985) observed a difference between the drying kinetics of isolated particles and the same particles being dried in a layer. The drying tunnel used by Langrish (1984) and Keey *et al.* (1985) is shown in Figure 2.16.

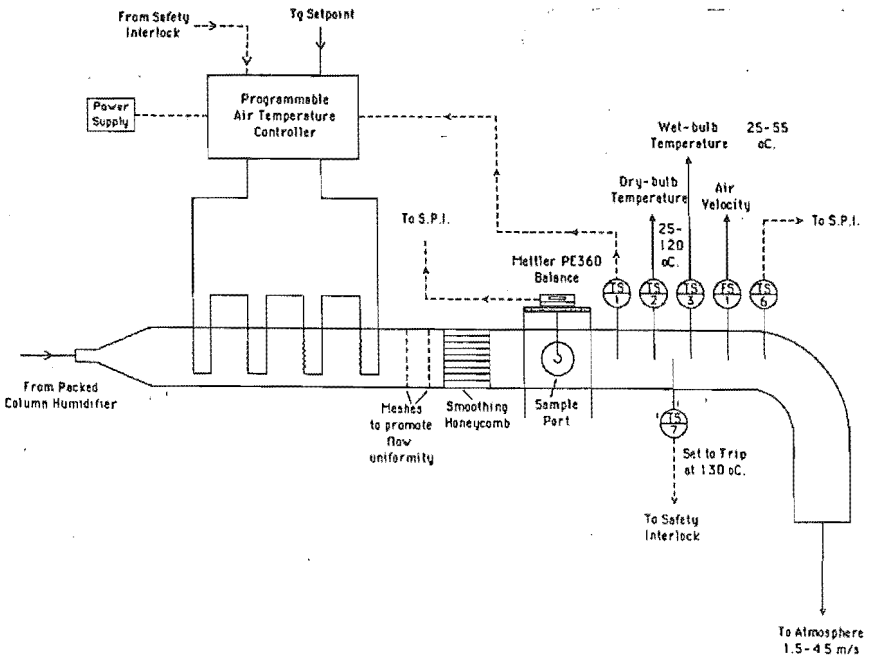

Figure 2.16 Drying tunnel (after Keey, *etal.*, 1985)

The isolated vermiculite particles used were hollow unglazed porcelain cylinders, typically used in industrial and household electrical appliances. Discrete particles were suspended on metal pins from the balance before drying. A tray (Figure 2.17) was used to dry these vermiculate particles in a cross-circulated layer. Drying was performed with a range of conditions described in Figure 2.16

The characteristic drying curves for drying isolated particles and layer arrangements from these tests are reproduced in Figure 2.18. Notice the extreme variability in drying descrete particles. Monitoring drying rates of individual particles is very difficult and experimentally inaccurate.

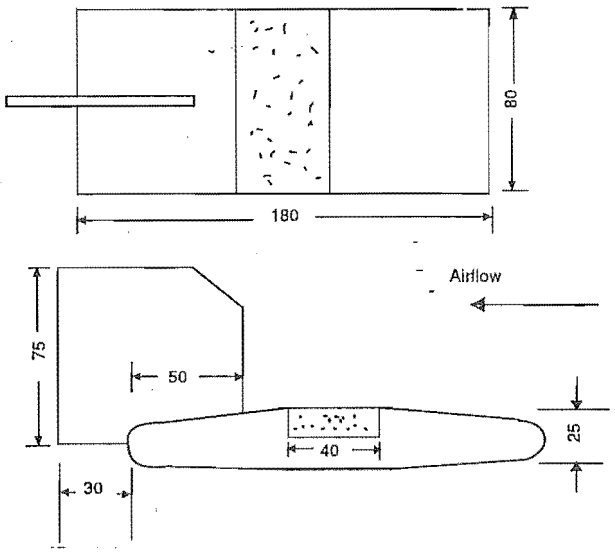

Figure 2.17 Diagram of wooden boat for cross-circulated layer drying used by Langrish (1984)

2.8.2 Using Canterbury thin layer apparatus, Keech (1992)

Figures 2.19 and 2.20 indicate the differences in drying behaviour with layer depth by using characteristic drying curves. The drying of thinner layers is different from the drying of thicker layers.

2.9 ANALYTICAL METHODS USED TO CHARACTERISE SORPTION

2.9.1 Thermogravimetric analysis and differential scanning calorimetry

Analytical techniques available to help characterise solid/moisture bonding at low moisture contents

There are some traditional techniques (equilibrium isotherm determination) commonly used for drying to give an indication of the nature of the water held in particle structures, but mostly the methods are sensitive to moisture contents only above about 1%. For example, it is difficult to obtain relative humidities below 5% accurately for moisture characterisation in the region where linear desorption kinetics are thought to exist (Hobson and Chapman, 1972).

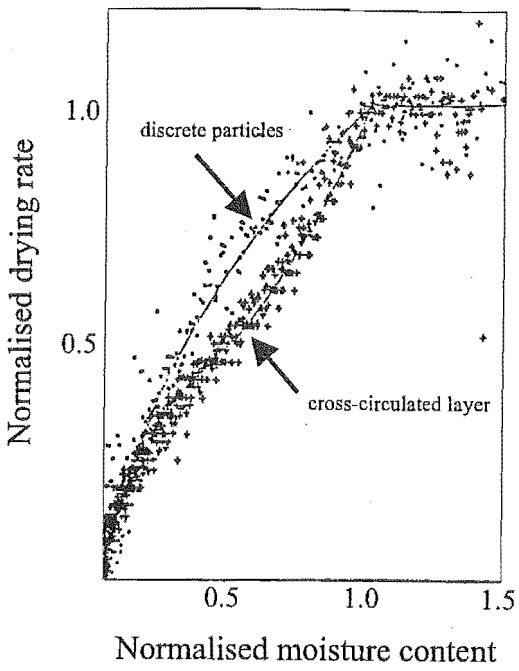

Figure 2.18 Relative drying rate of vermiculite particles (6 *mm* diameter) when dried individually and when dried in a cross-circulated layer 12 *mm* deep. Dry-bulb temperatures 61-95 $degC$; humidity 0.0170-0.0819 $kg\ kg^{-1}$; air velocity 1.56-3.00 $m\ s^{-1}$ (after Keey *et al.* 1985])

Analytical techniques used to extend the characterisation of moisture/solid relationships for the drying of material to low moisture contents include the following.

1. Nitrogen sorption to determine pore topology from isotherms and single point nitrogen sorption to obtain surface areas using the BET equations (Suzuki, 1988).

2. Neutron scattering (NS) techniques using a light-scattering technique to quantify different configurations of light elements up to oxygen (MW 16) (Manley, 1989).

3. Thermal methods of analysis, which are techniques that measure the change in some property of a material. [Thermal methods subjected to a defined temperature programme include: differential thermal analysis (DTA), derivative thermogravimetry (DTG), thermomechanical analysis (TMA), hot-stage microscopy (HSM), differential scanning calorimetry (DSC)] (Manley, 1989).

4. Infrared (IR) spectroscopy, which scans the IR region and records sections of material vibrating, stretching, etc. and can identify free water and different hydroxyl stretches depending on how the water is held (Anderson and Wickersheim, 1964).

5. Near infrared (NIR) spectroscopy, which scans the NIR region, identifying the stretching associated with different hydroxyl groups (Anderson and Wickersheim, 1964).

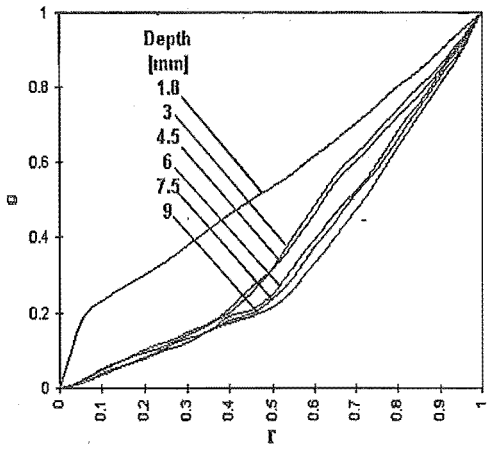

Figure 2.19 Characteristic drying curves for varying layer depths (1 to 6 layers). Air velocity 5.2 $m\ s^{-1}$; temperature; $=100 degC$, humidity = 0.02 $kg\ kg^{-1}$; X_o = 0.283 $kg\ kg^{-1}$ (after Keech, 1992)

6. Fourier transform infrared (FTIR) spectroscopy, electron beam scattering from the sample surface; diffuse reflectance FTIR spectroscopy to quantify free water levels in solids (Compton *et al.*, 1991).

7. Thermogravimetric analysis (TGA), which measures the weight of a sample as a function of temperature or time (Chris Manning, Stanton-Redcroft Ltd., London, 1988, *private communication*).

8. X-ray diffraction (XRD), which records crystal parameters and information about the solid phase (N Jogenson, AEA intec, 1993, *private communication*).

9. Mass spectroscopy (MS), which characterises materials by performing an evolved gas analysis as they are heated or dried in a controlled atmosphere (Sazanov, 1989).

Using a number of these techniques together helps to identify changes taking place while the material is subjected to external changes, such as temperature, gas conditions, electromagnetic radiation. Often a number of these techniques have been "coupled" to prevent performing separate tests and to help identify the changes that take place in materials once subjected to different environmental conditions (Compton *et al.*, 1991). Persistent problems can arise in using different samples and getting slightly

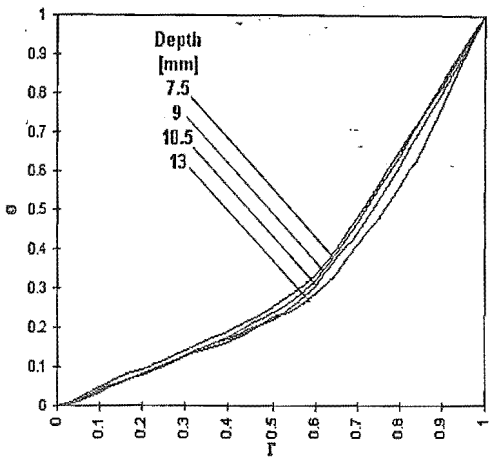

Figure 2.20 Characteristic drying curve for varying layer depths (4 to 8 layers). Air velocity 5.2 $m\ s^{-1}$; temperature $=100 deg C$; humidity = 0.02 $kg\ kg^{-1}$; X_o = 0.283 $kg\ kg^{-1}$ (after Keech, 1992)

different results due to sample size and morphology. Configurations include combining the following:

1. Differential scanning calorimetry, X-ray diffraction and mass spectroscopy. This combination enables the user to identify structural deformations in a material exposed to a temperature profile, along with the energy required to deform the lattice, and finally to monitor the evolved vapours that accompany this deformation (C Manning, Sales Department, LabTherm Scientific, London, *private communication*).

2. Thermogravimetric analysis, Fourier transform infrared spectroscopy and mass spectroscopy. The weight loss of free water can be accounted for using FTIR spectroscopy with a monitoring of evolved vapours other than water (C Manning, Sales Department, LabTherm Scientific, London, *private communication*).

3. Thermogravimetric analysis, differential scanning calorimetry and infrared gas analysis. The energy associated with removing bound water from a matrix is determined and quantified by both a weight loss profile and a humidity measurement (C Manning, Sales Department, LabTherm Scientific, London, *private communication*).

2.9.2 Description of thermal methods for moisture characterisation

2.9.2.1 Thermal methods of analysis (Manley, 1989)

Thermal methods of analysis are defined as techniques that measure the change in some property of a material as it is subjected to a specified temperature programme. This programme may be dynamic, in which the sample is heated or cooled at a constant rate over the temperature range of interest. It may also consist of holding the temperature at a predetermined value and examining changes that occur over a time period. When the material is cooled or heated, it will adsorb or desorb moisture respectively, the amount of sorption depending of the material's moisture-binding behaviour. Desorbing moisture from a material by a thermogravimetric device can help to identify the nature of the attached moisture, and to find the optimum drying temperature.

Other properties that have been measured by thermal methods include the following.

1. Structural changes - glass transitions, melting, boiling, sublimation, solid-phase transitions.
2. Mechanical properties - hardness, expansion.
3. Thermal constants - specific heat, melting points.
4. Thermal reactivity - solid/solid and solid/gas reactions, dehydration, curing reactions. Two special aspects are the thermal stability of materials in various gaseous atmospheres and thermal decomposition reactions.

In addition, thermoanalytical techniques are invaluable aids in the identification and characterisation of a material.

2.9.2.2 Thermogravimetric analysis

In thermogravimetric analysis (TGA) , a thermobalance is used to give a direct plot of weight loss versus temperature for any sample over the temperature range from ambient up to $1500 degC$. The technique thus gives a quantitative analysis of the amount of moisture desorbed at temperatures below the material's melting point. The resulting thermogram also records valuable information (i.e. weight loss against time or temperature or temperature curves) on the following physical and chemical phenomena.

1. Physical changes: vaporisation, sublimation, adsorption/desorption.
2. Chemical changes: decomposition, oxidative degradation, desolvation (especially dehydration), solid/solid reactions involving loss of weight, solid/gas reactions (for example, oxidation and reduction).

2.9.2.3 Differential scanning calorimetry

Differential scanning calorimetry (DSC) is an important technique that is very useful for phase characterisation. It is based on heating a sample along with an inert reference material. The sample and reference are heated at the same rate, and the difference in energy required to maintain the same rate of temperature increase (or decrease) is monitored and recorded. For example, losses of moisture below the melting point can be identified by the heat loading required on the sample side to maintain the temperature of the sample and reference cells. There are several other reasons why there may be a difference in the amount of energy required by the reference and the sample, as tabulated below.

1. Melting/solidification - Solid state transformation, eg. polymorphic transformation, glass transition.
2. Sublimation.
3. Thermal decomposition.
4. Polymerisation.
5. Evaporation/condensation.
6. Desolvation.

2.9.3 Comments on thermal analysis methods

Rees and Richards (1986) were successful in performing isothermal desorption work with a thermogravimetric (TG) unit to find adsorption/desorption rates with various solvents on zeolites. TG units of this type allow drying rates to be evaluated simply by using the derivative function (DTG) installed in the unit which converts the TG signal into its first derivative form, i.e. rate of weight change against time. These results can be complemented by using differential thermal analysis (DTA) or DSC. These measure energy changes by monitoring the temperature difference between an inert reference material and the sample. When such a temperature difference exists, a signal results and is recorded as a peak. Idealised DTA (polymer) and DSC (elastomer compound) curves (Figure 2.21) show the kinds of behaviour possible with polymers and organic compounds. The graphs show exothermic peaks, typical for chemical reactions such as oxidation, and endothermic peaks, i.e. from melting.

Over the past two decades, DSC has superseded DTA in the thermal analysis of polymers as little work is done above $400 deg C$. Further, the use of high pressure DSC has enabled significant advances to be made in studies on crystallisation and curing (Manley, 1989). Until recently, the use of these techniques for drying purposes

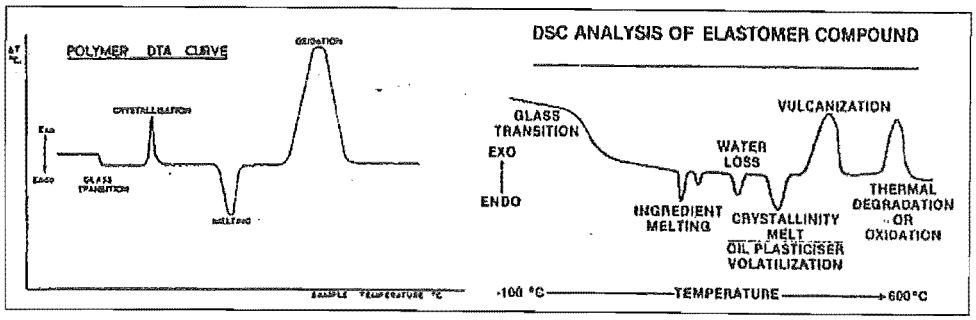

Figure 2.21 DTA curve for a polymer and DSC curve for an elastomer compound (Manley, 1989)

was unfortunately limited to finding the optimum drying temperature for condensed vapour/solid systems, as well as how the material responds in heating to that optimum drying temperature. Now these techniques may be used to perform drying tests on single particles or small agglomerates of particles.

2.9.3.1 Disadvantages of using TG equipment

The main disadvantage is asserting whether all the weight lost recorded by the balance is entirely due to one solvent or one type of moisture. Can one be sure that trace solvents, fragments of the material or the material itself are not also removed?

In certain situations, where the material may contain more than one condensed vapour, it is useful to know both qualitatively and quantitatively what gases are being evolved in the drying process, thus indicating any preferential desorption of these vapours. Many evolved gas analysers are adequate for this purpose, such as a mass spectrometer, with either the magnetic or rapid-scan quadrupole sensors. Infrared spectrometers or gas chromatographs are also suitable. Determining the composition of the evolved gas is possible by performing a purity analysis of the final product or evolved vapour, by analytical means such as mass spectroscopy (MS), proton-nuclear magnetic resonance spectroscopy (p-NMR), high pressure gas chromatography (HPLC), gas chromatography (GC), infrared spectroscopy (IR), or Karl Fischer titrations (KFT). A simpler less expensive method would be to specifically adsorb the evolved gas, say water, on to a zeolite molecular sieve (3A specific for H_2O, NH_3 and He; or 13X, general drying purposes). The final difference in weight between the sample and the amount of moisture adsorbed on to the molecular sieve at the end of drying should give the sum of

1. the amount of desorbed species other than water given off from the sample, and

2. the amount of water adsorbed on to the unit.

To limit the amount of water adsorbed on to the unit walls, it is important to minimise the distance between the sample and the adsorption unit containing the molecular sieve.

2.9.3.2 Direct methods of evolved gas analysis

Mass spectroscopy (MS) (Sazanov, 1989)

MS is probably the most effective evolved gas analysis system, as MS gives a qualitative as well as a quantitative description of the desorbed species. Most MS units identify a range of molecules between 0 and 500 *m.u.* in size (mass units or molecular weight). The evolution curves of the gas products express the time (t) and temperature (T) dependence of the peak heights (h) for the corresponding values of *m.u.* The quantitative analysis of these gases or vapours can be simply carried out with the aid of graphical integration of the curves $h_m = f(t_m)$:

$$Q_m = \psi_m \sum_{t_1}^{t_2} t_m \, dt \tag{2.154}$$

where Q_m is the content of the gas product m in the temperature range corresponding to the time interval $t_2 - t_1$, and ψ_m is the coefficient of sensitivity to the substance m. This coefficient of sensitivity may be difficult to determine or may vary in non-homogeneous materials.

At low moisture contents, relatively small amounts of water vapour are desorbed, because water molecules have a high affinity for most surfaces, and moisture builds up around the internal surfaces of the mass spectrometer. This increases the background noise for detecting water, giving inaccurate water desorption profiles. For this reason, a dew/frost point meter could be used in parallel with the mass spectrometer to attempt to account for all the water desorbed.

Proton-nuclear magnetic resonance spectroscopy (pNMR)

pNMR has been used previously by Hatakeyama and Hatakeyama (1992), and Hirai and Nakajima (1988) to investigate the effect of relaxation due to water desorption from various polymers. This technique has very accurate resolution of water peaks, but baseline noise can be a problem at low-moisture levels. However, continuous, *in situ* desorption profiles are impossible and readings are possible only at standard temperature and pressure.

Infrared (IR) spectroscopy

An infrared spectrometer is probably the most widely used device in analytical chemistry. It gives a different fingerprint for each individual organic compound by

recording the frequencies of adsorption in the electromagnetic near-to-far infrared region. At low solvent/water concentrations, baseline noise destroys the accuracy in determining the amount of desorbed vapour.

Infrared hygrometry (IRGA)

Determining the amount of desorbed water from a sample and/or air flow down to low humidities is possible (2000 *ppm*), provided a long path length for the IR beam is available, say 500-1000 *mm*. Water adsorbs strongly at bands of 1.9, 2.7 and 6.3 *mm* (Servomex Ltd., 1993, *private communication*) where the humidity of the gas is recorded.

Capacitive sensors (Weiderhold, 1982)

Advantages of the aluminium oxide sensor are as follows.

- It can be made small and is suitable for *in situ* use.
- It can be used very economically in multiple sensor arrangements.
- It is suitable for very low frost point levels without the need for sensor cooling (as in condensation-type sensors). Typically, frost points down to -80*degC* (0.1 *ppm* water) can be measured without great difficulties.
- It can cover a wide span.

Limitations of this sensor are as follows.

- The sensor is a secondary measurement device and must be periodically calibrated against a primary standard to accommodate aging effects, hysteresis and contamination.
- Sensors are not reproducible, calling for separate calibration curves for each sensor, and are non-linear with moisture content.
- Each sensor often has a limited life of around 6 months.

The electrolytic hygrometer (phosphorus pentoxide) (Wiederhold, 1982)

Typically the electrolytic hygrometer offers an accuracy of the order of $\pm$ 5% of the maximum reading. Detecting humidities at *ppm* levels is possible with clean gas flows, but contaminants that can block the capillaries (alkynes, alkadienes and alkenes higher than propylene) or react with P_2O_5 (chlorine) must be avoided.

2.9.3.3 Indirect methods of evolved gas analysis

High pressure liquid chromatography (HPLC)

HPLC is very useful in identifying very low concentrations of vapours or gases (a few parts per trillion *ppt.*). It has been used to identify species desorbed from molecular sieves. HPLC is a very expensive technique and MS should be employed in preference if suitable.

Karl Fisher titration

Although Karl Fischer titration is an accurate method (sensitive to less than 1-10 *ppm* of contaminants in liquid solution) to determine the amount of water contained in certain powdery materials, it is essentially an off line method and is not ideally suitable as a method of evolved gas analysis (C Price, *private communication*).

Optical condensation hygrometers (Wiederhold, 1982)

With the availability of thermoelectric coolers and solid state instrumentation, the optical condensation-type dew point hygrometer has become one of the most accurate and reliable humidity instruments offering a broad dew point range (-50$degC$ to 100$degC$) and excellent repeatability ($\pm$ 2 $degC$). These features are achieved at the expense of increased complexity and initial cost. In the optical dew point hygrometer, a surface is cooled by a thermoelectric or Peltier cooler until a dew or frost begins to condense on the mirror. The condensate surface is maintained electronically in vapour pressure equilibrium with the surrounding gas, and surface condensation is detected by optical or, in some cases, electrical techniques.

The optical dew point hygrometers are well suited to many applications where contamination of other condensable vapours (such as hydrocarbons) is mild to severe. Most instruments employ condensation chambers which can be quickly opened, allowing the mirror to be cleaned with a suitable swab. Routine maintenance schedules can be applied to keep the instrument in operation.

2.9.3.4 Comment

During the process of crystallisation, solvent may be incorporated into the crystal structure. Hydrates form when water is the solvent of crystallisation. The most commonly used techniques for quantifying the water content in hydrates are TGA, Karl Fischer titrimetry (KFT) and evolved gas analysis (EGA). All these methods are limited to some extent in their application to determine moisture residues in solids. For example, it may be difficult to decide the cut-off point on a TGA step, or TGA may not differentiate between the various binding states or water locations. KFT may not extract all the water/solvent held in the material. It is thus impossible to quantify the exact amount of residue remaining in the solid matrix. Pyrolysis of solids has been the most effective analytical technique to estimate the true amount of water in solids, once all

side reactions of water condensation have been identified. Combining this with KFT in an evolved gas set-up would provide the most accurate determination of water in solids.

The DSC curve can show several desolvation endo/exotherms, whereas the TGA thermogram shows only one desolvation step.

TGA does not differentiate between the various states of binding or water location in a hydrate, because these states of binding often have overlapping heats of wetting. KFT provides an accurate determination of water in many compounds provided the water molecules can be removed from the material, but interference from side reactions is frequently encountered mainly due to the oxidation-reducing properties of the iodine-iodine couple involved in the KFT reaction. KFT and EGA determine the total water content and therefore do not differentiate between adsorbed moisture and water of crystallisation.

It appears that a dew point hygrometer with a triple cooling plate device which is a three stage humidity analyser would be the best type of equipment to obtain concentration profiles of water in a gas (between -75$degC$ and 75$degC$ dew/frost points). Coupled with a suitable microprocessor and application MSDOS software that is available, accurate drying kinetic data at low moisture levels from materials can now be obtained.

2.9.3.5 Present technology to determine drying behaviour

State of drying equipment

At present, the equipment to measure drying behaviour uses gravimetric methods or perform gas analysis (EGA) by using techniques such as infrared hygrometry (IRGA), infrared (IR) spectroscopy, mass spectroscopy (MS) or optical hygrometrys (Weiderhold, 1982). Kinetics can also be obtained by monitoring a weight loss profile as the sample dries. Some indirect methods are useful when sensitive measurements are required. These include HPLC, KFT and solid phase microextraction (SPME) followed by gas chromatography/mass spectroscopy (GC/MS).

These techniques are adequate provided the sample size is neither too large nor too small. With large sample sizes, it is difficult to interpret the kinetic data because of the variations in local conditions, such as concentration profiles throughout the sample; with small sample sizes, the readings can become inaccurate.

At low moisture levels, moisture adsorption on to the sample housing usually becomes a significant source of error. Results can be uncertain unless great care is taken in designing an experimental procedure that will limit the introduction of such errors, or very sophisticated analytical equipment is used.

Three ways of improving accuracy are by:

- improving the sensitivity of weighing equipment,
- limiting the size of the chamber and tubing to reduce adsorption of moisture vapours on equipment surfaces, and
- using more sensitive gas analysis equipment.

2.9.3.6 Equipment investigated for low moisture drying

Weight loss of moisture against time

Continuous or *in situ* weighing under vacuum is an accurate method of determining the drying rate when the moisture is a single substance. The advent of more sensitive electronic microbalances in the last 10 years enables drying kinetics data under vacuum to be obtained. Besides being used under vacuum, the apparatus may be used under through-flow or cross-flow conditions. However, the air flow velocities are limited to avoid excessive vibrations in the sample balance pan. Continuous or *in situ* weighing under vacuum has been used effectively by Schlünder (1976) over the last 20 years. However, employing standard gravimetric equipment to establish drying kinetics at low-moisture contents would be impractical because of the insensitivity of standard balance equipment.

Advantages of using TGA

TGA presents many advantages in comparison with a loss-on-drying assay owing to the principle of the determination. TGA gives a dual record of the change in material temperature with the loss in weight. Degradation or sublimation in isothermal experiments can be detected if a TGA is coupled with a differential scanning calorimeter (DSC), and if necessary a mass spectrometer (MS).

TGA and a DSC enables heats of vaporisation and wetting as a function of moisture content to be evaluated (Etzler and Conners, 1991). Also the types and amounts of bound water or solvent can be determined on a qualitative and quantitative basis, and the dehydration or desolvation steps can be found. The technique requires only traces of samples (5-5000 *mg*) which is a great advantage for expensive samples or expensive calibration materials. TGA is also valuable for determining the volatile part of an aroma, for composition analysis, for kinetics analysis or for studying solid-liquid or solid-vapour equilibrium. As the carrier gas can be chosen, experiments can be strictly well controlled.

Operating costs for TGA units are minimal. Air conditioning systems for drying under moist or dry gas flows are comparatively small compared with conventional drying kinetics rigs. These gas flows are limited to about 100 $ml\ min^{-1}$ by the sample balance, as turbulent gas flows fluctuate the balance arms, affecting its accuracy, but these flows ensure small adsorption columns of silica gel or 13X zeolite to remove the water as less air is dried.

DSC and TGA are accurate methods of analysis which can be used as alternatives to classical melting point determinations and isothermal drying as routine methods. The correlation of DSC with the classical melting point determination has been validated (Giron-Forest *et al.*, 1989). DSC and TGA are more precise, quicker and give the same information about purity.

The thermobalances in these units consist of an electronic microbalance inside a glass head. They are sensitive to 1 *mg* and have the capacity to hold samples up to 5 *g*. So weight differences down to 1 *ppm* could be detected with good accuracy, which was of interest for this work.

2.9.4 Variations in amounts of heat required to dry solids

2.9.4.1 Effect of particle size

Zhang *et al.* (1992) showed that particle size has an effect on the drying behaviour of particulate solids. The heats of desorption should not be affected by particle size. The difference in drying behaviour should be dependent on the diffusion coefficients of moisture which relate to the distance required for moisture to travel to the surface.

2.9.4.2 Non-swelling solids

Constant rate drying of solids with a hydrophilic surface

(I) Drying solids with moisture content greater than the X_{cr}

(a) The amount of heat required to vaporise moisture from a free liquid surface is dependent on the temperature of the moisture (heat of vaporisation at that drying temperature).

(b) Free moisture that is being removed from spaces between particles can be described by capillary-driven forces. The amount of heat required to vaporise the moisture is still equivalent to the heat of vaporisation. A smaller porosity would slow down the drying process, but the heat required to desorb the moisture is not affected.

(II) Drying from cracks and macropores (moisture content less than or equal to X_{cr})

A constant-rate period of drying may continue if moisture from the particle can maintain a free wetted surface in the macropores or cracks or maintain a saturated vapour pressure at the surface in any way (van Brakel, 1980). In terms of the heat required to desorb this moisture, this should be equivalent to the heats required in evaporating free moisture.

Falling-rate period drying

(III) Drying from mesopores

(a) As the size range of mesopores is so wide (0.2-200 *nm*), there are two ways in which moisture can be bound to the active surface, either directly or indirectly

with different heats of sorption. Hydrophilic surfaces such as silica gel have been shown to increase the heats of desorption for water (heat of wetting plus the heat of vaporisation) up to five layers away from the hydrophilic surface (Staszczuk, 1986). This corresponds to layers 0.1-0.2 *nm* thick, so a heat of vaporisation would exist for moisture in pores less than 0.2-0.4 *nm* in diameter (from the diameter and packing nature of water molecules). Moisture in mesopores with pore diameters between 0.4 and 200*nm* would have the same heat of vaporisation as that in free moisture.

(b) The heat of desorption increases for smaller mesopores (0.2-0.4 *nm*). This is a result of removing moisture in layers that are partially hydrogen bonded to the hydrophilic surface. The layers of moisture closer to the surface have a higher heat of desorption than the indirectly bound layers.

(IV) Drying of solids covered in a monolayer of moisture

Removing moisture from a monolayer on a pore surface is effected at elevated temperatures, and can be modelled by surface diffusion forces. For example, the energy required to remove that bound moisture is determined solely by the local heat of sorption.

(V) Drying of microporous solids

(a) Removal of moisture not directly bonded to the particle surface from micropores requires similar energy to that for smaller mesopores. Moisture loss may be restricted by the diffusion through a microporous structure and thus adds additional diffusion resistances. Pore necking of a microporous structure may also limit the drying behaviour.

(b) Removal of moisture directly from microporous walls requires the same energy as that for monolayer desorption, except that additional diffusion resistances may be found.

(c) In the removal of moisture from smaller micropores ($\phi < 0.6$ *nm*) where the moisture is held in a force field (i.e. is influenced by the particle's surface surrounding the entire water molecule), this heat of desorption is strongly influenced by the microporous topology and pore necking. However, the energy required to desorb this type of bound moisture would be difficult to calculate without deforming, or sufficiently stretching, the lattice. As a result of pore necking and structural hindrance for moisture removal, the heats of sorption for trapped microporous moisture are likely to be very large compared with the heats of sorption required for other types of moisture discussed previously.

2.9.4.3 Swelling solids

There are a number of differences to the behaviour of drying when swelling solids are considered. This swelling may be either swelling of the particle's internal structure

(timber fibre or polymer-based compounds) or swelling of a particulate mass (clay).

Swelling of a particle's internal structure

If a dry amorphous solid (timber or a polymer-based compound) with a low porosity is exposed to a saturated or wet environment, water will vapour diffuse into the particle which may have either a hydrophobic or a hydrophilic surface. Water vapour will continue to diffuse even after the initial dry microporous structure has been saturated. Now particularly for hydrophobic surfaces, water molecules will hydrogen bond with neighbouring molecules and induce a local swelling of a pore. Swelling will continue until the hollow fibres (tracheids as in timber) or surrounding polymer chains present a mechanical restriction on further swelling (Keey, 1992). A general plot of particle swelling as a function of moisture content shows this type of restriction (Figure 2.22).

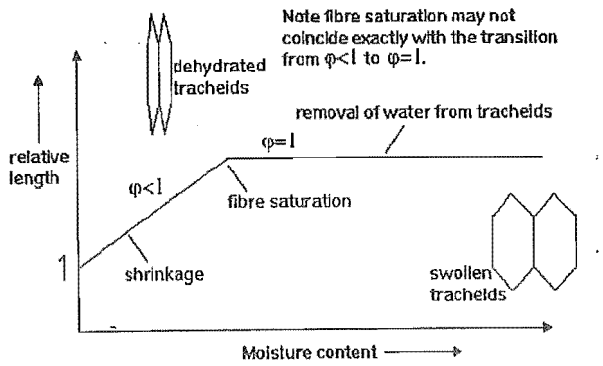

Figure 2.22 The effect of intraparticle swelling with moisture content for a woody material (Keey, 1992)

Heats of sorption during intraparticle swelling will be similar to that of free liquid water at that temperature provided liquid transport within the particle can maintain a saturated external surface. Relaxation or swelling of amorphous material should not significantly increase the heats. If a local mean free path for water transportation is absent, then the moisture is trapped in the lattice.

Swelling of a particulate mass

If a dry crystalline solid (non-porous non-swelling particulate) with a low porosity is exposed to a saturated or wet environment, water again will vapour diffuse into the particle with either a hydrophobic or a hydrophilic surface. Water vapour adsorption and/or intraparticle capillary action will cease once the porous structure reaches the moisture content at consolidation. Further exposure to a wet environment promotes the adsorption of liquid water into the interparticle particulate structure by capillary forces. This swells the particulate mass (R Keey, 1994, private communication). Heats of

sorption of the moisture (during the swelling process), which is held outside individual particles, would be similar to that of liquid water at the same temperature. Graphically, this can be represented as shown in Figure 2.23.

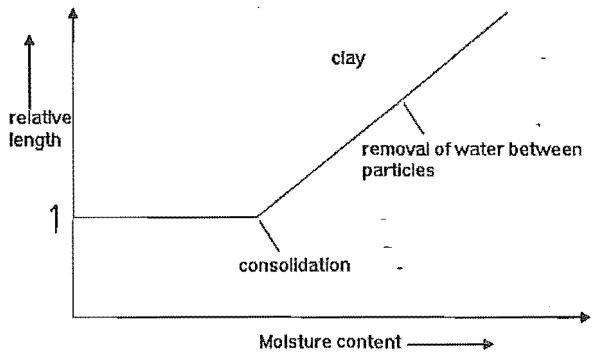

Figure 2.23 The effect of interparticle swelling with moisture content for a colloidal material (Keey, 1992)

In short, each drying material has its own porous structure/s. Varying pore sizes can result in varying heats of sorption. Therefore in order to fully explain the drying behaviour especially at low moisture contents, it is useful to know the amorphous or crystalline character of the particle and its nature of bonding between moisture and solid. From such information, the drying kinetics may be inferred.

2.9.5 Calculating the heats of wetting of particulate/powdery material at low moisture contents

In drying solids to low moisture contents (well into the falling-rate period of drying), it is important to know the quantity of moisture held in the solid and how strongly it is held in the solid structure. Section 2.1 gives a full characterisation of such solid/moisture relationships. As described in Section 2.2, water held in the solid particles can be either "water of crystallisation" or "water of constitution", e.g. water is held with varying degrees of strength to solid surfaces. Hydrophilic surfaces require more energy to remove water molecules than hydrophobic surfaces that may constitute free water (hydrophobic interactions) at the surface of the particles.

The total enthalpy for moisture evaporation $(\Delta H_v + \Delta H_w)$ $[kJ\,kg^{-1}\ dry\ material]$ is composed of the latent heat of vaporisation for free moisture ΔH_v, and the latent heat of vaporisation for bound or held moisture in solids (heat of wetting, ΔH_w). A graph of total enthalpy for moisture evaporation against moisture content of a solid

gives a clear indication of the quantity of energy required to remove varying amounts of water from the solid. This graph can be obtained by two distinct methods.

Firstly and most commonly, it can be obtained directly from plotting the moisture isotherms for a solid/solvent system at varying temperatures. Here the temperature and relative humidity must be strictly controlled when using either the dynamic or static methods (Keey, 1978). Adsorption and desorption isotherms must be sought to locate any hysteresis before the heats can be calculated. The latent heat of vaporisation for bound moisture ΔH_w (commonly called the *enthalpy of wetting*) can be obtained here by the Clausius-Clapeyron relationship (Equation 2.155). Graphically, this can be calculated from the change of relative humidity (relative pressure of vapour) with temperature (Figure 2.24).

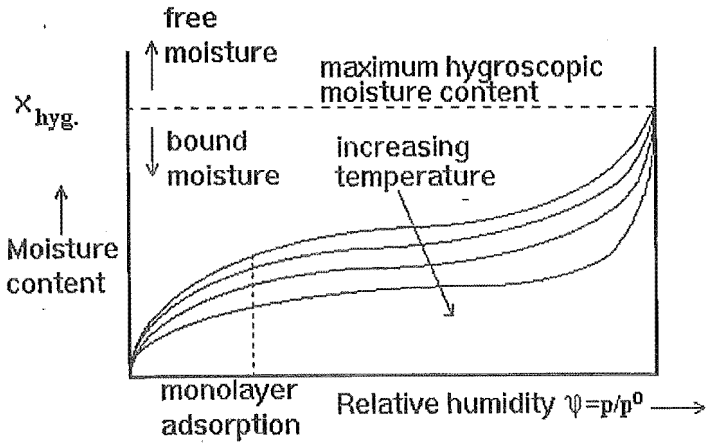

Figure 2.24 Typical moisture isotherms with the effect of temperature on sorption

$$\left[\frac{d(lnp/p^{\circ})}{d(1/T)}\right]_x = -\frac{\Delta H_w}{R} \tag{2.155}$$

For liquids, the heat of vaporisation is easily calculated in the same way from the variation of temperature with vapour pressure. This method can be extended to moisture held in porous particles. As the vapour pressure of moisture in particles decreases appreciably below moisture contents of the order of 0.1 $kg\ kg^{-1}$, the enthalpy for moisture evaporation increases due to the heat of wetting of the bound moisture.

The total enthalpy for vaporisation is thus given by.

$$\left[\frac{d(lnp^o)}{d(1/T)}\right]_X + \left[\frac{d(lnp/p^o)}{d(1/T)}\right]_X = -\frac{(\Delta H_v + \Delta H_w)}{R} \tag{2.156}$$

When drying solids to low moisture contents, the added heat of wetting for the bound moisture has a significant effect on the energy required to dry the particles, and contributes to lengthening the drying times when the heat transfer to the near-dry material is limiting. A typical plot of sorption isotherms at different temperatures (Figure 2.24) shows a decrease in sorption with increasing temperature and lower relative humidities. The differences between the curves represent the heats of wetting (Figure 2.25).

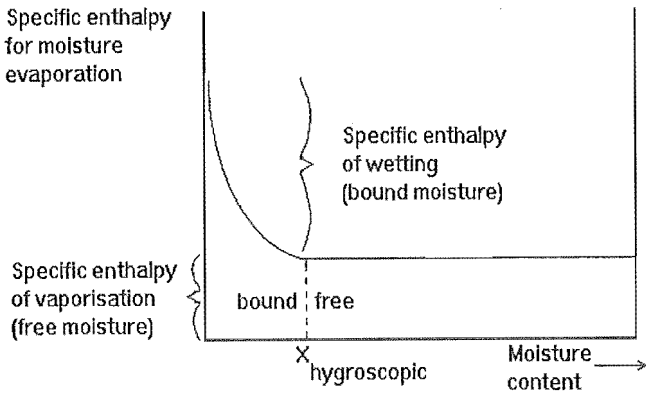

Figure 2.25 A graph of total enthalpy for moisture evaporation with moisture content of a solid

Secondly, a more recent technique involves coupling the results from a TG unit with those from DSC (C Manning, Stanton Redcroft, Ltd., 1993, *private communication*). A TG unit enables a sample to be heated at a given rate while recording the weight loss against time. A differential scanning calorimeter is analogous to a TG unit in which the sample is heated at a constant rate, but records the amount of energy required to hold the heating rate constant. On combining these techniques, by heating a sample at a known rate, the amount of desorbed moisture and the heat needed to desorb it are known; thus the heats of wetting plus the heat of vaporisation (energy needed to vaporise unit mass of liquid) can be determined as a function of moisture content. Simultaneous DSC/TGA allows for the measurement of the time or temperature dependence of both mass and energy flux. If the sample mass changes during

the experiment, e.g. vaporisation of liquid, chemical reaction etc., an additional term is added to the equation for the measured instantaneous power flux, dH/dt:

$$\frac{dH}{dt} = m(t)Cp(T)\frac{dT}{dt} + \frac{dm}{dt}\Delta H_{v,w}(T) \tag{2.157}$$

where $m(t)$ is the sample mass at time t, dT/dt is the scan rate, dm/dt is the sample loss in weight with time DTG and $\Delta H_{v,w}(T)$ is the energy needed to vaporise the liquid either from its pure state or held in a porous structure. All variables that are a function of temperature (e.g. specific heat) may also be parameterised as a function of time.

2.10 LITERATURE SURVEY ON PHYSICAL PROPERTIES OF MATERIALS

2.10.1 Silica gel

2.10.1.1 Silica gel preparation

Silica gel is the absorbent particle prepared by the coagulation of a colloidal solution of silicic acid (3-5 nm) followed by controlled dehydration. Liquid sodium silicates are neutralised by sulphuric acid and the mixture is then coagulated. Then it is dried, crushed and sieved. Spherical silica gel particles are prepared by spray drying of the hydrogel in hot air. Its chemical structure, whether it is microporous or mesoporous, is shown in Figure 2.26.

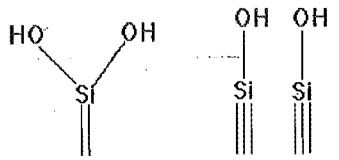

Figure 2.26 Surface hydroxyl groups on silica surface

2.10.1.2 Types of silica gel

Silica gels of two types of pore size distribution are frequently used for commercial purposes. These types are commonly called A and B and have different shapes of adsorption isotherms of water (Figure 2.27). This difference originates from the fact that *Type A* is controlled to form pores of 20-30 $\dot{A}$, whereas *Type B* has larger pores of about 70 $\dot{A}$. Internal surface areas are about 650 m^2g^{-1} (*Type A*) and 450 m^2g^{-1} (*Type B*).

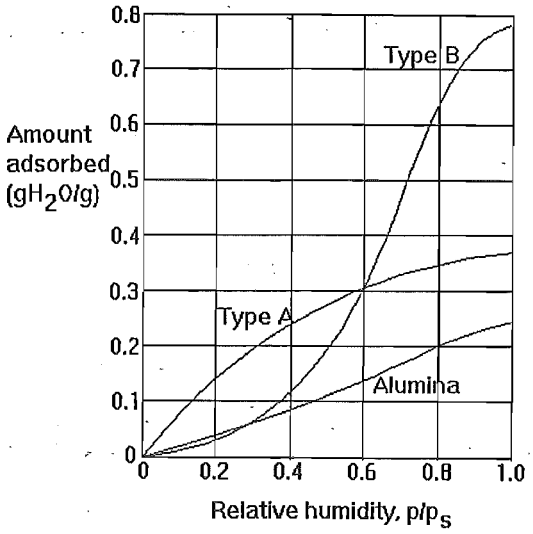

Figure 2.27 Typical examples of adsorption isotherms of water vapour on silica gel *Type A* and *Type B* and active alumina.

Silica gel contains about 0.04-0.06 *g combined water/g dry silica gel* of combined water after heating at $400 degC$. If it loses this water, it is no longer hydrophilic and loses adsorption capacity for water. The main use of silica gel is dehumidification of gases such as air and hydrocarbons. *Type A* is suitable for ordinary drying, but *Type B* is more suited for use at relative humidities higher than 50%. For the purposes of this work, a *Type A* silica gel was used, consistent with material used in earlier research at Canterbury by Zhang *et al.*, (1992) and Keech (1992).

2.10.1.3 Physisorbed and chemisorbed water on silica gel

The physical and chemical interaction of water vapour with the surfaces of silica gel has been extensively studied by measuring the isotherms over the past 45 years. It is well known that the hydroxyl groups on the silica surface act as primary sites for the physisorption of water molecules. Morimoto *Et al.*, (1971) determined that the ratio of surface hydroxyl groups to physisorbed water molecules at monolayer coverage was 1:1. On the other hand, Kiselev and Lygin, (1959) reported that a 1:2 ratio between physisorbed water molecules and surface hydroxyl groups can occur. Naono *et al.*, (1980) showed that the above ratio depends on the surface density of the hydroxyl groups on the silica, shown in Figure 2.28.

The removal of surface hydroxyl groups by thermal treatment leads to a marked

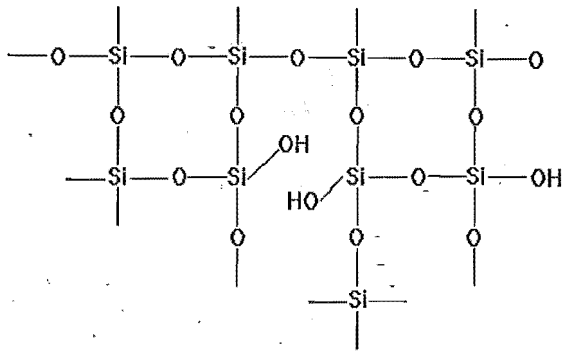

Figure 2.28 Variation of surface density of hydroxyl groups

reduction in the uptake of water on a given surface and, as a result, the silica surface becomes hydrophobic (Bassett *et al.*, 1968). Baker and Sing (1976) pointed out that the interpretation of water adsorption data for dehydroxylated silica is complicated by the fact that the surface can undergo slow rehydroxylation as the water vapour pressure is increased. The degree of the rehydroxylation of silica gel has been determined (Naono *et al.*, 1980),) and is reversible below $400 degC$, but is not reversible above that temperature.

Pure silica, SiO_2, is naturally a chemically inactive non-polar material with a visual structure of a colloidal silica particle as a network of interlinking SiO_4 tetrahedra. However, when it has a hydroxyl functional group (silanol group), the surface becomes very polar and hydrophilic. Under microscopic examination, the apparent loss of moisture is not easily recognisable. In Figure 2.29,

The photographs show small clusters of silica gel particles ($d_p = 1.5\text{-}2mm$), before drying and after drying. The right-hand side photographs are the same wet single particles before drying. No major differences are apparent, except that the wet particles appear slightly darker and fuzzier. This is probably due to the water in the wet particles diffusing the light from the microscope. Note, the light intensity and drying conditions of the particles were kept constant throughout the tests.

Generally, only two kinds of "end groups" are possible on the surface (Figure 2.30): the more reactive silanol groups existing at low temperatures, and the less reactive siloxane group existing at high temperatures due to the dehydroxylation of the silanol group. Removal of the last traces of water requires very high temperatures.

Hofmann *et al.* (1934), as cited by Boehm (1966), were probably the first to postulate that the free valence of silicon atoms in the surface of silicates must be saturated with silanol groups before preheating. The existence of siloxane bonds on

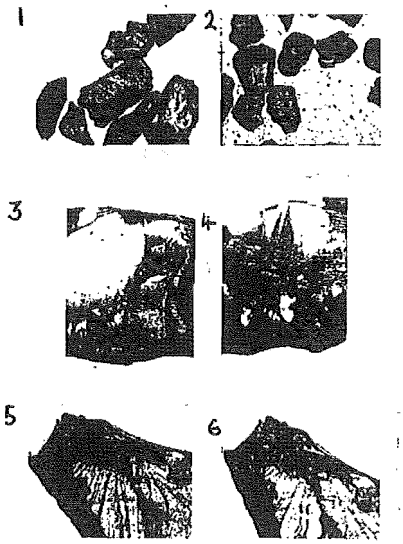

Figure 2.29 Photographs of dry (left-hand side and the same wet silica gel particle/s (right-hand side) (d_p=1.5-2 mm). Notice the clearer appearance of the dry particles

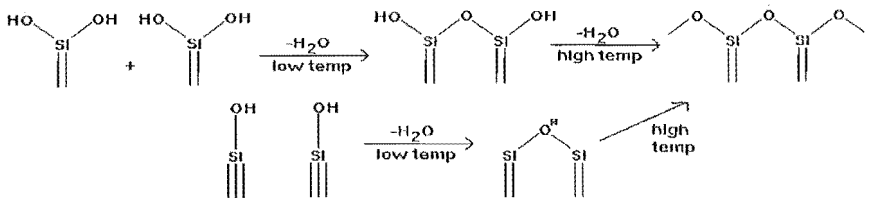

Figure 2.30 The two types of end groups on the surface. Silanol on the left-hand side to siloxane on the right-hand side

the surface of silica has been inferred mainly from the fact that the number of observed silanol groups is not sufficient for complete surface coverage. Practically no silanol groups are present in silicas heated to high temperatures. The siloxane bonds are quite unreactive. This results in the inertness of fused silica vessels towards chemical attack. When siloxane bonds are open, sintering will occur throughout the material and the silicon-oxygen bonds may eventually break. The oxygen atom in the siloxane group loses much of its basicity and shows an extremely weak tendency to make hydrogen bonds. This is manifested by the surface of silica turning hydrophobic after heating to high temperatures. No rehydration will occur on adsorption of water vapour below saturation pressure if the silica has been heated to temperatures higher than $400 degC$. Only dehydration of silanol groups is reversible and rehydroxylation of the siloxane bonds will take place instantaneously if the dehydration has been carried out below

400-450*degC* (Young, 1958; Boehm, 1966; and Naono *et al.*, 1980).) This irreversibility is illustrated in Figure 2.31 for a silica with a particle diameter of around 6.5 *nm* (65 *Å*).

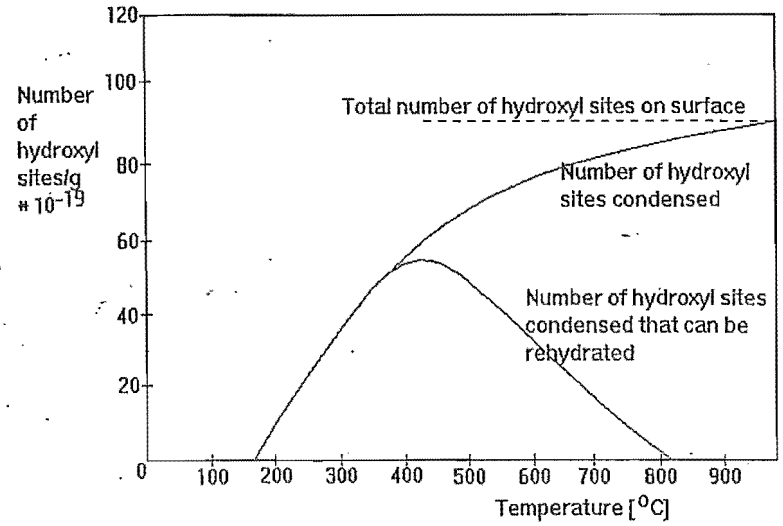

Figure 2.31 Change in surface silanol sites with sample heat treatment (Young, 1958)

The total number of hydroxyl sites originally present on the surface, as given by water adsorption, is shown at the top of the graph. The curve shows the number of silanol groups removed by activation at various temperatures, which was determined from weight loss data and also independently by measuring the amount of water evolved. Each molecule of water removed from the sample is assumed to be equivalent to the condensation of two silanol sites (Figure 2.32). The curve giving the number of hydroxyl sites that could be rehydrated by water vapour after once being removed from the surface was determined from the amount of chemisorbed water vapour and independently by measuring the number of adsorption sites by physical adsorption of water vapour after chemisorption.

Figures 2.36 and 2.31 show that

1. condensation of the surface silanol groups does not occur until 220*degC*,
2. rehydration is reversible up to 400*degC*,
3. after 400*degC*, the number of dehydrated sites that could be reversibly rehydrated by water vapour below saturation is decreased until after heating to 850*degC*, where no chemisorption of water vapour occurred, and

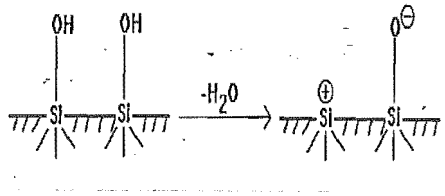

Figure 2.32 Reaction of two silanol groups

4. not all the surface silanol groups are removed even at the temperature where sintering starts to occur, at around $900 degC$.

Type III water vapour adsorption isotherm was found by Young (1958) with a heat-treated silica. Isotherms of this type are often found with water vapour adsorption on non-porous particles. This may suggest that adsorption in supermicropores and smaller mesopores is difficult because of the existence of siloxane and peroxo groups. Indeed, as mentioned before, the rehydroxylation of siloxane groups in the mesopores is difficult and does not exceed 3.3 $OH\,/\,100\,\dot{A}^2$ with samples subjected to pretreatment temperatures above $400 degC$ (Table 2.5).

Table 2.5 Recognised method of concentration of surface hydroxyl groups of *Type A* (03) and *Type B* (59, 81) silica gel

Sample	N_{OH}	Sample	N_{OH}
03-120	7.9	03-400	3.3
59-120	6.0	59-400	3.2
81-120	6.0	81-400	3.0

The strength of the stable siloxane group prevents complete rehydroxylation in the mesopores at temperatures above $400 degC$, and even at high relative humidities because water is only a weak nucleophile; breaking of the strong $(d\,\pi - \pi\pi)$ bonds is difficult but possible due to the strain on these bonds (compare the strained nature of organic epoxides). Opening of $Si\text{-}O\,(d\,\pi - \pi\pi)$ bonds, (2)(5), normally requires strong nucleophilic bases (Figure 2.33).

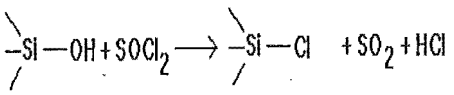

Figure 2.33 Reaction of a siloxane group with a lithium organic compound.

Rehydroxylation of the peroxo group in the supermicropores is impossible due to its unstrained nature depending on the width of the pore (distance between $Si\text{-}O$ groups)

and water being a weak nucleophile.

A major problem in dealing with silica gel surfaces is that of arriving at an estimate of the concentration of surface hydroxyls, n_{OH} (expressed as the number of OH groups per 100 $\dot{A}^2$). Methods of determining n_{OH} include isotropic exchange, X-ray analysis, reaction with OH-specific compounds and measurement of weight loss on heating. Agreement among the different methods, however, is generally poor (Boehm, 1966) . It is sometimes difficult to tell under what conditions physically adsorbed molecular water is completely eliminated. In Table 2.6 Naono *et al.*, (1980) assumed that all physisorbed water molecules can be removed from the adsorbent surface by the outgassing at $25 degC$ for 15 h under a reduced pressure of $2*10^{-5}$ $mmHg$. The surface hydroxyl groups per unit area (Γ_h) were estimated from the water content and the surface area of silica gel. (Γ_h of silica gel does not decrease appreciably up to $200 degC$).

Table 2.6 Surface area and water content of silica gel and chemisorbed and physisorbed water on silica gel

Pretreatment temp. (degC)	S_{BET} N_2	Γ_h (OH nm^{-2})	Γ_c (OH nm^{-2})	$\Gamma_h + \Gamma_c$ (OH nm^{-2})	Γ_p (H_2O nm^{-2})
25	358	5.4	0.0	5.4	4.0
200	357	5.2	0.0	5.2	4.1
400	356	4.2	0.9	5.1	4.1
600	355	1.5	2.2	3.7	3.6
800	331	0.4	2.0	2.4	3
1000	267	0.0	0.9	0.9	-

Boehm (1966) noted that the number of surface hydroxyl groups per unit area at $400 degC$ hardly ever exceeded 3.3 $OH/100\ \dot{A}^2$ and was at most 3.5. Mikhail and Shebl (1970), found from X-ray analysis of three samples of silica gel that the maximum number of surface hydroxyls per unit area is indeed 3.3 for microporous Davidson 03 silica gel (Table 2.5). Silica gel 59 and 81 contain only wide pores. These values may be compared with a higher value of 5.1 $OH/100\ \dot{A}^2$ at $400 degC$ determined by Naono *et al.* (1980) from water loss measurements. It is believed that the X-ray analysis method is more reliable, being a more direct technique.

It is difficult, in many cases, to be certain that all loss in weight on heating silica's to high temperatures is due exclusively to the chemical condensation of surface hydroxyls with loss of water. The loss of silanol groups against pretreatment temperatures for a silica, by Boehm (1966) , is shown in Figure 2.35. He used the reaction with thionyl chloride for the determination of silanol groups. For each hydroxyl group, one chlorine atom is retained on the surface. It is assumed that surface silanol groups are replaced by chlorine according to the reaction,

The chlorine is titrated after ion exchange with sodium hydroxide. It is uncertain whether all of the surface silanol groups react with the thionyl chloride, discounting the possibility of strongly adsorbed water. A more accurate picture of the loss of silanol

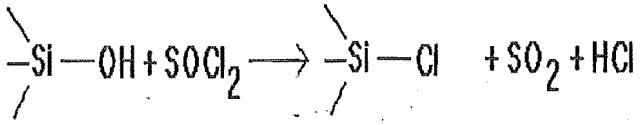

Figure 2.34 Reaction of thionyl chloride.

groups with temperature is given by differential thermal analysis (DTA) and is shown for a silica gel/water mixture in Figure 2.36 (Young, 1958).

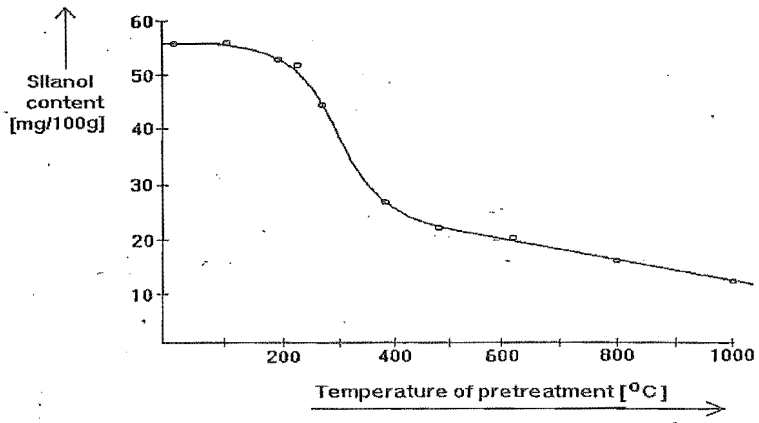

Figure 2.35 Content of silanol groups in "Aerosil", as determined by reaction with thionyl chloride (Boehm, 1966)

Bassett *et al.* (1968) undertook a gravimetric weight loss study on a non-porous silica (Figure 2.36).

Bassett *et al.* (1968) commented that not all physically adsorbed water was removed by heating at $25 degC$, contrary to Naono *et al.* (1980) who suggested that all was removed. However, there was also a significant loss between $25 degC$ and $110 degC$ due to adsorbed water being held in positions favourable for stronger bonding. In Figures 2.35 and 2.36 there is no accountable loss in silanol groups below $110 degC$. Beyond $110 degC$, the gradual decrease in weight in Figure 2.35 is due to the dehydroxylation of the silanol groups, also given in Figure 2.37.

Young (1958) also recorded the number of sites remaining on the silica surface that either exist as adsorption sites for water, or can be rehydrated to give silanol sites, as shown in Figure 2.31.

Under liquid water partial hydrolysis is possible over long periods, with boiling water in a limited time. However, the number of silanol groups found never exceeded 3.3

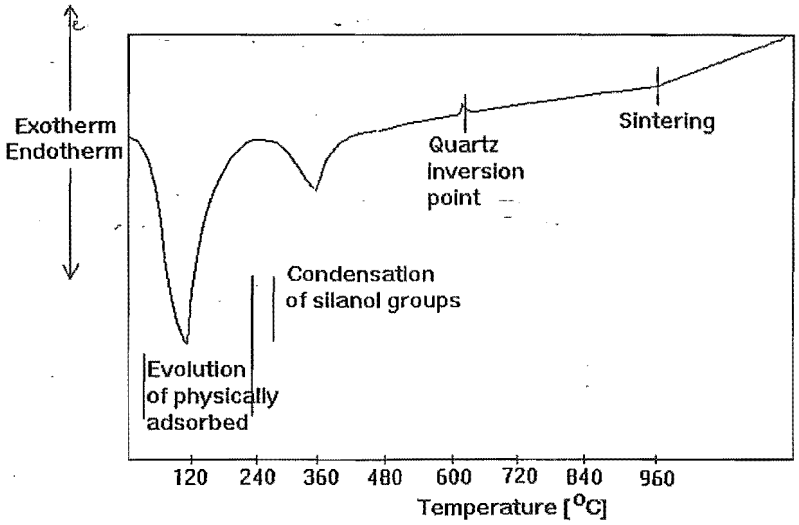

Figure 2.36 DTA curve for water on silica gel (Young, 1958)

$OH/100\,\dot{A}^2$. This value agrees with those from X-ray analysis, as mentioned previously.

From DTA of water on silica surfaces (Young, 1958), surface area changes show up as inflections due to changes in thermal conductivity of the sample, as indicated in Figure 2.36. At temperatures below $180 degC$, the removal of physically adsorbed water is predominant. At temperatures above $200 degC$, most of the dehydroxylation of the silanol groups can be seen from Figures 2.36 and 2.31. Dehydroxylation of the surface silanol sites as a function of temperature is given in Figure 2.38.

Anderson and Wickersheim (1964), using IR spectroscopy has identified at least two types of adsorbed water and two types of surface hydroxyl groups. The "species" inferred from the IR study are shown schematically in Figure 2.39.

They emphasised that the labelling scheme employed was based on the IR spectrum. They were not trying to imply that each spectroscopically distinguishable species corresponded to a unique surface configuration. The IR observations that led them to this picture were as follows.

1. Samples that had been fully dehydrated showed only a sharp OH stretching fundamental with an $Si\text{-}OH$ bending mode. At temperatures above $500 degC$, the bands became particularly sharp due to the absence of hydrogen bonded water. The exceptional high frequency of the stretching fundamentals indicate that this OH group, which they labelled OH_I, does not participate in hydrogen bonding.

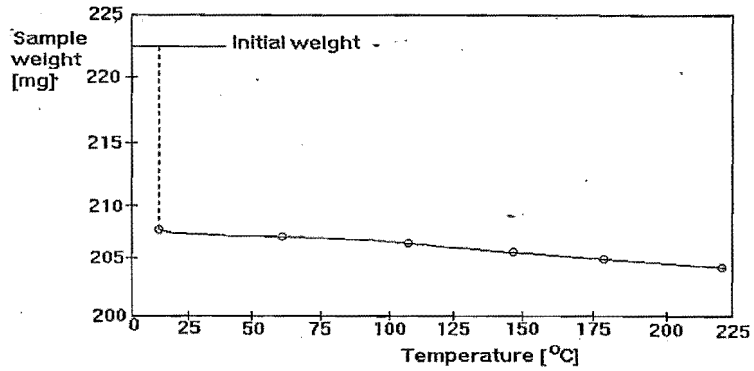

Figure 2.37 Gravimetric weight loss study on HiSil (Bassett *et al.*, 1968)

Therefore, above $500 degC$, the loss in weight of silica gel is due to dehydroxylation of hydroxyl groups.

2. At low levels of hydration, samples below a monolayer formation, the OH_I bands were less intense; in fully hydrated samples, they were missing altogether. The complete disappearance of this spectrum on hydration indicates that OH_I is a surface group that can interact with the adsorbing water molecules.

3. Consequently, as the OH_I adsorption bands decreased, a second type of hydroxyl ion (OH_{II}) was observed due to further hydration of hydroxyl groups.

4. Partnering these OH_{II} compounds, there was also an increase in water content. They labelled this type of water as H_2O_I. The fundamental high frequencies and the overall sharpness of the spectrum indicate that is monomeric water, i.e. individually adsorbed water molecules.

5. The simultaneous appearance of the OH_{II} and H_2O_I spectra on hydration and the reciprocal relation of the OH_I and OH_{II} band intensities indicate that an OH_I group was converted into an OH_{II} group by interaction with an adsorbing water molecule.

6. On further hydration, OH stretching bands of liquid water formed a hydrogen-bonded network on the surface. They called this network H_2O_{II}.

7. An interesting observation was made by Anderson and Wickersheim (1964) concerning the appearance of the H_2O_{II} fundamental spectrum. The broadening of combination bands, even at low water contents and the persistence of the H_2O_I spectrum to fairly high levels of hydration, suggest a certain "patchiness" in the

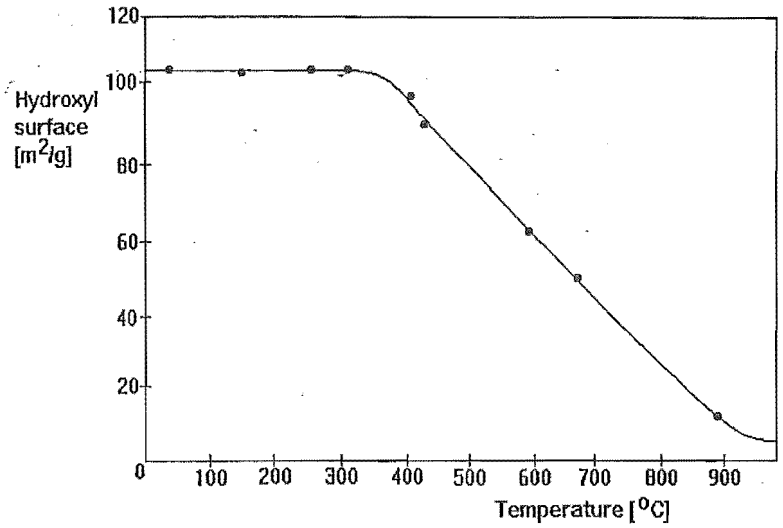

Figure 2.38 Change in total (rehydrated and per se) surface silanol sites with sample heat treatment (Young, 1958)

hydration process rather than the formation of complete molecular layers. Thus, even at lower levels of hydration, further adsorption may take place on OH or H_2 groups with nearly equal probability.

In conclusion, the chemisorption behaviour of water vapour on silica brings out an important point in the activation of silicas used for drying purposes. To be sure of future regeneration of the silica, moderate heating to $120 degC$ for a period of 48 h should limit the dehydroxylation of the surface silanol groups. Also instant loss of physically adsorbed water can be achieved at heating to approximately $180 degC$, but the former is recommended because of the tenacious way water is held in most silica adsorbents.

2.10.2 Crude terephthalic acid

Polymer-grade terephthalic acid is a petrochemical that is used in the production of polyesters. During 1979, the combined annual domestic production of dimethyl terephthalate and polymer-grade terephthalic acid exceeded $3.0*10^6$ *tonnes*. The Amoco process is used to purify terephthalic acid produced by bromine-promoted air oxidation of p-xylene.

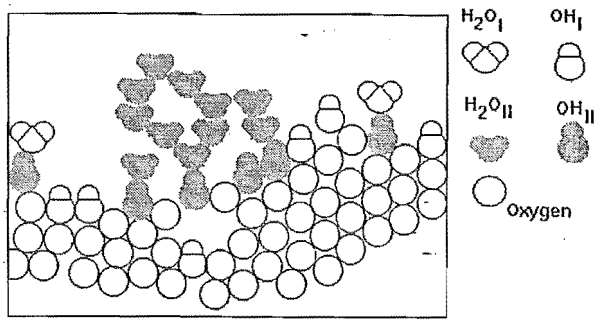

Figure 2.39 Molecular interpretation of water/silica gel bonding in the monolayer and in micropores. Schematic picture of a partially hydrated silica surface (Anderson and Wickersheim, 1964)

The drying kinetics and equilibrium characterisation of both pre-dried and pure forms of terephthalic acid were investigated in this work.

Polymer-grade terephthalic acid must conform to many specifications, because it is used to produce polyester fibre, film, and moulding resin. Specifications for polymer-grade terephthalic acid are shown in Table 2.7.

Table 2.7 Specifications for polymer-grade terephthalic acid.

Property	Specification	Test method
acid number, *mg KOH/g*	675 ± 2	titration
ash, *ppm*	15	pyrolysis
total significant metals (Mo, Cr, Ni, Fe, Ti, Mg), *ppm*	10 *max.*	atomic absorption
4-formylbenzioc acid, *ppm*	25 *max.*	polarography
moisture, *wt %*	0.5 *max.*	Karl Fischer
5 % dimethylformamide	10 *max.*	Colorimetry

2.10.3 Adipic acid (fine chemical)

Adipic acid is one of a family of dicarboxylic acids, and is obtained from a malonic ester synthesis. Adipic acid, *MW* 146.14, is a white crystalline solid with a melting point of about $152 deg C$. It is produced on a very large scale at several locations around the world (2 billion metric tons per year, 1989). Demands of high purity for such large scale production meant that adipic acid was an ideal material to be investigated in this work. A complete review on adipic acid chemistry, manufacture and uses can be found in the *Encyclopedia of Chemical Technology*, 4th edn, Vol. 1, pp.466-487.

The quality specifications for adipic acid production are shown in Table 2.8. Typical impurities include monobasic acids, trace metals, water, colour, and oils.

Table 2.8 Specifications for adipic acid production.

Parameter	Food grade	Other
melting range	151.5-154.0degC	
assay	99.6% *min.*	
water	0.2% *max.*	
residue on ignition	20 *ppm max.*	
arsenic (as As)	3 *ppm max.*	
heavy metals (as Pb)	10 *ppm max.*	
iron (as Fe)		2 *ppm*
ICV colour		5 *max.*
capronic acid		10 *ppm*
succinic acid		50 *ppm*
nitrogen		3 *ppm*
hydrocarbon oil		10 *ppm*

Water is determined by Karl Fischer titration of a methanol solution of the acid, as adipic acid is very soluble in methanol and ethanol.

Adipic acid is converted by treatment with acetic anhydride at a reflux temperature into a microcrystalline polymeric anhydride that melts after recrystallisation in the range 70-85*degC*. Properties and reactions of the substance indicate that it is a mixture of chain polymers of varying chain length with dehydration (Figure 2.40).

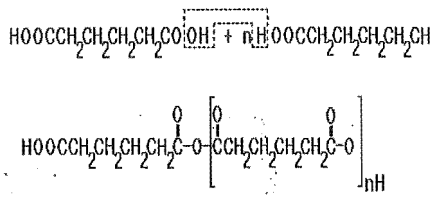

Figure 2.40 Monomeric to polymorphic forms of adipic acid via dehydration

Instead of intramolecular cyclisation to a 7-ring structure, the predominating reaction is intermolecular condensation (Fieser, 1961), and the contrast in behaviour to that of succinic and glutaric acids is attributable to a difference in relative opportunities for the two reactions. One carboxyl group separated from another by a chain of four methylene groups has many opportunities to combine with functional groups of other molecules and relatively few chances of colliding and interacting with the group attached to the same chain, because the chain can assume many positions and only a few of these bring the functional groups into proximity. Thus, the longer the chain, the less chance there is for intramolecular cyclisation and the greater is the tendency to form a polymeric material. Pimelic acid and subereric acid similarly yield chain polymers on treatment with dehydrating agents.

However, the monomeric form of adipic anhydride is not available by any known process of direct dehydration. When adipic anhydride (acid) is heated in high vacuum, a distillate slowly accumulates, consisting of the pure cyclic anhydride (Hill, 1940). Evidently the polymerisation is reversible and the volatile monomer distils from the equilibrium mixture, with eventual reversion of the bulk to the non-volatile polymer. Monomeric adipic anhydride is stable but reactive, and it is repolymerized by the catalytic action of a trace of water. This illustrates the principle of converting a polymeric substance into a cyclic monomer by heating in high vacuum to a temperature approaching the decomposition point.

To briefly add to this introduction on adipic acid, it is necessary at this stage to comment that, sorption isotherms were performed using the drying tunnel described in Section 2.8.2., and are later discussed in greater length in Chapter 6. Briefly, these isotherms indicated a very small maximum hygroscopic moisture content of unbound water. This equates to 0.4% free water content after exposing an adipic acid sample to a moist air stream for 2 *days* at $T_{dry} = 30 degC$, $T_{dew} = 30 degC$. Strongly held bound water from condensation of the dicarboxylic end groups of adipic acid to the polymorphic form (Figure 2.40) results in a further loss in water assay of 14%. This equates to the amount of condensable bound water held in an equivalent monolayer of bound water. Drying tests (Figure 6.13) indicate the large degree of difficulty in attempting to remove this bound water to produce a polymorphic form of the acid. This difficulty arises from the high relative vapour pressure of adipic acid compared with the high relative vapour pressure of the bound moisture of the dicarboxylic end groups. For example, drying adipic acid at $T_{dry} = 125 degC$ and $T_{dew} = 5 degC$ under a through-flow of air resulted in a slow release of bound moisture, producing fine needle-like crystals of the polymorphic adipic acid. However, these crystals began to appear after a few hours and a significant amount of the adipic acid (30% wet weight) monomer had been lost.

The removal of the free moisture from a maximum hygroscopic moisture content of 0.4% to a dry matrix showed a first-order drying kinetics characteristic drying rate curve, with the dual function parameters of A, B and C, shown in Equation 2.99.

Dehydration of the monomer units to the polymeric forms requires a low humidity drying environment. The sorption isotherm indicated that a relative humidity below 10% was enough to condense the monomer units. Drying to moisture contents below 1% may result in the formation of some monomeric adipic anhydride units, alongside long polymeric chains. From this sort of dehydration behaviour, it is envisaged that first order drying kinetics would pertain, due to the simple reaction kinetics nature of polymerisation.

Preliminary tests on exposing adipic acid to a saturated air stream resulted in its maximum hygroscopic moisture content reaching $\approx$ 6.5% (wet basis). This moisture

content was referenced on exposing the sample to dry air conditions ($T_{dry} = 80 degC$, $T_{dew} = 5$degC) for a period of 2 *days*. Unfortunately later experiments indicated that up to a further 7% water of crystallisation was present, which is in line with the stoichiometric value of 14% at monolayer saturation. From a stoichiometric standpoint, if no polymerised adipic acid was present, monomers only, on a dry mass basis there would be 14% maximum possible moisture content in an equivalent monolayer. This indicates that the sorption isotherm at $80 degC$ did not provide enough heat to fully desorb the condensed water. Drying adipic acid at $140 degC$ (adipic acid melting point $= 152 degC$) showed significant recrystallisation of the dried material from monomeric adipic acid into its polymeric form. Rehydrating this dried material, $T_{dry} = 32 degC$ and $T_{dew} = 30 degC$, showed a 1% loss in dry mass weight after rehydration.

2.10.4 Comments on the Variations in the Types of Materials Used in this Work

A little experimental work has been performed on adipic acid and one of the copolymers (III), under vacuum drying conditions. The bonding of the moisture on the solid matrix influences both the shape of the isotherm and the weight loss curve on drying. Expected shapes of isotherms and their respective weight loss drying curves are shown in Figures 2.41 and 2.42 (Hallstrome and Wimmerstedt, 1983).

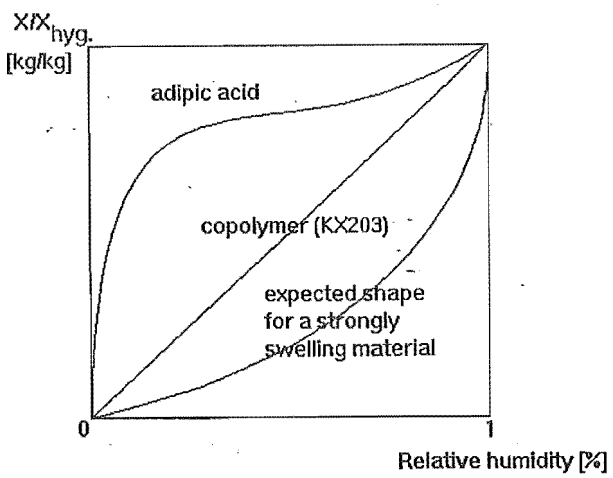

Figure 2.41 Guessed typical shapes of normalised isotherms

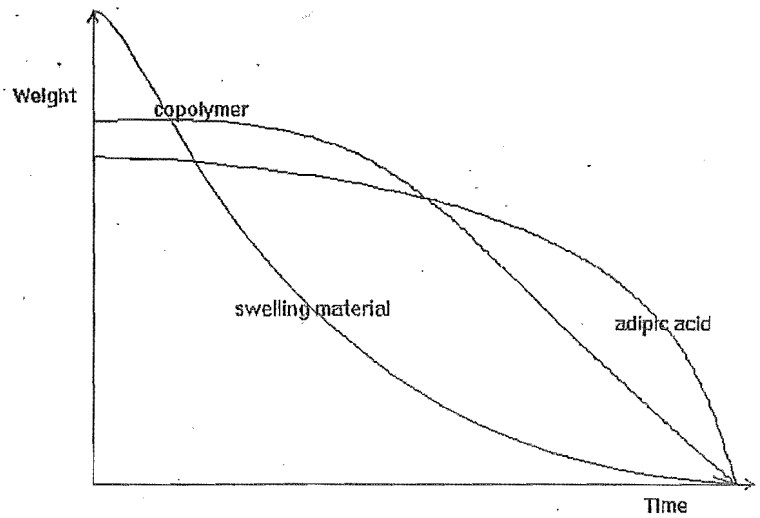

Figure 2.42 Expected weight loss profiles

Chapter 3

APPLYING EXISTING MODELS TO LOW MOISTURE CONTENT DRYING

3.1 INTRODUCTION

At low moisture levels, moisture bound to solid surfaces in porous particles has been described to be transported by means of surface diffusion and internal gas-phase flow provided a free path for diffusion to the particle's surface exists (Suzuki, 1988). If no free path exists, moisture is trapped in the solid matrix. For example, the moisture residue from chemical reactions is often trapped in solidifying polymer matrices and can be removed only by deforming the matrix, either by stretching it under vacuum or by softening and/or melting.

In this work, the removal of these moisture residues from desiccating agents, polymers and fine chemical particles was of principal interest. Generally, these types of materials are either non-porous or microporous, and the traditional Fickian models of diffusion may accurately describe the drying of bound moisture for some materials at low moisture contents, but not others. Diffusion at low-moisture contents is believed to occur under two widely different sets of conditions: molecular diffusion and surface diffusion mechanisms.

Molecular diffusion under isothermal conditions can be adequately described by Fick's equations, although they assume that a concentration gradient is the fundamental force responsible for diffusion. In gaseous diffusion, a partial pressure gradient is the force responsible and can be applied even under non-isothermal conditions. However, Fick's equations may, not always apply to surface diffusion. For example, Fick's equations fail to describe the equilibrium conditions in sorption systems with hysteresis. Moisture can and does diffuse against a density difference, where liquids absorb vapours under isothermal conditions; thus Fick's equations do not describe accurately interphase mass transfer.

Consequently, under both isothermal and non-isothermal conditions, a spreading pressure in surface diffusion (sorption diffusion) is the force responsible for the diffusion of multilayered moisture not directly bound to the solid. Its validity under

non-isothermal conditions is demonstrated by experimental data from the literature. Thus, surface diffusion differs from molecular diffusion in that it requires an activation energy.

If the order of the kinetics over a portion of the characteristic drying curve does not change, then the drying kinetics may be accurately described by an emperical drying rate equation, which is different from the numerical expression shown in Equation 3.3. However, if at any stage during the drying process there is a change in drying kinetics, as would be the case if silica gel was dried through the physisorption-chemisorption transition, then a single value of n may not accurately describe the drying kinetics over the whole range. A modified two-stage expression may then be written for the silica gel material:

$$\frac{dX}{dt} = kX^n; n = 1 \qquad X_s < X < X_{cr} \tag{3.1}$$

and

$$\frac{dX}{dt} = kX^n; n = 2 for X_e < X < X_s \tag{3.2}$$

where X_s is the transitional moisture content between the physisorbed and chemisorbed moisture, n is the order of the kinetics, and k is a constant.

The order of the drying kinetics can be determined from the physio-chemistry of the solid/moisture bonding. This may be all that is required for the drying of very thin-layers of particles and isolated particles that are small ($< 0.5\ mm$). Zhang *et al.* (1992), indicated a difference in the drying kinetics of larger particles due to the intraparticle mass/heat transfer resistances. However, most industrial drying operations involve the production of larger quantities and would be simulated by the drying of thicker layers. It then makes it difficult to determine the appropriate drying kinetics model to adopt for an industrial process. However, this difficulty is normally overcome by using a empirically based model, such as the concept of the characteristic drying curve that has a shape specific to that material and its initial moisture content. This curve can then be used to design an industrial drier as described by Keey (1992).

3.2 PHYSIO-CHEMICAL DRYING KINETICS

When the monolayer of moisture is no longer complete, the sorption behaviour is governed by the collision frequency, and the rate of desorption can be described by:

$$rate = collision frequency * energy factor * probability factor(orientation factor) \tag{3.3}$$

The **collision frequency** depends upon:

1. how closely the particles are crowded together, that is, concentration or pressure;
2. how large they are;
3. how fast they are moving, which in turn depends upon their weight and temperature.

By far the most important factor determining the collision rate is the **energy factor**: the fraction of impacts that are sufficiently energetic. This factor depends upon the temperature and upon the energy of activation, which is characteristic of the heat of sorption.

The **probability factor** depends upon the geometry of the particles and the kind of reaction that is taking place.

If it is assumed that physio-chemical kinetics are the rate-determining step in the drying, then mass transfer and heat transfer resistances within the particle or a thin-layer of particles would be negligible. Thus, the drying rate may be described in terms of the collision frequency, the energy factor and the probability factor. The effects of each parameter can be elaborated further.

- The collision frequency is dependent firstly on how closely the particles are crowded together, and is thus dependent upon the pressure on drying at constant humidity. If the atmospheric pressure is decreased, i.e. on drying under a vacuum, the collision frequency of the gaseous molecules in the bulk, with a wet pore surface, decreases. This in turn decreases the vapour pressure or partial pressure of the bound moisture, or decreases the heat of sorption, thus significantly increasing the drying rate.

- The energy factor is the most important rate-determining term. Surface diffusion of moisture during drying processes has been well described by Suzuki (1988) to be determined solely by temperature, and quantifying its effect is described later. Under vacuum conditions, the partial pressure of the bound moisture decreases, thus, the activation energy is reduced.

- The probability factor depends on the steric nature of the reacting species and the chemistry. For example, the reaction or drying kinetics of removing physisorbed moisture from a pore surface can be described by a first-order reaction: $A \rightarrow B+C$

where the *rate=k[A]*. Here species A may be a silica gel, i.e. $-O_3Si\text{-}OH - H_2O$, with B as $-O_3Si\text{-}OH$ and C as H_2O. Condensing a reactive silica gel surface by reacting two neighbouring $-O_3Si\text{-}OH$ groups is a second-order reaction as both A species have to form their own stable, but opposite, intermediate before the reaction is to be completed: $2A \rightarrow B+C$ where the $rate=k[A]^2$. Here species A is $-O_3Si\text{-}OH$ with species B as $-O_3Si\text{-}O\text{-}SiO_3$ and species C as H_2O. The reaction chemistry is $2^*\text{-}O_3Si-OH \rightarrow -O_3Si-O^- + -O_3Si^+ \rightarrow -O_3Si-O-SiO_3+H_2O$. Second-order kinetics are determined by the formation of the two transition state intermediates. As a silica gel surface is dried in a "patchy" manner, the transition from physisorbed to chemisorbed drying kinetics is masked. This is typified by observing no noticeable changes in drying kinetics when drying into an equivalent monolayer of moisture on a silica gel surface.

If the removal of physisorbed and condensed moisture from a silica gel surface is described by a characteristic drying curve, then drying through this transition may show a change in drying kinetics from a first-order to a second-order process. This transition may not always be visible as other mass and heat transfer resistances may exist through the particle.

The terms in Equation 3.3 indicate the possible factors affecting rates of desorption from a physio-chemical stand point. The weighting of each of the described factors would be determined from calculations on the energy factor. Previous surface diffusion models that accurately calculate the drying rates indicate the importance of the energy factor term (Staszczuk, 1986). Thus, other factors responsible for the physio-chemical model would have less importance.

3.3 SURFACE DIFFUSION MODEL FOR BOUND MOISTURE

In surface diffusion, a concentration gradient along the micropore wall exists, permitting lateral diffusion along the pore wall. Surface diffusion is more likely than the total removal of moisture molecules from the surface because of the lesser energy involved. The temperature dependence of the surface diffusivity can be expressed in terms of the Arrhenius law,

$$D_s = D_* e^{-\frac{E}{RT}} \tag{3.4}$$

where D_* is a constant found from experiment.

Thus there exists a temperature dependence on drying to low-moisture contents, and a rate expression of similar form to Equation 3.3 could be used to predict the

drying kinetics. In other words, the rate of desorption from the particle's surface = (desorption constant)*(probability that the desorption carries enough energy), i.e.

$$\ddot{n}_d = ze^{-\frac{E_a}{RT}} \tag{3.5}$$

where z is the probability factor multiplied by the collision frequency (as described earlier), E_a is the activation energy of the moisture-solid bond and $e^{-E_a/RT}$ is the fraction of collisions with energy greater than E_a.

By correlating experimental data on viscosity versus temperature, Bird *et al.* (1960) state that the free energy of activation in a "stationary fluid" can be related to the internal energy of vaporisation ΔU_v by an empirical expression

$$E_a = 0.408\Delta U_v \tag{3.6}$$

For a stationary fluid E_a is related to the heat of vaporisation by

$$= 0.369\Delta H_v \tag{3.7}$$

For the drying of porous solids, assume a linear relationship:

$$= b'\Delta H_v \tag{3.8}$$

where b' is a constant determined from experiment.

From these relationships it is now possible to construct a drying rate curve as shown in Figure 3.1 which is derived entirely from heats of wetting information, which is given for each material in the Results Section.

From Equation 3.7, activation energy can be evaluated as a function of moisture content. The curves of 3.1 (as given in the Chapter 6) are constructed for each drying test, and indicate the significance of the drying temperature on drying rates. Thus, verifying the possible existence of surface diffusion for the drying of smaller particles whenever other mass transfer diffusion mechanisms may not exist. However, drying rates at low moisture contents may be small enough such that diffusion mechanisms are not rate-determining and emphasise the importance of sorption diffusion. Dislocation theory (Atkins, 1988) for the movement of molecules on unstable solid surfaces as not been considered for drying of bound moisture. Moisture molecules should be threated as separate entities from sorptive sites on a solid.

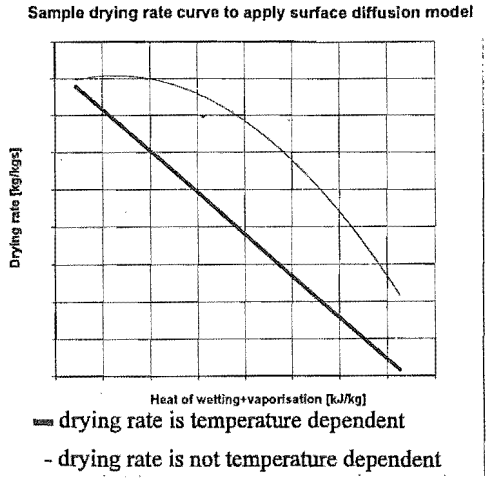

Figure 3.1 Drying rate against heat of vaporisation + heat of wetting

3.4 WATER CLUSTERING AT LOW MOISTURE CONTENTS (< 1%)

The concentration dependence of the diffusion coefficient decreases with increasing concentration for several less hydrophilic polymers. Very often this decrease in diffusion coefficient is distinctly noticeable with increased concentration. Rouse (1947) proposed that such behaviour was explicable by postulating clustering of the water in a polymer so as to render a proportion of it comparatively immobile. Clustering may be initiated at polar centres or, for the harder plastics, in microcavities existing in the polymer matrix. Cluster growth in the polymer will differ from that in free species because of the potential field of the surrounding polymer and because of steric factors which effectively limit the size of a cluster to that of the microcavity (Barrer and Barrie, 1958). On the other hand, with highly flexible polymers such as polydimethalsiloxane, association of the water may occur in a completely random fashion throughout the polymer. Non-active hydrophobic surfaces in particle structures favouring water molecules binding to this type of surface are driven by entropic electrostatic forces (hydrophobic interaction) and enthalpic (hydrogen-bonding) processes. Poor fitting of the LBGAB sorption isotherm correlation indicates that the bonding of a solvent to hydrophobic or non-active surfaces in the materials investigated resulted in simultaneously occurring "entropic and enthalpic driven process" (Franks, 1972). Once an equivalent monolayer has been formed, the developing progressive layers indicate the formation of water clusters in the solid structure, as non-active surfaces do not induce stronger bonding in higher layers as active surfaces do (silica gel). Although drying involves simultaneous heat and mass transfer, it is possible, under given conditions, to consider desorption as an isothermal process (Cobbinah, 1984) This is specially the

case when the moisture content is low. To a first approximation, the drying may be described as a vapour diffusion process. Drying of these water clusters can then be evaluated by solving Fick's second law of diffusion. In the case of radial diffusion, where linear flow exists in one dimension, Fick's second law of diffusion may be written

$$\frac{\partial u}{\partial t} = D\frac{\partial^2 u}{\partial x^2} \tag{3.9}$$

Note that Equation 3.9 is a derived form where

$$u = Cr \tag{3.10}$$

and C is the moisture concentration.

Keey (1992) reported that generally the surface moisture content will generally fall progressively rather than instantaneously to the equilibrium moisture content. For example, in the drying of polymer-based media, the large population of water clusters at or near the particle's surface may decrease in number as drying proceeds. For a first-order process, one expects an exponential decline,

$$X_s(t) = X_o\left[1 - e^{-\frac{\beta_x t}{R}}\right] \tag{3.11}$$

which corresponds to the boundary condition

$$-D\left(\frac{\partial X}{\partial r}_R\right) = \beta_x(X_s - X_e) \tag{3.12}$$

where β_x is an effective mass transfer coefficient, on the assumption that the rate of moisture loss is directly proportional to the excess moisture content above equilibrium.

The solution of Fick's second law for this boundary condition is given by Crank (1970), resulting in the mean moisture content of the particle as described by Keey (1992):

$$\frac{X - X_e}{X_o - X_e} = \sum_{n=1}^{\infty} \frac{6Sh^2 exp(\gamma_n^2 Dt/R^2)}{\gamma_n^2\left[\gamma_n^2 + Sh(Sh-1)\right]} \tag{3.13}$$

Figure 3.2 shows curves of $(X - X_e)/(X_o - X_e)$ plotted as a function of $Fo_M^{1/2} = (Dt/R^2)^{1/2}$ for several values of Sh for which Newman (1931) gave tabulated values. For

Sh>1, the moisture loss curves are exponential with time, consistent with a first-order process implicit in the assumed surface boundary conditions.

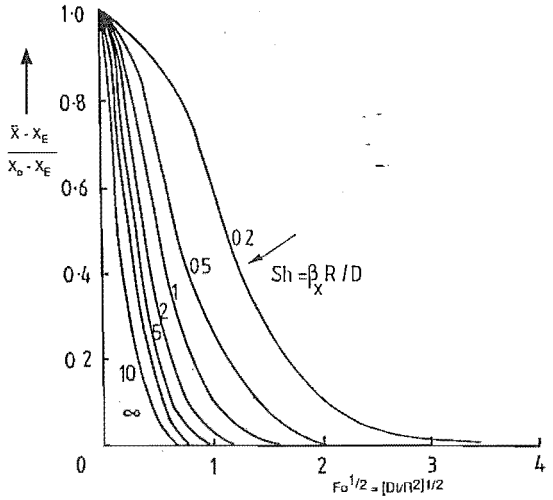

Figure 3.2 Mean moisture content of a drying sphere with an initial moisture content X_o, subjected to the stated surface boundary condition above. The parameter is the effective Sherwood number (adapted from Crank, 1970; Keey, 1992)

In the case where the surface moisture concentration is maintained at a uniform moisture content X_e (say the equilibrium value with respect to the particle's surroundings); this may be the case with the drying of single particles or a very thin-layer. When the surface moisture is exposed to a faster decrease in moisture content to the equilibrium value when compared with increasing layers, the moisture content profile at any time t becomes

$$\frac{X-X_o}{X_e-X_o}=1+\frac{2a}{\pi}\sum_{n=1}^{\infty}\frac{(-1)^n}{n}sin\frac{n\pi r}{a}exp(-\frac{Dn^2\pi^2}{a^2}) \tag{3.14}$$

The concentration at the centre is given by the limit as $r\rightarrow 0$, that is by

$$\frac{X-X_o}{X_e-X_o}=1+2\sum_{n=1}^{\infty}(-1)^n e^{-\frac{Dn^2\pi^2 t}{a^2}} \tag{3.15}$$

The average relative moisture content is given by

$$\Phi = \left(\frac{X - X_{eq}}{X_o - X_{eq}}\right) = \frac{6}{\pi^2}\sum_{n=1}^{\infty}\frac{1}{n^2}e^{-\frac{Dn^2\pi^2 t}{a^2}} \tag{3.16}$$

The solution to this equation can be written in terms of the dimensionless parameter Φ as a function of Dt/a^2, the Fourier number for mass transfer. For values of the ratio Dt/a^2 greater than 0.1 (Steinmetz *et al.*, 1991), Equation 3.16 can be limited to the first term of the series. It is then equivalent to

$$ln\Phi = ln\frac{6}{\pi^2} - \pi^2 D\frac{t}{a^2} \tag{3.17}$$

If the isothermal diffusion model is applicable, experimental values of relative moisture content can be fitted by Equation 3.17. The slope value of the straight line $ln\Phi$ with t allows the calculation of the diffusion coefficient. If a straight line is not achieved by using Equation 3.17, then Equation 3.16 can be used to extract the diffusion coefficient.

For the case of a variable diffusion coefficient in Equation 3.13 i.e. say when D decreases with diminishing moisture content, which is the normal case in the drying of moist materials, the shape of the moisture loss curve is only moderately influenced by the nature of the concentration-dependent function of the diffusion coefficient can be calculated from the plot in Figure 3.3. Crank's ideas (Crank, 1970) suggest that, to describe the individual drying of small particles in isolation, one should use an empirical, constant moisture diffusion coefficient.

3.5 CONDUCTIVE HEAT DRYING MODELS AT LOW MOISTURE CONTENTS

General

In many types of industrial driers, such as cylinder driers for sheet materials or vacuum freeze driers for foodstuffs or medicines, the moist material is in contact with a heated metal surface. In such conductive drying, heat is directly conducted through the material and higher drying rates can be obtained than in the usual hot air drying. For the drying of particulates with low moisture contents, conductive heat drying under vacuum is probably the most successful technique. For this type of drying, not only external heat transfer coefficients are important, but also the transport properties of moisture through the particulates are significant. Producing a vacuum increases the ability for molecular diffusion of the moisture vapour in the porous networks. In most practical cases convection can be excluded because the Grashof numbers are usually relatively low. The combined effect of temperature and vacuum level on the drying of

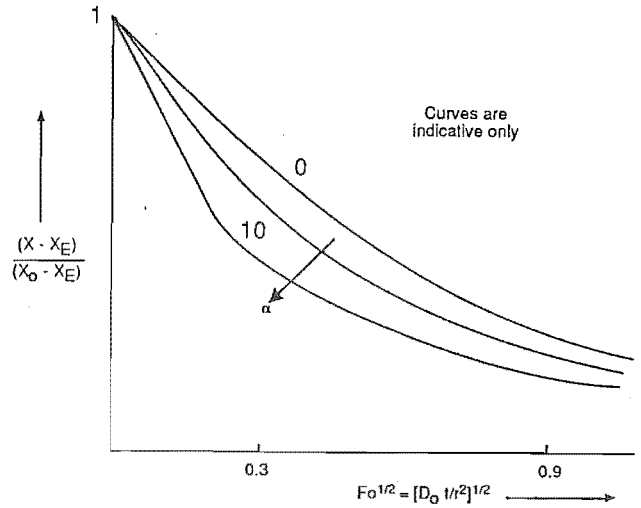

Figure 3.3 Generalised moisture loss curve for a linear concentration-dependent diffusion coefficient, $D = D_o(1 + \alpha X/X_o)$(adapted from Crank, 1970; Keey, 1992)

particulates with low moisture contents is the main factor for successful drying into an equivalent monolayer in individual particles.

Heat/mass transfer equations given by Okazaki *et al.* 1978

The process of conductive heat drying without the transfer of liquid water has been described by Okazaki *et al.* (1978) by the following set of non-linear partial differential equations.

- The heat transfer equation is given by noting that the conduction provides both heating of the material and the evaporative heat load:

$$(C_{ps}\rho_b + X_v \varepsilon C_{pw}\rho_w)\frac{\partial T}{\partial t} - \Delta H_v \varepsilon \rho_w \frac{\partial X_v}{\partial t} = \frac{\partial}{\partial x}\left(\lambda_e \frac{\partial T}{\partial x}\right) \qquad (3.18)$$

where the initial boundary conditions are the following:

- $X_v = X_{vo}$ and $T = T_o$ at t=0
- $T\,|_{x=L} = T_b$ and $X_v\,|_{x=0} = 0$ at $t > 0$
- $\lambda_e \partial T/\partial x\,|_{x=0} = \alpha(T_a - T\,|_{x=0})$ at $t > 0$

- $[-DM_w/RT]\partial p/\partial x\,|_{x=0} = \beta(p\,|_{x=0} - p_a)$ at t>0

Okazaki *et al.* (1978) had limited success in accurately predicting their experimental drying rates, probably from assuming a linear relation of temperature with water vapour pressure and from not having heat of desorption data on the solids investigated. Okazaki and colleagues used dual receding evaporative fronts approaching one another. One away from the top surface of the drying bed, which was exposed to vacuum, and the other away from the heated contact surface at the base of the bed. They used this approach to model the removal of liquid moisture from interparticle drying at low moisture contents. However, at very low moisture contents, a receding evaporative front from the upper surface would be unlikely to occur, due to the absence of interparticle moisture or capillary movement of moisture. In this work, Okazaki's model was modified (equations follow) to look only at a possible receding evaporative front extending away from the contact heated surface. Accurate fitting of this model may suggest the existence of a sharp evaporative drying front extending away from the contact surface, instead of a more even loss of moisture from the entire bed as drying proceeds.

Simple prediction of drying time (modification of work by Okazaki *et al.* (1978)

The process of contact drying from a heated surface may be described using (Figure 3.4

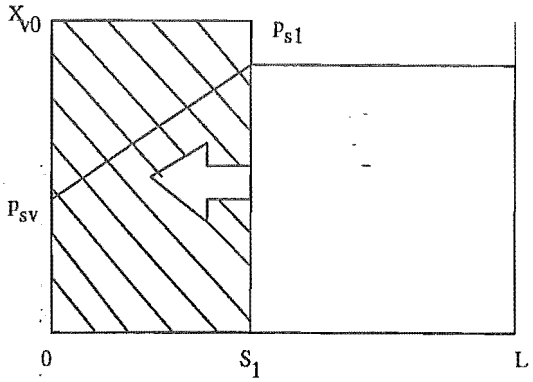

Figure 3.4 Evaporative plane from base of drying chamber

The moisture content in the moist zone is assumed to remain constant during the whole period of drying. Only one-dimensional heat and mass flows, normal to the surfaces, are considered. Evaporation occurs at the moving boundary parallel to, and at distances $0 < x(s_1) < L$ from, the bottom of the sample. The thickness of the moving boundary is taken to be infinitesimal. The dried regions are considered to be homogeneous, of constant thermal properties described by equivalent thermal

quantities. The sides of the particulate bed are assumed to be perfectly insulated against the transfer of heat and mass. The set of equations describing the positions of the evaporative planes and temperature profile are as follows.

From the model shown schematically in Figure 3.4, the heat balance equation at $x=s_1$ is

$$\lambda_{ed}\frac{T_b - T_1}{L - s_1} - \lambda_{ew}\frac{T_1 - T_v}{s_1} = \frac{DK_p\Delta H_v T_1 - T_v}{RTs_1} \tag{3.19}$$

or simply, heat conduction through vapour - heat conduction through liquid = heat involved with evaporation. Equation 3.19 incorporates a linear isotherm where K_p is the temperature coefficient of saturated vapour pressure of water shown by

$$p_s = K_p T + c \tag{3.20}$$

and c is a constant.

$$\lambda_{ed}\frac{T_b - T_1}{L - s_1} = \frac{DK_p\Delta H_v T_1 - T_v}{RTs_1} + \lambda_{ew}\frac{RT_m(T_1 - T_v)}{RT_m s_1} \tag{3.21}$$

$$\lambda_{ed}\frac{T_b - T_1}{L - s_1} = \frac{(T_1 - T_v)}{RT_m s_1}[DK_p\Delta H_v + \lambda_{ew} RT_m] \tag{3.22}$$

$$[T_1 - T_v] = \lambda_{ed}\frac{T_b - T_1}{L - s_1}\frac{RT_m s_1}{[DK_p\Delta H_v + \lambda_{ew} RT_m]} \tag{3.23}$$

Taking the mass balance at $x=s_1$;

$$\varepsilon X_{v0}\rho_w\frac{ds_1}{dt} = \frac{DK_p(T_1 - T_v)}{RT_m s_1} \tag{3.24}$$

The elimination of T_v from Equations 3.21, 3.24 gives the following equation:

$$\varepsilon X_{v0}\rho_w\frac{ds_1}{dt} = \frac{D_{eff.}K_p\lambda_{ed}(T_b - T_v)}{\lambda_{ew}(L - s_1) + \lambda_{ed}s_1} \tag{3.25}$$

which is then modified to

$$\varepsilon X_{v0}\rho_w \frac{ds_1}{dt} = \frac{DK_p}{RT_m s_1}\lambda_{ed}\frac{T_b - T_1}{(L - s_1)}\frac{RT_m s_1}{[DK_p\Delta H_v + \lambda_{ew} RT_m]} \tag{3.26}$$

$$\frac{ds_1}{dt} = -\frac{1}{\varepsilon X_{v0}\rho_w} DK_p\lambda_{ed}\frac{T_b - T_1}{(L - s_1)}\frac{1}{[DK_p\Delta H_v + \lambda_{ew} RT_m]} \tag{3.27}$$

$$(L - s_1)ds_1 = -\frac{DK_p\lambda_{ed}(T_b - T_1)}{\varepsilon X_{v0}\rho_w[DK_p\Delta H_v + \lambda_{ew} RT_m]}dt \tag{3.28}$$

$$\left[Ls_1 - \frac{s_1^2}{2}\right]_{s_{1o}}^{s_1} = -\frac{DK_p\lambda_{ed}(T_b - T_1)}{\varepsilon X_{v0}\rho_w[DK_p\Delta H_v + \lambda_{ew} RT_m]}[t]_0^t \tag{3.29}$$

Boundary conditions: $s_1 = 0$ at $T = T_1$, $s_1 = L$ at t=0, $s_1 = 0$ at $t = \infty$

Solving the equations for s_1 using a quadratic expression gives

$$s_1 = L - \sqrt{\frac{2DK_p\lambda_{ed}(T_b - T_1)}{\varepsilon X_{v0}\rho_w[DK_p\Delta H_v + \lambda_{ew} RT_m]}t} \tag{3.30}$$

The velocity of the projected evaporative front is

$$\frac{ds_1}{dt} = -\frac{DK_p\lambda_{ed}(T_b - T_1)}{\varepsilon X_{v0}\rho_w[DK_p\Delta H_v + \lambda_{ew} RT_m]}\sqrt{\frac{2DK_p\lambda_{ed}(T_b - T_1)}{\varepsilon X_{v0}\rho_w[DK_p\Delta H_v + \lambda_{ew} RT_m]}t} \tag{3.31}$$

This model will predict the velocity of an equivalent evaporative plane (if one exists) progressing through the particulate bed during drying. However, this model would neglect intraparticle heat/mass transfer resistances. Limited success with fitting this drying model to experimental results would accentuate the importance of intraparticle effects during residual drying processes. Also, the heat of wetting data on drying a solid should be incorporated in to this type of approach. A good agreement with experimental results with matching temperature profiles would indicate that local bed temperatures do affect the kinetics, and that interparticle vapour diffusion resistances in the bed exist.

Plotting the progressive temperature profiles within the bed as a function of time (Figure 3.5), and simultaneously plotting the velocity of an equivalent evaporative plane would indicate what important factors (discussed above) effect the kinetics.

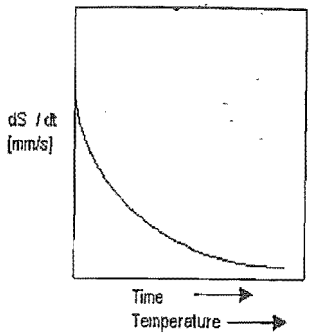

Figure 3.5 Velocity of evaporative front as a function of time and layer thickness of dried layer (compare Figure 6.11)

Heat/mass transfer equations (Mollekopf and Schlünder, 1986)

Particles with residual moisture have a negligibly small capacity for latent heat of adsorption when compared with sensible heat adsorption. There is no evaporation but only heating of the particles. Thurner and Schlünder (1986) often commented that, in contact drying of granulated product, the contact resistance of heat transfer between the particulate mass and the contact surface, rather than the thermal resistance within the particulate bed controls the drying rate. Calculations at low moisture contents indicate that the contact time is not as significant as the bed's thermal resistance. There is no reduction in low moisture drying rates by agitating a particle bed under vacuum (R Keey, *private communication*)

The theoretical drying rate in an isothermal particulate bed in contact drying at steady state can be given by

$$\dot{n} = \dot{n}_{max.} = \frac{\alpha_{ws}(T_H - T_S)}{\Delta H_{v,w}} \tag{3.32}$$

where T_H is the temperature of the submerged surface, T_S is the temperature of the particulate material, ΔH_v is the latent heat of evaporation which a function of vacuum pressure, and α_{ws} is the surface-to-particle heat transfer coefficient. On noting that the heat conductivity of the dilute gas depends on the pressure, and that the surface-to-particle heat transfer coefficient α_{ws} is given by both conductive and radiative effects

$$\alpha_{ws} = \frac{\pi\lambda_g}{d}\left(\frac{d+2(l+\delta)}{d} ln \frac{d+2(l+\delta}{2(l+\delta)} - 1\right) + \frac{4-\pi}{2}\frac{\lambda_g}{\sqrt{2}d+2(l+\delta)} + 5.67 * 10^{12} A(T_1^4 - T_2^4) \quad (3.33)$$

where λ_g is the heat conductivity of the continuum gas, d is the particle diameter, δ is the roughness of the particle, A is the cross-sectional area of the contact surface, T_1 is the temperature of the contact surface or horizontal section, T_2 is the temperature of the "black-box" surroundings. The modified free path is given by

$$l = \frac{2\Lambda(2-\gamma)}{\gamma} \quad (3.34)$$

where Λ is the mean free path of the gas molecules, depending on the pressure, and γ is the accommodation coefficient (water vapour = 0.9). For a static bed (long contact time), heat conduction through a particulate bed is significant. Thus, the time-averaged surface-to-bed heat transfer coefficient is

$$\alpha = \frac{2\alpha_{ws}}{(2+\sqrt{\pi\frac{\alpha_{ws}^2 t_c}{(\lambda_b(\rho c)_b)}}} \quad (3.35)$$

This equation takes into account the rarefied gas effect which applies to vacuum conditions.

When evaluating the drying of particulate beds at atmospheric pressure, one has to consider the convective heat transfer effects of the continuum gas flow. The inverse of individual heat transfer effects may then be added to obtain the reciprocal of the overall heat transfer coefficient.

It is important to know this heat transfer resistance through a particulate bed, given by the effective heat conductivity of the bed, either by theoretical calculation or by experimental determination. Bauer and Schlünder *et al.* (1978) gave the effective heat conductivity of the bed as

$$\frac{\Lambda}{\lambda_b} = F\left(\frac{\lambda_S^*}{\lambda}, \frac{\lambda_R}{\lambda}, \varphi, \psi, \zeta_r, Z_r, \frac{d_{bed}}{d}\right) \quad (3.36)$$

Here, λ is the thermal conductivity of the fluid phase in an infinitely expanding space, λ_S^* is a mean thermal conductivity of the solid phase, and λ_R is the thermal conductivity between the surfaces of the solid phase due to the Smoluchowski effect. The term φ denotes that fraction of the heat transfer due to possible contact surfaces

between the particles, ψ is the mean porosity and ζ_r is the particle size distribution. A influence parameter is expressed by Z_r and the wall influence quantity denoted by d_{bed}/d. A large number of variables are needed to calculate the thermal conductivity of a particulate bed. However, experimental evaluation of local heat transfer (and thus the thermal conductivity) within a particulate bed can be found from the temperature profiles within it.

For non-isothermal drying of a particulate bed, the drying rates can be better described by

$$\dot{n} = \frac{\alpha(T_H - T_S)}{\Delta H_{v,w}} \tag{3.37}$$

where α is the time-averaged surface-to-bed coefficient, rather than α_{ws} the surface-to-particle coefficient applicable to isothermal drying.

3.6 DISCUSSION

Okazaki *et al.* (1978) used a combined heat and mass transfer model to estimate the drying rates. On assuming that simple evaporative drying front would proceed through the drying particulate bed, he then applied both heat and mass balances at this evaporative front to estimate its velocity profile with time.

Mollekopf *et al.* (1986), on the other hand, predicted the drying rates of both isothermal and non-isothermal particulate beds in contact drying, by placing more emphasis on the heat conduction of the particulate bed, and not on the mass transfer resistances. Once the heats of evaporation (heat of wetting plus heat of vaporisation) are known as a function of moisture content and applied vacuum, modelling these small drying rates may be easy for single particles and thin-layers. For thicker beds of particles, other mass transfer resistances may need to be accounted for.

The heat of wetting becomes increasingly significant while drying well into the second falling-rate period; thus the lower drying rates observed in this region may be described in Equation 3.37 by the increase in the heat of wetting. It may be useful to know under what conditions this idea may hold, and the applications where mass transfer resistances become significant.

A number of drying models have been described above in the context of low moisture content drying. Each model has taken a different approach to simulate such drying behaviour.

In summary, progress in determining the transport phenomena of moisture migrating to the surface and then away from the surface at low-moisture contents cannot be described as accurately as when considering higher moisture contents where both

vapour phase and liquid transport occur simultaneously. No one mechanism is likely to dominate over the whole moisture content range of interest in drying. The wide range of materials dried in the laboratory and in commercial practices may result in materials being sub-categorised into groups with similar pore topology, chemical composition, and either isotropic or non-isotropic and swelling/non-swelling media.

Chapter 4

PRELIMINARY SORPTION AND DRYING KINETICS

4.1 CALIBRATION OF EQUIPMENT

4.1.1 Pressure gauges

Two pressure gauges were tested to check their accuracy in reading varying pressures over the range 30-1000 *mbar* (boiling point for pure water between 25 and 100*degC*). To do this, a saturation pressure curve for water was constructed from its Antione coefficients. Distilled water was put in a beaker, with a *k-type* thermometer, in the vacuum oven, the pressure of which was reduced until the water boiled. The oven temperature was increased and the boiling temperature was recorded. Figure 4.1 is a graph of the calibration results, in which the portable liquid crystal display (LCD) pressure gauge is compared with the vacuum oven pressure gauge against the known atmospheric pressure for that test time taken from an accurate barometer and calculated from the Antione coefficients for water at lower pressures.

Figure 4.1 indicates that the portable LCD and the vacuum oven pressure gauges were accurate enough to use because their readings corresponded well with the barometric calculated pressures, and little deviation existed between pressure instruments.

4.1.2 Thermometers

The accuracy of selected thermometers was investigated to see if they were suitable for these preliminary sorption studies. Two mercury thermometers in glass and two *k-type* thermocouples were used. It was found that one of the mercury thermometers was reading 4*degC* above the rest; it was removed from the experiments.

Note: the dead time for the glass mercury thermometers was up to 15 *min* longer than that for the thermocouples. This was probably due to the additional heating required to heat the glass surrounding the mercury bulb.

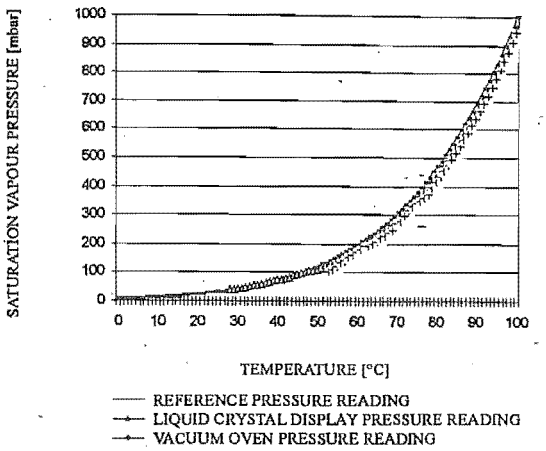

Figure 4.1 Pressure calibration curves

4.2 SORPTION STUDIES AT HARWELL

4.2.1 Static method used to find isotherms

Fifteen 10 g samples of silica gel were placed in separate crucibles, and each was exposed to a different relative humidity using salt solutions, as described by Keey (1978), and was stored at $20 degC$. The types of salt solutions are listed in Table ??. The crucibles were sealed and left to equilibrate over 12 months. It was assumed that equilibrium had been reached after this period. This was a reasonable assumption as the isotherms obtained in this work were similar to those from the dynamic method (thermogravimetric unit).

4.2.1.1 Equilibrium moisture isotherms using SPS dynamic (Figure 4.2) equilibrium moisture content (emc) rig and possible alterations to rig

4.2.1.2 Results of static sorption studies

Table 4.1 shows relative humidities produced from various saturated salt solutions. A silica gel sample was left over 12 months while exposed to a saturated salt solution. The equilibrium moisture contents from the static tests reported in Table 4.1 were com-

paribly similar to those obtained from a dynamic method using the thermogravimetric unit.

Table 4.1 Relative vapour pressures of water from various salt solutions (Keey, 1972)

Saturated solution	Relative humidity, φ	Equilibrium moisture content for silica gel
Lithium chloride LiCl	0.126	7
Potassium acetate CH_3COOK	0.20	12
Calcium chloride $CaCl_2$	0.323	14.8
Potassium carbonate K_2CO_3	0.45	20
Sodium nitrite $NaNO_2$	0.66	23
Ammonium chloride NH_4Cl	0.792	26
Potassium bromide KBr	0.84	26.5
Potassium chromate K_2CrO_4	0.88	27.1
Lead nitrate $Pb(NO_3)_2$	0.98	28
Distilled water	1.00	28.2

The salt solutions provided a range of relative humidities. Each solution was stored in a sealed container with a portion of silica gel 124. The containers were stored in a dark cuboard at a constant temperature ($T_d = 20 degC$) sufficient to remove only mobile or free water from the silica gel particles. A significant amount of free moisture (Zhang *et al.*, 1992) is present in the silica gel material (0.36 $g\ H_2O/gdrysolid$), compared with 0.28 $gH_2O/gdrysolid$ which was desorbed at $T_d = 20\ degC$. Thus, 0.12 $gH_2O/gdrysolid$ remained in the solid matrix during the desorption isotherm. It was therefore proposed that the isotherms be repeated over a larger temperature range to account for the desorption of not only free water but also tightly bound physisorbed water. Using static methods, equilibrium should be allowed to form over a longer period of time (12 months), which can present a time problem. However, this was possible given that the first 12 months of this work programme was at Harwell. It is important to allow complete equilibration to remove residual moisture.

4.2.2 The importance of minimising the experimental scatter in isotherms

This preliminary sorption work done on Harwell's emc rig, was not suitable for plotting sorption isotherms for particulates with low hygroscopic moisture contents. Since the accuracy of plotting sorption isotherms is very important, these tests were performed on an apparatus at Canterbury. The tunnel drier at Canterbury (Figure 2.16) has been shown and discussed in Chapter 2.

The degree of scatter when plotting isotherms very much depends on the control of external conditions. Minimal scatter would provide a more accurate fitting of the correlations. However, regardless of the degree of scatter, the fitting equations to be used should provide a stable "best-fit" solution. It should be possible to decipher the general shape of an isotherm and manually correct the experimental scatter, rather

than input this scatter directly into the fitting equations. Quite often any such scatter can be attributed to the experimental technique rather than to any discontinuity in the solid's behaviour, but also taking into account any possible observed hysteresis from the isotherms. In deciphering scatter from such discontinuities in the solid, often separating the scatter from true sorptive behaviour can be put down to one's experience of plotting isotherms.

4.2.3 The emc apparatus and isotherm experiments at Harwell

A schematic description of the apparatus is shown in Figure 4.2. Air was continuously passed through the sample section causing dynamic sorption between a controlled humid air stream and the particulate solid sample. This was very different from the static sorption technique used above. The water bath capacity was 10 litres so the level of water remained reasonably static for each sorption point plotted. The secondary air heater was used to top-up and control the final sorption temperature.

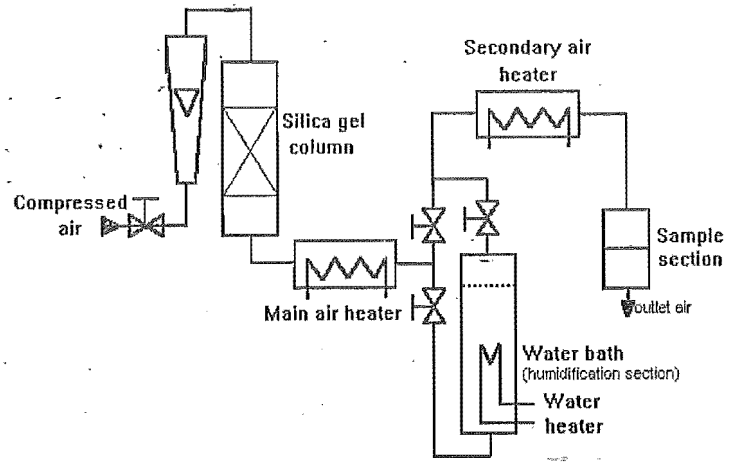

Figure 4.2 Diagram of SPS emc rig

The air flowrate, and dry-bulb and wet-bulb conditions of the air were controlled manually with the help of three on/off controllers for the air and water heating. The secondary air heater was found to be underpowered, even for low flowrates of air. The air velocity significantly affected the heat transfer coefficients in the air heaters. Maintaining a constant dry-bulb temperature over the complete relative humidity range

proved to be very difficult because of the fluctuating heat transfer coefficients and the fluctuating pressure drop in the water bath, see Figure 4.2. It was extremely difficult to obtain the desired accuracy with the air conditions, especially as most of the materials investigated had a very small hygroscopic moisture content range (<1%). More accurate sorption isotherms are possible using this apparatus for larger moisture content ranges. Chapter 5 section sets out the equilibrium isotherms at $20 degC$ for the fine chemicals, adipic acid and terephthalic acid. Inaccuracies with these sorption studies led to the use of the thermogravimetric unit for sorption studies.

4.2.3.1 Alterations to sample section

To prevent introducing errors while reading the sample weights (once equilibrium had been reached), it was proposed to introduce an *in-situ* weighing device for the sample section. Figure 4.3 illustrates the alteration. This modification to the emc rig was not approved by SPS staff, so these modification were not implimented.

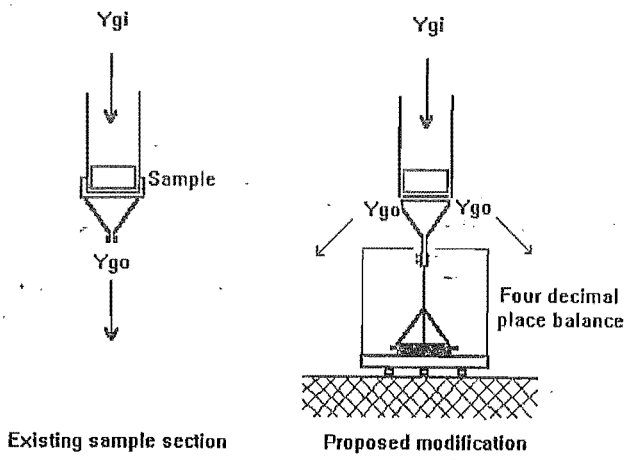

Figure 4.3 Modification to SPS emc rig

4.2.3.2 Connecting a line from the emc rig to the inlet gas section of the thermogravimetric (TG) unit

The TG unit was provided with an inlet gas section to permit a controlled flow of wet or dry gas to pass through/around the sample. This permitted an *in situ* weighing of

the sample, but limited the evaluation of the isotherms to that at room temperature, because there was insufficient insulation material to maintain a constant temperature around the sample section. As a result, vapour was condensing in the gas transfer line when hot air from the humidification column condensed before entering the TG unit.

4.2.4 Nitrogen sorption by single point BET (AEA intec)

The materials listed in Table 4.2 are all mostly microporous (at the surface, macroporous cracks may be present). Sorption studies and drying kinetic studies were also performed on New Zealand West Coast iron sand (titaniumagnite). Table 4.2 also indicates the general appearance and dimensions of the materials used in this work.

Table 4.2 Some characteristics of the selected materials in this work

Sample	BET specific surface area, $(m^2 g^{-1})$	Mean particle size and shape (μm)	Comment
Silica gel (type B)	450 [1]	1850, spherical	very rigid microporous structure
Alumina	150 [2]	140, spherical	white cohesive powder
Terephthalic acid	0.21	130, spherical	wet terephthalic acid
Adipic acid	1.04	50, spherical	white cohesive powder
Terephthalic acid	0.21	130, spherical	dry terephthalic acid
Copolymer # 1	0.58	700, spherical	non-porous white rubber
Copolymer # 2	< 0.05	4000, spherical	gelatinous white rubber
Copolymer # 3	0.51	500, spherical	non-porous yellow rubber

4.2.4.1 Using the TG unit for equilibrium isotherms

The Stanton-Redcroft TG760 thermobalance is designed to give a direct plot of weight loss against temperature for any sample over the temperature range from ambient to $1000 degC$. A diagram of such an apparatus is shown in Figure 4.4.

The following features may be seen.

- The sample is contained in an 8 mm diameter sample crucible made from platinum.
- The sample temperature is measured by a thermocouple carried in a twin-bore alumina rod.
- The plate has been positioned accurately at a distance of approximately 0.5 mm from the sample pan and suspension.
- The sample is heated using a microfurnace mounted in the body of the unit.

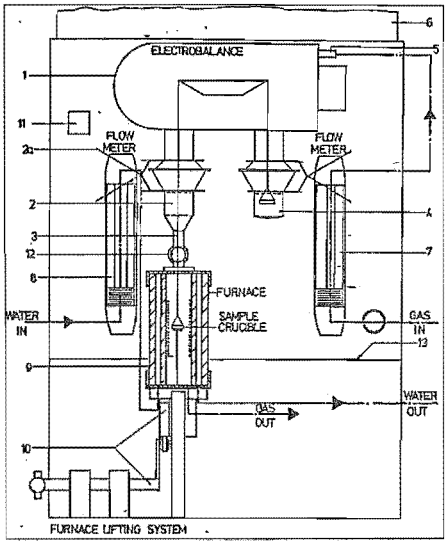

Figure 4.4 Furnace and sample section

- Another thermocouple is carefully positioned in contact with the furnace wall and is used as the temperature controller.

In the Harwell unit, analogue signals are plotted continuously on a chart recorder. From Figure 4.4, it can be seen that a flow of gas can pass around or through the sample (dry or wet gas). The allowable flows are between 1 and 100 $ml\ min^{-1}$, although a flow of 80 $ml\ min^{-1}$ is a convenient flow to use, as suggested in the TG apparatus operating manual. The features shown in Figure 4.4 are as follows.

1. The electronic microbalance and glass vacuum assembly.
2. Glass ball and socket joint, 2a - spring clip.
3. Glass hangdown tube.
4. Glass cap to cover poise pan.
5. Vacuum connectors.
6. Metal front cover to protect balance from extraneous light.
7. Gas flow meter.
8. Water flow meter.

9. Furnace assembly.

10. Furnace lifting mechanism.

11. Level indicator.

12. Hangdown tube retaining bracket.

13. Top of furnace assembly console.

A section through the microfurnace unit is shown in Figure 4.5. The body is made from chromium-plated brass and is watercooled by means of a number of interconnected vertical channels. The features shown in Figure 4.5 are as follows.

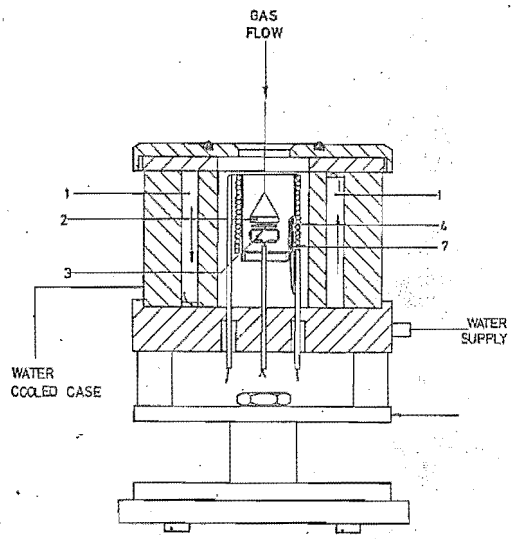

Figure 4.5 View of sample section and furnace of TG unit

1. Interconnecting vertical channels

2. Sample pan.

3. Thermocouple.

4. Microfurnace.

5. Thermocouple.

With a sensitivity of the balance, given at installation by manufactures, of $5 \pm 0.1 \mu g$ and the excellent control of gas flow temperatures ($< \pm 0.1 degC$), the TG unit could be used to obtain moisture isotherms accurately. Because considerable information on the behaviour of silica gel is available, this material was chosen as an initial material to test the procedure of getting sorption isotherms.

An air line was connected from the existing emc rig close by to the gas inlet line on the TG unit. Isotherms were done at $20 degC$ and $40 degC$.

4.3 THERMOGRAVIMETRIC ANALYSIS

4.3.1 Thermogravimetric analysis (TGA) of silica gel from 25 to 1000

Further experiments were performed on the same electronic microbalance to get an insight into:

- the operation of such a device;
- its possible use in the new vacuum drying apparatus at Canterbury;
- the reproduction of previous thermal analyses on a known material.

The TG unit was calibrated using calcium oxalate monohydrate with known changes in chemical structure with increasing temperature (calibration procedures for the TG760, operating manual by Stanton-Redcroft Ltd., London, U.K.) Using an electronic microbalance has both advantages and disadvantages with it being used in the new drying kinetics apparatus.

4.3.1.1 Advantages of TGA

1. The apparatus gives continuous weight loss profiles of samples weighing up to $5g$ with a reproducibility of $1/10$ μg. Thus, even if weight losses were observed below 1% percent moisture content (50 000μg), the microbalance would be able to resolve any differences in weight loss.
2. The microbalance has a rigid glass housing which can sustain an internal vacuum of down to $10^{-4} Pa$.
3. It is available with a 20 bit A/D card to increase the frequency of measurements
4. Software allows once mechanical tasks to be done from the keyboard.
5. It is relatively inexpensive when compared with other methods of monitoring desorption profiles of gases to resolve drying behaviour.

4.3.1.2 Disadvantages of TGA

1. The unit requires careful installation and is prone to damage if the operator is careless during loading/unloading of samples.
2. For cross/through circulation of air, flows are small due to air causing the sample to move, requiring careful design of the sample housing.
3. The balance requires an extremely stable environment to reduce vibrations from external sources.
4. Like all balances, it must be kept at a constant operating temperature to minimise offset in balance readings.
5. Components of the balance, such as counterweights and balance arms, must be kept clean and in a place such that they will not get misplaced.

There were some clear positive attributes for microbalances for use in the new vacuum drying rig, but it was important to minimise the problems associated with installation and operation of microbalance equipment.

In an attempt to duplicate previous results on the thermal analysis of silica gel, an experiment was designed to use the Stanton-Redcroft TG unit, and thus get a feel for the operation of such an instrument.

4.3.2 Sorption studies by thermogravimetric analysis (TGA)

TGA was found to be very useful for plotting successive single points for sorption isotherms for silica gel at temperatures of $20 degC$ and $40 degC$, although for other materials it was necessary to use higher temperatures to get adequate desorption. A very low flow of air 10 $ml\ min^{-1}$ was used. Once a stable reading was obtained (normally over 24 hours), the air flow was dropped for plotting desorption isotherms. Modified TGA units for automated sorption isotherms are currently available (CI Electronics, Ltd., Wiltshire, U.K.). However, this unit, it was not possible handle a high humidity air flows. Figure 4.6 shows a comparison between the isotherms obtained using the static method and dynamic sorption isotherms from the TG unit.

Isotherm temperatures were limited to near ambient temperatures. For low-moisture sorption, higher sorption temperatures were required; thus TGA was not suitable for sorption isotherms at low moisture contents.

A thermal analysis curve for silica gel indicated the temperatures at which both physisorbed and chemisorbed moisture were removed. A small sample of silica gel (d_p =0.4 mm) was placed in a platinum crucible and heated at a constant rate of $10 degC\ min^{-1}$ from 25 to $1000 degC$. The loss in weight, which was plotted as a function of temperature, is shown in Figures 4.7 and 4.8.

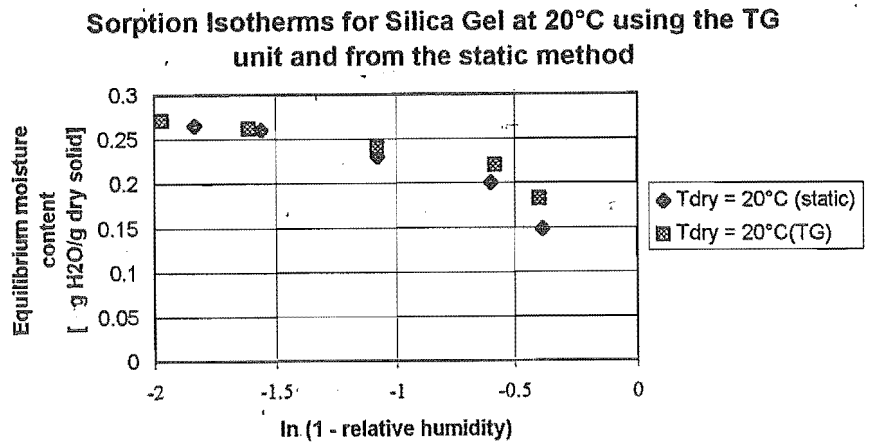

Figure 4.6 Comparing two methods of obtaining isotherms at 20degC

Both graphs indicate that the removal of free water from the microporous structure of silica gel takes place between 25 and $170 degC$, although the resolution of the desorption of bound water was less evident in the Harwell experiment. The Harwell microbalance plotted the results on to chart paper, so only a limited number of points could be transferred into computer data by hand. The new microbalance eliminates this problem by providing more frequent data logging. This result indicated that the low-moisture drying kinetics apparatus should then be designed to produce temperatures of at least $150 degC$ (design constraint) for the removal of all physisorbed moisture from particulate materials.

The sorption isotherms from the static and TG units were comparible (Figure 4.6. This was probably a result of using two different types of silica gel from different vendors. However, one should question the usefulness of the TG unit for sorption isotherm work for the types of materials used in this work, because of the limited range of air humidities that can be produced in a TG unit. Recent work by CI Electronics Ltd., Wiltshire, U.K., have recognised and solved this problem by modifying and automating a TGA/DSC unit for use in plotting complete sorption isotherms for a range of temperatures. However, earlier in this research programme it was recommended, that sorption isotherm work be done on very thin-layers of particulate materials, fully exposed to a very low continuous air stream, for the entire isotherm, with excellent control on the air conditions. Unless the drying chambers are pressurised (for use with saturated steam) so that isotherms can be evaluated, the upper limit for full sorption isotherms (plot complete range of relative humidities) was found to be up to $90 degC$ to fully desorb all physisorbed low-moisture.

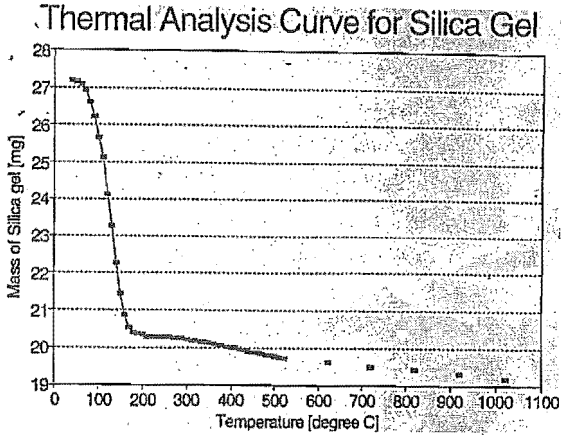

Figure 4.7 A plot of weight loss of water from silica gel from a temperature of 25 to $1000 degC$, (gas flowrate $60 ml\ min^{-1}$ of nitrogen; diameter of furnace $10 mm$)

4.3.3 Experimental test conditions for TGA/DSC work at Harwell

Experiments were performed on a Torledo Mettler differential scanning calorimeter, model no. 1105 and a Stanton-Redcroft thermogravimetric unit, model no. 760 in parallel in an attempt to duplicate results obtainable from a coupled DSC/TG apparatus. In-house software enabled data logging of the heat flow (mW), heat rate ($10 degC/min$), temperature from the DSC, and weight loss ($\pm$ 1/10 μg), temperature readings ($degC$) from the TG unit. The evaporation of pure liquids (distilled water, methanol, cyclohexane) and of pure liquids from porous substrates was investigated. Materials were pre-dried in a silica gel desiccator for 7 days, and then were exposed to a free liquid surface for a further 7 days, the three liquids being in separate chambers, after which time it was assumed that enough liquid was able to diffuse into the separate materials to reach equilibrium. All the sample scans containing water, methanol or cyclohexane were run from 30 to $175 degC$. Three separate runs were made for each material. First, the empty sample cup was measured against the empty reference cup. The blank run was subtracted from the sample run in order to obtain the absolute instantaneous heat flux (dH/dt) required for the subsequent calculations. A dry sample run (minus the blank run) was then subtracted from the sample run. This eliminated the power resulting from the heat capacity of the dry matrix, on the assumption that the heat capacity of the matrix material was not a function of hydration.

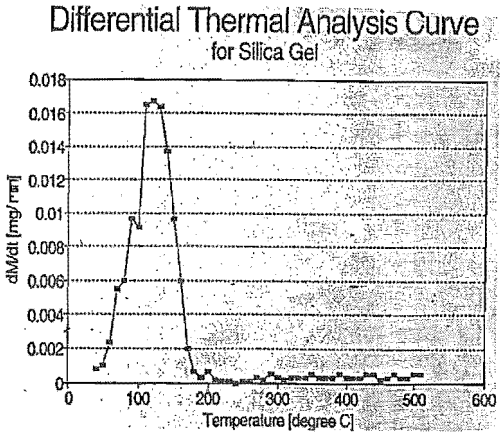

Figure 4.8 Rate of weight loss taken from Figure 4.7, compare similarity to 2.36

4.3.3.1 Sample preparation for TGA and DSC tests

A sample was first removed from the humidification chamber and divided into two equal parts. They were then made to have equivalent weights ($\pm$ 0.005g) by an accurate balance (with sensitivity 0.0001 g). After this, the samples (including pans) were placed in the respective instruments. Once the experiment was finished, the samples were again weighed to account for the weight loss during the experiment.

Both the TG unit and the DSC units' were run under identical conditions, e.g. heat rate 10degC, air flowrate over/through sample 60-70$ml\ min^{-1}$ dry air/nitrogen, except that contact heating was the source for the DSC unit, with conductive and radiation heating for the TG unit.

4.3.4 TGA/DSC Results

4.3.4.1 Effect of varying scan rate in DSC tests

The temperature dependence of the heat of vaporisation of water has been found to be a function of scan rate. The TGA/DSC unit was first calibrated by drying water only using the TGA/DSC crucibles. Figure 4.9 shows a plot of the heat of vaporisation of water measured at $75 degC$ as a function of scan rate. The asymptotic value plotted for the asymptotic limit of 0 $degC\ min^{-1}$ scan rate is the literature value (Etzler and Conners 1991) of the heat of vaporisation within a few percent. The calorimeter should be operated at a scan rate that is slow enough to avoid a significant lag between power and mass measurements that may be due to different response times of the calorimetric and mass signals, as well as to thermal and mass transport effects within

the calorimetric zone of the instrument. The line drawn through the data points is the least squares fit of the measured points. Etzler and Conners (1991) measured the scan rate up to 5 ($degC\ min^{-1}$) and further extrapolation of their least squares fit (dotted line) shows a very low heat of vaporisation of water if the scan rate was taken at 10 ($degC\ min^{-1}$). Experiments here at $75 degC$ had scan rates of 10 [*degC/min.*] and this additional parameter is plotted on the graph with an adjusted least squares fit (full line). From steam tables at 75 $degC$, $\Delta H_v = 2319.2 kJ kg^{-1} = (2319.2/4186.8) * 100 = 553.9 cal g^{-1}$.

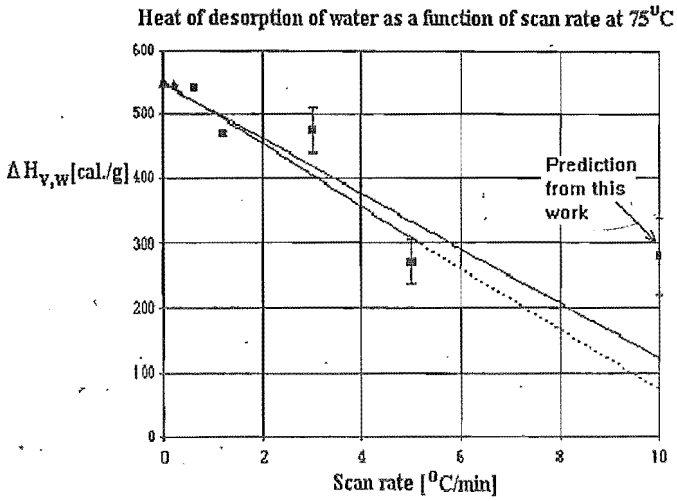

Figure 4.9 Effect of varying the scan rate in DSC tests. Original graph from Etzler and Conners (1991) and this work

The effect of varying the heat scan rate on the DSC unit has a predominant effect on the calculating the heat of wetting at low moisture levels. The typical heat scan rate for measuring the heat of vaporisation of liquids is 10 $degC\ min^{-1}$ but Figure 4.9 illustrates that greater accuracy is possible using lower scan rates. A further point was plotted on this graph to help extend the region of the plot. However, this further point was calculated from data for material that had interparticle moisture removed.

Etzler and Conners (1991) gave a proportional relationship over a scan rate up to 5 $degC\ min^{-1}$. A further point was added to show a further propagation of error under a 10 $degC\ min^{-1}$ scan rate. The result does indicate that as slow as possible scan rate should be used to calculate accurate heat of vaporisation or heat of wetting values. This is especially the case for the calculation of heats of wetting of moisture

from particulate material at low moisture contents. Based on these results, a scan rate of 1 $degC\,min^{-1}$ was used in these tests.

This work on the heat of vaporisation of pure water was used as a basis to examine the heat of desorption (heat of vaporisation + heat of wetting) of water from porous matrices. A range of materials was investigated. Most of the water, not bound directly or indirectly to the material's surface, had a heat of vaporisation equal to that of pure water. However, once drying commenced below the low moisture contents (which most of these materials had), there appeared to be a marked increase in heat of desorption.

Figure 6.18 shows the heat of desorption against moisture content of water from silica gel with an average pore size of 5 *nm*. Because the surface area of this silica gel sample was known, it was possible to calculate the equivalent monolayer loading on the silica gel surface. This indicated that all water molecules in the 5 *nm* pores experienced an anomalously high heat of desorption, which suggests that the active surface slightly changes the molecular arrangement of liquid water, to that of molecular bonding of water with silanol sites on the silica gel surface. This figure also shows a comparison of the three methods of obtaining the heats of desorption from porous matrices. The method from sorption isotherms using the Clausius-Clapeyron relationship is the most widely used method of obtaining heats of sorption data, and this work recommends its use over the other two methods. Often the lengthy time periods involved with the static methods of obtaining sorption isotherms have discouraged workers, but improved dynamic methods with very good control of wet-dry and dry-bulb temperatures and air flow, and continuous weight measurement have reduced the time period required for isotherm experiments significantly.

The heat of desorption obtained from the isotherms may be used as a standard to compare the other two methods. It can be seen from Figure 6.18 that both the thermodynamic and DSC/TGA methods of obtaining the heats of desorption are similar, but the data show steeper transitions into the monolayer region for silica gel. It has been shown (Anderson and Wickersheim, 1964) that this transition of drying into an equivalent monolayer for silica gel results in uneven drying of the monolayer/multilayer regions, parching some areas of the silica surface while leaving adjacent zones fully hydrated, so a more gradual increase in heat of desorption into the monolayer would result.

The other comparisons between heats calculated from isotherms and by the DSC/TG method are shown in Chapter 6.

As a result of these TG and DSC tests, a number of comments can be made. Firstly, in calculating the heat of wetting with moisture content to low moisture contents, the most accurate technique was found to be from sorption isotherms. This is a reliable technique to estimate the heat of sorption and it is recommended to have an extended use to low moisture contents. Combined TGA/DSC results are very much

faster in estimating the heats of sorption. This method can be made more accurate at lower moisture contents if the heating scan rate is taken as slow as possible, i.e. less than $1 degC\ min.^{-1}$. However, the larger the particles or the greater the estimated interparticle mass transfer resistances, the greater is the error in estimating the heats of sorption at low moisture levels. The Langmuir fitting equation, which is based on thermodynamic principals to calculate the heats of wetting was first presented by Polanyi (1932), this mothod was found to be surpassed by the use of the Clausius-Clapeyron equation, Equation 2.32. Secondly, the main objective of these extensive tests was to calculate accurately the heats of sorption at low moisture contents, and measure the asymptotic behaviour of heats previously inaccurately estimated in this region. It was found that even at very low removable moisture levels, $< 0.01\%$, the heats of sorption had a finite value. However, trapped moisture held in rigid microporous cavities, does exhibit much larger heats of wetting because the solid structure would have to be deformed during the removal of this moisture. The amount of trapped moisture held in a rigid lattice can be determined under pyrolysis of the material, or by drying the solid structure under extreme vacuum conditions.

4.4 DRYING KINETICS STUDIES

4.4.1 Apparatus for experiments

Again the Stanton-Redcroft thermogravimetric analyser (TG761) was used, which yields profiles of weight loss against temperature, was to be used to perform isothermal drying of silica gel samples.

Changes to the TG unit so that isothermal drying experiments could be performed were as follows:

1. Apparatus to produce a gas flow of known humidity, flow rate and temperature was connected to the unit.

2. The temperature programmer (U.T.P.) was set to operate at a constant temperature.

3. A steel mesh crucible ($d_p = 8\ mm$) was made to fit on the pan carrier, large enough to minimise air flow around the crucible, but small enough to ensure that the carrier did not touch the sides of the furnace so that a through-flow of air would be possible.

4.4.2 Types of experiments performed

4.4.2.1 Single particle drying experiments

Single particles of silica gel each of diameter 1.85 ± 0.2 *mm* at an initial moisture content of X_e =0.23 *kg water/kg moist solid* were placed in the mesh pan at varying positions to each other (Figure 4.10). Silica gel particles were prepared by keeping them in an enclosure containing saturated air at 25*degC* for 3 weeks. Wall effects for the drying of a particle at the edge of the pan and for the drying of a single particle at the centre were compared. Two particles were placed at opposite ends of the mesh pan, i.e. at a distance of approximately 4 *mm* apart, to compare the drying of a single particle with the drying of two particles at a distance of two particle diameters.

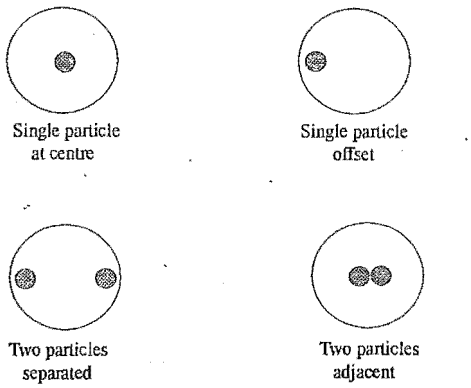

Figure 4.10 Arrangements of single particles

4.4.2.2 Single layer drying

To form a single layer, seven to ten particles were laid side-by-side on the mesh pan and the kinetics were observed.

4.4.2.3 Multiple layer drying

Successive experiments of two (14 particles, shown below), three (28 particles) and four (35 particles) layers were performed and the characteristic drying curves were

compared.

4.4.3 Constructing drying kinetics curves

4.4.3.1 Filtering of data, Raw data → drying kinetics curves

The raw data can either be filtered or, if the raw data are smooth enough, replotted directly as a first-derivative drying rate. Smoothing was performed by applying a nth-order forward-difference by determining the first-derivative drying rate curves. The derivation of the smoothing procedures are shown in Appendix B.

4.4.3.2 The first-derivative drying rate curves

From an evolved gas analysis, which gives an outlet gas humidity profile, the drying rate (*-dX/dt*) can be found by doing a mass balance around the drying sample:

$$-W_s \frac{dX}{dt} = W_g(Y_{go} - Y_{gi}) \tag{4.1}$$

where W_s is the mass of dry material $[kg]$, W_g is the mass flowrate of dry air ($kg\ s^{-1}$), X is the average moisture content ($kg\ kg^{-1}$), Y_{go} is the outlet gas humidity ($kg\ kg^{-1}$), and Y_{gi} is the inlet gas humidity ($kg\ kg^{-1}$). From weight loss measurements, the profile of moisture content against time can be easily calculated.

Drying kinetics curves can be obtained in a number of ways, depending on the form of the raw data. The data can be obtained from either an evolved gas analysis, i.e. from an outlet gas humidity or a mass spectrometer profile, or from a profile of weight loss against time from accurate weighing of the material *in situ*. Outlet gas humidity profiles, by Keech (1992), for the drying of 1-4 layers are reproduced in Appendix A.1.

Once the air conditions (humidity, gas flow) and furnace temperature ($100 degC$) were constant, particle/s were quickly removed from the saturated environment and placed in the mesh pan. The pan was then placed on the suspended carrier arm and lowered into the furnace. A weight loss profile was noted on a chart recorder. When no further weight loss was observed, the unit was reset to the beginning to perform another experiment.

The initial moisture content was calculated from the weight loss and final moisture contents, and checked by exposing a previous sample to an oven at a temperature of $100 degC$ for a day. There was an insignificant initial moisture content difference of $X_I < 0.5\%$ between drying for $< 30 min$, and drying for 1 day. The first derivative of the curve of moisture content against time was found either by a first-order difference between two adjacent points, or by using a forward difference of order 6, followed by curve fitting it to a polynomial of order 2-9 to obtain a smooth curve through the data.

Then to obtain a reduced form of the characteristic drying curve for the falling-rate period, the drying rates ($\ddot{n}$) were normalised to yield the ordinate value

$$g = \frac{\ddot{n}}{[\hat{n}]_o} \tag{4.2}$$

where $[\ddot{n}]_o$ is the drying rate at a moisture content X_o at the beginning of the falling-rate period. The characteristic moisture content (Γ) formed the abscissa:

$$\Gamma = \frac{X - X_e}{X_o - X_e} \tag{4.3}$$

where X is the average moisture content at any time t ($kg\ kg^{-1}$), and X_e is the final or equilibrium moisture content ($kg\ kg^{-1}$).

The results on the effect of bed thickness (1-4 layers) were then compared with those reported previously by Keech (1992), where 1-4 layered experiments were performed on a larger diameter bed of particles. The differences are described:

Two types of experiments are described in this thesis. Firstly, experiments were undertaken to look at the effects on drying kinetics using large samples (6-30 g, as reported by Keech, 1992), and small samples (0.020-0.050 g) using a TG unit. Thicker layers permit the establishment of heat and drying profiles through the layer. The more concave-upward nature of the characteristic drying curves (Figures 2.19 and 2.20 compared to Figure 4.13, in summary of these characteristic drying curves on silica gel 124, see Figure 2.20) showed the difference in drying kinetics behaviour of this bed configuration compared with thinner layers. Smaller samples have a much reduced external vapour diffusion coefficient in the bulk and less resistance to heat transfer through smaller particulate beds of particles, so increased drying rates are observed. Secondly, single particle drying kinetics and the effects of a particle drying within the close proximity of another were investigated, and are shown in Figure 4.13.

4.4.4 Test Conditions for Harwell and Canterbury Drying Kinetics Experiments

4.4.4.1 Harwell experiments - isolated particles and single particle agglomerate trials

These experiments were designed to test the concept of the characteristic drying curve for isolated and agglomerated silica gel 124 particles during exposure to low air flows. These initial experiments at Harwell in 1993 were designed to compare the preliminary tests done on a TG unit, with the same experimental conditions and material. The

new apparatus had a larger bed diameter of 50 mm compared with that of 10 mm in the TG unit. The mass flowrate of air, its inlet temperature and its inlet humidity were kept constant and the drying rates during drying were obtained from a weight loss microbalance (C.I. Electronics, MK2 vacuum head) with a reproducibility of ($\pm$ 1/10 μg). Weight loss and outlet temperature were recorded with drying time. The total drying time of the experiments had a range of 800-2000 s. A forward finite-difference method was used to help extract the drying rate from the loss-in-weight information.

The operating conditions of the experiments using silica gel (SG124) are given in Table 4.3.

Table 4.3 Experimental conditions on new apparatus for single particle trials

	Exp. 1a	Exp. 2a	Exp. 3a	Exp. 4a	Exp. 5a	Exp. 6a
Inlet air temp. ($\pm$ 1$degC$)	100	100	100	100	100	100
Inlet air humidity ($\pm$ 0.005$kgkg^{-1}$)	0.015	0.015	0.015	0.015	0.015	0.015
Layer thickness (mm) ($\pm$0.1)	1.86	1.86	1.86	1.86	1.86	1.86
Initial moisture content ($kgkg^{-1}$) ($\pm$ 0.005)	0.16	0.18	0.18	0.18	0.23	0.21
Superficial air velocity (ms^{-1}) ($\pm$0.002)	0.017	0.017	0.017	0.017	0.017	0.017

The bed configurations for the experiments were as follows.

1. Experiment # 1a: Single particle dried at the centre of the pan.
2. Experiment # 2a: Single particle dried at the edge of the pan.
3. Experiment # 3a: Two particles dried separated by two particle diameters.
4. Experiment # 4a: Two particles dried at the centre of the pan.
5. Experiment # 5a: One layer drying.
6. Experiment # 6a: Two layer drying.

These experimental conditions, listed in Table 4.3, were used to test the effects of varying the bed configurations and to test the effects of using a laminar through-flow of air. The results of varying the bed conditions are tabulated in Table C.1 in the appendix, and are plotted in Figure 4.13. The results of changing the laminar through-flow of air are tabulated in Tables C.2. and C.3. in the appendix, and these are plotted in Figure 6.39.

4.4.4.2 Canterbury experiments - isolated particles and single particle agglomerate trials

These experiments extended those done at Harwell. At higher air velocities (Zhang *et al.*, 1992), it was apparent that SG124 has a single characteristic drying curve under various operating conditions. These conditions are: T_{dry} =100-150$degC$, Y_{gi} (inlet air humidity) = 0.02-0.052 $kg\ kg^{-1}$, superficial air velocity = 3.3-11.5 $m\ s^{-1}$. Very much lower air flowrates were used in the low moisture content drying kinetics rig. These lower air flows ranged between 0.00085 and 0.017 $m\,s^{-1}$, and the drying curves of Figure 6.38 (experiments performed at Canterbury) and Figure 4.13 (experiments performed at Harwell) can be compared. A good match of the characteristic drying curves at low flows to higher flows would indicate a possible extension on the existing limiting conditions on the curves for SG124. Other external conditions were also investigated to extend the application of the characteristic drying curve for SG124 and these can be observed in Figure 6.39.

The operating conditions of the experiments using silica gel were: T_{dry} =100$degC$, T_{dew} = -2$degC$, Y_{gi} = 0.005 $kg\ kg^{-1}$, X_i = 0.17-0.18 $kg\ kg^{-1}$, mass air velocity G = 0.016 $kg\ m^{-2}\,s^{-1}$. The bed configurations for the experiments were as follows.

1. Experiment # 1b: Single particle dried at the centre of the pan.
2. Experiment # 2b: Single particle dried at the edge of the pan.
3. Experiment # 3b: Two particles dried separated by two particle diameters.
4. Experiment # 4b: Two particles dried at the centre of the pan.
5. Experiment # 5b: One layer drying.
6. Experiment # 6b: Two layer drying.

4.4.5 Results of drying kinetics studies

4.4.5.1 Vacuum drying of silica gel (preliminary vacuum drying experiments)

Some preliminary vacuum drying experiments were performed at Harwell to determine:

- the length of time required to drying particulated material to low moisture contents (<0.01%);
- insight into designing the new vacuum/through circulating drying rig at Canterbury;
- the effect of removing samples from the drier to weigh them.

Silica gel was used for convenience in these tests because since it has well-known behaviour in drying. A particle bed of four layers was used, with average particle diameters (d_p) of 0.4 *mm*. Drying temperature =100*degC*, at a reduced pressure of 10^{-2} *mbar*.

It can be seen in Figure 4.11 that the desorption profiles are not uniformly decreasing with time, as expected by drying under vacuum, especially between 65-103 *mins*. (Observe the following plot of moisture content against time).

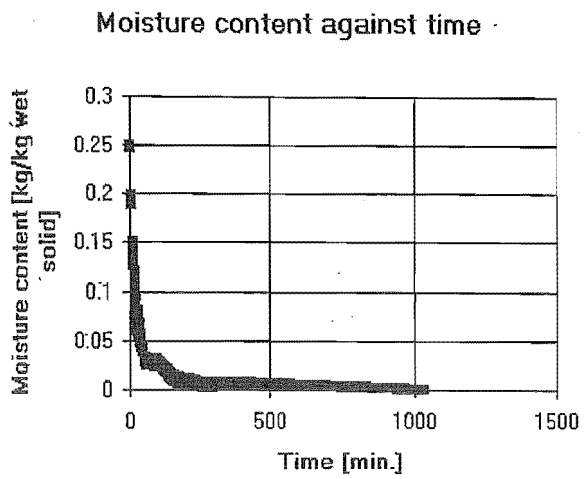

Figure 4.11 Loss in weight of silica gel on drying. Six identical samples were placed in a vacuum oven preheated to 100*degC* and the oven was evacuated to 10^{-2}*mbar*. The intermittent time periods between weighing were not the same, i.e. weights was recorded after: 10, 20, 50, 65, 78, 83, 93, 103, 163, 223, 283, 373, 1030 *min*

This is probably due to the problem of releasing air back into the vacuum chamber, weighing the sample, replacing it, and finally evacuating the system. When samples are being weighed they are exposed to a humid atmosphere, thus disturbing the drying process. During this time period (65-103 *mins.*), four measurements were taken introducing discontinuity's in the drying process over a relatively short period of time.

If the data are relatively smooth, a simple gradient function approach creates a first-derivative drying rate curve. If the data are not so smooth, a smoothing routine may be all that is required before finding the first derivative of the above curve. Notice, from Figure 4.12, the bunching up of data as the curves approach the origin.

This makes it very difficult to determine the drying behaviour in this region. The thicker curve used a sixth-order forward difference technique to provide a smooth fit through the drying rate curve. The thinner "rather wayward" line of Figure 4.12 is the first-order derivative of the original scattered data, calculated from differentiating neighbouring points. From this scattered date is was decided not to defferenciate

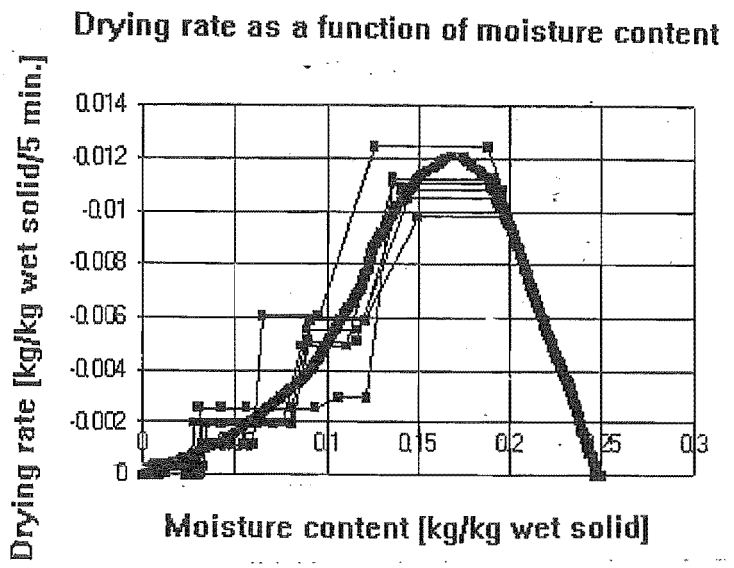

Figure 4.12 Drying rate curve established from noisy data of moisture content against time for silica gel

between each point, but to use forward differencing techniques (up to order 6) to estimate the drying rates for processing the low-moisture kinetics rig data.

From the raw data, it is easy to see the problems associated with removing samples to be weighed. It was therefore imperative that continuous weighing of the sample, or analysis of the continuously evolved gas, had to be used in the design of the new vacuum drying rig.

For each type of experiment, four graphs are presented to represent the drying process (Appendix A.3.1. - A.6.2).

1. Moisture content (X_c) of sample vs. time (t) (Appendix A.3.1, A.3.2).
2. $-dX/dt$ vs. time (t) (Appendix A.4.1, A.4.2).
3. $-dX/dt$ vs. normalised moisture content (Appendix A.5.1, A.5.2).
4. Normalised drying rate (g) vs. characteristic moisture content (Γ) (characteristic drying curve) (Appendix A.6.1., A.6.2).

Note that the normalised and characteristic moisture contents are the same as the final equilibrium moisture content (X_e) which is assumed to be zero.

Additional graphs for the drying of a single particle (Appendix A.1) include:

1. first-order forward difference (slope between two neighbouring points) vs. time;
2. sixth-order forward difference (using six further points) vs. time;
3. sixth-order central difference (using three points either side) vs. time.

These three additional graphs indicated which method of differentiation gave a more stable result. The derivation of the *nth*-order forward difference technique is given in Appendix B.

Attempts were made to smooth the data by applying either a fast Fourier filter, a smoothing routine or a combination of both.

A technical graphics and data analysis software package in WINDOWS, called ORIGIN Version II (MicroCal Software Ltd.), was used. It encompasses a number of methods to smooth data. The ORIGIN package uses a first-order difference to obtain the derivative of the curve simply by activating a key-stroke. For the sixth-order forward difference, the moisture content data had to be exported to a separately written program (which was put on a spreadsheet), changed to a sixth-order difference and then imported back into ORIGIN. The resulting drying rate curve was then fitted to a polynomial regression curve of varying order to obtain a smooth curve through the data. The normalisation procedures followed to form the characteristic drying curves are given below. These are programmed into the package as scripts written in the language of C and these scripts may be altered if the user wishes. These methods include the following.

1. Smoothing which reduces the noise in the data set by the user being asked to specify a number of adjacent points to be averaged. The more data points, the larger is the degree of smoothing.
2. FFT Filter which smooths by fast Fourier transform filtering (Press *et al.*, 1992) by eliminating high frequency noise from the data trend. A dialogue box again allows the user to specify how many data points at a time are to be considered by the smoothing routine.

ORIGIN Version II also has good curve-fitting options available, including three types of exponential decay and a polynomial regression function:

- Exponential decay

$$y = A_1 exp(\frac{-(x - x_o)}{t_1}) + A_2 exp(\frac{-(x - x_o)}{t_2}) \tag{4.4}$$

$$y = A_1 exp(\frac{-x}{t_1}) + A_2 exp(\frac{-x}{t_2}) \tag{4.5}$$

$$y = A_1 exp(\frac{-x}{t_1}) + A_2 exp(\frac{-x}{t_2}) + A_3 exp(\frac{-x}{t_3}) \tag{4.6}$$

- Polynomial regression

$$y = a_o + a_1 x^2 + a_2 x^3 + ... + a_n x^n \tag{4.7}$$

The most appropriate fitting function tested for typical drying rate shaped curves were the two dual exponential forms of Equations 4.4 and 4.5. In the fitting session, the user has complete control over the fitting process. The fitting parameters of $A_1, A_2, ..., x_0, t_1, t_2, ..., a_0, a_1, ...$ can be modified manually or automatically.

Whenever raw data are not smooth enough, calculating the slope between two adjacent points leads to instabilities in the estimated derivative. So it would be useful to use more than two neighbouring points. Here, up to six adjacent points were used in an attempt to predict a better approximation to the derivative at any point along the curve. For completeness, the derivation and mechanics behind forward differencing are given in Appendix B.

Provided the raw data are smooth or can be smoothed, two methods may be employed to enlarge the low moisture content region of drying. Firstly, normalise the drying rates from a number (say plot three separate graphs) of moisture contents on a curve ranging from X_{cr} *to* $X_{0.001}$. This would show any variations in drying kinetics by expanding and overlapping sections of drying in the falling-rate period. Secondly, another option, which contains all information on the same graph, is to plot the natural logarithms of both the drying rates and the moisture contents. A desorption profile can be represented using a relationship between the drying rate and the moisture content as a material dries:

$$\frac{dX}{dt} = f(X) \tag{4.8}$$

Thus, let us assume that this function is a simple algebraic function, where the drying kinetics behaviour can be obtained:

$$\frac{dX}{dt} = k_d (X - X_e)^n \tag{4.9}$$

Taking the natural logarithm of both sides:

$$ln\left[\frac{dX}{dt}\right] = lnk_d + nln(X - X_e) \tag{4.10}$$

A graph of *ln [dX/dt]* against *ln [X]* would give the slope n (order of drying kinetics) and the intercept k_d.

It may not always be possible to fit the drying rate curve to such a simple algebraic expression, Equation 4.8, over the entire moisture content range, but it can be made easier if fitting is performed over a large number of small increments of moisture content. If we make these increments small enough so that we can approximate the gradient between two incremental points to the first derivative, then:

$$n = g(X - X_e) \tag{4.11}$$

where n, the moisture content gradient or the kinetic order of drying, and is a function (called g) of the moisture content difference. k_d, is the rate of desorption and is a function (called h) of moisture content, by

$$k_d = h(X) \tag{4.12}$$

thus

$$\frac{\partial ln\left(\frac{dX}{dt}\right)}{\partial lnX} = I(X) = \begin{cases} n_1(X_1 - X_e) + k_{d_1} \\ n_2(X_2 - X_e) + k_{d_2} \\ \vdots \\ n_z(X_e - X_e) + k_{d_z} \end{cases} \tag{4.13}$$

Graphs of the kinetic order of drying (n) against moisture content (X) and the rate of desorption (k_d) against moisture content (X) can be produced. The results would indicate any changes in drying kinetics during the drying process. If the kinetics do change, then may be this can be explained by the pore topology and/or heats of sorption. Equation 4.13 indicates the slopes (n) and intercepts (k_d) over small increments, thus showing any possible progressive changes in the drying kinetics behaviour.

It was found that Equation 4.13 proved to be unsuitable for fitting the experimental drying data for this work, because here more emphasis was placed on drying kinetics at moisture contents less that 1% physisorbed moisture. No changes in kinetics were observed for the materials tested at low moisture levels, so it is possible that a

single equation of the form given by Equation 4.9 would be all that is required, since n=constant. Notice the characteristic drying curves for the materials investigated in this work: Figures 6.41 to 6.44 indicate little deviation from first-order kinetics (linear appearance of characteristic drying rate curves). However, for the drying of materials with high initial moisture contents to very low levels, a change in the kinetics order of drying may be observed (such is the case for the extreme drying of silica gel from 0.28 $kg\ kg^{-1}$ (physisorbed moisture) to moisture contents less than 1% because patches of chemisorbed moisture from the microporous silica gel surface are removed at this level of drying). In this example using silica gel, Equation 4.13 would be an ideal method of indicating the drying behaviour of materials with high initial moisture contents to extreme drying of a particulate. One of the main points is that, once the drying rate curves have been established, a method of determining the kinetic order is has been shown to be possible.

4.4.5.2 Single Particle - Multiple Particle Drying Kinetics

Using Harwell's TG unit

From Figure 4.13 on particle drying, the relative ease of the drying of single particles is more pronounced than the drying of particles in close proximity to each other, as in layers or beds of particles, where the inital moisture contents were kept constant at 0.20 $kg\ kg_{-1}\ (wet - basis)$. The raw data are shown in Figures A.1 - A10.

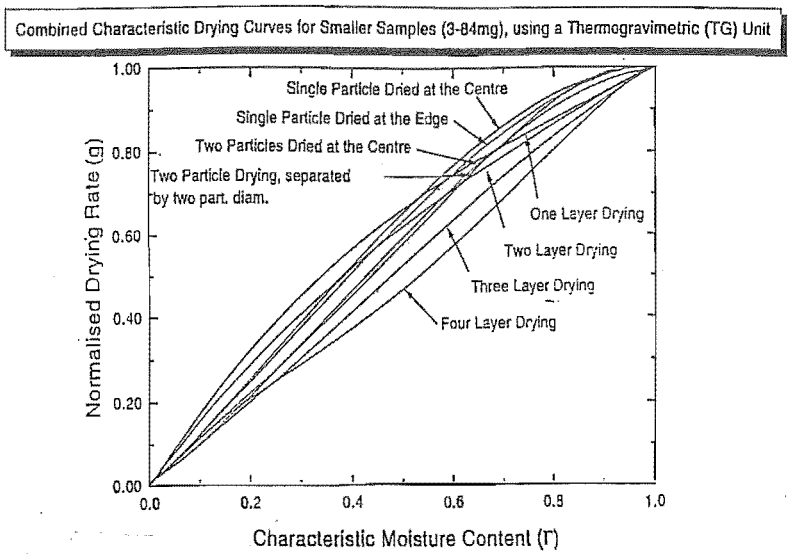

Figure 4.13 Characteristic drying curve for a smaller sample

4.4.5.3 Comparison of Harwell TG results with Canterbury thin-layer results

Figure 4.14 shows the differences in shape of the characteristic drying curves while drying silica gel particles under various bed geometries: using a microbalance sample pan (particle drying and small samples), compared with results obtained from previous work (Keech, 1992) (layer drying and large sample). Single particle agglomerates are small clusters of 7-20 particles of silica gel type 124 (d_p=1.85mm). The original raw data for Figure 4.13 and 4.14 are shown in Appendix A.

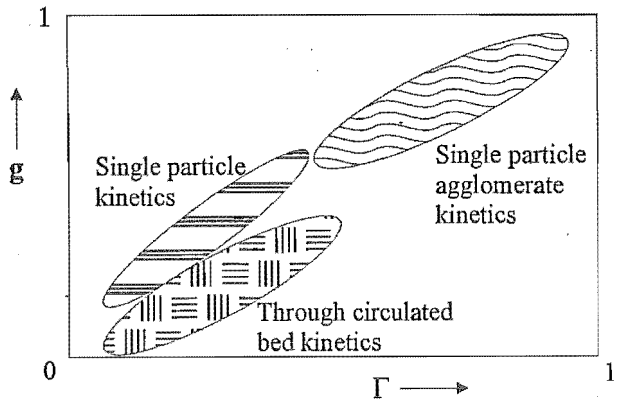

Figure 4.14 General characteristic drying curve appearance of small and large samples

4.4.5.4 Comparison of Harwell with Canterbury Results

Single particles of silica gel 124 are ideally suited for investigating drying kinetics, because the equilibrium characteristics of silica gel material is generally well understood. Also, its particle rigidity limits the effects of swelling on the kinetics of drying, and single particle trials keep the conditions of drying at the particle's surface constant. The chemistry of the drying silica is well understood.

Figure 6.38 shows the characterstic drying curves for single gel 124, for various isolated single particles and small clusters of silica gel particles. Discussion of the differences in kinetics is presented earlier in Chapter 6. However, here further discussion is needed. Under laminar flow conditions, individual silica gel particles of 1.85 mm

particle diameter had $Re_p = 70$), and high initial moisture contents ($X_o = 0.16\ kg\ kg^{-1}$), the higher external mass transfer coefficient in the gas phase (compared to lower moisture content particles) significantly contributes to increased drying rates of particle agglomerates. For particles with lower initial moisture contents (< 1%), the drying rates are likely to be low enough to ensure that the external mass transfer resistance is relatively negligible. These low drying rates of near dry particles reduce the boundary layer thicknesses compared to particles with higher moisture contents, under the same low flow drying conditions. The single particle drying kinetics performed at Harwell (Figure 4.13), was very similar to the drying kinetics of single particles done on the low moisture content drying kinetics apparatus (cf. Figure 6.38). Figure 6.39 also shows for drying a thin-layer of silica gel 124 particles, the same characteristic drying curve is produced that that single layer curve produced in Figures 4.13 and 6.38. Since these experiments revealed the same result, we should be confident that there is a consistency in reproducing drying kinetics results with other apparatus using a microbalance for weight-loss measurements.

Different methods of calculating the mass transfer coefficient for experiments 1-6 were used. For the single particle dried at the centre and the edge, and the drying of two particles separated by two particle diameters, Equation 2.136 was used to calculate the Sherwood number where an isothermal diffusion model was applied. For the drying of two particles at the centre of the chamber and the particles in layers, Equations 2.122 and 2.123 should be used to calculate the Sherwood number. The mass transfer coefficients calculated from these Sherwood numbers were compared to the experimental mass transfer coefficient calculated from Equation 2.111. The results are shown in Tables C.1, C.2 and C.3 for the drying of silica gel 124 single particles, and for the remander of the materials given in EXCEL files in the CD at the back of this thesis.

For the drying of thicker layers by a through-flow (> 3 layers), a temperature front may exist through the bed followed by a drying front. The speed of these temperature and successive drying fronts can be calculated from humidity and temperature probes positioned through the thick layer. An experimental programme on thicker layers of particulates was not investigated in this work. For drying in a fluidised bed, a large air flow is not possible as particle attrition limits the air flow. Although large fluidised particles may represent the drying of individual entities, thus increasing drying rates, the drying of finer particles in a fluidised bed may represent the drying of layered particles, because of the larger drying rates produced from smaller particles compared to larger particles. The size of the particles also influences the size of the external diffusion coefficient. Langrish (1988) found that coarse particles (> 1.4 *mm* diameter) when cascaded in a rotary drier behave as individual entities. However, Keey (1992) commented that, with finer material, the curtain of solid particles in a rotary drier acts like a fluidised bed. Thus a somewhat "large" change in shape factor should influence

the drying kinetics of particles. Keech (1992) noticed that the drying of particles with a shape factor difference of 21% was not enough to induce changes in the drying kinetics. There is now a greater demand for products with a high surface to volume ratio for a number of reasons; smaller particles produce higher drying rates, solubility of fine chemicals is increased, less residual moisture is trapped in smaller particles, etc. Significantly more time should now be concentrated on the drying of finer materials within the falling rate period. This is supported by the SPS members showing an interest in the drying of finer materials in this work. The currently preferred apparatus for the drying of finer grade material is the cascade rotary drier.

These results indicate that the characteristic drying curve for silica gel 124 can be extended to using air velocities in the range of laminar air flow conditions (Figure 6.39). A separate investigation of applying the concept of the characteristic drying curve under these low flow regions by varying the external conditions of air velocity, air temperature and air humidity showed a single characteristic drying *f-curve* when normalising against the reference critical moisture content of 0.38 $kg\ kg^{-1}$. Thus, a single chararcterstic drying curve is produced for the drying of a single layer of silica gel particles, with a low flow of air. This is an important result because even at very much lower air velocities, silica gel 124 still has the same characteristic drying curve for a very thin-layer. It looks now possible to use an electronic microbalance for single particle drying kinetic experiments at higher flow rates of air, more commonly used in commercial driers.

It may be important to note that this critical moisture content of $0.38kg\ kg^{-1}$ was determined for through-flow situations. This moisture content may be different when using a cross-circulated material, as noted by Ashworth (1979). The critical moisture content differs between through- and cross-circulated beds because: the end of the constant-rate period of drying through-flow beds is limited by the receding interface within discrete particles. Compared to cross-circulated drying, the end of the constant-rate period is limited to the receding evaporative interface into sucessive layers in a cross-circulated bed.

4.4.5.5 · Single Particle - Multiple Particle Drying Kinetics

These preliminary tests showed that using a TG unit (with a microbalance) to perform drying kinetics is suitable provided single particle drying is the only area of experimentation. By using the TG unit, if the amount of layers is increased from one to four, the results by Keech (1992) found, that of the curves becoming more concave-up. However, drying one to four layered small clusters of silica gel 124 in the the TG unit produced characteristic drying curves of similar shape to those produced by Keech (1992), but the small and large sample curves did not overlap. The reason is that the amount of material dried in the TG unit is significantly less than the amount of material dried in

the earlier tests. For example, for the drying of one layer in the TG unit, only seven particles were needed to cover the mesh crucible, whereas around 200 were required in the through-circulation rig used before. Thus, the use of small samples in the TG unit is more representative of the drying of single particles. Figure 4.14 incorporates general drying rate curves from previous work (Keech, 1992), and the general results found in this work on the same material. From Figure 4.14, the relative ease of drying of single particles is more pronounced than the drying of particles in close proximity to each another, as in layers or bed of particles. Similar conclusions were drawn from Keey *et al.* (1985) , whereby there was a recorded difference between the drying kinetics of isolated particles to the same particles being dried in a layer. The graph indicating this is reproduced as Figure 2.18.

The characteristic drying curve is independent of air temperature, air velocity and humidity, but dependent on the initial moisture content of the material being dried (Langrish *et al.*, 1991) . The present work showed that the thickness of the particulate layer or bed of particles and the size of the particles have an effect on the shape of the characteristic drying curve. These observed differences in drying kinetics behaviour between the drying of single isolated particles through to the drying of particulate beds represent the difficulties in designing industrial drying units from information on drying kinetics drawn from dissimilar particulate bed geometries. Therefore it is inappropriate to design a cascade rotary drier on the basis of single particle kinetics tests; rather those from thin-layer work should be used. The thickness of the layer used in this drying kinetics test should be the same as the physical thickness of the falling particulate layer from the baffles in the drier. This thickness would be a function of the flowability and speed of the rotating drum. Variations in thickness of the drying layer found result in variations in the drying kinetics and result in variations in the driers performance.

As can be seen from Appendix A.1 - A.6, the drying rates of single particles are five orders of magnitude higher than the drying rates of four layers under the same external drying conditions. The corresponding drying times to reduce the moisture content of these single isolated particles and single particle agglomerates (as described in Figure 4.10) from 17% to 1% are 550 s for single particles and 2000 s for four layers. Thus, for the drying of particles in close proximity to one another, as in fixed or moving beds of particles, the performance of a drier can be enhanced if these particle beds are not too deep, or are kept moving fast enough for the particle surface to be exposed longer to the drying gas, rather than having humid gas between clusters of particles. For this reason, large particles (> 500 mm) are dried in fluidised beds, to effectively dry as much material as the fluidised bed drier can handle without have problems with entrainment.

Moisture profiles are set up in fixed beds in the drying of particulate material with a high moisture content under vacuum or a reduced pressure. Nowadays, a significant

number of vacuum driers agitate the material as it is dried, in an attempt to prevent such moisture profiles being set up. For vacuum drying of material well within the second falling-rate drying period (at low-moisture contents < 1%), these moisture profiles within the bed become less predominant, so the need to agitate becomes less significant. Nevertheless "moving beds" are still used regardless of the material's initial moisture content and are now standard practice in industrial drying applications.

The partial theoretical foundation of the characteristic drying curve concept is described, as well as a method of calculating the number of transfer units experimentally from Equations 2.119 or 2.121. The external and internal mass transfer resistances are described and their weighting on different experimental conditions is emphasised. It was found that describing the drying kinetics of single particles can be helped by considering the internal mass transfer resistances alone. For the drying of single particle agglomerates and particles in layers, the external mass transfer resistances have to be taken into account especially under laminar conditions (Re_p =70). A brief description of the effects that large and small particle sizes (that alter the bed properties) have on the drying kinetics is presented.

The characteristic drying curves of individual entities and layered material were still shown to be different. Particles in layers appear to notice a "shadowing effect" by the drying of surrounding particles. With the drying under laminar conditions of layered particles (Re_p=70), the increase in gas phase diffusion resistance contributes to a reduction in drying rates. However, this resistance is minimised if particles are dried as individual entities. Significant external mass transfer resistances are found in laminar flow. This decreases the overall drying rates.

4.4.5.6 The effect of structural variations in a bed on the shape of the characteristic drying curve

In designing industrial drying equipment, the size and structure of the drying bed or layer, should be the same in the laboratory drying tests. For cascade rotary driers, the drying material falls in thin-layers from the baffles as the drum rotates; here hot moist material is exposed to the drying medium in thin-layers with very high bulk density. The thickness of this falling thin-layer can be measured and the same thickness of layer can be used in the laboratory tests. For the design of a fluidised bed, the hot air flow moves through the bed in a "bubbling" motion. Here the thickness of the drying layer very much depends on the velocity of the air flow. At low air velocities the bed bubbles at a moderate inhomogeneous rate, simulating the drying of a very much thicker layer. At higher air velocities, the bed bubbles with a more regular motion and material travels more up the sides of the fluidising chamber, increasing bed porosity and producing material being dried in thin-layers. At higher air velocities still, attrition becomes a problem and the drying medium no longer dries in a bubble arrangement,

but more a "spray formation".

As a result, this work has showed that, in designing and sizing a particular type of drying unit, the same particle size as in commercial production must be used. Analogous to Zhang's work (Zhang *et al.*, 1992), Keech (1992) found that, in order to obtain representative drying kinetic data from laboratory-scale tests, the test material must be representative of the type of material being dried. More specifically, if the material being used on a commercial scale has a known particle size distribution, then the same particle size distribution must be used in the laboratory tests. Again view Table 4.5 for suitable pilot plant tests that should be used in sizing industrial drying units.

4.4.6 Discussion of preliminary drying kinetics studies

4.4.6.1 Primary comments

Preliminary drying kinetics studies were performed to ascertain whether smaller samples (0.020-0.050 g) could give comparable results with existing drying kinetics data on larger samples (6-30 g). It was proposed that an apparatus to measure drying kinetics would involve the use of an electronic microbalance, which would give an accurate weight loss profile during the drying process. Such sensitive balances limit the sample sizes to 5 g and have a sensitivity of $\pm$ 1/10 mg, whereas traditional sample sizes used to determining drying kinetics are much larger (6-1000 g for laboratory-scale and up to two-fold larger samples for industrial pilot-scale units).

The Stanton-Redcroft TG unit (TG761) used was limited to holding a 50 mg sample. The same type of material and drying conditions used by Keech (1992) were used, but the differences between these and the present tests included air velocity, sample size and a slight difference in initial moisture content, as can be seen in Table 4.4.

Table 4.4 Comparison of experimental conditions used by Keech (1992) and in the present experiments

Material	Keech (1992)	Present experiments
-silica gel	Yes	Yes
Particle dia. (mm)	1.86 $\pm$ 0.2	1.86 $\pm$ 0.2
Solvent/moisture	water	water
Initial moisture-content X_e (wet) ($kg\ kg^{-1}$)	0.28	0.17-0.22
Sample size	6 - 30 g	0.08 - 0.3 g
Air Conditions		
-Temp. (dry bulb) ($degC$)	100	100
-Temp. (wet bulb) ($degC$)	25	25
-Air velocity ($m\ s^{-1}$)	4	0.033
Drying kinetics determined by	Evolved gas analysis (Infrared gas analyser)	*In situ* weight loss

Characteristic drying curves were constructed for each proposed experiment and then compared with those reported by Keech (1992).

From a plot of weight loss against time, the variation of moisture content with time was easily obtained. To obtain the drying rate from these data, it may be necessary to try either a first-order or higher forward difference relationship (Appendix B). Preliminary work here indicated that central and backward difference techniques were found to be less accurate. It is necessary to using a curve-fitting program such as a polynomial regression or exponential decay function to fit these weight-loss curves. Identifying the drying kinetic behaviour at low moisture contents from curves over a large moisture content range is difficult, because information at low moisture levels is "squashed". Therefore, as falling-rate drying curves appear to follow an exponential decay, taking the natural logarithms of these curves prevents loss of valuable information at low moisture contents.

Existing computer programs at Canterbury were used to help construct characteristic drying curves from outlet humidity profiles and were able to be used for evolved gas analysis on the new drying kinetics rig.

4.4.6.2 Secondary comments

A number of secondary objectives were investigated in this work. Firstly, it was necessary to determine whether there was a significant difference in drying behaviour between single particles, single particle agglomerates and particles dried in layers. Secondly, did the diameter of the layer/s have an effect on the drying kinetics? Thirdly, there was a call to develop alternative procedures to obtain a characteristic drying curve from a profile of weight loss against time. Finally, would drying smaller samples using microbalance (continuous weight loss) give similar results to larger thin-layer tests (continuous evolved gas analysis)?

The results from these preliminary drying kinetics tests indicated that there was a significant difference between the drying behaviour of single particles, single particle agglomerates and particles in layers. The relative ease of the drying of single particles was greater than for particle agglomerates, and in turn greater than for particles in layers.

After selecting a suitable industrial drying unit for a specific drying application, a knowledge of how the material would dry in the selected unit would be useful to help optimise its operation. The operations of industrial drying units are frequency optimised from drying kinetics studies on samples of the material. An application of this work was to determine which pilot plant kinetics test/s would be suitable for the wide range of industrial drying units. At this stage, after an extensive experimental programme, it is thought very useful to introduce a summary of the types of drying test methods against commercial drying units. Table 4.5 presents these pilot plant

techniques and designates a suitable drying test for each type of industrial drying method.

Table 4.5 Pilot plant techniques corresponding to various industrial drying methods

Batch driers		
Pilot plant technique	Type of industrial Drier	Comments
Single particle	Fluidised bed	Good fluidisation
Thin-layer	Fluidised bed	Poor fluidisation (bubbling of bed)
Thin-layer	Tray	
Schlünders equations for drying agitated beds	Agitated pan	
Thin-layer	Vacuum tray	
Schlünders model again	Paddle-type vacuum	
Schlünders model again	Contact vacuum	
Thin-layer	Tumble	
Continuous driers		
Thin-layer	Plate	
Single particle	Milling airlift	
Thin-layer	Band	
Single particle	Flash	
Thin-layer	Conductive disk	
Thin-layer	Convective rotary	
Single particle	Fluidised bed	Good fluidisation
Thin-layer	Fluidised bed	Poor fluidisation (bubbling of bed)
Single or thin-layer	Spray	Best modelled from velocity profiles in CFD modelling; however, CFD models currently use single particle kinetics

This work extended the particle arrangement to the drying of isolated single particles and the drying of particle agglomerates. The results confirmed this difference and extended the shape of the characteristic drying curve to be more convex-upwards for the drying of single particles. This can be seen in Figure 4.13. It must be taken in to account that the 1-4 layers shown in Figure 4.13 are only span 3-4 particles in layer diameter. So these layers should be refered to "single particle clusters" or "single particle agglomerates", as discribed in Figure ??.

There is a difference in drying kinetics behaviour between drying of isolated single particles through to particles dried in thick layers (Figure 4.14). The results here also indicated that the characteristic drying curves for the drying of two silica gel particles were different not only when drying them at varying distances from each other, but also when the air velocity was reduced to 1/10th of the other. This difference can be explained by the difference in boundary layer thickness between the two air velocities. At the lower air velocity, a thick boundary layer existed and overlapped the boundary layer of the other, affecting the drying behaviour of the other particle. However, at the higher air velocity, the boundary layer was very much thinner and did not overlap the other particle's boundary layer. Variations in air velocity, at low flows (Reynolds numbers (< 100)), does affect the shape of the characteristic drying curve. Thus, it is

important to keep air flow constant for drying kinetic tests at low air flow rates.

A particle's apparent internal diffusion coefficient (D) can be determined, where necessary, using Fick's second law, once the appropriate boundary conditions have been found. For the drying of isolated single particles, irrespective of initial moisture content and superficial air velocity, this coefficient is higher because of the lack of interference from other particles; however, for the drying of single particles agglomerated together (clusters of a few particles dried together), and layers under a laminar air flow, the air conditions at the particle's surface provide non-uniform boundary conditions when solving the relevant drying models.

These drying kinetics tests were performed on silica gel with an initial moisture content of 0.28 $kg\ kg^{-1}$ (dry basis). It was unknown whether the shape of these characteristic drying curves would be the same as that for other particulate material at very low moisture contents, which is related to the drying kinetics in this work. However, the drying kinetics of silica gel particles was seen to vary with moisture contents (Zhang *et al.*, 1992) of 0.28-0.36 $kg\ kg^{-1}$ (dry basis). Preliminary drying kinetics tests on the same material with varying moisture contents in this work (0.17-0.28 $kg\ kg^{-1}$ wet basis) did indicate that the characteristic drying curves approach first-order kinetics (linear characteristic drying curve). As a result, the characteristic drying curves of particulate material with low moisture contents have variable shapes but their shapes have a more linear appearance. A difference in drying kinetics behaviour exists for different moisture contents and particulate bed configurations. Note, this work also showed that at low moisture contents the physio-chemical nature of the moisture/solid bonding also affects the drying kinetics. This has to be considered when designing and selecting industrial drying units for specific applications.

Porous particulate material with a hydrophilic surface, that contains a small amount of moisture can be modelled entirely by a surface diffusion model. Porous particulate material with a non-homogeneous hydrophilic/hydrophobic surface can be modelled by combining both surface and Fickian diffusion effects. Thus, the chemistry of the solids surface and the type of moisture affect the drying behaviour.

The diameter of the layer does have an effect on the drying kinetics. Therefore wall effects cannot be neglected using particles of similar size in a microbalance. Wall effects are claimed to be eliminated if the particles that are dried have more than 42 particles spanning the layer (Martin, 1977). Only 7 silica gel particles spanned the preliminary drying kinetics tests, but the new low moisture content drying kinetics apparatus had a sample pan designed to have at least 42 silica gel particles spanning the sample bed. The shapes of the characteristic drying curves for the preliminary tests at Harwell and the preliminary tests on the new drying kinetics rig at Canterbury appeared to be slightly different as a result of the wall effects during drying. Note the same silica gel material was used for both preliminary tests. With the existing

thin-layer drying kinetics rig at Canterbury, particles of silica gel, d_p =1.85 *mm* and a sample holder diameter of 78 *mmID*, the ratio is 78/1.85 = 42. Therefore wall effects cannot be neglected using the same size particles in a microbalance with a sample holder diameter of 8 *mm*.

Figures 2.19 and 2.20 indicates that as the number of layers increases or the size of the drying sample increases, the curves become more concave-upwards. Figure 4.13 shows a similar result for the drying of isolated single particle and single particles agglomerated together. Figure 4.14 gives a summary of the expected shapes of characteristic drying curves for different particulate configurations. However, because the results for the small and large diameter layers do not overlap, it was considered satisfactory to go ahead with the newly proposed vacuum drying kinetics rig at Canterbury to obtain drying kinetics data for small samples using the microbalance, provided the ratio bed diameter/particle diameter was no less than 42. Because most of the material to be investigated had a particle diameter less than 1.25 *mm*, a sample holder of 50 *mmID* was adequate, provided the total weight of the sample holder and the sample was less than 5 *g* (maximum operating weight of the microbalance) for thin-layer through flow and vacuum experiments. For the drying of larger particles (up to d_p =4 *mm*) in thin-layers, the microbalance could be decoupled and the drying kinetics obtained solely by evolved gas analysis. Also, the microbalance is an ideal tool to determine the drying kinetics of single particles under vacuum and through-flow conditions.

Chapter 5

EXPERIMENTAL

5.1 DEVELOPMENT OF LOW MOISTURE CONTENT KINETICS RIG

5.1.1 Preliminary design of new drying kinetics rig

5.1.1.1 Preliminary design ideas

Effect of thermal currents on accurate weighing of hot samples in cold balances

The microbalance was be kept at a constant temperature (by monitoring the temperature around its electronic head), to avoid errors produced from convection currents around the sample section.

5.1.1.2 Determining whether infrared hygrometry or Karl Fisher titrimetry would be sensitive enough to record profiles of low humidity air

Infrared hygrometry

From manufacturers' specifications on current infrared hygrometry devices, it was found that the lower limits of detection of humidity profiles exist at frost points not less than -10 *degC* (200 *ppm* water), which is not sensitive enough for following low-moisture drying profiles. Although the path length for the infrared beam is only about 100 *mm*, it could be lengthened (or include a shorter section and a longer section) to compensate for lower humidity levels. These modifications are currently not available "off the shelf", but modifications could be made "in-house". It was determined that infrared hygrometry was not suitable for this work.

Karl Fischer titrimetry

This is a widely used technique to establish the amount of water that can be removed from a powdered solid. It is especially useful in determining very low moisture contents. By adsorbing the moisture vapour in dry methanol, Karl Fischer titrimetry can be adapted to measure low humidities in a gas stream (the operating manual of

the Karl Fischer apparatus suggests that readings are reproducible to 10 *ppm* water concentration in a dry methanol solution), so it may be considered to be a useful proposition in the design of the new vacuum drying rig.

To record evolved gas profiles containing traces of water vapour, the gas flow could be bubbled through a dry methanol solution to collect the water. The concentration of water in the bottles could be monitored periodically. However, the very large quantities of methanol this method requires made, the use of Karl Fischer titrimetry a non-viable option for repeated use.

Two-stage dew/frost point meter

Presently, two-stage dew/frost point meters are capable of recording frost points down to -50 *degC* with relative ease, and to -70 *degC* with auxiliary cooling of the optical mirror in the cell, but this modification introduces numerous experimental errors into the operation of the instrument, as it is forced to operate outside its normal limits of between -50 and 30 *degC*. This dew/frost point meter would be used to continuously monitor desorption profiles of water vapour from the drying of thin/thicker layers (after decoupling the microbalance).

Configuration of instruments for establishing the water desorption profiles in the new drying rig

The final configuration chosen (Figure 5.1) gave a complete evolved gas analysis of both water and organic vapours.

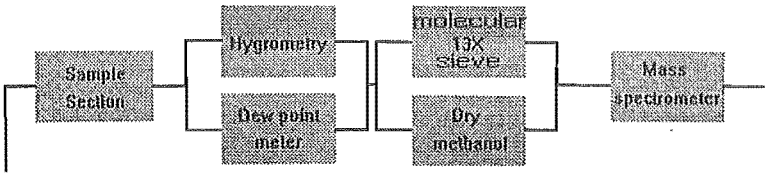

Figure 5.1 The preliminary configuration to be used in the new drying kinetics rig at Canterbury. The final configuration is shown in Figure 5.4

Calibration of vapour desorption profiles by integration of the mass spectrometer curves was done using the microbalance in the sample section. For example, by drying a solid with only one known solvent, and by recording the desorption profile on the mass spectrometer, one can equate the area under each vapour profile or vapour fragment profile with the weight loss from the microbalance. Once these integral values are known for each vapour, further experimental configurations, such as decoupling the microbalance and using the drying vacuum chamber (for larger samples) as the sample section, can then be employed.

Adsorption columns

It was initially proposed that the new vacuum drying rig should have total gas

recycle, as the cost of purchasing very dry air (bottled nitrogen, liquid/compressed gas) was found to be too expensive as long drying times were predicted for low moisture drying. However, very low flow rates of nitrogen were required so nitrogen gas was finally selected as the drying medium for through-flow conditions in the new drying kinetics rig.

Drying chambers

The sample housing needed to be designed once the electronic microbalance was decided to be a major component of the new rig. As the vacuum head for the microbalance was made of glass, this material was also used for the main sample housing. It was then decided to use standard Quick-fit glassware in a novel configuration, simple but effective for the required flow and heating patterns inside the sample housing. Initially the sample was to be heated indirectly using either a bomb calorimeter or a hot liquid (Figure 5.2).

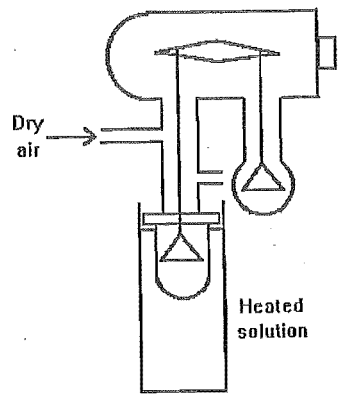

Figure 5.2 Heating configuration (initial idea). Shown is the microbalance head, a QuickFit condenser, a glass sample enclosure and a liquid heating bath

This was not the final configuration. It was decided later that electrical heating would have better control and pose a more effective heat transfer method to the sample. Two electrical elements were used to heat the sample suspended on the microbalance sample pan. The first heated the sample from just beneath the suspended pan. This provided most of the heat to the sample. A second element was used to reduce the effects of heat currents being set up around the sample section. This second element

followed the edge of the sample pan, and was generally turned on to 10 s before the first element is activated.

To avoid vibrations and lateral movement of the sample pan and balance arm, gas was introduced at a steep angle with a reduced flow volume, thus reducing the induced vibrations on the balance arm.

A detachable base section was included so that samples could be inserted quickly into the sample housing.

Sample housing

The overall configuration of the glass housing (less electrical fittings, thermocouples and capillaries) for the sample is shown in Figure 5.3.

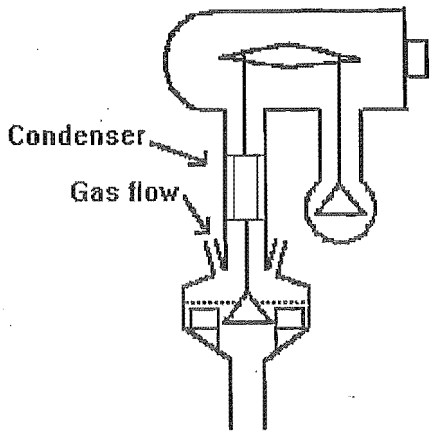

Figure 5.3 Sketch of microbalance configuration. Alterations to that shown in Figure 5.2 are to the sample housing. A photograph of this complete sample section is shown in Figure 5.10

Most components are of standard Quickfit glassware: apart from the balance, there is a standard condenser (to prevent heat escaping up into the microbalance producing offsets in readings) and a five-port Quickfit beaker is coupled to the microbalance housing (the ports are used for the input gas flow line, thermocouples above and below sample and the microbalance arm in the centre). A detachable base is provided so access to the sample is possible. As part of the detachable base, another condenser, as part of the detachable base, pre-cools the evolved gas at a predetermined temperature above the dew point, before the gas passes into the vapour detection instruments. All these details are shown in Figure 5.8.

5.1.2 Design of drying kinetics apparatus

5.1.2.1 Overall design

The apparatus has the flexibility of determining drying kinetics under vacuum or using a cross/through circulating air stream. Switching the operation between vacuum and cross-circulation consists of no structural change to the experimental section; only opening/closing a number of valves is required. Essentially, the apparatus permits a sample to be dried under a continuously weighing electronic microbalance, with sample sizes ranging from a single particle to aggregates of 4.5 g. The drying kinetics data can be retrieved from the processed digital signals via multiple RS232C inputs from the microbalance, the mass spectrometer and/or the dew/frost point meter, and then transferred to the relevant software programs for data analysis. The microbalance quantifies the amount of moisture/solvent lost in drying, whereas the mass spectrometer and the dew/frost point meter provide a qualitative and quantitative description of the desorbed species. All data are plotted using the same time base. A block diagram of the overall set up for the design is shown in Figure 5.4. A more detailed flow diagram (Figure 5.5) and an instrumentation diagram (Figure 5.6) are illustrated.

The microbalance is capable of holding samples up to 5 g, which provides data to overlap these single particle tests undertaken at Harwell. The new rig has the flexibility to perform drying kinetics tests with larger samples under a reduced pressure as well as a cross/through circulated air flow. The rig has the capability of performing vacuum drying and through/cross-circulation experiments for large and small samples, i.e. single particle drying as well as the drying of agglomerates.

Vacuum head containing electronic microbalance

The vacuum head (Figure 5.7) provides the opportunity to work at a high vacuum ($1.33*10^{-4}$ Pa) in a controlled environment. Essentially, it is the housing around the electronic microbalance.

Specifications of the microbalance are shown in Table 5.1.

The electronic microbalance consists of a moving coil and infrared detector which are employed to produce accurate and stable results. Both the sample and the counterweight are suspended from two rigid lattice arms, which offer uniform expansion at elevated temperatures.

The movement support and framework are nickel plated with suitable fixing points for mounting in most applications. The head is mounted on a rigid framework free from vibration and direct sunlight to obtain the specified performance.

Balance arm housing

The suspended balance arm between the balance head and the sample is encased in an adaptor to link the balance head to condenser C1 (Figure 5.8), which has a 60 mm effective length. The condenser prevents heat escaping up the balance arm into the

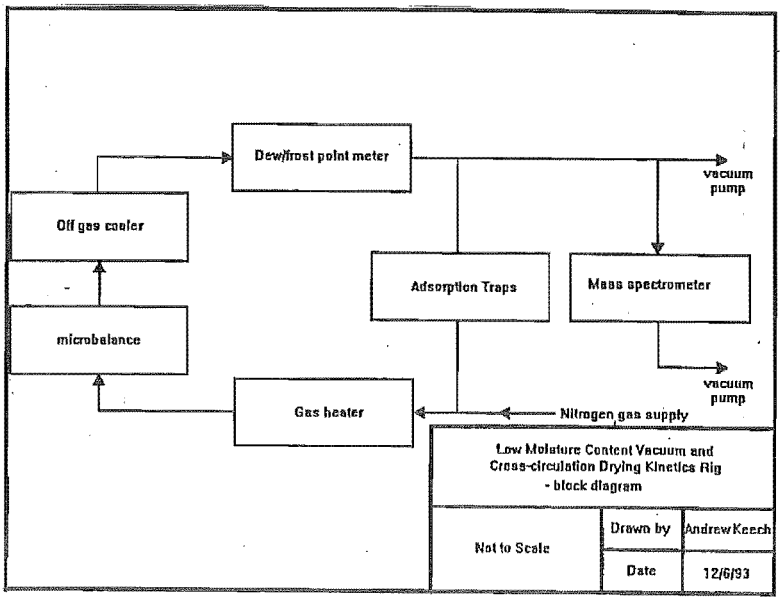

Figure 5.4 Preliminary block diagram of proposed drying kinetics rig, but not part of the final design as shown in Figure 5.8. Notice adsorption columns are excluded from the final design

head, thus inhibiting a temperature drift during operation. A variable flow of water enters condenser C1 and leaves condenser C2. The water is continuously recycled using a water bath and a peristaltic pump.

Gas cooling

The gas cooling section consists of one or more condensers with an effective length of 200 mm, depending on the required cooling duty and the maximum attainable flowrate of water. The maximum operating temperature of the sensor for the mass spectrometer is $100 degC$, so, for drying at temperatures well below this, cooling of the evolved gas may not be necessary. The maximum operating temperature of the dew/frost meter is $+75 degC$ with a dew point depression of $60 degC$. To achieve a frost point of around $-50 degC$, the temperature of the evolved gas has to be about $20 degC$, and the auxiliary

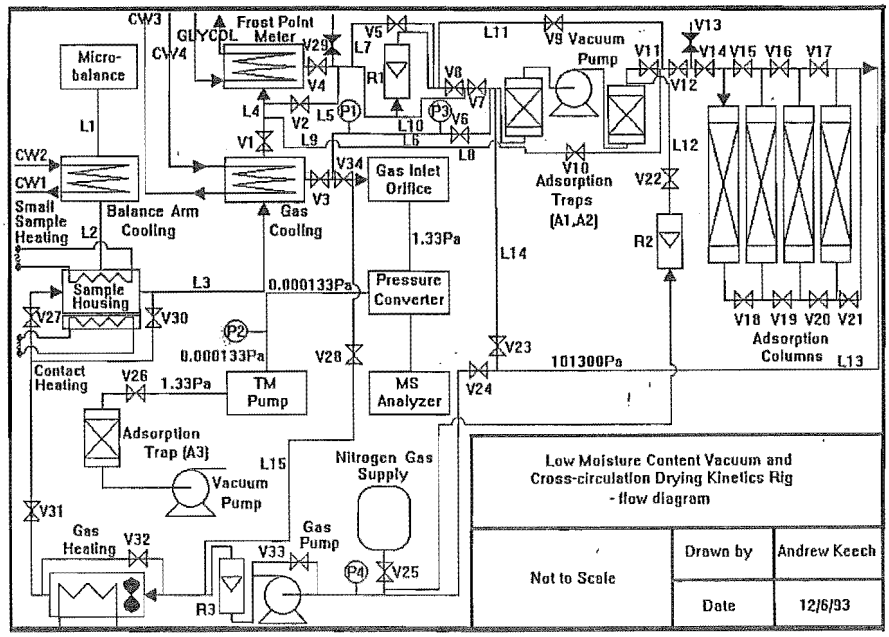

Figure 5.5 Preliminary flow diagram.

coolant of the mirror has to be between 0 and 10*degC*.

Sample housing

The sample housing prevents any water vapour entering an already dry environment while the sample is inserted on to the balance arm. Substantial heat loss is eliminated as the compartment is lined with polystyrene foam.

Sample container

Before, or after, an experiment, the lower section of the sample container can be raised or lowered, so the sample can be inserted or removed. During an experiment, the container is held in place by two clamps. Its lid has three openings: the first houses the balance arm from the microbalance, the second allows a thermocouple wire to record the temperature of the sample, and the third may contain a pressure indicator or be plugged for possible future modifications.

Mass spectrometer

A steady flow of evolved gas passes the gas inlet valve/s V9, V10 and V11 in Figure

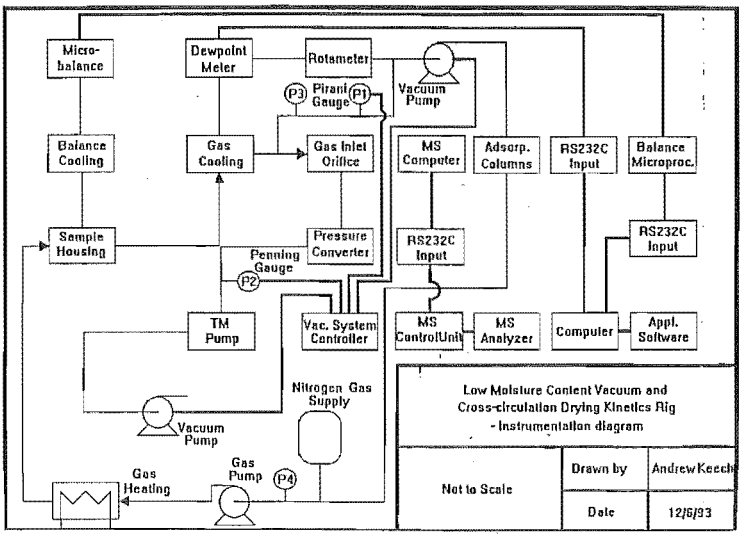

Figure 5.6 Preliminary instrumentation diagram

5.8. The mass spectrometer unit operates under a reduced pressure of $1.33*10^{-4}$ *Pa*, so a high vacuum pump and a turbomolecular pump are used to achieve this. Data profiles on species present in the gas are logged on a personal computer which also accepts information simultaneously from the microbalance (weight loss vs. time) and the dew/frost point meter (evolved gas humidity vs. time).

The following is a list of components required to operate the mass spectrometer.

1. Turbomolecular pump.

   This provides a reduced pressure of around 10^{-9} *Pa* from an upstream pressure of 10^{-7} *Pa*. An additional high vacuum rotary pump is also required. These are photographed in Figure 5.9

2. Pressure converter and extension set.

   This is intended to admit process gases in the pressure range between 1000 *mbar* and 10^{-4} *mbar* and residual gases at pressures above 10^{-6} *mbar*, whereby the

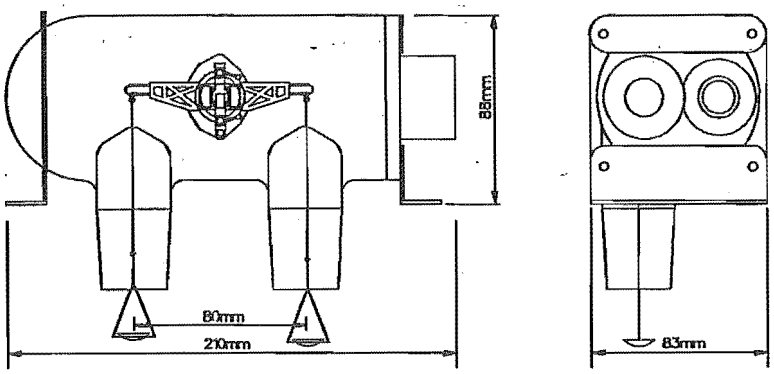

Figure 5.7 Vacuum head containing the electronic microbalance

Table 5.1 Specifications of the microbalance

Head capacity	1 g, 1 g sample + 1 g counterweight 5 g, 5 g + 5 g counterweight
Electrical range/readability	1 g, 100 mg / 10mg or 10mg / 1 mg 5 g, 200 mg / 10mg or 20 mg / 1mg
Reproducible to	Typically 10 mg or 1 mg
Temperature drift	Typically 10 $mg/degC$
Vacuum	1.33*10^{-4} Pa (maximum)
Vacuum flange	15 mm ID (nickel-plated brass)
Glass joints	B34 or S35
Movement temperature	100 $degC$ (maximum)
Weight	1 kg
Head connector	7 pin locking DIN

composition of the admitted gas remains unchanged. Up to two inlet gas valves can be connected to the pressure converter. The adaptation to the pressure range is done by fitting interchangeable orifices to the gas inlet valve. The full admission range is divided into five ranges between 10^{-4} and 1000 *mbar*. In the low pressure ranges, the pressure is reduced in a single stage, whereas above 10 *mbar*, the pressure is reduced in two stages. In all ranges, the composition of the admitted gas will remain unchanged.

3. Mass spectrometer unit.

   Two communication links, RS232C for single sensors and RS485 for multiple sensor configurations, connect the microprocessor to an existing computer, or a choice of one of several PCs and DOS software packages available.

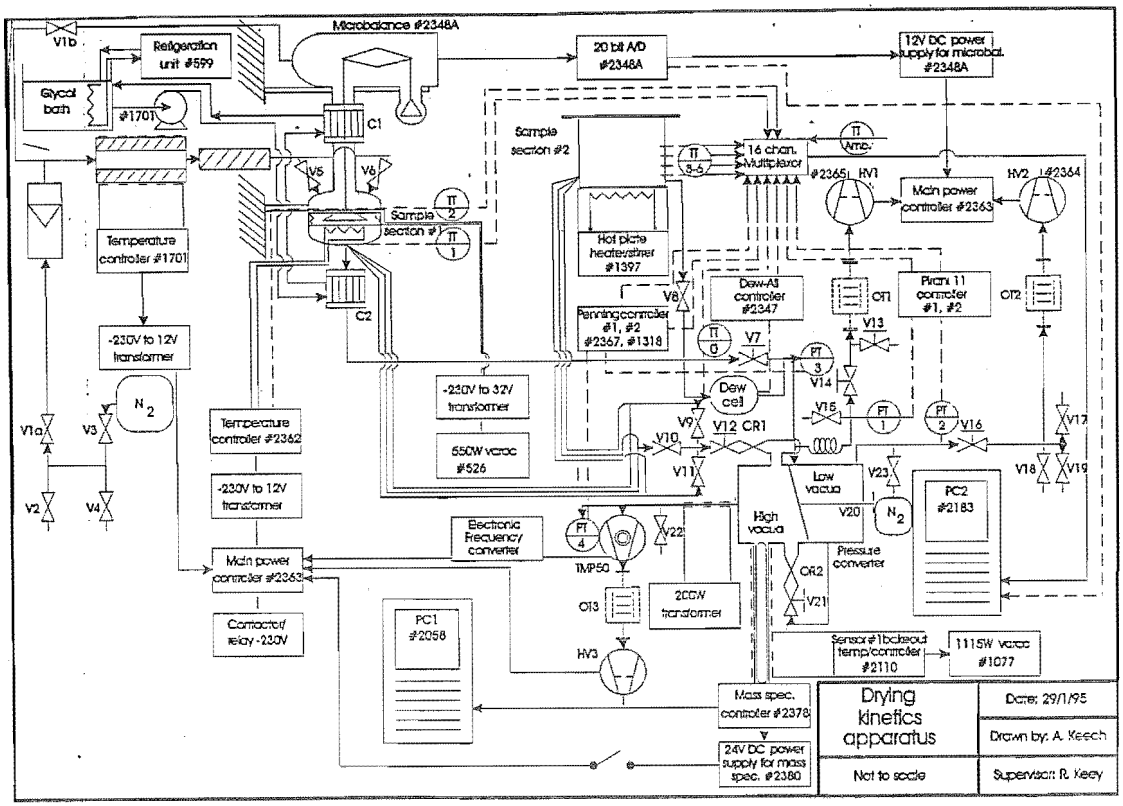

Figure 5.8 Complete schematic of the apparatus

At the lowest partial pressure ratio (above the noise baseline), this mass spectrometer unit can read a gas concentration of down to 1 *ppm*. At low water humidities in a gas, a mass spectrometer finds it difficult to resolve a concentration profile due to the build up of water molecules around the ion source, resulting in a large background noise in the water spectrum. As the determination of water in a gas was a prime consideration in this project, the frost point meter was operated simultaneously in parallel to the mass spectrometer.

Computer hardware and software

Experimental data were to be taken from the microbalance (weight loss vs. time), mass spectrometer (intensity vs. time in individual mass units) and the dew/frost point meter (concentration of water in the evolved gas vs. time). They were to be

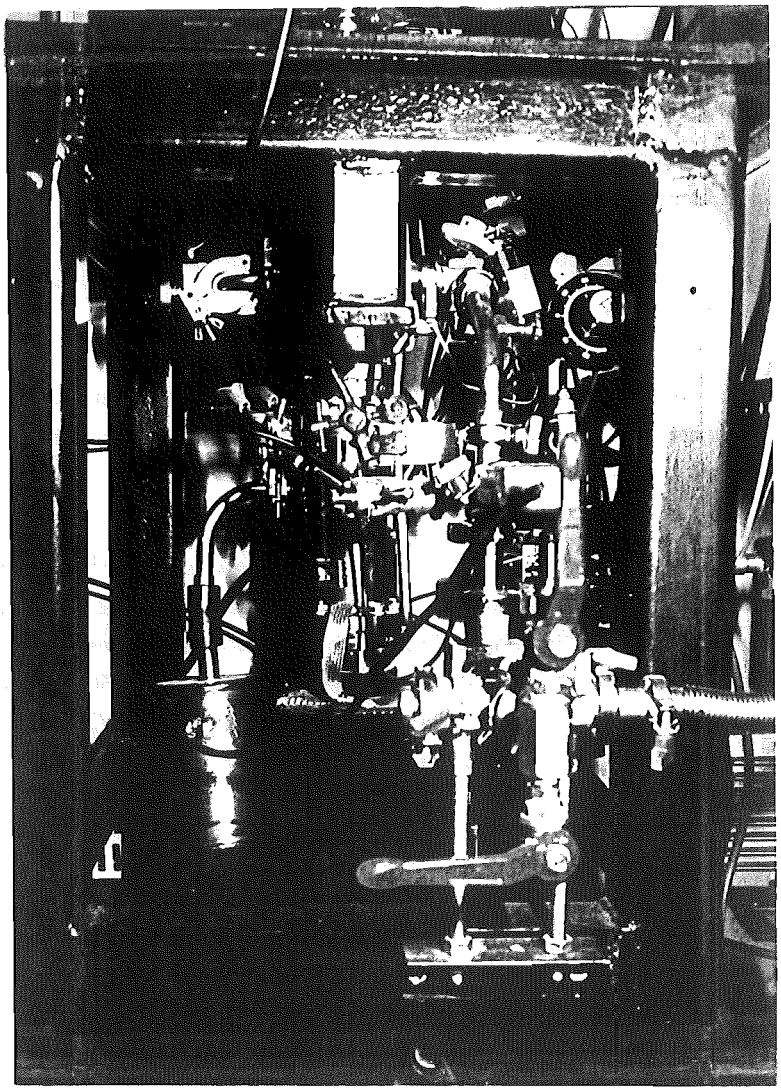

Figure 5.9 Photograph of vacuum system

simultaneously logged in a personal computer. Each sensing system has an RS232C serial communications interface which presents a digital signal compatible with the computer. The three devices have their own software packages stored in the computer which are simultaneously sourced using the main computer program written for this low-moisture drying kinetics rig. The computer is equipped with a multiple serial port to receive all data and to be recorded on the same time scale. As an analogue signal comes from the microbalance, it has its own separate microprocessor which is not built into the balance.

The application software as mentioned is incorporated into the computer's hard drive, but also other packages are needed to process the data. The software required to process the data include:

1. a suitable spreadsheet package;
2. application software for the
   (a) mass spectrometer
   (b) dew/frost point meter
   (c) electronic microbalance;
3. a technical graphics package (Mac. Curvefit or ORIGIN II).

Operating instructions for the drying kinetics rig are given in Appendix D. The software program required to read information from the multiplexer and to assemble data is shown in Appendix G.

Two-stage dew/frost point humidity analyser and microprocessor

This is designed to measure the water content in gases for a wide variety of laboratory and industrial applications. This continuously measures the water humidity of a vapour or gas flow. In-line corrections are possible for contamination of the cooled sensor without loss of real time data. Measurements range from -50$degC$ (30 ppm water) to +100$degC$, and at ambient temperatures of between -50$degC$ and 130$degC$ with manual cooling of the mirror (sensor) possible. Readings are accurate to $\pm$ 0.2$degC$.

Remaining items

Pumps - high vacuum

Two Edwards high vacuum pumps are required. The first is part of the degassing section of the mass spectrometer. The second is used in the vacuum drying of the material, by degassing the experimental section and associated lines. The vacuum pump oil is designed to exert a very low vapour pressure to help minimise oil loss. Each of the pumps has an adsorption trap (A1, A2, A3) (see flow diagram) which minimises the amount of oil begin emitted into the process lines.

Pressure indicators

Three pressure indicators are used in the rig. The first is a Pirani gauge which monitors the vacuum drying pressure around the sample (10^{-2} - 1000 $mbar$) and is inserted into line 8 (L8), upstream from the vacuum pump. The second (P2) is a Penning gauge which records the outgassing pressure in the pressure converter. If the pressure is above 10^{-4} $mbar$, the mass spectrometer will automatically cut out. The third is a less expensive indicator to observe possible deviations from atmospheric pressure.

Gas heating

A simple air gas heater was constructed to produce a constant temperature and variable flow of air to dry the sample.

Range of sample sizes, configurations

A photograph of sample section 1 is shown in Figure 5.10. Sample section 2 is cylindrical and has dimensions, base diameter = 200 *mm* and height 200mm. It contains a bank of four *k-type* thermocouples spaced at 2 *mm* apart, the first at 3 *mm* from the bottom surface.

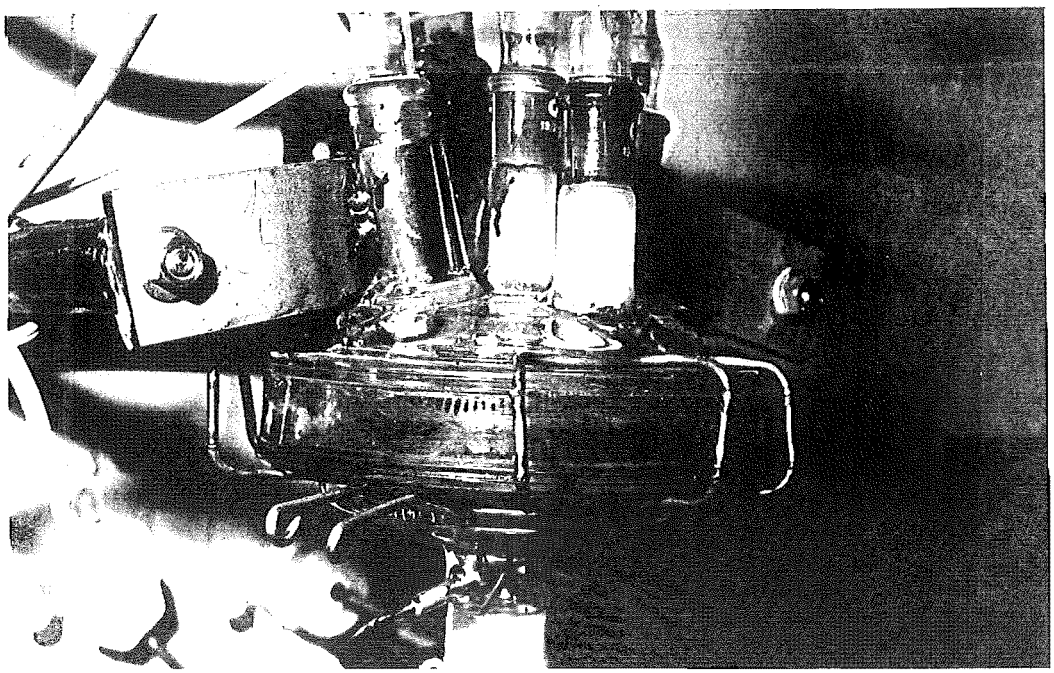

Figure 5.10 Photograph of sample section #1

The range of drying conditions are shown in Table 5.2:

Table 5.2 Test conditions for apparatus

Condition variable	Through or cross circulating	Vacuum
Dry bulb temperature (*degC*)	25 - 160	25 - 160
Dew/frost point temperature (*degC*)	-70 (instrument grade N_2) - 5	N/A
Gas mass velocity (kg m^{-2}/s)	0.00080 - 0.015	N/A
Vacuum (*mbar*)	N/A	1.2*10^{-5} - 1000

Processing method of data to drying rate curves

The main processing personal computer receives all (digital) signals via the multiplexer. These signals are divided into two groups: (1) weight loss data (μg) from the microbalance and/or dew/frost point temperatures; (2) temperatures from various

Table 5.3 Possible drying conditions

Conditions	Sample section	Sample configuration	Gas mass velocity ($kg/m^2 s^{-1}$)	Minimum sample size (mg)
Through-flow or cross circulation	1	Single particle	0.00158 0.00709	100 200-300
	1	1-4 layers, diameter = 50 mm	0.00158 0.00709	100 200-300
1	1-4 layers	diameter = 100 mm (without microbalance)	0.00158 0.00709	6000-30000 6000-30000
Vacuum	1	Single particle		35-2000
	1	1-4 layers, diameter = 50 mm	-	35-2000
	2	1-4 layers	-	5000-200000
	2	Particle bed (4 layers)	-	5000-200000

thermocouples or pressure readings ($mbar$) set around the apparatus. The thermocouple and pressure readings do not require further processing.

The dew/frost point signal is converted into a humidity via the psychrometric correlations for water in air, to then be converted into drying rate data from a mass balance of the drying sample:

$$W_s\left(-\frac{d\bar{X}}{dt}\right) = W_g(Y_{go} - Y_{gi}) \tag{5.1}$$

where W_s is the mass of dry material, W_g is the mass flowrate of dry air, Y_{go} is the outlet humidity as recorded by the dew/frost point meter, Y_{gi} is the inlet gas humidity and dX/dt is the moisture loss rate or drying rate.

The microbalance capacity is 5 g, reproducible to 1/10 (μg). The electrical readability has a weight loss "window" of 200 mg of the drying sample. The combined weight of the sample pan and balance rods on the sample side equates to 2 g, thus permitting a 2.5-3 g drying sample to be recorded from the microbalance. Before a sample is dried, the microbalance is calibrated with the equivalent dry weight of the sample. After the insertion of the sample on to the microbalance, a microgram drying profile is output to the computer. This yields an unprocessed signal plot as recorded in the Chapter 4. This unprocessed signal may require smoothing. If so, a moving average subroutine is available on the microbalance 20 bit A/D eurocard, which is accessible from the PC keyboard. Calibration and offset subroutines are also available from the eurocard. The moisture content (dry basis) against time profile is then obtained from the digital readings by

$$X_I = \frac{DSM|_{t=0} - DSM|_{t=\infty}}{Initial \quad dry \quad weight \quad of \quad sample} \tag{5.2}$$

where X_I is the initial moisture content, $\mu g \mu g^{-1}$, and DSM is the digital signal from the multiplexer, μg.

Selective drying at low moisture contents was investigated by using an infinity soluble binary mixture of isopropyl alcohol and water. The partial pressure of isopropyl alcohol (MW 60) was recorded by observing a fragment profile at 45 atomic mass units ($a.m.u.$) on the mass spectrometer. A software option [DEGAS] enabled the ion source for the current sensor to be cleaned prior to recording the desorption profile. This partial pressure profile of isopropyl alcohol was converted into a part-per-million quantity by using Dalton's law.

5.2 TEST CONDITIONS FOR DRYING TUNNEL SORPTION STUDIES

5.2.1 Equipment

5.2.1.1 General

Measuring the sorptive behaviour of materials is normally done over long periods using either static methods and/or less time-consuming dynamic methods. The measurement of accurate equilibrium isotherms is complicated for materials that have a low critical moisture content because the adsorption of moisture on metal or glass walls of the apparatus. This difficulty can be overcome by using a large sample (used here for isotherms) or sensitive electronic microbalances (used here for desorption kinetics).

Equilibrium loading was measured using a dynamic method in a controlled atmosphere ($T_w, T_d \pm 0.2 degC$). This is shown in Figure 2.16. So that the time required to establish equilibrium was reduced from the damp air value of several days/months using static methods to a matter of hours. The experimental apparatus consisted of a packed column humidifier and a temperature/flow controlled tunnel, as shown previously in Figure 2.16, and further described below.

5.2.1.2 Procedure for sorption experiments at Canterbury

A sample (1-10 g) was placed on the suspended balance pan and exposed to a controlled air flow (0.5 $m\ s^{-1}$) that had been first heated by passing it up through a packed column (with a water recycle heated by a 6 kW heater). PID control maintained the dry-bulb (T_d = 25-120$degC$) and wet-bulb (T_w = 25-65$degC$) temperatures to within 0.1$degC$ of both temperatures (once steady state had been reached after about 30 min). The

sample remained under these controlled conditions until a constant weight had been reached (minimum of 24 h), after which the wet-bulb humidity of the apparatus was increased/decreased depending on whether adsorption or desorption isotherms were required. An IBM286 personal computer was used to control (using PID) the operating conditions.

As most of the solids had a low critical moisture content (approximately $X_{cr} < 1\%$), it was imperative to maintain strict conditions throughout experimental runs to obtain accurate sorption isotherms and heats of sorption.

5.2.1.3 Test conditions

Table 5.4 indicates the humidity conditions for the sorption isotherms.

Table 5.4 Ranges of T_{dry} and T_{wet} values *degC* used for sorption isotherms

Dry-bulb temperature	Wet-bulb temperatures		Relative humidities		Dew point temperatures	
	low-high		low-high		low-high	
45	18	41	7	83	1	41.4
65	24	64	3	89	1	62.5
80	28	62	1	41	1	59.6

5.2.1.4 Material investigated

The materials that were used in this work were: silica gel, alumina, fine iron sand, adipic acid, pure terephthalic acid, non-dried terephthalic acid and three polystyrene-butadiene copolymers: I, II, III. Details on these copolymers are not able to be disclosed in the body of this thesis.

Three different types of materials were used to investigate the drying behaviour at low moisture contents: two common particulate drying agents (silica gel and alumina), two fine organic chemicals (one aromatic and one aliphatic dicarboxylic acids) and three polymer-based compounds (one gelatinous copolymer, two other particulate copolymers with higher comparative surface areas).

The mean particle diameters of each material with one standard deviation were: silica gel ($1855 \pm 50\mu m$), alumina ($120 \pm 30\mu m$), two fine organic chemicals ($110 \pm 50\mu m$), $70 \pm 30\mu m$), three copolymers ($4000 \pm 50\mu m$, $550 \pm 100\mu m$, $550 \pm 200\mu m$).

Alumina was selected to test the sensitivity of this apparatus under various flow regimes and particulate geometries. A more complete solids characterisation of alumina materials is given. Aluminium oxide (Al_2O_3), appearance fine white powder, very cohesive. Physiochemical data: bulk density 850 [kg m^{-3}], particle density 1150 [kg m^{-3}]. Applications: Desiccant, typical drying research material, raw material for production of aluminium.

5.2.2 Experimental

5.2.2.1 Measurement of sorption isotherms and binding energy

The internal structure of porous or non-porous particulate/powdery material can be characterised by fitting the sorption isotherms to either of the above materials. By plotting isotherms at different temperatures (45, 65, 80$degC$), the heats of wetting against equilibrium moisture content can be evaluated using the Clausius-Clapeyron equation, thus giving an indication of the binding energies between the material and the moisture.

Plots of sorption isotherms at varying temperatures were made for certain typical adsorbents and the binding energy between material and moisture was calculated. The materials under investigation were as follows;

1. Adipic acid.
2. Terephthalic acid (pre-dried and pure forms).
3. Activated silica gel.
4. Non-activated silica gel.
5. Alumina.
6. Three polystyrene-butadiene copolymers.

5.3 TEST CONDITIONS FOR DRYING KINETICS EXPERIMENTS UNDER VACUUM

Materials:

1. Silica gel (SG124, d_p =1.86 mm)
2. Alumina (d_p =100μm)

Table 5.5 indicates the thickness of the drying layer of the particulate material as well as the external conditions. The effects of vacuum level, temperature and bed geometry were investigated to observe the differences in drying kinetics behaviour for each case. The dew point for all runs was about 0.6± 0.05 $degC$

Table 5.5

Bed configuration	Vacuum (*mbar*)		T_{dry} (*degC*)
	high	low	
Single isolated particles	10^{-2}	10^{-3}	100
Single isolated particles	10^{-3}	10^{-5}	100
One layer	10^{-2}	10^{-3}	100
One layer	10^{-3}	10^{-5}	100
Two layers	10^{-2}	10^{-3}	100
Two layers	10^{-3}	10^{-5}	100
Three layers	10^{-2}	10^{-3}	100
Three layers	10^{-3}	10^{-5}	100
Single isolated particles	10^{-2}	10^{-3}	80
Single isolated particles	10^{-3}	10^{-5}	80
Single isolated particles	10^{-2}	10^{-3}	120
Single isolated particles	10^{-3}	10^{-5}	120
Single isolated particles	10^{-2}	10^{-3}	140
Single isolated particles	10^{-3}	10^{-5}	140
Single particle agglomerates	10^{-2}	10^{-3}	
Single particle agglomerates	10^{-3}	10^{-5}	
Uneven layer	10^{-2}	10^{-3}	100
Uneven layer	10^{-3}	10^{-5}	100

5.4 TEST CONDITIONS FOR DRYING KINETICS EXPERIMENTS AT LOW MOISTURE CONTENTS OF ALUMINA CONTAINING A BINARY SOLUTION OF WATER AND ISOPROPYL ALCOHOL

The conditions for this experiment were as follows: $T_{dry} = 100 degC)$, $T_{dew} = 0.6$degC, *Gas mass velocity* $= 0.00709\ kgm^{-2}s^{-1}$.

Bed configuration	*Concentration of isopropyl alcohol*
1 mm *thick sample*	*0.5* mol l^{-1}
3 mm *thick sample*	*0.5* mol l^{-1}
1 mm *thick sample*	*2* mol l^{-1}
3 mm *thick sample*	*2* mol l^{-1}

Chapter 6

RESULTS

6.1 ACCURACY OF THE NEW DRYING KINETICS APPARATUS

6.1.1 Drying using a through flow of air

6.1.1.1 Drying alumina - raw data

Figure 6.1 shows the electronic signal profile from drying alumina with an initial weight of 100 mg with a high air flow of 0.00709 $kg\ m^{-2}\ s^{-1}$. The y-axis signal in Figure 6.1 is a weight -loss signal in micrograms. A very noisy signal is produced under these conditions, which is unacceptable for determining drying kinetics information at low moisture contents.

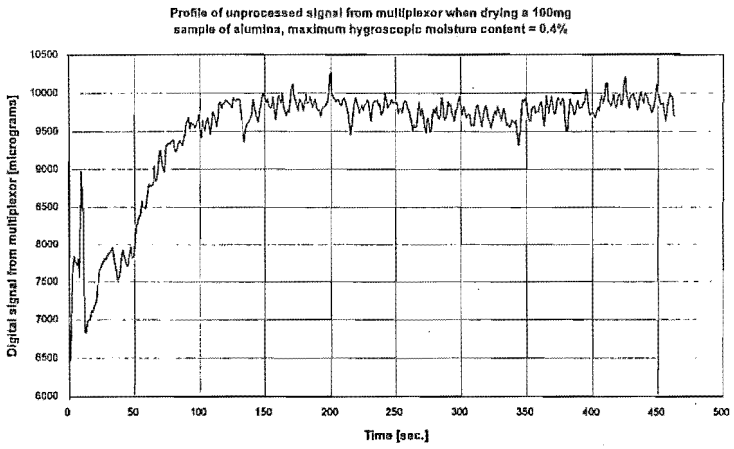

Figure 6.1 Raw signal data of alumina, T_{dry} = 120$degC$, T_{dew} = 5$degC$, sample weight = 100 mg, air mass velocity G = 0.00709 $kgm^{-2}s^{-1}$

Figure 6.2 shows the electronic signal profile of alumina with an initial weight of 100 mg with a lower air flow of 0.00158 $kg\ m^{-2}\ s^{-1}$. Reducing the air flow reduces the noise observed in Figure 6.1. Note, the gas flow past the sample creates vibrations in the sample pan, causing noise in the raw data readings, so is it necessary to use a very low gas flow. These conditions are acceptable for determining the drying kinetics.

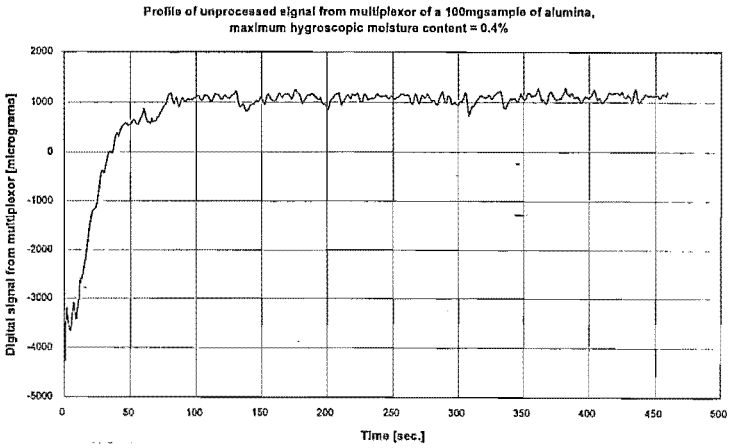

Figure 6.2 Raw signal data of alumina, $T_{dry} = 120degC$, $T_{dew} = 5degC$, sample weight = 100 mg, air mass velocity G = 0.00158 $kgm^{-2}s^{-1}$

Figure 6.3 shows the electronic signal profile of alumina with an initial weight of 300 mg with a higher air flow of 0.00709 $kg\ m^{-2}\ s^{-1}$. Increasing the weight of the sample by 300% compared with the data given in Figure 6.1 appeared to dampen the noise, providing suitable drying conditions.

Figure 6.4 shows the electronic signal profile of alumina with an initial weight of 300 mg with a lower air flow of 0.00158 $kg\ m^{-2}\ s^{-1}$. Again accurate drying profiles are obtained under these conditions.

6.1.1.2 Conclusion

The observed limits on extracting accurate weight loss profiles lie somewhere between a 200 and 300mg sample size for the larger air flow of 0.00709 kgm^2s^{-1}. For the smaller air flow of 0.00158 $kg\ m^2s^{-1}$, the size of sample is limited to 100mg. For this work it was not required to find more limitations of the apparatus, just locate a suitable sample size against a low gas flow rate.

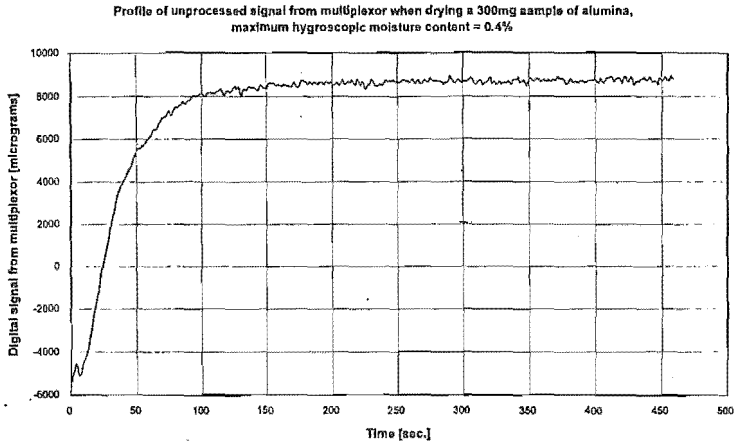

Figure 6.3 Raw signal data of alumina, $T_{dry} = 120degC$, $T_{dew} = 5degC$, sample weight = 300 mg, air mass velocity G = 0.00709 $kgm^{-2}s^{-1}$

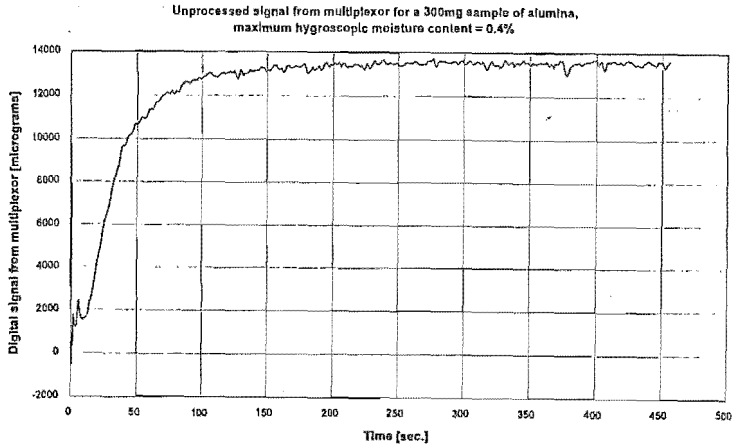

Figure 6.4 Raw signal data of alumina, $T_{dry} = 120degC$, $T_{dew} = 5degC$, sample weight = 300 mg, air mass velocity G = 0.00158 $kgm^{-2}s^{-1}$

6.1.2 Drying using vacuum conditions

The preceding graphs indicate a problem with obtaining accurate weight loss profiles under an air flow. Under vacuum conditions and low drying rates, the only perceived disturbances would be to the degassing of the chamber of air past the sample holder during the initial stage of drying.

6.1.2.1 Drying alumina - raw data

Figure 6.5 shows the electronic signal for the drying of alumina with an initial mass of $35mg$ under a vacuum of 0.027 $mbar$ absolute pressure. Degassing time to 0.027 $mbar$ absolute pressure was 46 s. The overall drying time was 800 s

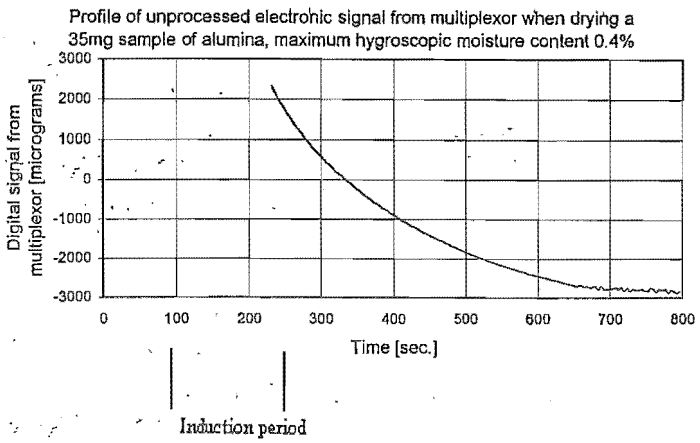

Figure 6.5 Raw signal data of alumina under a vacuum of 0.027 $mbar$ absolute pressure, T_{dry} = $100 deg C$

Figure 6.6 shows the signal when the sample mass was increased to $100mg$ under the same conditions, leading to an increased drying time of 1000 s.

The microgram readings here are negative because the weighing is performed using a horizontal balance arm that can only deviate a maximum of 200 mg during a experimental run. The combined weight of the sample pan, balance arm and sample must initially be the same as the counterweights on the other side of the balance arm. Sometimes it is possible to observe the readings pass through zero as the sample dries. However, this is acceptable as an overall weight loss reading is still recorded on the y-axis.

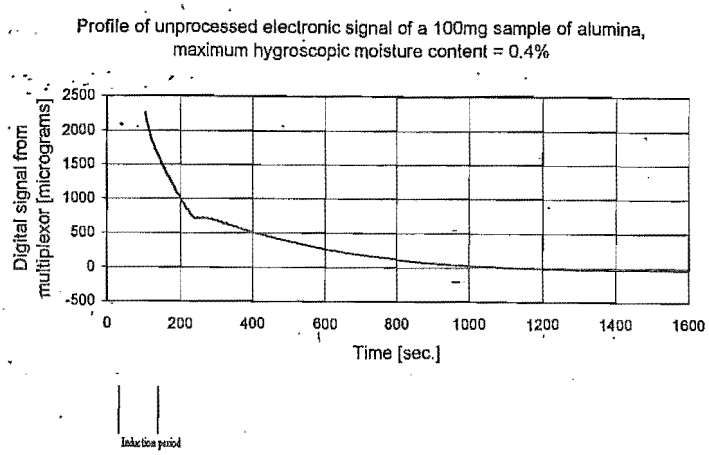

Figure 6.6 Raw signal data of alumina under a vacuum of 0.027 *mbar* absolute pressure, $T_{dry} = 100 degC$

6.1.2.2 Conclusion

The observed practical limit on extracting and accurate weight loss profile under vacuum conditions for alumina is approximately a 35 *mg* sample size under a vacuum of vacuum of 0.027 *mbar*. A smaller sample could be tested but much of the drying would be performed under the degassing stage of the drying process.

These limits for obtaining accurate drying profiles depend strongly on minimising the environment disturbances of room temperature, avoiding direct sunlight on the balance electronics, pump noise, size of air flows and minimising ground movement. Electronic microbalances are sensitive to baseline shift on detecting tidal fluctuations throughout the day if your microbalance is located near the ocean or a busy road (A Roberts, CI Electronics, Wiltshire, U.K., private communication, 1993). This is why the low moisture content drying kinetics apparatus was solidly bolted to a corner pillar, and constructed in an old radiochemical lab in the basement of a large concrete building.

6.2 TESTING THE LOW-MOISTURE CONTENT MODELS

The drying models presented in Chapter 3 indicate the possible mechanisms for moisture and heat transport through particulate material containing low levels of moisture. The following subsections show the experimental verification of these individual models for each material investigated.

6.2.1 Testing the surface diffusion model on the materials at low-moisture contents

The surface diffusion model for the desorption of bound moisture from a particulate matrix, shown in Chapter 3, is governed by the simple rate expression

$$rate \quad of \quad desorption = ze^{-\frac{E_a}{RT}} \tag{6.1}$$

Equation 6.1 is depended only on temperature for drying. For the drying of very thin-layers or small isolated particles, temperature profiles are not easily set up through the drying sample. The drying temperature remains relatively constant for the long drying times that are typical of low-moisture drying.

The following four graphs (Figures 6.7, 6.8, 6.9, 6.10) shows the application of the temperature dependent surface diffusion model to two very different solid particulates. Alumina, a porous hydrophilic solid has water bound to its internal porous structure, and a copolymer, which is very much temperature independent because of its hydrophobic nature. Alumina is a common dessicant and water sorption in alumina is very much temperature dependent. The characteristic shape of the drying rate verses heat of wetting data for very thin-layers ($0.2mm$) is shown in Figure 6.7, and for a slightly thicker layer ($1.0mm$) shown in Figure 6.8. These Figures show a strong dependence between the drying rates and heat of wetting. The copolymer shows very different characteristic shapes in Figures 6.9 (for isolated particles, $d_p = 1$mm, and Figure 6.10 for thicker layers ($2mm$). This charactersitic shape in the last two Figures is typical for hydrophobic particulates. The drying kinetics of this type of material is more dependent on mass transfer resistances than temperature effects. The scatter in these Figures are almost entirely due to experimental error, because it is still very difficult to accurately measure drying rates at very low moisture contents.

6.2.1.1 Alumina

Table 6.1 and Figures 6.7 and 6.8 show the applicability of the surface diffusion expression for varying thicknesses of the particulate bed. Alumina was the material selected to test this bed-thickness effect. Figure 6.7 gives a relatively non-linear appearance through the drying period. Which maps the heat of wetting data obtained for these materials, suggesting that, for very thin-layers of alumina at low moisture contents, a surface diffusion model "alone" should account for the mechanism of moisture transport. However, for the thicker layer, a less linear appearance pertains (concave-downwards), suggesting that, even at lower moisture contents with low drying rates, a resistance through the particulate bed would have to be considered to account for the overall diffusion coefficient.

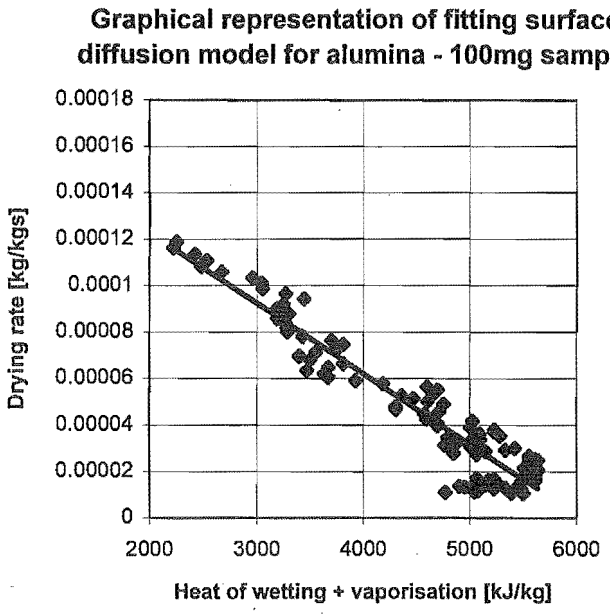

Figure 6.7 Graphical representation of the surface diffusion equation for a very thin-layer (0.2mm) of alumina (Exp. 28)

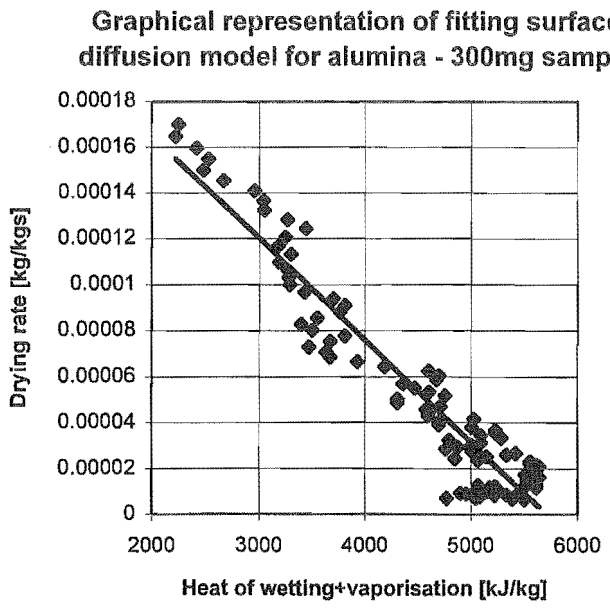

Figure 6.8 Graphical representation of surface diffusion equation for a thicker-layer (1mm) of alumina

Table 6.1 Testing the surface diffusion model for alumina

Exp. No.	z	b'	Sample weight (mg)	Temp. ($degC$)	Air velocity (kg m$^2 s^{-1}$)
Exp. # 24a	0.0001046	0.398	300	120	0.00709
Exp. # 24b	0.0001021	0.398	300	120	0.00709
Exp. # 25a	0.0000951	0.398	300	120	0.00115
Exp. # 25b	0.0000966	0.398	300	120	0.00115
Exp. # 25c	0.0000918	0.398	300	120	0.00115
Exp. # 26a	0.0001143	0.398	300	140	0.00709
Exp. # 26b	0.0001158	0.398	300	140	0.00709
Exp. # 26c	0.0001125	0.398	300	140	0.00709
Exp. # 27d	0.0000921	0.398	300	80	0.00709
Exp. # 27e	0.0000934	0.398	300	80	0.00709
Exp. # 27f	0.0000928	0.398	300	80	0.00709
Exp. # 28a	0.0001254	0.399	100	120	0.00709
Exp. # 28b	0.0001289	0.399	100	120	0.00709
Exp. # 28c	0.0001275	0.399	100	120	0.00709

6.2.1.2 Iron sand

To test the effect of bed thickness on whether a surface diffusion equation alone could account for the drying mechanism, further studies were performed on other materials. These particulates included iron sand (see Table 6.2), and pure and pre-dried terephthalic acid.

Table 6.2 Testing the surface diffusion model for iron sand

Exp. No.	z	b'	Sample weight (mg)	Temp. ($degC$)	Air velocity (kg m$^2 s^{-1}$)
Exp. # 30a	0.0000939	0.402	300	120	0.00709
Exp. # 30b	0.0000926	0.402	300	120	0.00709
Exp. # 31a	0.0000856	0.402	300	120	0.00115
Exp. # 31b	0.0000866	0.402	300	120	0.00115
Exp. # 31c	0.0000852	0.402	300	120	0.00115
Exp. # 32a	0.000119	0.402	300	140	0.00709
Exp. # 32b	0.000110	0.402	300	140	0.00709
Exp. # 32c	0.000121	0.402	300	140	0.00709
Exp. # 33d	0.0000851	0.402	300	80	0.00709
Exp. # 33e	0.0000834	0.402	300	80	0.00709
Exp. # 33f	0.0000897	0.402	300	80	0.00709
Exp. # 33g	0.0000832	0.402	300	80	0.00709
Exp. # 34a	0.000156	0.402	100	120	0.00709
Exp. # 34b	0.000150	0.402	100	120	0.00709

6.2.1.3 Pure terephthalic acid

The difference between pure and pre-dried terephthalic acid was the type of solvent used: the pure form contained water and the pre-dried form contained cyclohexane. Table 6.3 and 6.4 showed that showed a surface diffusion model may be applied for either solvent.

Table 6.3 Testing the surface diffusion model for pure terephthalic acid

Exp. No.	z	b'	Sample weight (mg)	Temp. ($degC$)	Air velocity (kg $m^2 s^{-1}$)
Exp. # 36a	0.0000867	0.403	300	120	0.00709
Exp. # 36b	0.0000839	0.403	300	120	0.00709
Exp. # 36c	0.0000865	0.403	300	120	0.00709
Exp. # 37a	0.0000812	0.404	300	120	0.00115
Exp. # 37b	0.0000795	0.403	300	120	0.00115
Exp. # 37c	0.0000786	0.403	300	120	0.00115
Exp. # 38a	0.000108	0.404	300	140	0.00709
Exp. # 38b	0.000110	0.404	300	140	0.00709
Exp. # 38c	0.000107	0.403	300	140	0.00709
Exp. # 39d	0.0000752	0.403	300	80	0.00709
Exp. # 39e	0.0000754	0.403	300	80	0.00709
Exp. # 40a	0.0000976	0.404	100	120	0.00709
Exp. # 40b	0.0000955	0.404	100	120	0.00709

6.2.1.4 Pre-dried terephthalic acid

Table 6.4 is the corresponding table for pre-dried terephthalic acid.

Table 6.4 Testing the surface diffusion model for pre-dried terephthalic acid

Exp. No.	z	b'	Sample weight (mg)	Temp. ($degC$)	Air velocity (kg $m^2 s^{-1}$)
Exp. # 42a	0.000178	0.403	300	120	0.00709
Exp. # 42b	0.000168	0.403	300	120	0.00709
Exp. # 42c	0.000176	0.403	300	120	0.00709
Exp. # 43a	0.000163	0.403	300	120	0.00115
Exp. # 43b	0.000167	0.403	300	120	0.00115
Exp. # 43c	0.000170	0.403	300	120	0.00115
Exp. # 44a	0.000189	0.403	300	140	0.00709
Exp. # 44b	0.000182	0.403	300	140	0.00709
Exp. # 44c	0.000184	0.403	300	140	0.00709
Exp. # 45a	0.000181	0.404	100	120	0.00709
Exp. # 45b	0.000183	0.403	100	120	0.00709
Exp. # 45c	0.000189	0.404	100	120	0.00709
Exp. # 46d	0.000156	0.403	300	80	0.00709
Exp. # 46e	0.000157	0.403	300	80	0.00709
Exp. # 46f	0.000154	0.403	300	80	0.00709

6.2.1.5 Copolymer III

Table 6.5 and Figures 6.9 and 6.10 show the applicability of the surface diffusion model for varying thicknesses of the particulate bed for the copolymer III. The moisture used for this copolymer was water.

Table 6.5 Testing the surface diffusion model for copolymer III

Exp. No.	z	b'	Sample weight (mg)	Temp. ($degC$)	Air velocity (kg $m^2 s^{-1}$)
Exp. # 48a	0.0000689	0.401	300	120	0.00709
Exp. # 48b	0.0000645	0.401	300	120	0.00709
Exp. # 48c	0.0000609	0.401	300	120	0.00709
Exp. # 49a	0.0000597	0.401	300	120	0.00115
Exp. # 49b	0.0000594	0.401	300	120	0.00115
Exp. # 49c	0.0000587	0.401	300	120	0.00115
Exp. # 50a	0.0000756	0.401	300	140	0.00709
Exp. # 50b	0.0000789	0.401	300	140	0.00709
Exp. # 50c	0.0000767	0.401	300	140	0.00709
Exp. # 51a	0.0000876	0.401	100	120	0.00709
Exp. # 51b	0.0000862	0.401	100	120	0.00709
Exp. # 51c	0.0000889	0.401	100	120	0.00709
Exp. # 52d	0.0000512	0.401	300	80	0.00709
Exp. # 52e	0.0000510	0.401	300	80	0.00709
Exp. # 52f	0.0000529	0.401	300	80	0.00709

6.2.2 Conductive heat drying models - testing Okazaki conductive heat drying model

Figure 6.11 shows a comparison between the location of the unfiltered experimental drying front data in a sample bed and that predicted using Okazaki's conductive heat drying model.

6.3 SOLIDS CHARACTERISATION

6.3.1 Using microscopic photographs to observe particle's surface before and after drying

The photomicrographs in Figure 2.29, with 100 times magnification, show the dry (left-hand side) and wet (right-hand side) forms of silica gel with particle diameters of between 1.5 and 2.0 mm. Samples were taken before and after exposing them to T_d = $100 degC$, T_{dew} = $3.0 degC$, until a steady weight was recorded (equilibrium moisture content). Before drying, silica gel (X_I = 28% wet basis) particles appeared "hazy", as the free water inside the particles diffused the light from the microscope. After drying the particles had a more clearer appearance due to the absence of free water in the

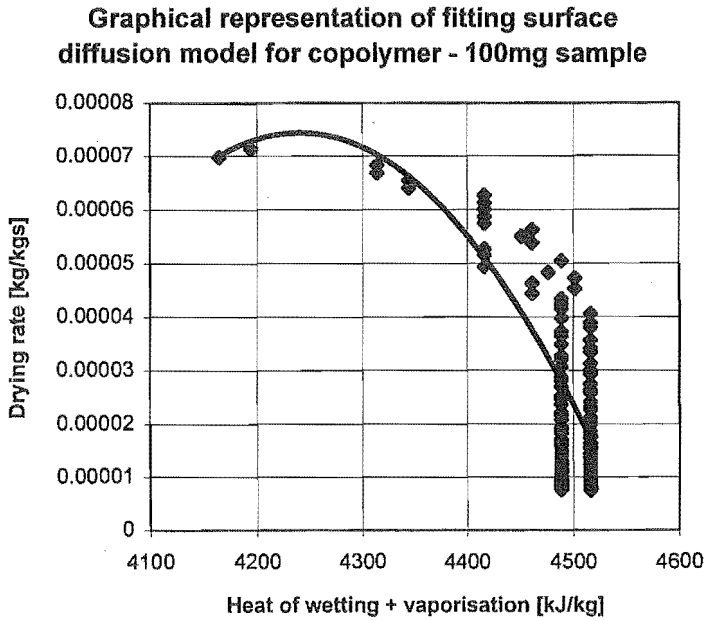

Figure 6.9 Graphical representation of the surface diffusion equation for the drying of isolated particles of copolymer III

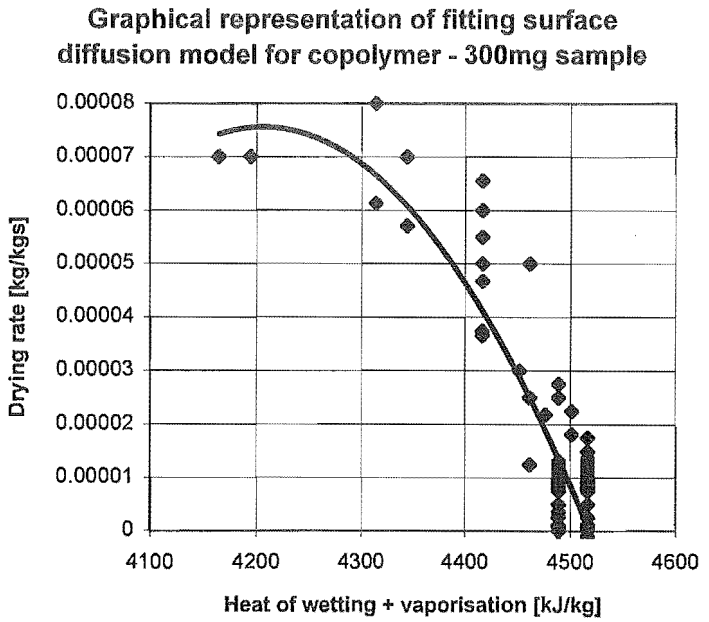

Figure 6.10 Graphical representation of the surface diffusion equation for the drying of a thin-layer ($2mm$) of Copolymer III

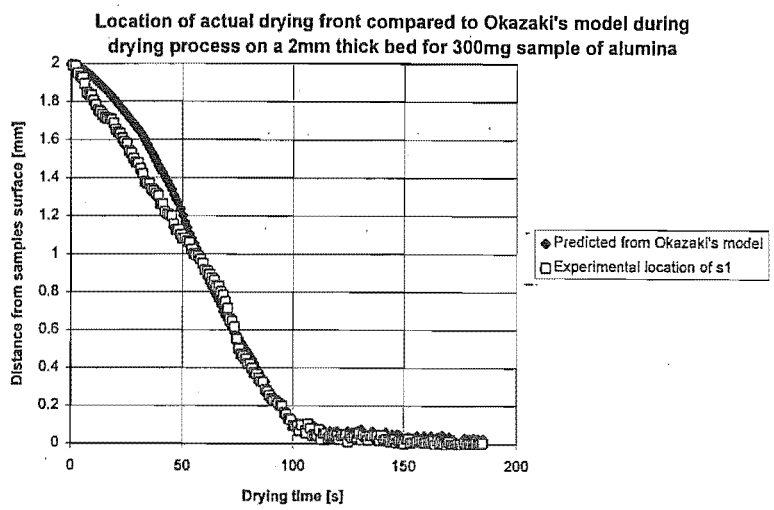

Figure 6.11 Comparison for location of drying front for predicted and experimental drying profiles for alumina, T_{dry}=120$degC$, T_{dew}=0.5$degC$, mass gas velocity=0.00709 $kgm^{-2}s^{-1}$, sample size=300mg

microstructure. Hydroquinone before and after drying appeared clear, with little if any evidence of water removal (from the weight loss in drying assay).

6.3.2 Variations in the types of materials used in this work

The adipic acid sorption isotherm is given in Figure 6.31, and that for Copolymer II copolymer is given in Figure 6.35. The observed weight loss drying profiles for these two materials are shown in Figure 6.13 (adipic acid) and Figure 6.12 (Copolymer II). The basic shapes of these curves are consistent with what could be expected, as shown in Figures 2.41 and 2.42. Notice the degree of scatter for Figure 6.12. This is raw data and is not filtered.

Figure 6.13 shows another form of scatter caused by electrical disturbances from the balance head.

6.3.3 Physical appearances

6.3.3.1 Silica gel

Silica gel. Name: silica gel (SG124). Appearance: clear (dry) to milky (wet) rigid particles. Physio-chemical data: bulk density, 1250 (kgm^{-3}), particle density, 1500 (kgm^{-3}); C_{ps}, specific heat capacity, 0.80 (kJ $kg^{-1}K^{-1}$), applications, desiccant and

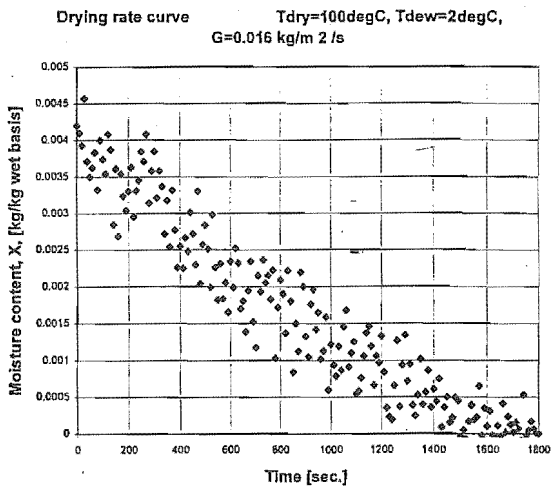

Figure 6.12 Weight loss profile for copolymer II

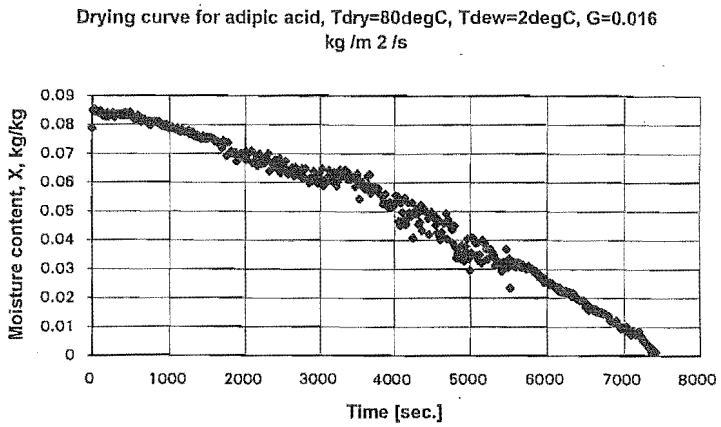

Figure 6.13 Weight loss profile for adipic acid

typical drying research material, particle size distribution; 1.86 ± 0.05 *mm* (one standard deviation)

Silica gel is widely used as a standard reference material in adsorption/desorption studies, and there is considerable information about moisture bonding. As there is a significant amount of drying kinetics literature on silica gel, drying kinetics results from new rigs are checked and calibrated against the published data for this material.

6.3.3.2 Alumina

Alumina. Name: Aluminium oxide (Al_2O_3). Appearance: Fine white powder, very cohesive. Physio-chemical data: bulk density, 850 (kgm^{-3}), particle density, 1150 (kgm^{-3}); C_{ps}, specific heat capacity, 0.80 (kJ $kg^{-1}K^{-1}$), applications, desiccant and typical drying research material, particle size distribution; 120 ± 30 μm (one standard deviation)

6.3.3.3 Pre-dried terephthalic acid (before drying) (fine chemical)

Terephthalic acid. Name: Terephthalic acid (1,4-benzenedicarboxylic acid). Appearance: Off-white powder with slight odour of acetic acid. Physio-chemical data: bulk density, 860 (kgm^{-3}), particle density, 1513 (kgm^{-3}); C_{ps}

Particle size distribution measured by sieve analysis. Figure 6.14 is a plot of weight percentage as a function of the different sieved particle diameters. For drying tests particles of average diameter were selected. These particle size distributions indicated the commercial variations produced for these products.

6.3.3.4 Adipic acid (fine chemical)

Adipic acid. Name: adipic acid (1,4-butenedicarboxylic acid). Appearance: white fine powder, cohesive. Physio-chemical data: melting point, 151-153 *degC*), bulk density, 1090 (kgm^{-3}), particle density, 1363 (kgm^{-3}); C_{ps}, Physical properties: Solubility in water at $10 degC$- 1.4 parts in 100.

Particle size distribution measured by sieve analysis. Figure 6.15 is a plot of weight percentage as a function of the different sieved particle diameters.

6.3.3.5 Styrene-butadiene copolymer (I)

Physio-chemical properties at $20 degC$ and 1013 *mbar*. The relative molecular mass is approximately 100 000 (unless otherwise stated). The glass transition temperature is approximately $100 degC$. Copolymer III is insoluble in water and hardly soluble in mineral oils. Copolymer III is a hydrogenated block copolymer of styrene and isoprene. It is a white odourless and tasteless solid. It is rubbery in texture. Particle size

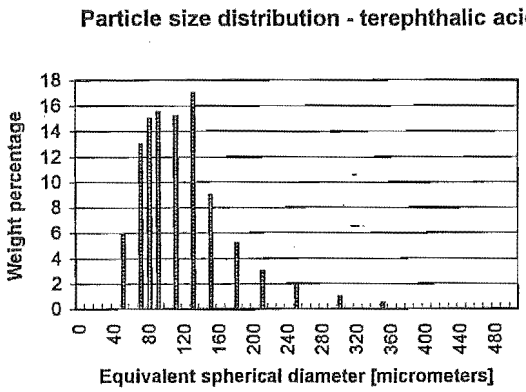

Figure 6.14 Particle size distribution for terephthalic acid

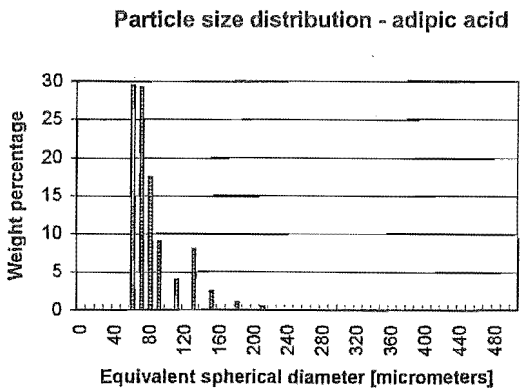

Figure 6.15 Particle size distribution for adipic acid

distribution measured by sieve analysis. Figure 6.16 is a plot of number percentage as a function of the different sieved particle diameters.

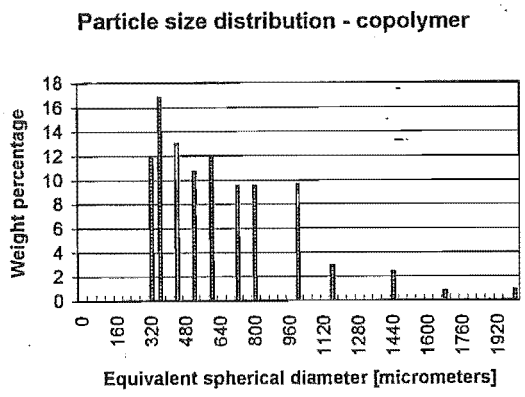

Figure 6.16 Particle size distribution for copolymer (I)

6.3.3.6 Styrene-butadiene co-polymer (II)

Clear copolymer based on styrene and butadiene. Particle size distribution measured by sieve analysis. Figure 6.17 is a plot of weight percentage as a function of the different sieved particle diameters.

6.3.3.7 Styrene-butadiene co-polymer (III)

Physio-chemical data: density, 930 (kgm^{-3}). It is a clear copolymer based on styrene and butadiene. Particle size distribution, extruded pellets all of around $4mm$ in diameter

6.3.3.8 Titaniferous iron sand

From the west coast shores of New Zealand. Name: titaniferous iron sand. Appearance: black and sandy, with tiny igneous crystals. Physio-chemical data: bulk density, 850 (kgm^{-3}), particle density, 1350 (kgm^{-3}); C_{ps}, particle size distribution; $120 \pm 35\ \mu m$ (one standard deviation)

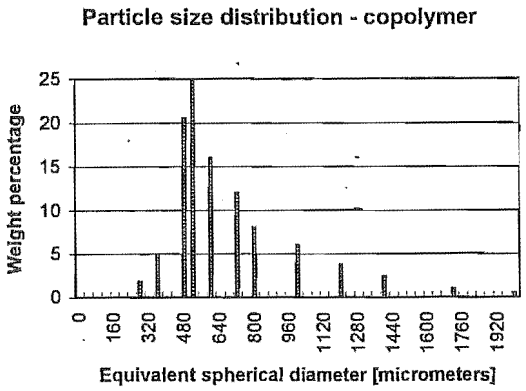

Figure 6.17 Particle size distribution for copolymer (II)

6.3.4 Heat of vaporisation + wetting against moisture content at low moisture contents

Figure 6.18 shows SG124 plotted for heat of wetting+vaporisation against moisture content. Three methods of calculating the heats of sorption against moisture content were attempted. Clausius-Clapeyron (the most accurate), monolayer estimation based on thermodynamic principals from Polyani (1916) with appeared to be the least accurate (this is called Langmuir fitting in the following graphs on heats of wetting against moisture content), and the heats of sorption calculated from simultaneous DSC/TGA tests (Etzler and Conners, 1991). For clarity, the heat of desorption is equivalent to the heat of vaporisation plus the heat of wetting.

Other comparisons of heats of wetting between isotherms and DSC/TGA tests for the remainder of the materials used in this work are shown in Figure 6.19 onward. The horizontal solid line is the heat of vaporisation of water at the highest sorption temperature ($80 degC$). It is shown to indicate a reference baseline to illustrate the extra heat required to remove the bound moisture from within the solid matrix of the particulate material.

Alumina

Alumina appears to show a steep rise in heat of wetting (see Figure 6.19) as more and more bound moisture is removed from the solid. Notice the very low initial moisture

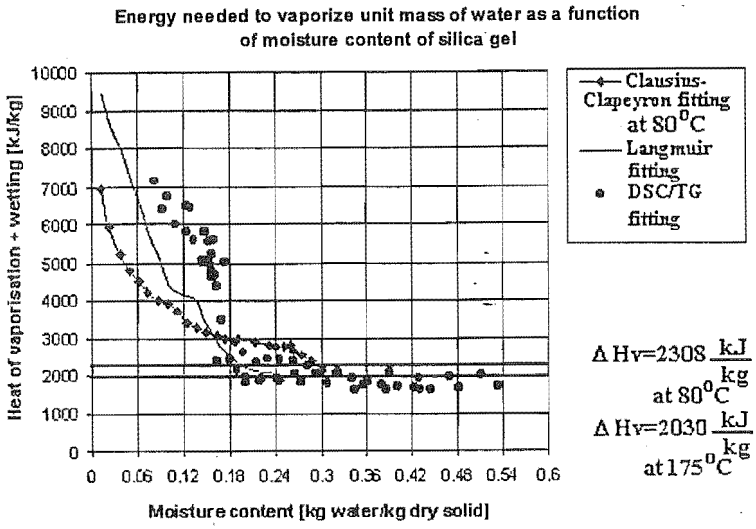

Figure 6.18 Comparison of calculated heats of vaporisation and heat of wetting with moisture content of silica gel type124

content of approximately 0.6% in these tests. The calculated heat of wetting by using DSC/TG unit gave a very non-linear increase as the moisture content was reduced to near zero. Note the initial moisture contents are the same for these heat of desorption curves as the drying rate curves for each material, unless otherwise stated.

Adipic acid

The heat of wetting for adipic acid showed a more gradual increase over a larger moisture content range (see Figure 6.20). This indicates the similar heats of wetting of physisorbed and chemisorbed moisture for this material, thus emphasising the difficulty of drying this type of product commercially (D Gravatt, Merck, Manufacturing Division Elkton, USA, *private communication*).

Pure terephthalic acid

DSC/TG again predicted a non-uniform increase in heat of wetting, which is questionable, because of the reasons discussed earlier in this section (see Figure 6.21).

Pre-dried terephthalic acid

A lower heat of wetting is shown in Figure 6.22 because cyclohexane exerts a greater vapour pressure than water (cyclohexane and other organic residues are the moisture of this pre-dried material). However, the trend in the strength of bound moisture was similar to that observed for pure terephthalic acid.

Copolymer of polystyrene-butadiene - I

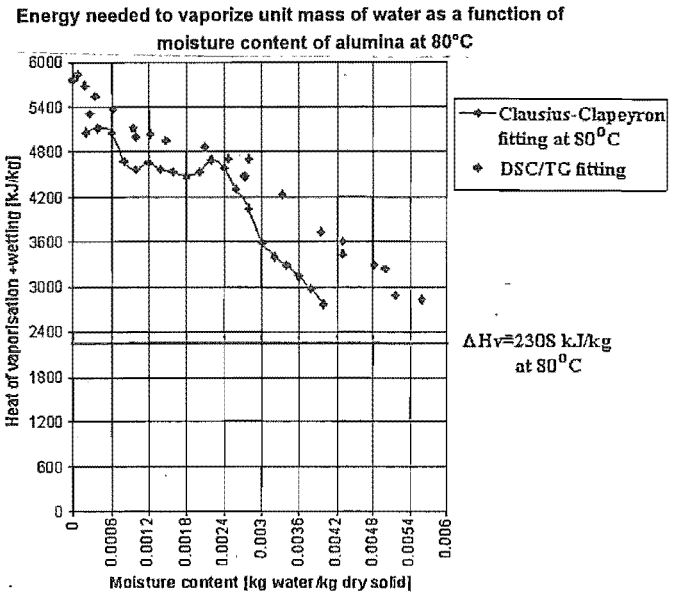

Figure 6.19 Comparisons of heats of wetting calculated from isotherms and DSC/TGA fitting for alumina

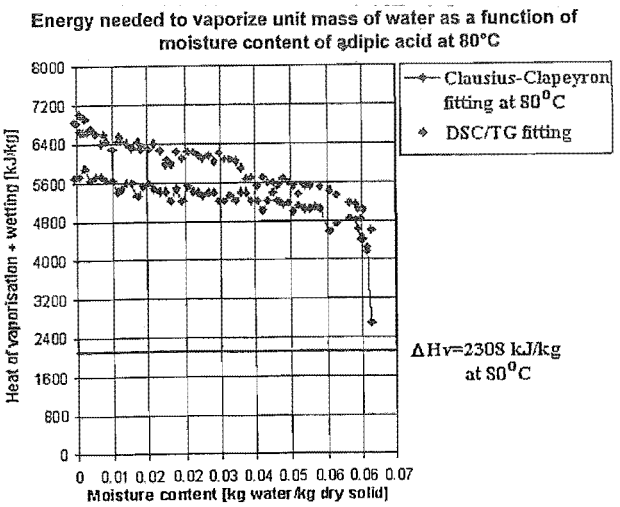

Figure 6.20 Comparisons of heats of wetting calculated from isotherms and DSC/TGA fitting for adipic acid

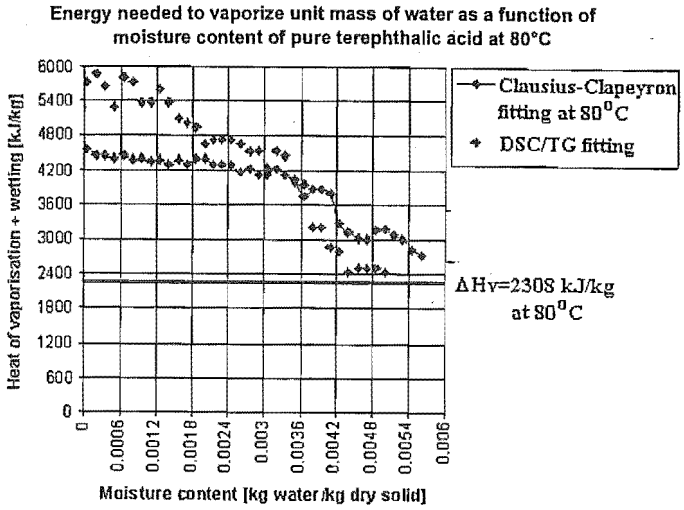

Figure 6.21 Comparisons of heats of wetting calculated from isotherms and DSC/TGA fitting for pure terephthalic acid

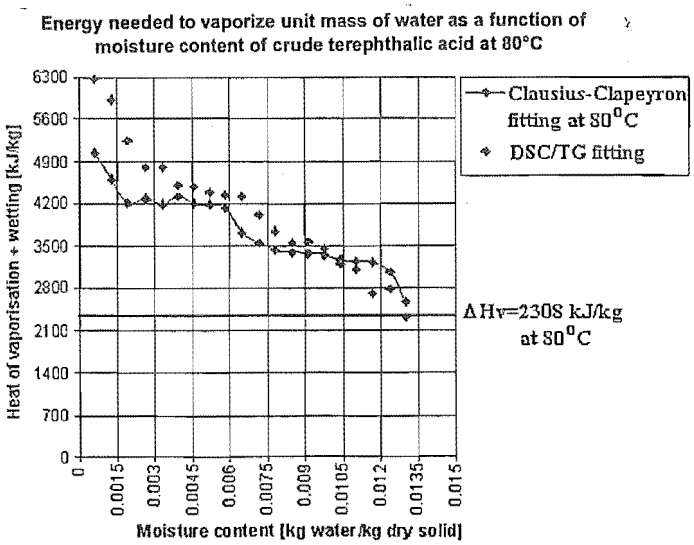

Figure 6.22 Comparisons of heats of wetting calculated from isotherms and DSC/TGA fitting for pre-dried terephthalic acid

A very gradual heat of wetting was observed for the polystyrene-butadiene copolymers because this type of material is hydrophobic (see Figure 6.23).

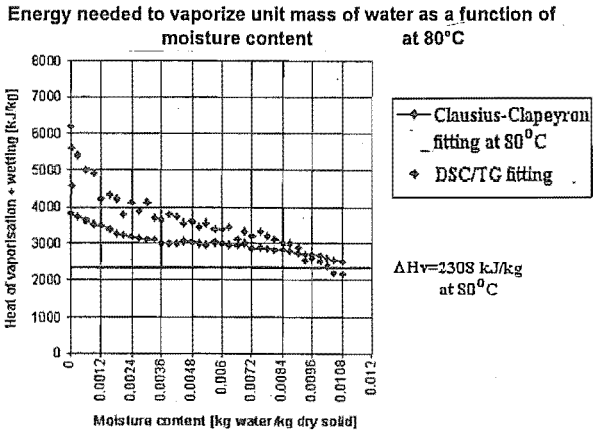

Figure 6.23 Comparisons of heats of wetting calculated from isotherms and DSC/TGA fitting for copolymer I

Copolymer of polystyrene-butadiene - copolymer II

(see Figure 6.24)

Copolymer of polystyrene-butadiene - copolymer III

(see Figure 6.25)

Titaniferous iron sand

(see Figure 6.26)

Heat treated silica gel 124

(see Figure 6.27)

6.4 DRYING TUNNEL SORPTION STUDIES - GRAPHS OF SORPTION ISOTHERMS

Silica gel

The shape of the sorption isotherm in Figure 6.28 is typical of a silica gel material, fitting a IUPAC H2 hysteresis loop. The shape of the H2 hysteresis loop is shown in Figure 2.3 in Chapter 2.

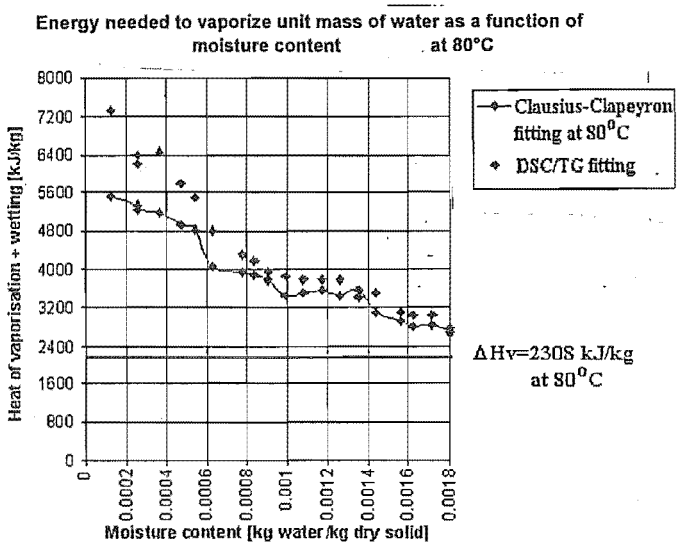

Figure 6.24 Comparisons of heats of wetting calculated from isotherms and DSC/TGA fitting for copolymer II

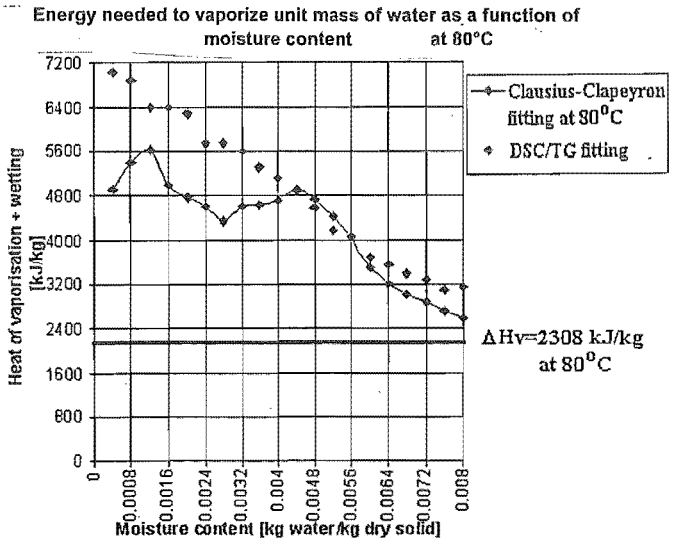

Figure 6.25 Comparisons of heats of wetting calculated from isotherms and DSC/TGA fitting for copolymer III

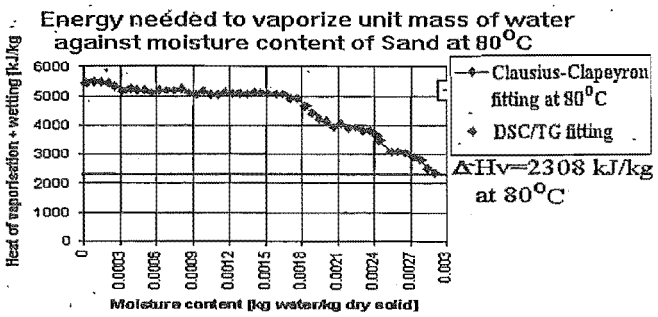

Figure 6.26 Comparisons of heats of wetting calculated from isotherms and DSC/TGA fitting for titaniferous iron sand

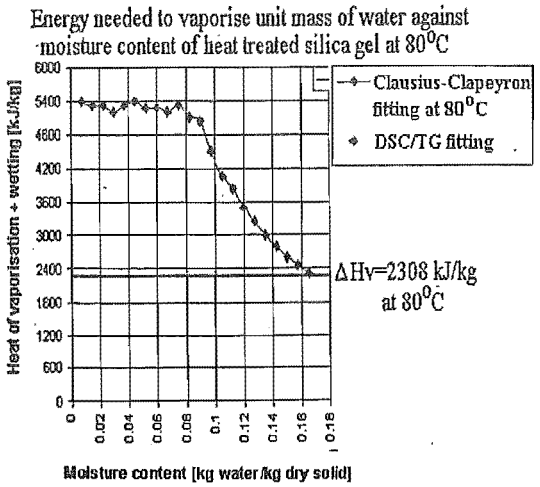

Figure 6.27 Comparisons of heats of wetting calculated from isotherms and DSC/TGA fitting for heat-treated silica gel

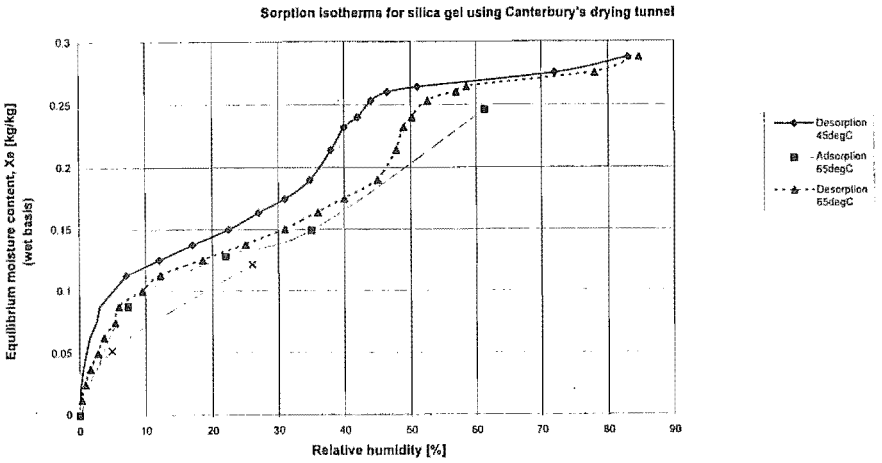

Figure 6.28 Sorption isotherms for silica gel

Alumina

Linear sorptive bahaviour (Figure 6.29) was observed for most of the loosely bound moisture. This suggests that this bound moisture is similar to liquid water held in layers of moisture not directly bound to the pore surface of alumina. More strongly bound moisture was evident below 0.2%, which was probably moisture bound directly to the pore surface.

Iron sand

A significant amount of moisture was bound very tightly to the iron sand (Figure 6.30), probably in the form of water complexes typical of transition elements. Very little of the moisture appeared to be held in layers, because of the microporous structure of this material.

Adipic acid

Most of the moisture in adipic acid (Figure 6.31) appeared to be directly bound to the monomer units or represented as removable chemisorbed moisture from monomer adipic acid units.

Pure terephthalic acid

Small amounts of moisture (Figure 6.32) was held in multilayers for terephthalic acid, but there is a significant amount bound tightly to electrophilic carboxyl end groups on the terephthalic acid unit.

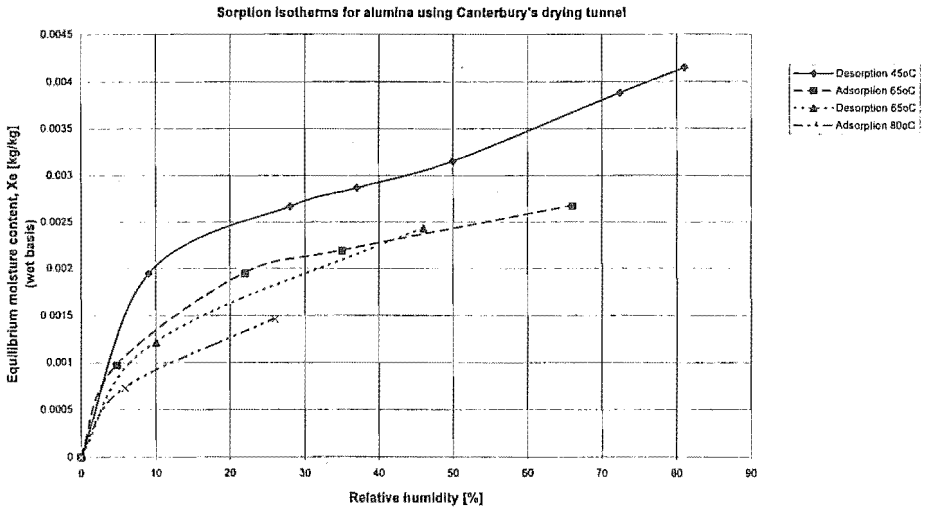

Figure 6.29 Sorption isotherms for alumina

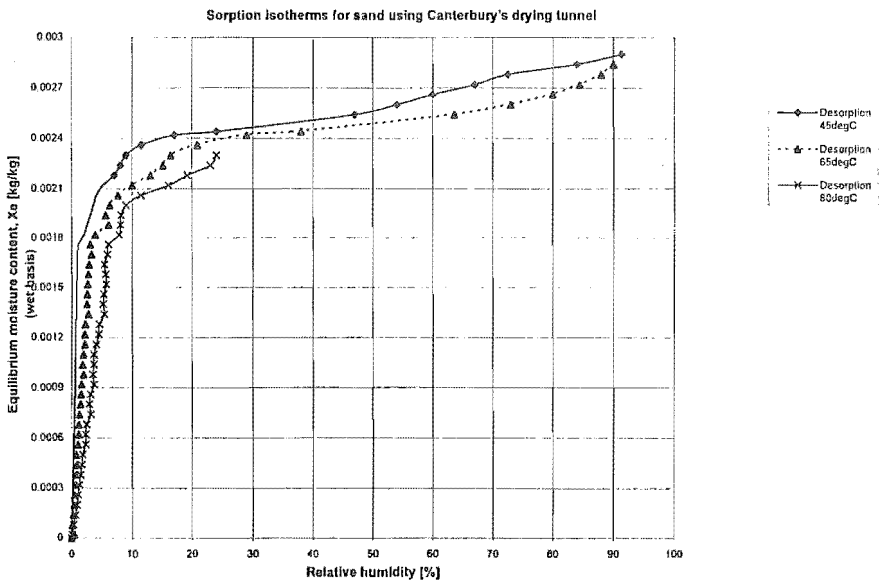

Figure 6.30 Sorption isotherms for iron sand

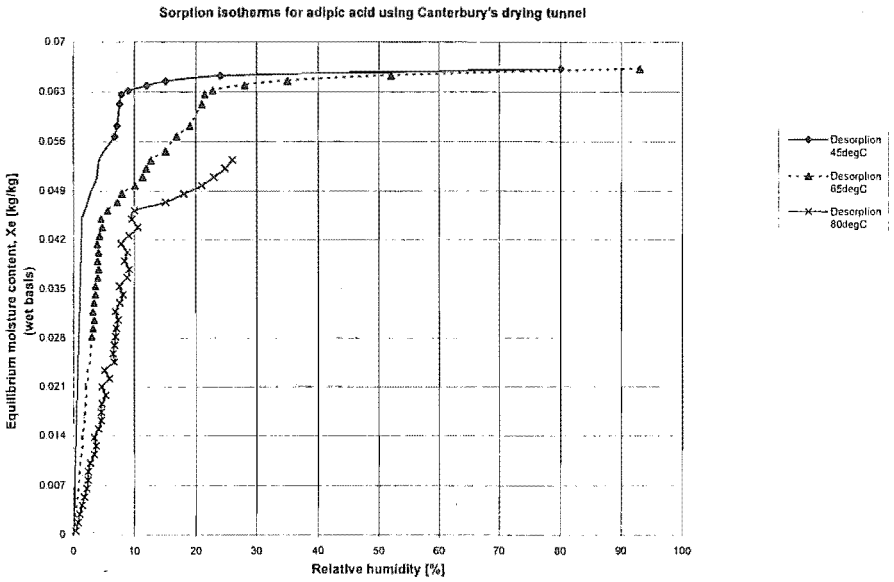

Figure 6.31 Sorption isotherms for adipic acid

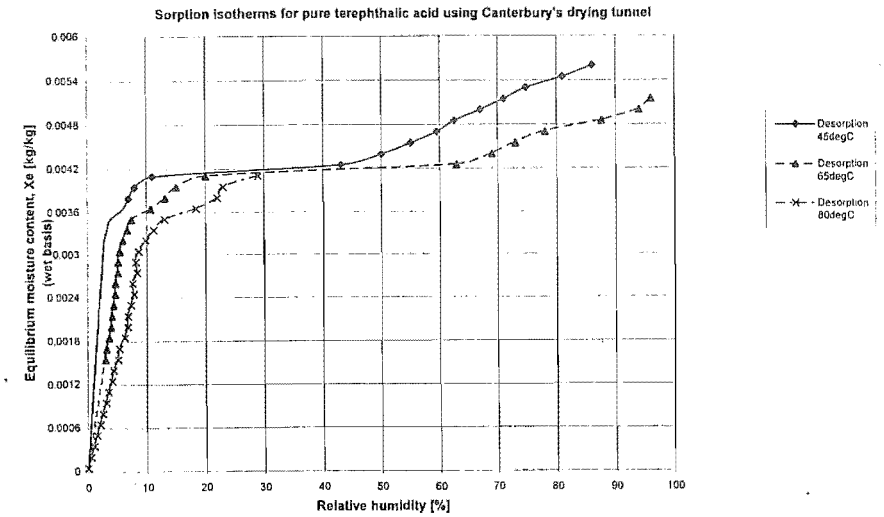

Figure 6.32 Sorption isotherms for pure terephthalic acid

Pre-dried terephthalic acid

Observations were made of any favourable substitution of the cyclohexane with water vapour from the humidified air stream. It appeared that, at 45 *degC*, the sample appeared to preferentially bind the cyclohexane already present in the terephthalic matrix. No displacement was observed after steady state conditions were reached. The isotherm was a similar shape to that observed for pure terephthalic acid (compare Figure 6.32 to Figure 6.33). However, at lower sorption temperatures, the non-polar organic cyclohexane appeared to favour binding to the organic terephthalic acid.

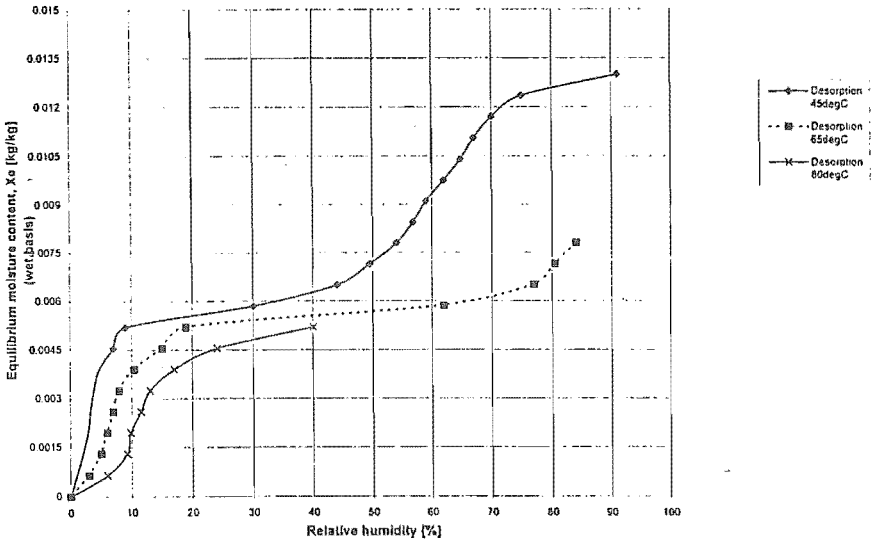

Figure 6.33 Sorption isotherms for pre-dried terephthalic acid

Copolymer I

The copolymers of polystyrene-butadiene all appeared to show water being held in clusters, which is a typical explanation of the linear appearance of the following sorption isotherms in Figures 6.34, 6.35 and 6.36. The linear sorptive behaviour over the range of relative humidities is typical of water molecules being held in "water clusters", and not directly bound to the solid material (Hallstrom and Wimmerstedt, 1983)

Copolymer II

(see Figure 6.35)

Copolymer III

(see Figure 6.36)

Heat treated silica gel 124

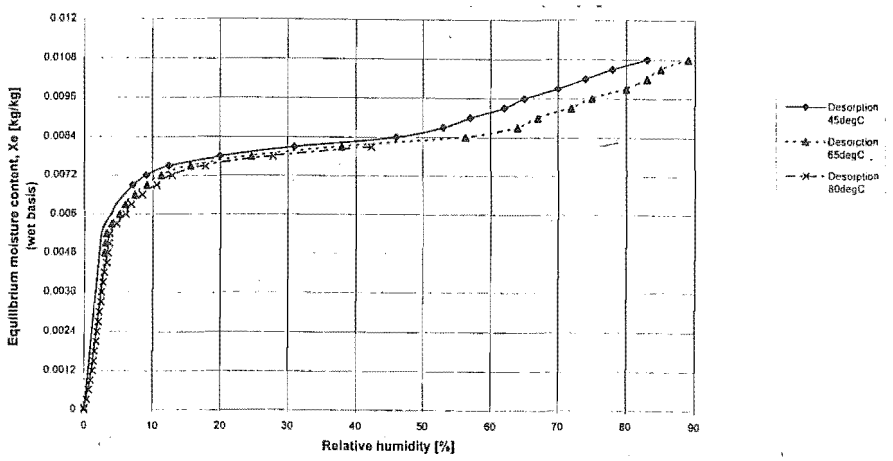

Figure 6.34 Sorption isotherms for copolymer I

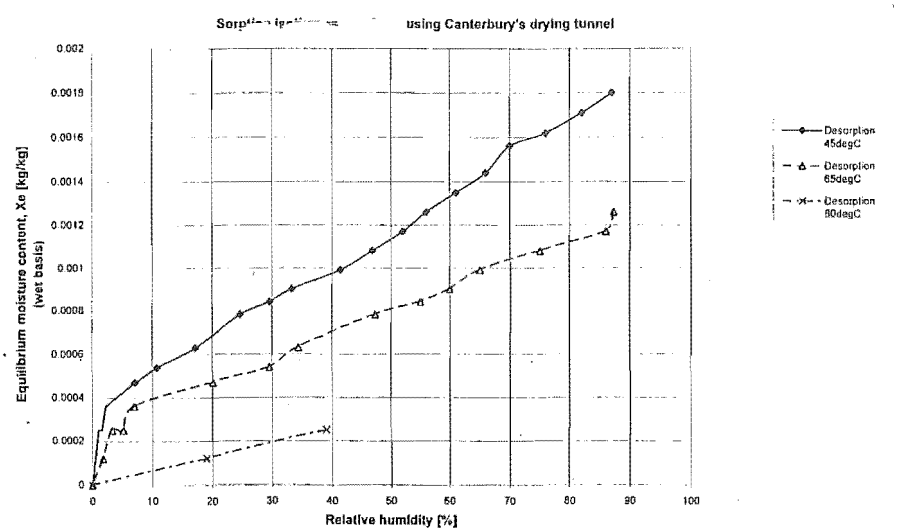

Figure 6.35 Sorption isotherms for Copolymer II

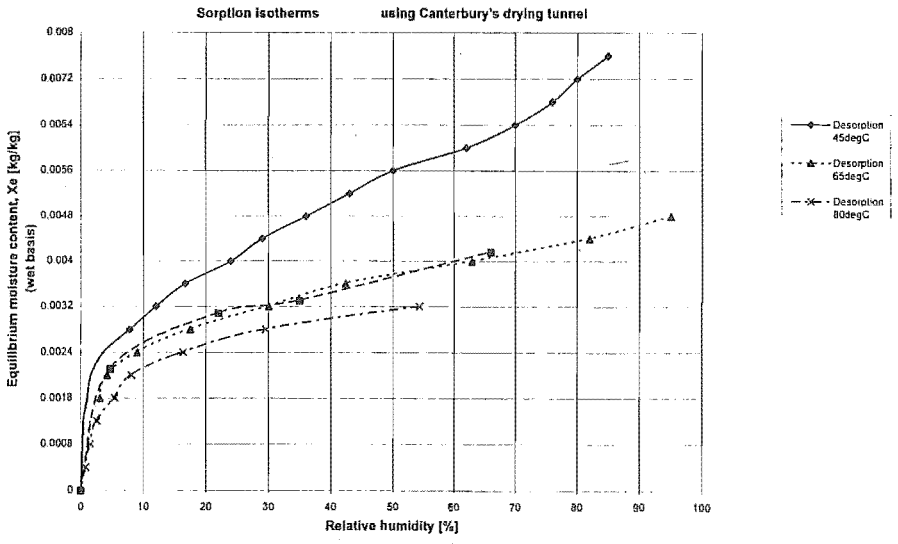

Figure 6.36 Sorption isotherms for Copolymer III

(see Figure 6.37)

6.5 EXPERIMENTAL PROGRAMME WITH NEW DRYING KINETICS RIG

A complete description of all the experimental conditions is given in Appendix C.

Alumina, sand, pure terephthalic acid and pre-dried terephthalic acid were exposed to the same air conditions as listed in Table 6.6. The experimental conditions for Copolymer I are given in Table 6.7.

Table 6.6 Experimental conditions for alumina

	T_{dry} $(degC)$	Humidity $(kg\ kg^{-1})$	Air velocity $(kg\ m^{-2}\ s^{-1})$	Sample weight mg	Layer thickness mm
Exp. # 1 - 3	120	0.0005	0.00709	300	2
Exp. # 4 - 6	120	0.0005	0.00158	300	2
Exp. # 7 - 9	140	0.0005	0.00709	300	2
Exp. # 10 - 12	120	0.002	0.00709	300	2
Exp. # 13 - 15	120	0.0005	0.00709	100	0.7

Materials: Copolymer I

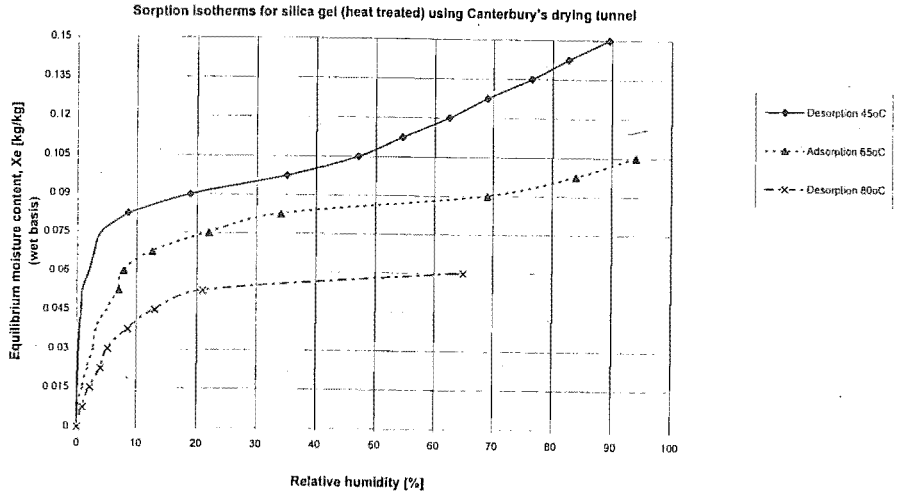

Figure 6.37 Sorption isotherms for heat treated silica gel

Table 6.7 Experimental conditions for Copolymer 1 only

	T_{dry} $(degC)$	Humidity $(kg\ kg^{-1})$	Air velocity $(kg\ m^{-2}\ s^{-1})$	Sample weight mg	Layer thickness mm
Exp. # 1 - 3	120	0.0005	0.00709	300	4
Exp. # 4 - 6	120	0.0005	0.00158	300	4
Exp. # 7 - 9	140	0.0005	0.00709	300	4
Exp. # 10 - 12	120	0.002	0.00709	300	4
Exp. # 13 - 15	120	0.0005	0.00709	100	2

6.6 DRYING KINETICS OF SELECTED MATERIAL AT LOW-MOISTURE CONTENTS USING THE NEW APPARATUS

In this section, the validity of the characteristic drying curve for the selected materials is tested.

6.6.1 Comparisons between Harwell's drying kinetics rig with new apparatus - characteristic drying curves

6.6.1.1 Effect of changing bed configurations under a laminar through-flow of air

The experimental conditions for Figure 6.38 are listed in Table C.1 of the appendix.

A single silica gel 124 particle ($X_o = 0.16\ kg\ kg^{-1}$ wet basis) was dried by subjecting it to a dry-bulb temperature of $100 degC$, wet-bulb temperature of $36 degC$ at an air velocity with $Re_p = 70$. The observed maximum drying rate at the start of the falling-rate period was $0.0011\ kg\ kg^{-1} s^{-1}$. Another particle with the same characteristics was dried at the edge of the drying chamber, and the observed drying behaviour was the same as that of the particle dried at the centre. Under the same external drying conditions, two single particles separated by two particle diameters were observed to dry at a rate again equivalent to that of the aforementioned tests. However, for the next experiment, two equivalent silica gel particles were placed touching each other in the centre of the drying chamber; under the same laminar flow ($Re_p = 70$, with the characteristic length sill that of a single particle), the observed drying rates were found to be $0.0007\ kg\ kg^{-1} s^{-1}$, a 50% drop due presumably to an increase in the external mass transfer resistance, because each particle is influenced by the drying of the neighbouring particle, i.e. the boundary layers for each particle overlap. This simulated the drying of one particle layer because the observed drying rates for two particles dried adjacent to each other and for one particle layer were the same. Again, under the same drying conditions, the drying of two, three and four layers gave maximum drying rates of 0.00033, 0.00023, $0.00023\ kg\ kg^{-1} s^{-1}$ respectively. Notice that the drying behaviour of thicker beds may have drying rates similar to drying three and four layers, once heat and mass transfer fronts are established in the thicker layer. Earlier work by Keech (1992), showed similar characteristic drying curves for 4-8 layers. As the moisture pick-up is small, the external drying conditions are effectively constant over the second and succeeding layers. The characteristic drying curves of 3-8 layers in a bed were observed to be equivalent to those in earlier tests (Keech, 1992).

6.6.1.2 Effect of changing external flow conditions under a laminar through-flow of air

The second group of experiments was an attempt to extend the current limits on air velocity when applying the characteristic drying curve to the silica gel 124 material. The air velocities used were 0.0009-0.017 $m\ s^{-1}$. A range of drying temperatures (T_{dry} = 80-140$degC$) and slight variations in bed configurations (single particle and particles in one layer) were used to investigate any variations in drying characteristics.

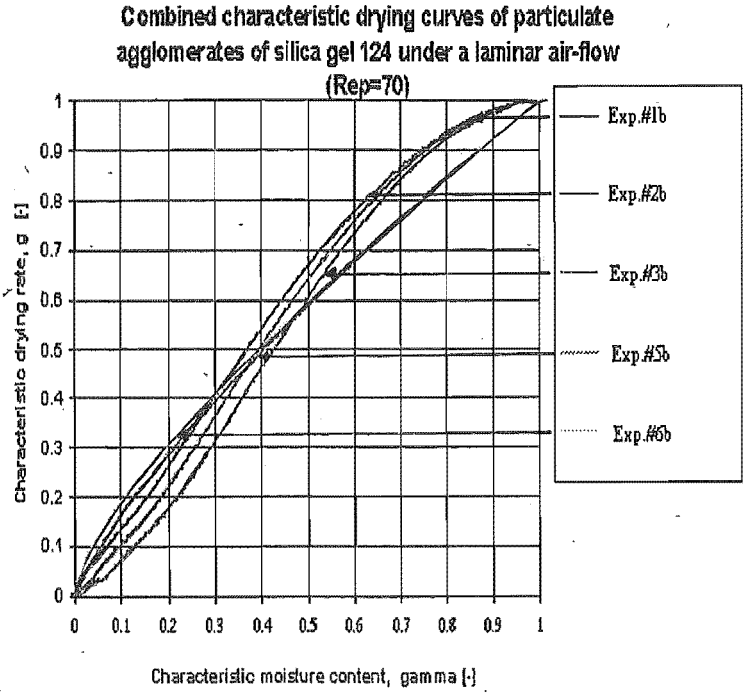

Figure 6.38 Characteristic drying curves (*g-curves*), X_o = 0.16 ($kg\ kg^{-1}$), of varying bed configurations with new apparatus

The experimental conditions for Figure 6.39 are listed in Tables C.2 and C.3 of the appendix.

6.6.2 Determining the critical moisture content of the copolymer - I

Bed configuration: single isolated particles, T_{dry}=100$degC$, T_{dew}=0.6$degC$, gas mass velocity = 0.00709 $kgm^{-2}s^{-1}$ (8 $l\ min^{-1}$ through 150 mm sample section with 50 mm sample pan. Small ribbons located under the sample pan indicated that the flow was the same through the thin-layer as surrounding the pan). Other material have very small particle diameters, so we can assume $X_{hyg}/X_{cr} \approx$ =1. Table 6.8 shows the three sizes of particles sizes used to calculate the copolymer critical moisture content.

Table 6.8 Varying particle size for Copolymer I to determine the critical moisture content

Material (shell polymers)	Particle size
Copolymer I	small particle size (100 μm)
Copolymer I	medium particle size (1000 μm)
Copolymer I	large particle size (2000 μm)

The experimental conditions for this set of experiments are shown in Table C.4 in the appendix, the results are shown in Figure 6.40, and the raw data are given in Appendix F.

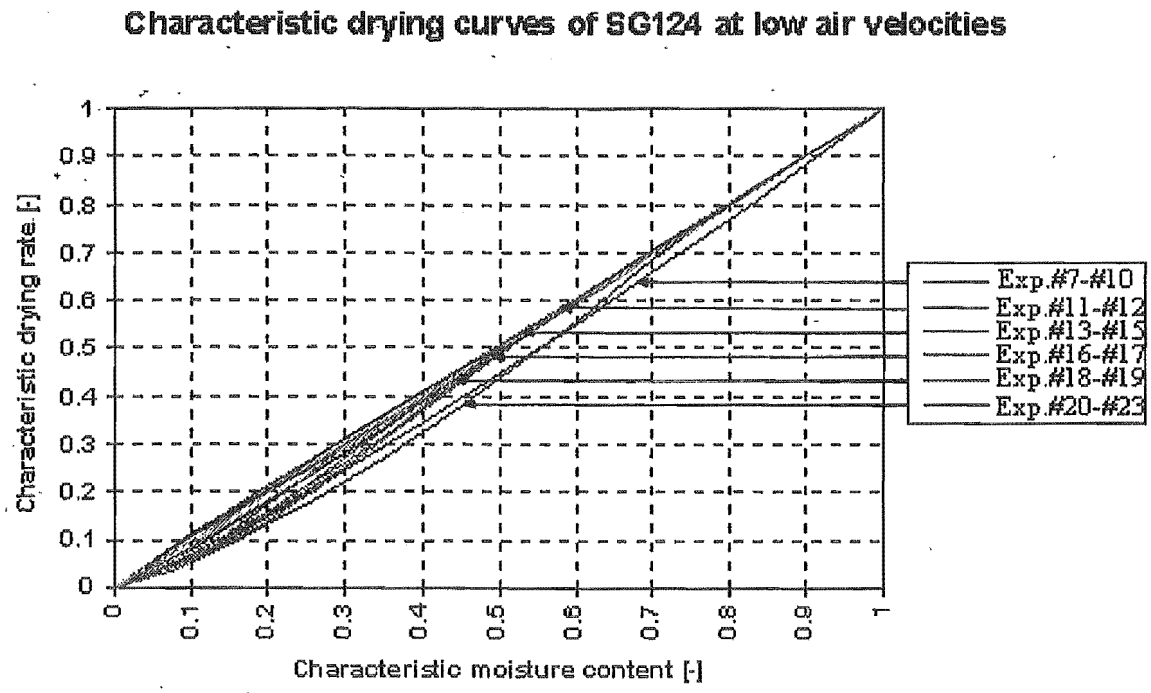

Figure 6.39 Characteristic drying curves (*f-curves*), $X_{cr} = 0.38$ ($kg\ kg^{-1}$), of silica gel 124. Changing the drying conditions for a thin-layer of particles.

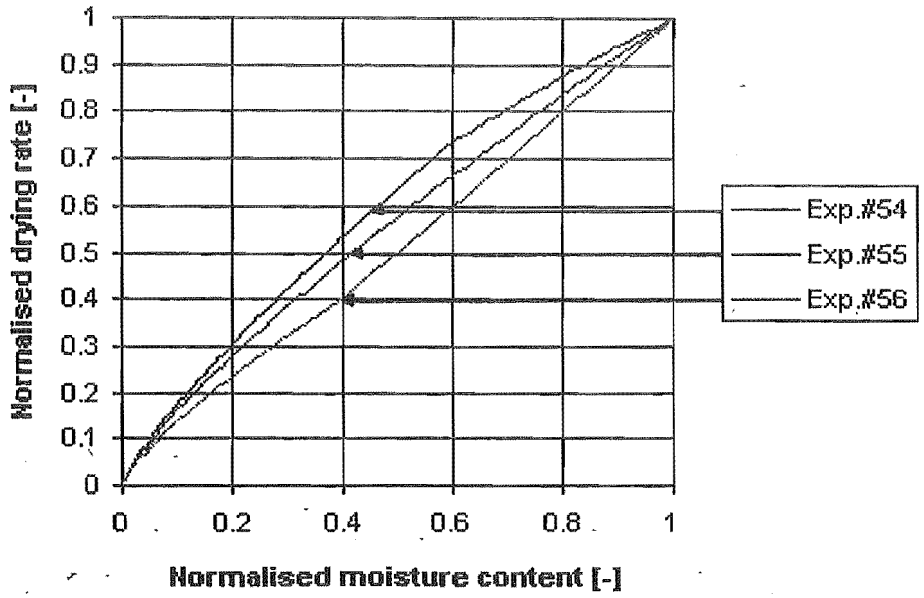

Figure 6.40 Characteristic drying curve (g vs. Γ), to determine the critical moisture content of the copolymers Copolymer 1

Based on the method given in Chapter 2 of this work on calculating a particle's critical moisture content, the following equation describes the relationship of particle size to its critical moisture content. A limitation on this approach on calculating the critical moisture content was found. A difficulty arose in ariving at this equation, since from sorption isotherms it was very difficult to obtain an exspression relating the equilibrium moisture content at high relative humidities (for silica gel see Equation 2.150, which is needed to calculate the critical moisture content. This probably a result of the uncertain degree of possible swelling of the copolymer and the variable sizes of water clusters. Thus, if the material has a finite maximum hygroscopic moisture content or does not swell, the critical moisture content can be estimated.

$$\frac{X_{cr}}{X_o} = [0.71 + 0.06d_p](0.283d_p)^{-1/(0.599+0.2d_p)} \tag{6.2}$$

Table 6.9 The parameters of the mean characteristic drying curves for Copolymer I

Particle size mm	A	B	C	X_{cr}/X_o
0.1	0.2599	0.603	0.806	0.013
1	0.8	0.502	0.79	0.25
2	1	0.402	0.773	0.38

Table 6.9 does indicate different critical moisture contents. This can probably be explained by the swelling of the three sizes of particles as they hydrate. This copolymer appears not to favour a characteristic drying curve approach to identifying its kinetics.

6.6.3 Determining the drying kinetics of selected materials at low moisture content

Bed configuration: single isolated particles, $T_{dry} = 100 degC$, $T_{dew} = 0.6 degC$, gas mass velocity $= 0.00709\ kg\ m^{-2}\ s^{-1}$

(see Table 6.10)

Table 6.10 Materials used for low-moisture content experiments and the bed configurations used for all of these materials

Material	Bed configuration
Adipic acid	Single isolated particles
Alumina	One layer
Iron sand	Multilayered bed
Pre-dried terephthalic acid	
Copolymer I	
Copolymer II	
Copolymer III	

The following graphs test the applicability of the characteristic drying curve for a limited range of conditions, which are listed in Appendix C. Characteristic drying curves have not previously been developed for low moisture solids. It was useful to ascertain whether it was possible to use this approach to model drying kinetics. The following characteristic drying curves (Figures 6.41, 6.42, 6.43, 6.44 and 6.45) tested this concept by constructing curves for various flow conditions. The raw data for each of the curves is shown in Appendix F, and the remaining raw data points for other experiments are given in the compact disc at the back of this thesis.

For alumina, Figure 6.41 shows a number of characteristic drying curves for the range of conditions listed in Table C.5 in the appendix.

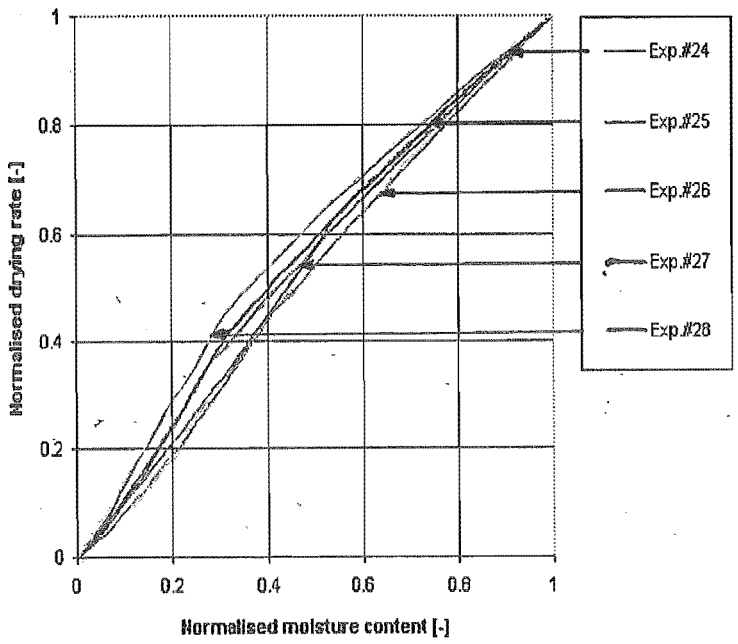

Figure 6.41 Testing the characteristic drying curve (g vs. Γ) for the materials at low moisture contents - alumina. There are approximately 100 data points on each curve, so only fitted lines are given

For iron sand, Figure 6.42 shows a number of characteristic drying curves for the range of conditions listed in Table C.6 in the appendix.

For pre-dried terephthalic acid, Figure 6.43 shows a number of characteristic drying curves for the range of conditions listed in Table C.7 in the appendix.

For pure terephthalic acid, Figure 6.44 shows a number of characteristic drying curves for the range of conditions listed in Table C.8 in the appendix.

For Copolymer III, Figure 6.45 shows a number of characteristic drying curves for the range of conditions listed in Table C.9 in the Appendix.

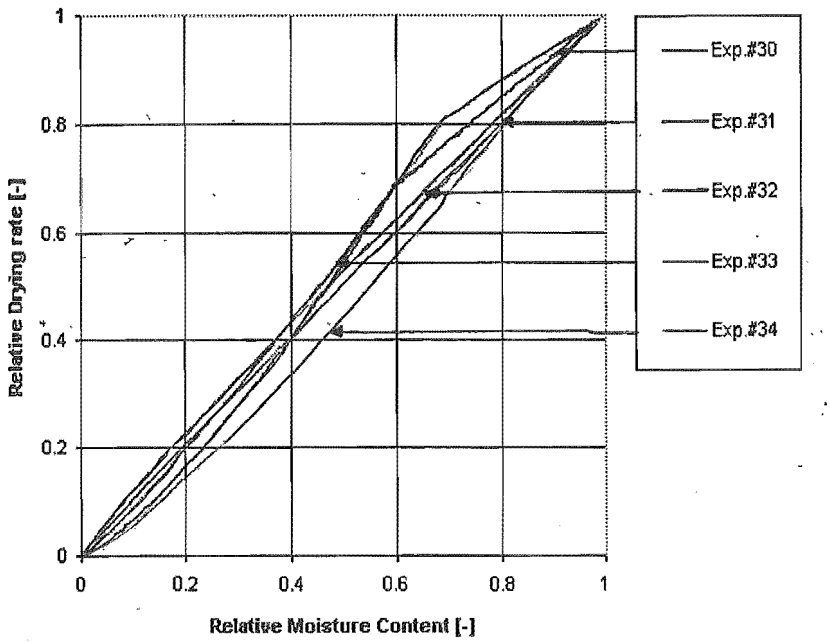

Figure 6.42 Testing the characteristic drying curve (g vs. Γ) for the materials at low moisture contents - iron sand. Again, there are approximately 100 data points on each curve, so only fitted lines are given

6.6.4 Vacuum drying

6.6.4.1 Single particle tests

Four materials (alumina, iron sand, pre-dried terephthalic acid, Copolymer I) were used to determine the effects on the shape of the characteristic drying curve under an isolated single particle arrangement. This is shown in Figure 6.46 and listed in Table C.10 in the appendix. Various bed and drying conditions were tested for isolated silica gel particles and alumina under vacuum conditions. Their characteristic drying curves were constructed and are plotted in the following graphs (Figures 6.46, 6.47 and 6.48).

6.6.4.2 Vacuum drying tests of silica gel 124 and alumina

For silica gel 124, Figure 6.47 shows a number of characteristic drying curves for the range of conditions listed in Table C.11 in the appendix.

For alumina, Figure 6.48 shows a number of characteristic drying curves for the range of conditions listed in Table C.12 in the appendix.

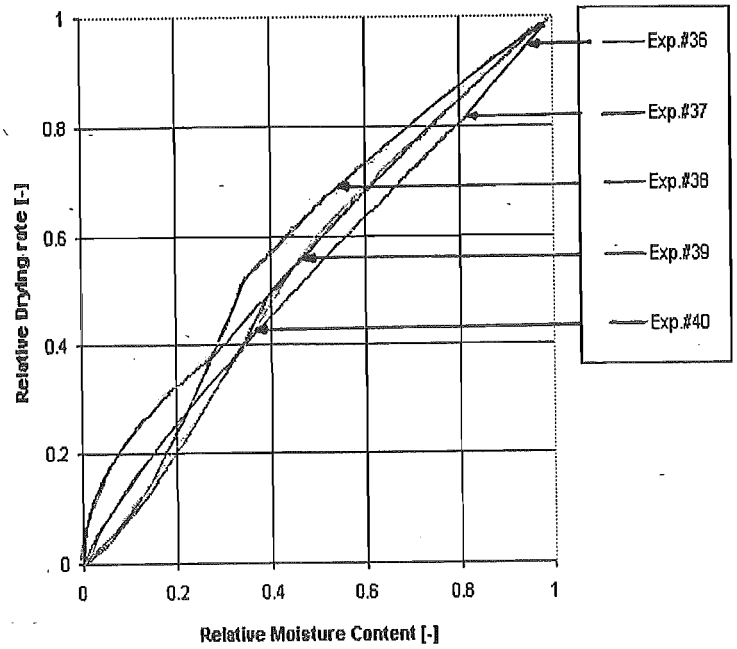

Figure 6.43 Testing the characteristic drying curve (g vs. Γ) for the materials at low moisture contents - pre-dried terephthalic acid. There are approximately 100 data points on each curve, so only fitted lines are given

6.6.5 Drying kinetics at low-moisture contents of alumina containing a binary solution of water and isopropyl alcohol

For alumina containing a binary solution of isopropyl alcohol and water, Figure 6.49 shows a number of characteristic drying curves for the range of conditions listed in Table C.13 in the appendix.

The experimental and estimated drying rates are shown in Figure 6.50.

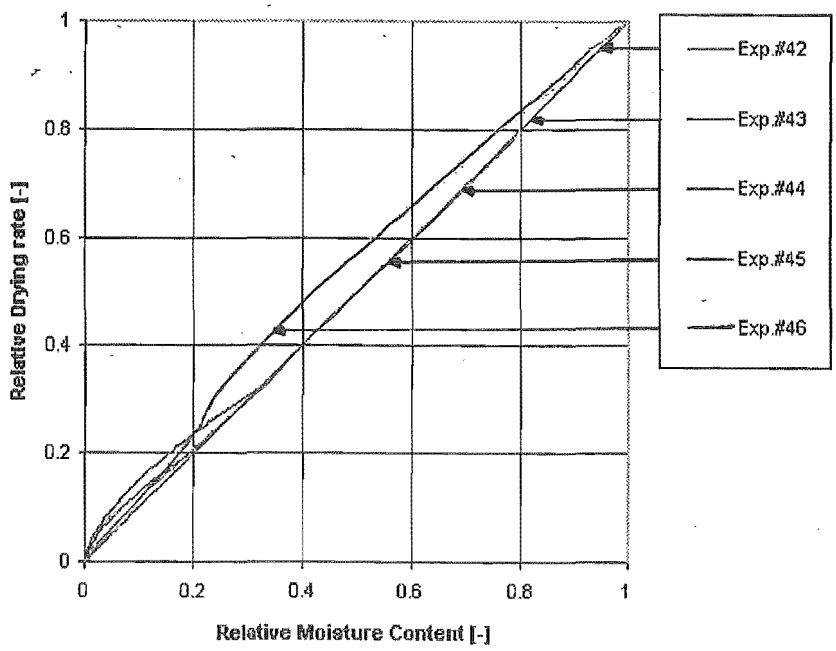

Figure 6.44 Testing the characteristic drying curve (g vs. Γ) for the materials at low moisture contents - pure terephthalic acid. There are approximately 100 data points on each curve, so only fitted lines are given

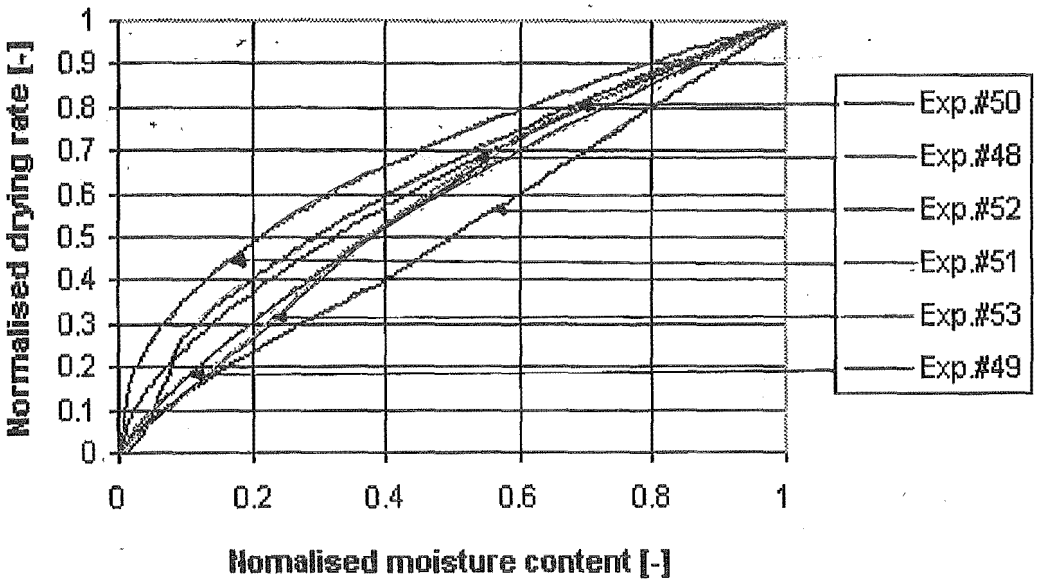

Figure 6.45 Testing the characteristic drying curve (g vs. Γ) for the materials at low moisture contents - Copolymer III. Because to the large spread of the data in this curve, the data are given in Appendix F

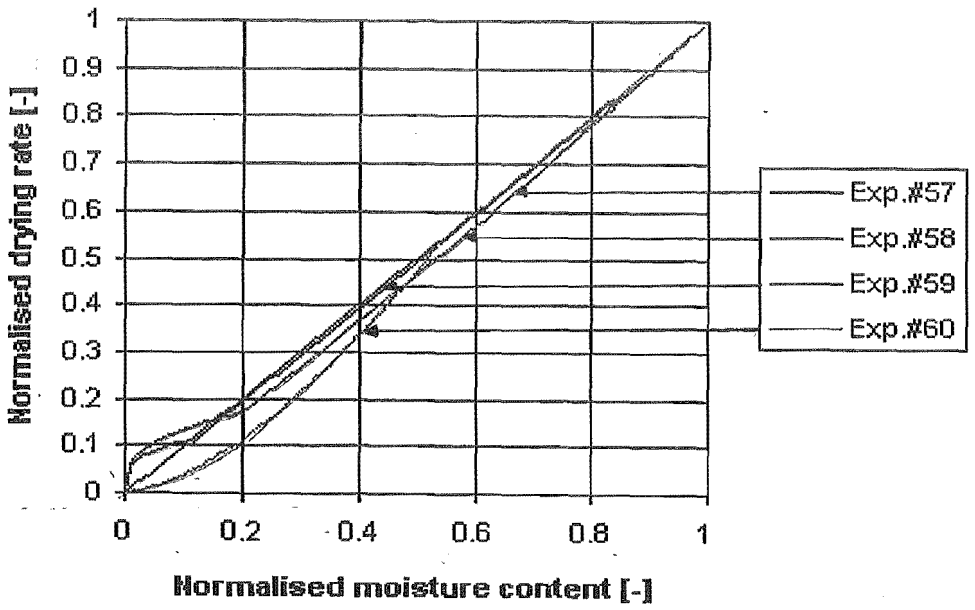

Figure 6.46 Testing the characteristic drying curve (g vs. Γ) for isolated particles at low moisture contents

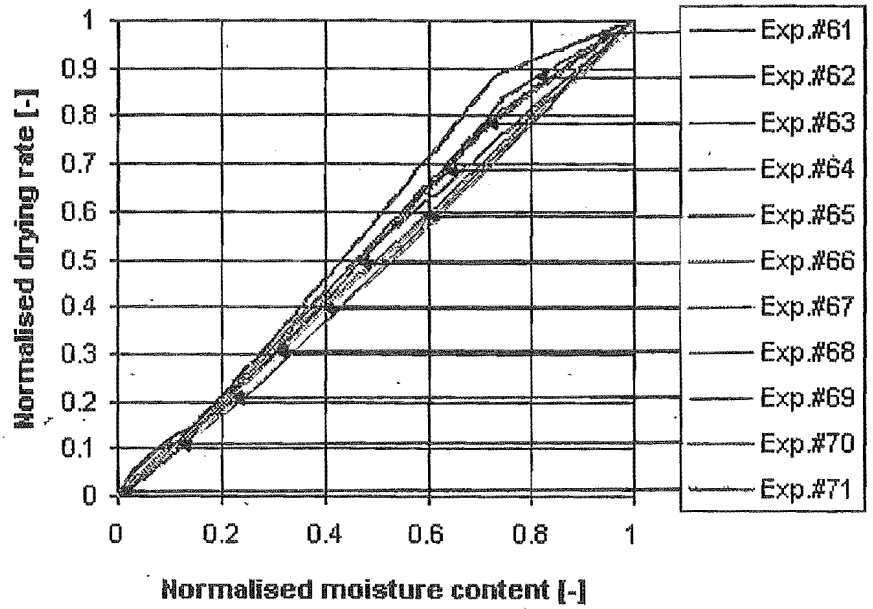

Figure 6.47 Testing the characteristic drying (g vs. Γ) for silica gel 124 under varying vacuum conditions

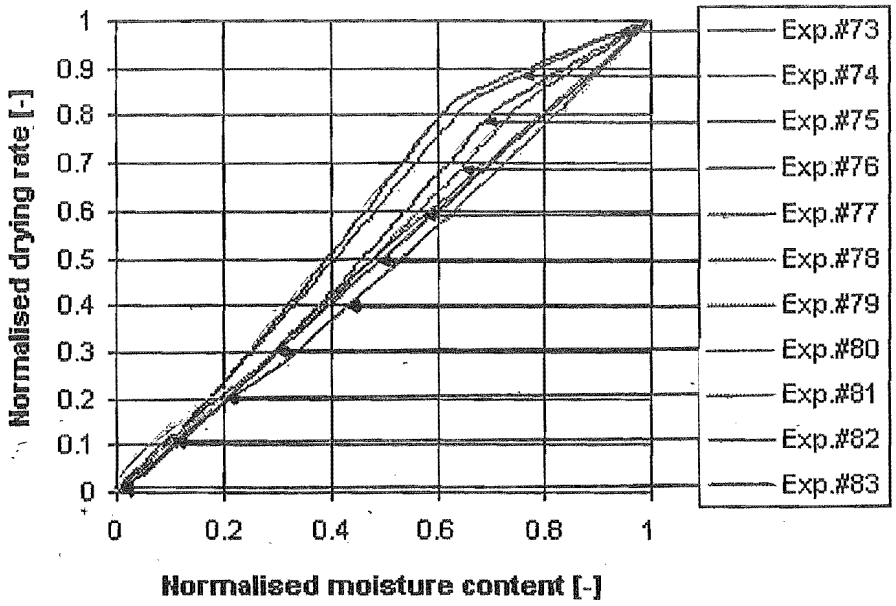

Figure 6.48 Testing the characteristic drying curve (g vs. Γ) for alumina under varying vacuum conditions

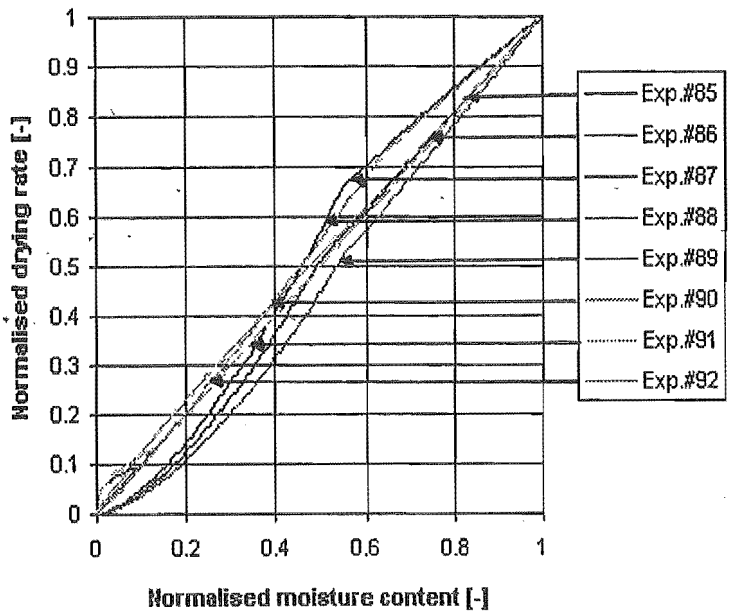

Figure 6.49 Testing the shape of the characteristic drying curve (g vs. Γ) for alumina containing a binary solution of water and isopropyl alcohol

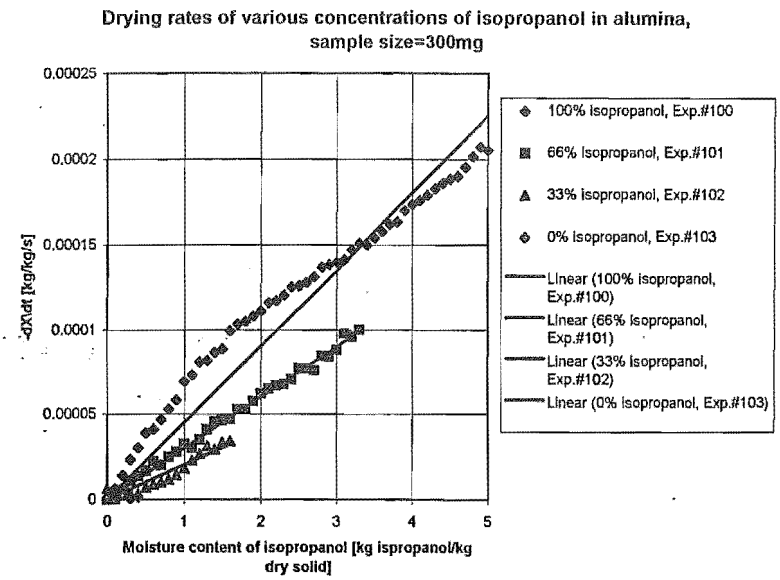

Figure 6.50 Drying rate of isopropyl alcohol in alumina sample containing a binary solution of water and isopropyl alcohol

Chapter 7

DISCUSSION

7.1 SORPTION STUDIES

The salt solutions provided a range of relative humidities. Each solution was stored in a sealed container with a portion of silica gel 124. The containers were stored in a dark cuboard at a constant temperature ($T_d = 20 degC$) sufficient to remove only mobile or free water from the silica gel particles. A significant amount of free moisture (Zhang *et al.*, 1992) is present in the silica gel material (0.36 $g\ H_2O/gdrysolid$), compared with 0.28 $gH_2O/gdrysolid$ which was desorbed at $T_d = 20\ degC$. Thus, 0.12 gH_2O/g dry solid remained in the solid matrix during the desorption isotherm. It was therefore proposed that the isotherms be repeated over a larger temperature range to account for the desorption of not only free water but also tightly bound physisorbed water. Using static methods, equilibrium should be allowed to form over a longer period of time (12 months), which can present a time problem. However, this was possible given that the first 12 months of this work programme was at Harwell. It is important to allow complete equilibration to remove residual moisture.

The sorption isotherms from the static and TG units were comparible (Figure 4.6. This was probably a result of using two different types of silica gel from different vendors. However, one should question the usefulness of the TG unit for sorption isotherm work for the types of materials used in this work, because of the limited range of air humidities that can be produced in a TG unit. Recent work by CI Electronics Ltd., Wiltshire, U.K., have recognised and solved this problem by modifying and automating a TGA/DSC unit for use in plotting complete sorption isotherms for a range of temperatures. However, earlier in this research programme it was recommended, that sorption isotherm work be done on very thin-layers of particulate materials, fully exposed to a very low continuous air stream, for the entire isotherm, with excellent control on the air conditions. Unless the drying chambers are pressurised (for use with saturated steam) so that isotherms can be evaluated, the upper limit for full sorption isotherms (plot complete range of relative humidities) was found to be up to $90 degC$ to fully desorb all physisorbed low-moisture.

Heat of sorption calculations from isotherm experiments indicated a gradual increase in heats of sorption as drying proceeded. Thermodynamic calculations for ideal monolayer sorption indicate (Langmuir fitting calculations) a distinctive increase in heat of vaporisation with drying. Reasons for this non-ideality may indicate:

1. the hydrophilic adsorption sites on the pore surface are non-uniform;
2. gradual desorption from the pore surface is not layer-by-layer;
3. some water molecules may be trapped in smaller micropores rather than bound directly to the pore's surface;
4. the exact monolayer loading cannot be determined by correlations, and the isotherm may not have a classical sigmoidal shape

Thermodynamic calculations appeared to show a greater increase in heat of vaporisation when compared with the heats calculated from sorption isotherms, but did not accurately predict the surface effects and bond strengths of multilayer water molecules on active surfaces. Calculations from using the Clausius-Clapeyron equation gave a gradual increase in heat of desorption, which indicates a homogeneous active pore surface with desorption, not layer-by-layer but by uneven drying of both monolayer and multilayer water molecules at the same instant.

7.2 COMPARISON OF HARWELL WITH CANTERBURY RESULTS

Single particles of silica gel 124 are ideally suited for investigating drying kinetics, because the equilibrium characteristics of silica gel material is generally well understood. Also, its particle rigidity limits the effects of swelling on the kinetics of drying, and single particle trials keep the conditions of drying at the particle's surface constant. The chemistry of the drying silica is well understood.

Figure 6.38 shows the characterstic drying curves for single gel 124, for various isolated single particles and small clusters of silica gel particles. Discussion of the differences in kinetics is presented earlier in Chapter 6. However, here further discussion is needed. Under laminar flow conditions, individual silica gel particles of 1.85 mm particle diameter had $Re_p = 70$), and high initial moisture contents ($X_o = 0.16\ kg\ kg^{-1}$), the higher external mass transfer coefficient in the gas phase (compared to lower moisture content particles) significantly contributes to increased drying rates of particle agglomerates. For particles with lower initial moisture contents ($< 1\%$), the drying rates are likely to be low enough to ensure that the external mass transfer resistance is relatively negligible. These low drying rates of near dry particles reduce the boundary layer thicknesses compared to particles with higher moisture contents, under the same

low flow drying conditions. The single particle drying kinetics performed at Harwell (Figure 4.13), was very similar to the drying kinetics of single particles done on the low moisture content drying kinetics apparatus (cf. Figure 6.38). Figure 6.39 also shows for drying a thin-layer of silica gel 124 particles, the same characteristic drying curve is produced that that single layer curve produced in Figures 4.13 and 6.38. Since these experiments revealed the same result, we should be confident that there is a consistency in reproducing drying kinetics results with other apparatus using a microbalance for weight-loss measurements.

Different methods of calculating the mass transfer coefficient for experiments 1-6 were used. For the single particle dried at the centre and the edge, and the drying of two particles separated by two particle diameters, Equation 2.136 was used to calculate the Sherwood number where an isothermal diffusion model was applied. For the drying of two particles at the centre of the chamber and the particles in layers, Equations 2.122 and 2.123 should be used to calculate the Sherwood number. The mass transfer coefficients calculated from these Sherwood numbers were compared to the experimental mass transfer coefficient calculated from Equation 2.111. The results are shown in Tables C.1, C.2 and C.3 for the drying of silica gel 124 single particles, and for the remander of the materials given in EXCEL files in the CD at the back of this thesis.

For the drying of thicker layers by a through-flow (> 3 layers), a temperature front may exist through the bed followed by a drying front. The speed of these temperature and successive drying fronts can be calculated from humidity and temperature probes positioned through the thick layer. An experimental programme on thicker layers of particulates was not investigated in this work. For drying in a fluidised bed, a large air flow is not possible as particle attrition limits the air flow. Although large fluidised particles may represent the drying of individual entities, thus increasing drying rates, the drying of finer particles in a fluidised bed may represent the drying of layered particles, because of the larger drying rates produced from smaller particles compared to larger particles. The size of the particles also influences the size of the external diffusion coefficient. Langrish (1988) found that coarse particles (> 1.4 *mm* diameter) when cascaded in a rotary drier behave as individual entities. However, Keey (1992) commented that, with finer material, the curtain of solid particles in a rotary drier acts like a fluidised bed. Thus a somewhat "large" change in shape factor should influence the drying kinetics of particles. Keech (1992) noticed that the drying of particles with a shape factor difference of 21% was not enough to induce changes in the drying kinetics. There is now a greater demand for products with a high surface to volume ratio for a number of reasons; smaller particles produce higher drying rates, solubility of fine chemicals is increased, less residual moisture is trapped in smaller particles, etc. Significantly more time should now be concentrated on the drying of finer materials within the falling rate period. This is supported by the SPS members showing an

interest in the drying of finer materials in this work. The currently preferred apparatus for the drying of finer grade material is the cascade rotary drier.

These results indicate that the characteristic drying curve for silica gel 124 can be extended to using air velocities in the range of laminar air flow conditions (Figure 6.39). A separate investigation of applying the concept of the characteristic drying curve under these low flow regions by varying the external conditions of air velocity, air temperature and air humidity showed a single characteristic drying *f-curve* when normalising against the reference critical moisture content of 0.38 $kg\ kg^{-1}$. Thus, a single chararcterstic drying curve is produced for the drying of a single layer of silica gel particles, with a low flow of air. This is an important result because even at very much lower air velocities, silica gel 124 still has the same characteristic drying curve for a very thin-layer. It looks now possible to use an electronic microbalance for single particle drying kinetic experiments at higher flow rates of air, more commonly used in commercial driers.

It may be important to note that this critical moisture content of $0.38 kg\ kg^{-1}$ was determined for through-flow situations. This moisture content may be different when using a cross-circulated material, as noted by Ashworth (1979). The critical moisture content differs between through- and cross-circulated beds because: the end of the constant-rate period of drying through-flow beds is limited by the receding interface within discrete particles. Compared to cross-circulated drying, the end of the constant-rate period is limited to the receding evaporative interface into sucessive layers in a cross-circulated bed.

7.3 SINGLE PARTICLE - MULTIPLE PARTICLE DRYING KINETICS

These preliminary tests showed that using a TG unit (with a microbalance) to perform drying kinetics is suitable provided single particle drying is the only area of experimentation. By using the TG unit, if the amount of layers is increased from one to four, the results by Keech (1992) found, that of the curves becoming more concave-up. However, drying one to four layered small clusters of silica gel 124 in the the TG unit produced characteristic drying curves of similar shape to those produced by Keech (1992), but the small and large sample curves did not overlap. The reason is that the amount of material dried in the TG unit is significantly less than the amount of material dried in the earlier tests. For example, for the drying of one layer in the TG unit, only seven particles were needed to cover the mesh crucible, whereas around 200 were required in the through-circulation rig used before. Thus, the use of small samples in the TG unit is more representative of the drying of single particles. The relative ease of drying of single particles is more pronounced than the drying of particles in close proximity to each another, as in layers or bed of particles. Similar conclusions were drawn from Keey

et al. (1985) , whereby there was a recorded difference between the drying kinetics of isolated particles to the same particles being dried in a layer. The graph indicating this is reproduced as Figure 2.18.

The characteristic drying curve is independent of air temperature, air velocity and humidity, but dependent on the initial moisture content of the material being dried (Langrish *et al.*, 1991) . The present work showed that the thickness of the particulate layer or bed of particles and the size of the particles have an effect on the shape of the characteristic drying curve. These observed differences in drying kinetics behaviour between the drying of single isolated particles through to the drying of particulate beds represent the difficulties in designing industrial drying units from information on drying kinetics drawn from dissimilar particulate bed geometries. Therefore it is inappropriate to design a cascade rotary drier on the basis of single particle kinetics tests; rather those from thin-layer work should be used. The thickness of the layer used in this drying kinetics test should be the same as the physical thickness of the falling particulate layer from the baffles in the drier. This thickness would be a function of the flowability and speed of the rotating drum. Variations in thickness of the drying layer found result in variations in the drying kinetics and result in variations in the driers performance.

As can be seen from Appendix A.1 - A.6, the drying rates of single particles are five orders of magnitude higher than the drying rates of four layers under the same external drying conditions. The corresponding drying times to reduce the moisture content of these single isolated particles and single particle agglomerates (as described in Figure 4.10) from 17% to 1% are 550 s for single particles and 2000 s for four layers. Thus, for the drying of particles in close proximity to one another, as in fixed or moving beds of particles, the performance of a drier can be enhanced if these particle beds are not too deep, or are kept moving fast enough for the particle surface to be exposed longer to the drying gas, rather than having humid gas between clusters of particles. For this reason, large particles (> 500 mm) are dried in fluidised beds, to effectively dry as much material as the fluidised bed drier can handle without have problems with entrainment.

. Moisture profiles are set up in fixed beds in the drying of particulate material with a high moisture content under vacuum or a reduced pressure. Nowadays, a significant number of vacuum driers agitate the material as it is dried, in an attempt to prevent such moisture profiles being set up. For vacuum drying of material well within the second falling-rate drying period (at low-moisture contents $< 1\%$), these moisture profiles within the bed become less predominant, so the need to agitate becomes less significant. Nevertheless "moving beds" are still used regardless of the material's initial moisture content and are now standard practice in industrial drying applications.

The partial theoretical foundation of the characteristic drying curve concept is

described, as well as a method of calculating the number of transfer units experimentally from Equations 2.119 or 2.121. The external and internal mass transfer resistances are described and their weighting on different experimental conditions is emphasised. It was found that describing the drying kinetics of single particles can be helped by considering the internal mass transfer resistances alone. For the drying of single particle agglomerates and particles in layers, the external mass transfer resistances have to be taken into account especially under laminar conditions (Re_p =70). A brief description of the effects that large and small particle sizes (that alter the bed properties) have on the drying kinetics is presented.

The characteristic drying curves of individual entities and layered material were still shown to be different. Particles in layers appear to notice a "shadowing effect" by the drying of surrounding particles. With the drying under laminar conditions of layered particles (Re_p=70), the increase in gas phase diffusion resistance contributes to a reduction in drying rates. However, this resistance is minimised if particles are dried as individual entities. Significant external mass transfer resistances are found in laminar flow. This decreases the overall drying rates.

In designing industrial drying equipment, the size and structure of the drying bed or layer, should be the same in the laboratory drying tests. For cascade rotary driers, the drying material falls in thin-layers from the baffles as the drum rotates; here hot moist material is exposed to the drying medium in thin-layers with very high bulk density. The thickness of this falling thin-layer can be measured and the same thickness of layer can be used in the laboratory tests. For the design of a fluidised bed, the hot air flow moves through the bed in a "bubbling" motion. Here the thickness of the drying layer very much depends on the velocity of the air flow. At low air velocities the bed bubbles at a moderate inhomogeneous rate, simulating the drying of a very much thicker layer. At higher air velocities, the bed bubbles with a more regular motion and material travels more up the sides of the fluidising chamber, increasing bed porosity and producing material being dried in thin-layers. At higher air velocities still, attrition becomes a problem and the drying medium no longer dries in a bubble arrangement, but more a "spray formation".

As a result, this work has showed that, in designing and sizing a particular type of drying unit, the same particle size as in commercial production must be used. Analogous to Zhang's work (Zhang *et al.*, 1992), Keech (1992) found that, in order to obtain representative drying kinetic data from laboratory-scale tests, the test material must be representative of the type of material being dried. More specifically, if the material being used on a commercial scale has a known particle size distribution, then the same particle size distribution must be used in the laboratory tests. Again view Table 4.5 for suitable pilot plant tests that should be used in sizing industrial drying units.

7.4 EQUILIBRIUM MOISTURE ISOTHERMS USING SPS EQUILIBRIUM MOISTURE CONTENT (EMC) RIG AND POSSIBLE ALTERATIONS TO RIG

The importance of minimising the experimental scatter in isotherms

This preliminary sorption work done on Harwell's emc rig, was not suitable for plotting sorption isotherms for particulates with low hygroscopic moisture contents. Since the accuracy of plotting sorption isotherms is very important, these tests were performed on an apparatus at Canterbury. The tunnel drier at Canterbury (Figure 2.16) has been shown and discussed in Chapter 2.

The degree of scatter when plotting isotherms very much depends on the control of external conditions. Minimal scatter would provide a more accurate fitting of the correlations. However, regardless of the degree of scatter, the fitting equations to be used should provide a stable "best-fit" solution. It should be possible to decipher the general shape of an isotherm and manually correct the experimental scatter, rather than input this scatter directly into the fitting equations. Quite often any such scatter can be attributed to the experimental technique rather than to any discontinuity in the solid's behaviour, but also taking into account any possible observed hysteresis from the isotherms. In deciphering scatter from such discontinuities in the solid, often separating the scatter from true sorptive behaviour can be put down to one's experience of plotting isotherms.

7.5 THERMOGRAVIMETERIC ANALYSIS AND DIFFERENTIAL SCANNING CALORIMETRY

Heat of sorption calculations from isotherm experiments indicated a gradual increase in heats of sorption as drying proceeded. Thermodynamic calculations for ideal monolayer sorption indicate (Langmuir fitting calculations) a distinctive increase in heat of vaporisation with drying. Reasons for this non-ideality may indicate:

1. the hydrophilic adsorption sites on the pore surface are non-uniform;
2. gradual desorption from the pore surface is not layer-by-layer;
3. some water molecules may be trapped in smaller micropores rather than bound directly to the pore's surface;
4. the exact monolayer loading cannot be determined by correlations, and the isotherm may not have a classical sigmoidal shape

Thermodynamic calculations appeared to show a greater increase in heat of vaporisation when compared with the heats calculated from sorption isotherms, but did not

accurately predict the surface effects and bond strengths of multilayer water molecules on active surfaces. Calculations from using the Clausius-Clapeyron equation gave a gradual increase in heat of desorption, which indicates a homogeneous active pore surface with desorption, not layer-by-layer but by uneven drying of both monolayer and multilayer water molecules at the same instant.

Effect of varying scan rate in DSC tests

The effect of varying the heat scan rate on the DSC unit has a predominant effect on the calculating the heat of wetting at low moisture levels. The typical heat scan rate for measuring the heat of vaporisation of liquids is 10 $degC\ min^{-1}$ but Figure 4.9 illustrates that greater accuracy is possible using lower scan rates. A further point was plotted on this graph to help extend the region of the plot. However, this further point was calculated from data for material that had interparticle moisture removed.

Etzler and Conners (1991) gave a proportional relationship over a scan rate up to 5 $degC\ min^{-1}$. A further point was added to show a further propagation of error under a 10 $degC\ min^{-1}$ scan rate. The result does indicate that as slow as possible scan rate should be used to calculate accurate heat of vaporisation or heat of wetting values. This is especially the case for the calculation of heats of wetting of moisture from particulate material at low moisture contents. Based on these results, a scan rate of 1 $degC\ min^{-1}$ was used in these tests.

This work on the heat of vaporisation of pure water was used as a basis to examine the heat of desorption (heat of vaporisation + heat of wetting) of water from porous matrices. A range of materials was investigated. Most of the water, not bound directly or indirectly to the material's surface, had a heat of vaporisation equal to that of pure water. However, once drying commenced below the low moisture contents (which most of these materials had), there appeared to be a marked increase in heat of desorption.

Figure 6.18 shows the heat of desorption against moisture content of water from silica gel with an average pore size of 5 nm. Because the surface area of this silica gel sample was known, it was possible to calculate the equivalent monolayer loading on the silica gel surface. This indicated that all water molecules in the 5 nm pores experienced an anomalously high heat of desorption, which suggests that the active surface slightly changes the molecular arrangement of liquid water, to that of molecular bonding of water with silanol sites on the silica gel surface. This figure also shows a comparison of the three methods of obtaining the heats of desorption from porous matrices. The method from sorption isotherms using the Clausius-Clapeyron relationship is the most widely used method of obtaining heats of sorption data, and this work recommends its use over the other two methods. Often the lengthy time periods involved with the static methods of obtaining sorption isotherms have discouraged workers, but improved dynamic methods with very good control of wet-dry and dry-bulb temperatures and air flow, and continuous weight measurement have reduced the time period required

for isotherm experiments significantly.

The heat of desorption obtained from the isotherms may be used as a standard to compare the other two methods. It can be seen from Figure 6.18 that both the thermodynamic and DSC/TGA methods of obtaining the heats of desorption are similar, but the data show steeper transitions into the monolayer region for silica gel. It has been shown (Anderson and Wickersheim, 1964) that this transition of drying into an equivalent monolayer for silica gel results in uneven drying of the monolayer/multilayer regions, parching some areas of the silica surface while leaving adjacent zones fully hydrated, so a more gradual increase in heat of desorption into the monolayer would result.

The other comparisons between heats calculated from isotherms and by the DSC/TG method are shown in Chapter 6.

As a result of these TG and DSC tests, a number of comments can be made. Firstly, in calculating the heat of wetting with moisture content to low moisture contents, the most accurate technique was found to be from sorption isotherms. This is a reliable technique to estimate the heat of sorption and it is recommended to have an extended use to low moisture contents. Combined TGA/DSC results are very much faster in estimating the heats of sorption. This method can be made more accurate at lower moisture contents if the heating scan rate is taken as slow as possible, i.e. less than $1\,degC\,min.^{-1}$. However, the larger the particles or the greater the estimated interparticle mass transfer resistances, the greater is the error in estimating the heats of sorption at low moisture levels. The Langmuir fitting equation, which is based on thermodynamic principals to calculate the heats of wetting was first presented by Polanyi (1932), this mothod was found to be surpassed by the use of the Clausius-Clapeyron equation, Equation 2.32. Secondly, the main objective of these extensive tests was to calculate accurately the heats of sorption at low moisture contents, and measure the asymptotic behaviour of heats previously inaccurately estimated in this region. It was found that even at very low removable moisture levels, $< 0.01\%$, the heats of sorption had a finite value. However, trapped moisture held in rigid microporous cavities, does exhibit much larger heats of wetting because the solid structure would have to be deformed during the removal of this moisture. The amount of trapped moisture held in a rigid lattice can be determined under pyrolysis of the material, or by drying the solid structure under extreme vacuum conditions.

7.6 CONSTRUCTING DRYING KINETICS CURVES

Because the raw data curves of moisture content against time from the microbalance were not smooth, an appropriate curve-fitting function (polynomial or exponential decay function) was used to produce a very smooth profile. This was surpassed by the

use of a 6th-order forward differencing technique for final processing of data from the microbalance, but using a sinusoidal response curve as shown in 7.1 had to be tested.

When the central differences are compared with the forward difference values, it appears that they are not as accurate for a very smooth function. Both the forward and central difference approximations compare very well with the true derivatives of the basic sinusoidal function.

Simulated smooth drying rate curve

The falling-rate period of drying was isolated from this profile, and the characteristic drying curve was constructed. Drying rate curves are obviously not representable by one sigmoidal shape; therefore it is necessary to mathematically construct a typical drying rate curve from two sigmoidal curves. For a material that does not have a constant rate drying period, the first half of a sinusoidal curve, i.e. y=sin(x), 0 ¡ x ¡ π, can represent the induction period and first section of the falling rate period. The remaining section of the falling rate period can be simulated using an exponential decay function, i.e. y=exp(-x), x > π (Figure 7.1).

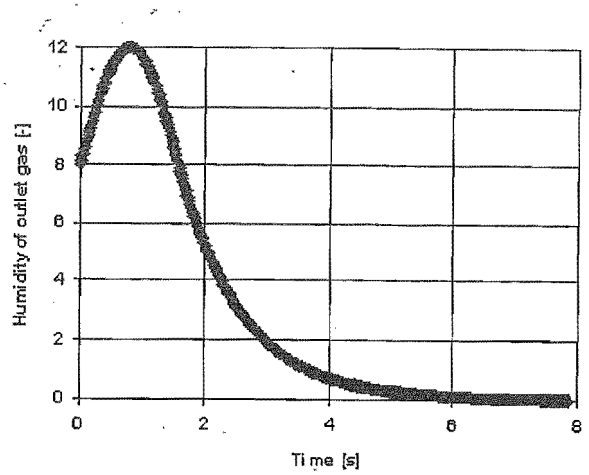

Figure 7.1 Simulated shape of drying curve

This curve is an ideal shape for a typical drying rate curve, which could be represented by:

$$Y = a + b * sincx, 0 < x < \pi/c \forall a, b, c \tag{7.1}$$

or

$$d * exp(-(x - \pi/2)), \pi/2 < x \forall c, d \tag{7.2}$$

Mathematically this curve takes the form:

$$8 + 4 * sin2x, 0 \leq x \leq \pi/2 \tag{7.3}$$

or

$$8 * exp(-(x - \pi/2)), \pi/2 < x \tag{7.4}$$

Experimental drying rate date contain a degree of scatter. The objective is to then construct the first derivative drying rate curves from either the scattered or smoothed data. Various fitting equations are possible to model the shape of the falling-rate period, e.g. finite difference techniques, splines, and various exponential decay functions. For the purposes of this work, it was necessary to fit the falling-rate period of drying without confusing the true kinetics effects of drying with experimental scatter. This difference can be distinguished by comparing the degree of scatter with the smoothness of the fitted equation. Identifying this difference was extremely important here as the calculated kinetics of drying differed greatly over very small variations in the shape of the falling-rate curves. Fitting smooth drying rate curves using ideal mathematical functions is generally not a good approach to take. The actual drying mechanisms are more complicated, and there is a fear here that experimentally determined information can be lost in this smoothing process. Thus, 6th-order forward differencing was used to filter the raw data from the microbalance. In this was the data is filtered rather than smoothed.

Non-smooth function

The TG unit plots an analogue signal of weight loss against time, on a chart recorder. Values every 20 s are then taken from the paper (Figure 7.2) and entered into a spreadsheet.

The curve is reconstructed and is shown below. If values were logged every second, which is possible from the new drying kinetics rig, then errors would be reduced accordingly. Even setting the chart to record over the full length of the paper, the errors introduced in transferring data to the spreadsheet were significant; smoothing or filtering may then be required to damp out these errors.

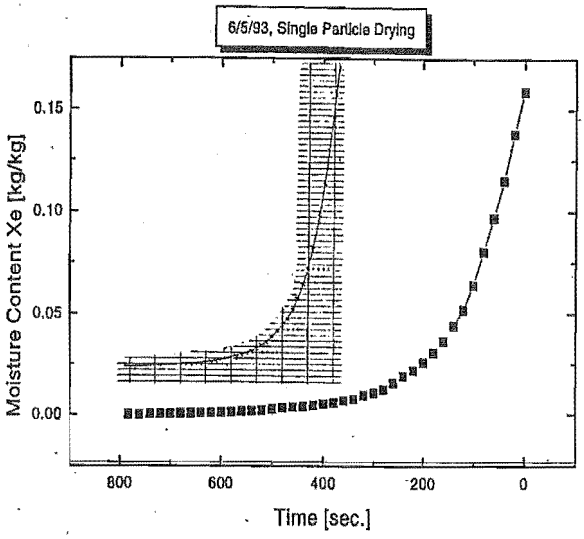

Figure 7.2 Reconstructed curve of moisture content against time compared with actual raw data

The inserted plot (Figure 7.2) is a photocopy of the actual data, and the main graph is the plot of moisture content against time. Taking "this" reconstructed curve, it was found that a first-order forward difference followed by applying a third-order polynomial regression curve produced a smooth result. Using a sixth-order forward difference, the drying rate curve (*-dX/dt vs. t*) was not quite as smooth. This indicates that the reconstructed curves from the chart paper were smoother than previously anticipated, so for raw data it would be best to try the first-, third- and sixth-order differences to find the drying rate curves.

The object of using such a curve-fitting function was to draw a smooth curve through the points, not by hand, but by making the computer generate a less subjective curve. Higher-order polynomial regression curves tended to follow plotted points too closely, this often producing another non-smooth curve. Lower-order curves tended to give an overdamped plot, producing a badly fitted curve through the data. Appendix A.1 shows the varying orders of fitted curves to the drying rate curves. There is no single order that fits all curves, although third-order or fourth-order polynomial regression curves appear to be the most effective.

For single particle drying, from the fitted curves, a first-order difference, a sixth-order central difference or a sixth-order forward difference gave similar fitting parameters as noted in Appendix A.1. The order of the fitted curve is the main consideration here. One has to be careful not to underdamp or overdamp the "true" drying rate

curve by comparing the fitted curve with the original data.

7.7 LIMITS OF ACCURACY ON MEASURING THE DRYING KINETICS OF PARTICULATE MATERIAL

One of the objectives of this work was to determine to what accuracy a drying profile could be constructed. These drying limits are influenced by the size of the sample that is dried, the low initial moisture content of the sample and the turbulent nature of the air flow, because higher air flows caused the sample to vibrate accordingly.

The observed limits on extracting accurate weight loss profiles for drying under a through-flow of air, in this apparatus, lie somewhere between a 200 and 300 *mg* sample size under the larger air flow of 0.00709 $kg\ m^{-2}s^{-1}$. For the smaller air flow of 0.00158 $kg\ m^{-2}s^{-1}$, the size of sample is limited to 100 *mg*. There was no need to find the suitable boundaries for operating the apparatus, this could take excessive time away from the main objedtives of this work, but it was necessary to find suitable drying conditions that produce accurate drying rate profiles.

The observed practical limit on extracting an accurate weight loss profile under vacuum conditions for alumina, in this apparatus, is approximately a 35 *mg* sample size under a vacuum of 0.027 *mbar*. A smaller sample could be tested but much of the drying would be performed under the degassing stage of the drying process.

These limits on accurate drying profiles depend strongly on minimising the environment disturbances of room temperature, avoiding direct sunlight on the balance electronics, pump noise, size of air flows and minimising ground movement. A good design and location of such an apparatus would minimise these disturbances and provide maximum accuracy during data recording. Samples ranging from 35 to 2500 *mg* may be dried by through-circulation, cross-circulation or under vacuum. The sensitivity of the microbalance permits the drying of single isolated particles, single particle agglomerates or particles in layers. A second chamber enables larger samples (5-200 *g*) to be dried under vacuum. The unit was used to follow the drying of fine pharmaceuticals and polymers, silica gel and alumina at dry-bulb temperatures between 80 and 140 *degC* and dewpoints of -5 and +5 *degC*, with through-circulating air flowrates of 0.00158 and 0.00709 kgm^2s^{-1} or vacua to $4*10^{-4}$ *mbar*. With a 35 *mg* sample, dried under vacuum, having an initial moisture content of 0.4%, the uncertainty in the electronic signal from the microbalance was ± 0.0003% moisture content on drying at 100 *degC* and a pressure of 0.027 *mbar*. A very stable reading was observed under vacuum conditions at long times and was reproducible to ± 0.1μ *g*. There was increased noise from the balance when the unit was used under through-flow conditions, the uncertainty being the order of ± 0.03% moisture content at the lower air flowrate with a sample size of 100 *mg*.

The maximum hygroscopic moisture content of water in alumina is approximately 0.4%, which makes it an ideal material to use to determine the limits on extracting

a drying profile and thus drying kinetics behaviour. Traditional methods of obtaining drying profiles at higher moisture contents are to use a weight loss balance or perform an evolved gas analysis. To extract a drying curve over a smaller moisture content range and at lower moisture content levels, a more sensitive electronic microbalance was used. It was found that the instability of the processed electronic signal during the operation of all pumps was negligible. So the only possible disturbances could be from air flows around the sample holder and degassing during vacuum operation.

7.8 ANSWERS TO THE MAIN OBJECTIVES OF THIS PHD WORK

7.8.1 Do isolated particles dry differently from particles in layers, both cross and through-circulated?

An earlier phase of this work (Keech, 1992) indicated that there is a difference in drying behaviour between thinner and thicker layers. It was then deemed necessary to understand further this difference by extracting the drying kinetics of single particles and single particle agglomerates in the preliminary drying kinetics work at Harwell. This was repeated and developed further using the new drying kinetics apparatus at Canterbury. The results indicated that there is indeed a difference in drying kinetics behaviour between the drying of isolated particles and the drying of particles in layers, so scaling up of the drying kinetics of isolated particles to particles in layers would be inaccurate. These results favour Langrish's thin-layer approach (Langrish *et al.*, 1991) to extracting the drying kinetics rather than that of Tsotsas (1992) who commented on being able to directly extract the drying kinetics of layers from the fundamental drying behaviour of single particles. As there may be such a difference, the drying kinetics of single particles and those held in layers should be dealt with separately. Most industrial drying of solids showing no constant-rate drying period tends to represent the drying of particles in layers rather than isolated particles. Even fluidised bed drying of particulates tends to represent the kinetics of particles drying in a thin-layer due to the close proximity of neighbouring particles. So a thin-layer approach to extracting the drying kinetics of most drying applications of particulates would be both direct and practical.

This is why the drying of this type of material in a drier such as a cascade rotary drier is best modelled using a thin-layer approach rather than scale-up of single particle kinetics.

7.8.2 Is it possible to use existing equipment to investigate drying kinetics at low moisture contents, or will a new design concept be required?

This question was resolved early on in the work, and traditional evolved gas methods were insufficient to extract the drying kinetics at low moisture contents. An electronic microbalance would give accurate weight-loss profiles below 1% initial moisture contents. However, the weight-loss of other solvents or solid fragments needed to be accounted for by the use of a mass spectrometer. A mass spectrometer is useful in giving an accurate evolved gas analysis of all species except water. A frost point meter was then required to obtain the evolved water vapour loss profile during drying. Two sample chambers allow the drying of single particles through to thick particulate beds. Through-flow, cross-circulated and vacuum drying applications are also possible. This instrumentation of the new apparatus has multitask capabilities to record simultaneous information about drying conditions and drying behaviour of particulated solids at low moisture contents.

7.8.3 Is the drying selective at low moisture contents when organic volatiles are present?

In this work, differences in drying kinetics between the drying of terephthalic acid wetted with an organic solvent (cyclohexane) and the drying of terephthalic acid saturated with water were investigated, both with varying maximum hygroscopic moisture contents of around 1.35% and 0.5% respectively. Selectivity in desorption for this case shows a consistency with the selective desorption mechanisms thought to occur at higher moisture contents.

In drying pre-dried terephthalic acid (moisture - organic residues from production, e.g. isopropyl alcohol or acetic acid, or cyclohexane) and pure terephthalic acid (moisture - water) behave very differently. Figure 6.32 and 6.33 have similar shaped isotherms at 65 and 80 *degC*. However, at low sorptive temperatures (45 *degC*, there was favourable sorption of the organic residues to the terephthalic acid particles. Because there was an increase in maximum hygroscopic moisture content from adsorbing theses organic residues, the lattice expanded to accommodate. The moisture content of terephthalic acid particles are respective to organic solvents because of its overall hydrophobic nature. So the drying of terephthalic acid is more surface diffusive drive for removing organic solvents, but Fickian diffusion driven for the removal of water. Also compare Figures 6.21 and 6.22.

The results in this work involving various concentrations of water and isopropyl alcohol indicated that selective drying was evident at low moisture concentrations but inconsistent with the Thurner and Schlünder (1986) ideas of selective drying at higher

moisture contents. At low concentrations of a water/isopropyl alcohol binary solution (mole fraction = 0.10) in alumina particles, indicated selective desorption of isopropyl alcohol was indicated. This would be believed to be caused by the higher heats of wetting of water on alumina than isopropyl alcohol, irrespective of the higher gas phase mass transfer of water compared with isopropyl alcohol, as water is bound directly to the alumina pore surface more favourably. Thus, the drying of an equivalent monolayer for a binary solution is more determined by the individual heats of wetting associated with each solute species on the material, rather that by what is normally expected from a binary solution at higher moisture contents. This indicates that the concepts of selective desorption of binary solutions at higher moisture contents cannot be extrapolated to the behaviour of drying selectivity at lower moisture contents.

7.8.4 Do the drying kinetics differ when moisture is held by volume filling and/or strongly adsorbed on pore surfaces at low moisture contents, compared with vapour diffusion and capillary action at higher moisture contents?

Even at higher particle moisture contents, volume filling or surface diffusion in some microporous materials may still prevail, especially those with an active pore surface would promote greater sorption. Very small particles ($< 200\ \mu m$), at low initial moisture contents that are dried as isolated particle aggregates, can be modelled entirely by a surface diffusion model. The drying of the copolymer material at low-moisture content was accurately described by applying Fickian-based ideas. This liquid diffusion process is commonly used at higher moisture levels to describe drying. However, for the majority of low-moisture content materials tested, including alumina, sand, pre-dried terephthalic acid and pure terephthalic acid, the drying kinetics are better described by a surface diffusion model which implies the need to provide enough sensible heat for the activation energy to be overcome. The characteristic drying curves are shown in Chapter 6; the copolymer characteristic curve (Figure 6.45), is very different from the curves of alumina, iron sand and terephthalic acid (Figures 6.41 to 6.44).

7.9 MOISTURE EQUILIBRIUM CHARACTERISTICS OF MATERIALS

Tables 7.1, 7.2 and 7.3 are a summary of the observed sorptive differences in the materials investigated in this work. A more complete description of these materials is given in Appendix E.

As a note, all materials fitted well to a Henry-type isotherm for their monolayer or equivalent monolayer, and all isotherms gave the best fit for the entire range by using a modified BET equation (four parameter fitting correlation explained in Chapter 2).

Table 7.1 Brief summary of sorptive characteristics of the materials - Part 1

Sorptive indicator hline $X_{hgr.}$ (wet basis)	Silica gel type 124 0.30	Alumina 0.004-0.005	Iron sand 0.0028-0.003
Monolayer saturation	0.110-0.135	0.002-0.0022	0.0023-0.0025
Internal surface area $m^2 g^{-1}$	450	72	7
Ratio of water held above monolayer or on particle's external surface to monolayer	2.7	0.3	0.8
Range of heats of wetting ($kJ\ kg^{-1}$ *dry solid*)	1500 - 5000	0-2300	0-2300
Comments	Surface dried in a patchy manner	No hysteresis, microporous isotherm	Isotherm shape typical of microporous material

Table 7.2 Brief summary of sorptive characteristics of the materials - Part 2

Sorptive indicator hline $X_{hgr.}$ (wet basis)	Adipic acid 0.07-0.08	Pure terephthalic acid 0.006-0.007	Crude terephthalic acid 0.013
Monolayer saturation	0.06-0.065	0.004	0.004-0.005
Internal surface area $m^2 g^{-1}$	1.02	0.21	0.21
Ratio of water held above monolayer or on particle's external surface to monolayer	very small	100 (moisture held) near external surface)	100
Range of heats of wetting ($kJ\ kg^{-1}$ *dry solid*)	0-2200 (including chem. moisture)	0-1800	0-1800
Comments	Strongly bonded chemisorbed moisture little physisorbed moisture	Moisture held by water clusters at or near external surface	Stronger sorption by organic polar solvents (residual processing moisture)

7.10 GENERAL FITTING CHARACTERISTICS OF CORRELATIONS

Comments on the empirical correlations. From the sorption programme carried out at Canterbury there were obvious trends in the following sorption correlations.

- A. Three-parameter correlations

  1. The BET correlation fits type III isotherms (IUPAC classification) well, as it assumes that a critical moisture content is not well defined.
  2. The modified BET and GAB equations appear to fit a wide body of isotherm shapes. These fitting correlations disclose information on a solids free and bound moisture with information about the heat of wetting on layered moisture in the particle.
  3. The SPS correlation appears to fit isotherms of type I, linear isotherms and moderately well for type II. However, it does not appear to like materials that have a lot of their moisture bound to the surface of the particle.
  4. The Schuchmann correlation fits type I isotherms very well, with no restrictions on the amount of bound moisture, and type II isotherms, again with no restriction on the amount of bound moisture.
  5. The Luikov correlation appears to fit type I isotherms, linear isotherms and moderately well for type II. However, it does not appear to like materials that have a lot of their moisture bound to the surface of the particle. Fitting is not as good as with the SPS correlation.

Table 7.3 Brief summary of sorptive characteristics of the materials - Part 3

Sorptive indicator	Co-polymer I	Co-polymer II	Co-polymer III	Heat treated SG
$X_{hgr.}$ (wet basis)	0.012-0.013	0.019-0.021	0.009-0.011	0.15-0.17
Monolayer saturation	0.007-0.008	0.0003	0.002-0.0022	0.06-0.08
Internal surface area $m^2 g^{-1}$	0.51	0.05	0.58	250
Ratio of water held above monolayer or on particles external surface to monolayer	98	167	72	2
Range of heats of wetting ($kJ\ kg^{-1}$ *dry solid*)	0-3500	0-3500	0-3500	0-3000
Comments	Non-spherical particles causing excessive sorption at the external surface	Gelatinous material	As Copolymer I	Deactivated surface cf. silica gel

6. The modified b correlation gives the same result as the Luikov correlation; the equations are very similar.
7. The Keey correlation again gives the same result as the Luikov and modified b equations, but often tends to favour the fitting of type III isotherms alone with the BET correlation.
8. The modified h correlation favours fitting of type III isotherms, but still attempts to fit the linear isotherms.
9. The Halsey correlation fits a type II isotherm moderately well with a limit on the amount of bound moisture.
10. The Henderson correlation fits a very flattened type II classification well.
11. The NBET correlation appears to fit linear isotherms, type I isotherms with a larger degree of bound moisture.
12. The PIR correlation appears to fit linear isotherms, type I isotherms with a larger degree of bound moisture.
13. The TLBET correlation appears to fit type II isotherms with a varying degree of bound moisture.
14. The SVBET correlation appears to fit type II isotherms with a small amount of bound moisture.

- B. Four-parameter models - because the number of fitting parameters has increased, there is more chance of accurate fitting by these correlations than any previously mentioned.

1. The NGAB correlation appears to fit type I isotherms permitting a small/large degree of water clustering (linear isotherm behaviour) and/or small/large amounts of bound moisture.
2. The PIRGAB correlation appears to fit type I isotherms with a small/large degree of water clustering and/or small/large amounts of bound moisture.
3. The TLGAB, TLNBET and SVBET correlations appears to fit type I isotherms with a small degree of water clustering and/or small/large amounts of bound moisture.

4. The LBGAB correlation gives a poor fit to all isotherms.

7.11 TESTING LOW-MOISTURE CONTENT MODELS

7.11.1 Physio-chemical kinetics drying model

Physio-chemical drying kinetics provide a link to understanding the dehydration of a porous particle for the drying behaviour of a solid and the chemistry of the drying process. Knowledge about the nature of the pore surface and the types of active bonding between the material and the sorbed species gives a preliminary insight into the type of drying behaviour that might be expected.

The drying through a physisorbed/chemisorbed transition for silica gel is a first-order to second-order drying kinetics process. The materials that have been investigated in this work mainly involve the removal of physisorbed rather than chemisorbed moisture, with the exception of silica gel 124 and adipic acid. For example, the drying stoichiometry of adipic acid could be seen to be first-to-second order for removing liquid water between the monomer units through to condensing the adipic acid monomer units to form the polymeric chains. The other dicarboxylic acid, terephthalic acid, also showed the chemisorbed dehydration of the lattice to be a second-order process. However, the immobility of the terephthalic acid solid prevented water diffusion through the lattice due to the rigid packing nature of the aromatic monomer units, so it was difficult to determine this second order drying experimentally. Removing chemisorbed moisture from such fine chemicals is of purely academic interest, because drying creates a polymorphic fine chemical, which is undesired.

7.11.2 Testing the surface diffusion model on the materials

The surface diffusion drying model occurs when molecules are diffusing through a solid matrix along the pore surface on which they are re-adsorbed. Surface diffusion differs from molecular diffusion in that the driving force for is temperature rather than concentration. Its driving force is not a concentration gradient but the movement is driven by an activation energy on or near the solids surface. Solid materials that have active (hydrophilic) surfaces often favour drying under surface or sorptive diffusion because of the lower activation energies required for a water molecule to jump to a neighbouring vacant active site. This is very dependent on the drying temperature. Accurate fitting of this model would suggest that the drying temperature is more responsible for the drying kinetics rather than the other mass transfer resistances such as diffusive and/or capillary forces.

The temperature difference in the drying medium is the driving force responsible for the rates of drying, which influences the degree of site hopping of the sorbed species.

Various types of materials, in this work, were used to test the applicability of this concept:

1. strongly active pore surface (silica gel 124);
2. weakly active pore surface silica gel (heat-treated silica gel, non-active alumina, sand);
3. fine chemical organic-based materials (terephthalic acid - pure and pre-dried forms);
4. polymer particulates (copolymers of butadiene and polystyrene).

It was useful to compare experimental drying data at low moisture levels with the above rate expressions. This helped to explain the importance of temperature in removing low levels of moisture from particles. This surface diffusion model is a very simplified approach to identifying a simple first-order drying process. Thus the accurate fitting of this theoretical model indicated first-order kinetics drying at low-moisture levels, which substantiated the absence of the multiple drying mechanisms that pertain at higher moisture contents.

At low moisture contents, the surface diffusion mechanism is assumed to dominate the drying behaviour. The results from this work indicated that this is indeed the case for the drying of non-swelling isolated particles, isolated particle agglomerates and very thin-layer particle beds. However, for thin-layers greater than 1 mm in depth, a surface diffusion model is not the only driving force for drying. Interparticle gas/bulk flow diffusive elements through the layer would have to be considered, and incorporated with surface diffusion coefficients, to calculate the effective bed diffusion coefficient, D_{eff}, from a sum of the individual reciprocals. Modelling diffusion at low moisture contents depends very much on the strengths of the sorbate-sorbent interactions. Knowledge about the heat transfer through the drying sample would also influence the rate of the effective diffusion of water vapour through the sample.

For swelling materials, other diffusive mechanisms become apparent. There is a significant amount of literature on the drying of polymer-based materials, which considers the effects of polymer relaxation and other structural effects on the drying behaviour. The drying behaviour of hydrophobic media is described in the next section.

7.11.3 Fickian diffusion at low-moisture contents?

Figures 6.9 and 6.10 show the applicability of the surface diffusion expression for varying thicknesses of particulate bed for the copolymer III. Figure 6.9 gives a drying rate against heat of wetting curve very different from that observed for alumina (surface diffusion material). It appears that, for the drying of isolated particles of copolymer III

at low moisture contents, a surface diffusion model "alone" cannot, if at all, account for the mechanism of moisture transport. For the larger sample, a less linear appearance pertains (concave-downwards), suggesting that, even at lower moisture contents with low drying rates, a diffusive resistance through the particulate bed would have to be considered to account for the overall diffusion coefficient. The poor fitting of this surface diffusion model amplifies the absence of strong bonding between solvent and material, and sidelines with the "water clustering" concept typical of water in polymeric solids. Figure 6.45 that indicates the characteristic drying curve method does not apply for this copolymer. The isotherms for the copolymers (Figures 6.34, 6.35) and 6.36 indicate that Fick's second law can be applied to these linear shaped isotherms (Steinmetz *et al.*, 1991). Thus, it was shown in this work that, at lower moisture contents, Fickian transport mechanisms commonly used at higher moisture contents can be extended to the regions of low-moisture content drying for this type of polymeric solid.

7.11.4 Testing Fick's laws of diffusion to drying at low moisture contents

Even at lower moisture contents ($< 0.5\%$), material that has hydrophobic surfaces, such as that formed in various polymers, has water still not bound to the pore surface of the material but favours "water clustering" in microcavities of the material. During adsorption of water in hydrophobic media, swelling of the lattice is promoted, resulting in the existence of more microcavities initially near the particle's surface.

A classification of non-active surfaces, such as in heat-treated silica gel or non-active alumina, show signs of water clustering and water bound weakly to the pore surfaces.

At low moisture contents, bound moisture is generally thought to be the predominant type of moisture in the pores for non-swelling hydrophilic media. However, for hydrophobic material, free water held in clusters of molecules may still exist at low moisture contents. Removing these free water complexes or "water clusters" can be modelled by Fick's second law, which could be used to simulate the drying of polymer-based materials.

Adsorption of water into these polymeric media is restricted to the regions of the particles surface. However, adsorption of water into smaller polymer particles (< 0.5 *mm*) may reach the centre of the particle. In this case, it would be useful to investigate the validity of a receding interface evaporative model. However, many polymeric solids are produced industrially in sizes greater than a particle diameter of 0.5 *mm*. Thus polymers that are washed with water before a drying stage may not necessarily contain a homogeneous spread of moisture throughout these sized particles. A receding evaporative interface drying model would be an unrealistic attempt at simulating the drying of these materials.

It is proposed that, having discarded most of the drying mechanisms such as capillary condensation, surface diffusion and the receding evaporative interface models, the use of a traditional Fickian diffusion model should be investigated.

7.11.5 Conductive heat drying models at low moisture contents

Drying to low moisture levels generally requires conductive heat drying under vacuum conditions. Two different models were used to simulate this.

- Does an evaporative front occur during low moisture content drying? A model predicting the movement of a drying front was compared with the moisture loss profile.

- A simpler model given by Thurner and Schlünder (1986) places emphasis in drying rates on the heats of desorption and heat transfer of the drying bed. Can the associated heats of wetting account for the low drying rates observed during drying at low moisture contents? A full list of the heats of sorption that should be predicted from the various types of interparticle pore geometries is given in Chapter 2, particularly from a classification of swelling and non-swelling solids. The non-uniform heat flux distribution over the particle's surface area will also generate non-uniform local rates of evaporation when moist particles are dried through contact with a hot air flow.

7.11.5.1 Okazaki's drying model (Okazaki , 1981)

This conductive heat drying model was formulated to predict the velocities of two evaporative planes coming together in a bed arrangement. The bottom surface was exposed to a conductive heating plate. A moist porous material was used in their studies; the water content was so low as to resist any transfer of liquid water within it.

For this work, it was useful to determine whether such a model could be used to describe the drying behaviour of material at low moisture contents ($< 1\%$).

These velocity profiles were formulated from traditional conductive mass and heat drying models with the appropriate boundary conditions, Equation 3.18. Solving the rigorous solutions to these heat and mass transfer equations is possible only by tedious and careful numerical calculation. With the appropriate boundary conditions, Okazaki showed how Equation 3.18 helps predict the existence of two receding evaporative planes. However, modification to Okazaki's model was made in this work to predict the existence of only one evaporative front moving away from the heated surface, while eliminating the desorption profile from the top surface of the drying bed. The modifications are described in Chapter 3 of this thesis.

Calculations indicate that, during the induction stage of drying (20-40 s) the temperature profiles are being set up through the sample bed. Applying Okazaki's model to low moisture content drying indicated a more stable evaporative drying front during the induction period than that expected. Thus a drying rate curve was poorly estimated for the induction period. However, once the drying fronts and temperature profiles had been set up it was found that Okazaki's model gave a good approximation to the actual drying rate measured.

A similar and more widely used model is the receding evaporative interface model. This is presented in van Meel's short-cut method in Chapter 2 of this thesis. A receding evaporative front is assumed when the characteristic drying curve for a particulate material is followed closely for changes in air temperature and humidity, but not for air velocity variations. This is because the boundary layer resistance has a negligible effect on drying once the interface has receded far into the solid. However, the materials investigated, with the exception of the copolymers, showed a similar shape in characteristic drying curve for various air velocities. The copolymers were shown to follow Fickian diffusion while removing the "water clusters" during a drying process. Thus this would suggest not applying a receding evaporative interface model at low-moisture contents. Using such a receding evaporative interface model does then appear to give an inaccurate description of the drying process at low moisture contents for small particle sized ($< 0.5\ mm$), non-swelling materials. However, this would be expected because of the wide range of binding energies observed in the equilibrium characterisation section of this work.

If accurate heats of wetting are known for materials, Okazaki's predicted evaporative drying front could be used to estimate the experimental drying rates at low-moisture contents. However, it is recommended that the surface diffusion and Fickian diffusion models be employed rather than Okazaki's model for low-moisture drying. This drying front is strongly related to the heat conduction through the bed rather that a traditional receding evaporative interface because of drying free liquid between particles.

7.11.5.2 Thurner and Schlünder's (1986) heat transfer drying model at low moisture contents

If the contact time is sufficiently long so that the temperature profile has deeply penetrated into the packed bed, then the bed could be considered as a continuum. In this case, Fourier's theory gives, for the regime of developing temperature profiles, the heat transfer coefficient

$$\alpha = C_1 \frac{\sqrt{(\lambda \rho c_p)_{so}}}{\sqrt{t}} \tag{7.5}$$

and, for fully developed temperature profiles, the heat transfer coefficient is

$$\lim_{n\to\infty} \alpha = C_2 \frac{\lambda_{so}}{H} \tag{7.6}$$

where λ_{so} is the effective heat conductivity of the packed bed and can be predicted by correlations given by Bauer and Schlunder (1978); $(\lambda\rho c_p)_{so}$ is the overall volumetric heat capacity of the packed bed. C_1 and C_2 are constants depending on the thermal and geometric boundary conditions. H is the bed depth.

This work, for the most part, involved the drying of isolated particles, single particle agglomerates and thin-layers in a through-flow air stream. So the effective heat transfer concerns were limited principally to the heat transfer through the individual particles.

Schlünder's heat/mass transfer equations appear as a simplified approach to resolving different drying rates. Schlünder compensated for the binding energy at low moisture contents by assuming an exponential relationship of heats of wetting with moisture content. This may be sufficient in roughly sizing a drier, because most drying units dry solids with a high initial moisture content ($> 1\%$). In an attempt to obtain as dry a product as possible, often the drier is slightly oversized by incorporating a safety factor into the drier sizing equations. Traditionally, this has been an effective method of designing a drying unit, for the reason of having limited knowledge about the drying behaviour at low moisture contents. This work indicated that assuming a typical exponential heat of wetting relationship with moisture content is mostly not correct. Thus this work has presented flaws in the accurate sizing calculations of a drier (poor fitting of experimental drying rate data found for using Okazaki *et al.* (1978) original model which used a exponential heat of wetting relationship), and showed that errors are indeed prevalent in assuming exponential heats of wetting relationships with moisture content.

Calculations indicated that only instance where this approach is applicable at low moisture contents is the drying of small ($d_p < 0.5\ mm$) isolated particles where there is little resistance to heat transfer. This work used small particles ($d_p \approx 0.1\ mm$) in thin-layers; thus very small heat transfer quantities were calculated by using the gas continuum as a transfer medium from Schlünder's heat transfer equations. His model is more applicable to the drying behaviour of material at higher moisture contents.

7.11.5.3 Comparison of models

Only the two models presented by Okazaki and Schlünder are discussed in this work. This work has showed that surface diffusion mechanisms simulate the drying of most particulate media containing residual moisture. Okazaki considered both mass and heat transfer effects and used this to predict a receding evaporative front. In this work,

Okazaki's model was used to predict the velocity profiles of a receding evaporative front for the drying of a particulate bed containing low initial moisture contents (alumina). His model gave a reasonably good fit to the experimentally measured drying rates, using both mass and heat transfer effects in drying a particulate bed. Schlünder's model, on the other hand, uses only a heat transfer expression to predict the drying rates of particulate beds at higher moisture contents. The heat transfer resistances affect the drying kinetics of the drying bed, and this often is the drying force behind the drying rates of particulates under vacuum. Experimental work on the drying of alumina in a thick layer indicated a poor fit to Schlünder's model. Thus, for the drying of particulate beds at low moisture contents, a receding evaporative interface model can be used to predict the drying performance. Also, for accurate prediction of drying low moisture particulate beds, a mass transfer effect has to be incorporated, which Okazaki's model uses. It should be remembered that for the drying of thin-layers and isolated single particles with low moisture contents, a mass transfer coefficient does not need to be included, a surface diffusion model alone is sufficient.

The application of Fick's equations to surface and gaseous diffusion has already been discussed. A simple temperature dependent rate expression, Equation 6.1 was developed for surface diffusion. Successful estimation of drying rates using Equation 6.1 for some/all of the solids investigated (with moisture contents $< 1\%$); emphasised the large effect of temperature on the overall drying kinetics behaviour. Poor fitting of drying rates would show the dependence of other factors, i.e. chemical kinetics, mass transfer resistances. Often it may become apparent that, with drying below an equivalent monolayer of moisture on a porous structure, the physio-chemical nature of the moisture/solid bonds may help characterise the drying kinetics. If it is assumed that physio-chemical kinetics is the rate determining step in the drying kinetics, then mass transfer and heat transfer resistances within the particle or thin-layer of particles would be neglected. The drying of water clusters (which were identified from the moisture isotherms) held in microvoids was evident with the polymer based compounds investigated and could be modelled using Fick's second law of diffusion. Once the boundary conditions at the particle surface have been identified during the drying process, calculating the diffusion coefficients and estimating the drying rates are possible. The merits of both conductive drying models are discussed previously in Chapter 3 of this thesis.

In summary, Okazaki used a combined heat and mass transfer model to estimate the drying rates. On assuming that a simple evaporative drying front would proceed through the drying particulate bed, he then applied both heat and mass balances at this evaporative front to estimate its velocity profile with time. However, Schlünder predicted the drying rates of both isothermal and non-isothermal particulate beds in contact drying, by placing more emphasis on the heat conduction of the particulate bed, and not on the mass transfer resistances. Once the heats of evaporation are known

as a function of moisture content and applied vacuum, modelling these small drying rates may be easy for single particles and thin-layers. For thicker beds of particles, other mass transfer resistances may need to be accounted for.

The heat of wetting becomes increasingly significant while drying well into the second falling rate period; thus the lower drying rates observed in this region may be described in Equation 3.32 by the increase in the heat of wetting. It may be useful to know under what conditions this idea may hold, and the applications where mass transfer resistances become significant.

7.11.6 Drying selectivity of a binary mixture at low moisture contents

For the drying of an isopropyl alcohol and water mixture in alumina, selectivity in drying is not consistent with higher moisture content situations, i.e. does not follow the selectivity predicted by molar composition curves such as in Figure 7.3. This is described in Section 6.8.1.3. Unlike some other fine organic chemicals (adipic acid, hydroquinone etc.), terephthalic acid has a relatively stable porous structure with water as the adsorbant at typical drying temperatures (T_{dry} =100-160$degC$), so drying of the particles physisorbed moisture is easier. However, the mobility of the dicarboxylic aromatic monomers of terephthalic acid is limited to such an extent as to eliminate the chemisorbed moisture by dehydrating the carboxyl end groups. The removal of chemisorbed moisture is easier in the aliphatic material, i.e. adipic acid, compared with the aromatic compounds because the less rigid nature of its crystal structure at typical drying temperatures.

Thurner and Schlünder's (1986) approach to the drying behaviour binary solutions.

Thurner and Schlünder's (1986) mechanisms for selective drying are discussed extensively in Chapter 2. They showed that selectivity in drying at higher moisture contents very much depends on the mole fraction of each of the components in the binary solution. In Figure 7.3, the calculated compositions of the moisture during drying for different initial compositions of moisture are shown.

For an initial composition of about 0.40, no selectivity is predicted. For lower initial compositions, isopropyl alcohol is preferentially removed, mainly, because of its higher volatility. For initial compositions above 0.40, the relative volatility approaches unity and therefore water is removed, mainly due to its higher gas phase mass transfer coefficient compared with that of isopropyl alcohol. This indicates that the concepts of selective desorption of binary solutions at higher moisture contents cannot be extrapolated to the behaviour of drying selectivity at lower moisture contents.

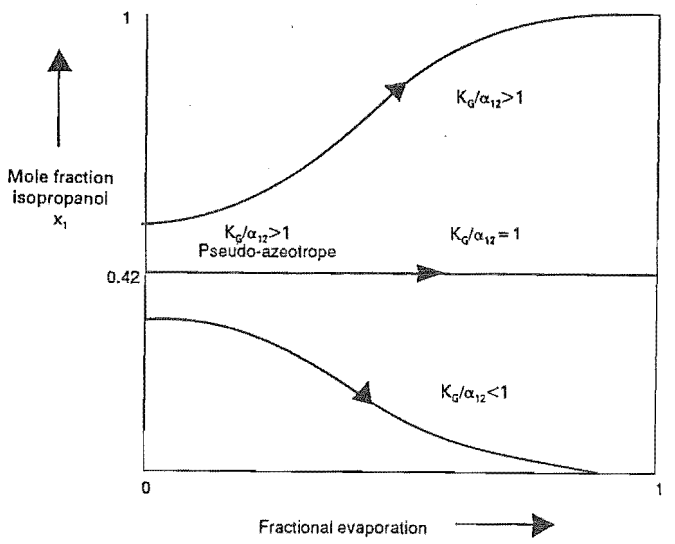

Figure 7.3 Calculated composition of the moisture for various initial compositions (shown by Thurner and Schlünder, (1986)

7.12 CHARACTERISTIC DRYING CURVES OF SELECTED MATERIALS AT LOW-MOISTURE CONTENTS

Characteristic drying curves were constructed under through-flow situations for the following materials: alumina, sand, pure terephthalic acid, pre-dried terephthalic acid and copolymer III. These are shown in Figures 6.41, 6.42, 6.43, 6.44, and 6.45. The thickness of the samples during these experiments remained relativity constant through all tests. Variations in air velocity, air temperature and air humidity showed minimal variation in the shapes of the characteristic drying curves for the drying of these materials with low-moisture contents. This stability in curve shapes again eliminates the possibility of wetted-surface, Fickian-based diffusion and receding evaporative interface models, but does not exclude the possibility of surface diffusion. There was an instability in the shapes of the characteristic drying curves for the copolymer material, thus again supporting the idea of Fickian-based diffusion processes even at low-moisture levels for polymeric materials.

Single particle and thin-layer experiments for these materials under vacuum conditions are shown in Figure 6.46. Figures 6.47 and 6.48 show characteristic drying curves under vacuum conditions for silica gel 124 and alumina. Similar conclusions can be drawn for these similar shaped characteristic drying curves under vacuum conditions. Variations in vacuum level from 0.022 *mbar* to 0.0004 *mbar* had no significant effect on

the shapes of the curves. Variations in curve shapes were observed from Figures 6.47 and 6.48. This difference can be accounted for by the thickness of the particulate layer, from the drying of single isolated particles to a 2 *mm* thick sample for both silica gel 124 and alumina materials.

Chapter 8

CONCLUSIONS

The drying kinetics differs when moisture is held by volume filling and/or is strongly sorbed on the pore surface at low moisture contents, compared with the situation when vapour diffusion and capillary action occur at higher moisture contents. Fickian diffusion processes do exist at low-moisture contents for the drying of polymeric-based materials and thus are not limited to higher moisture contents. The characteristic drying curves of the polymeric materials were found to have a variable spread of shapes under various external conditions of temperature and air velocity. However, the curves for alumina, sand, silica gel and the terephthalic acid materials were more consistently shaped. The shapes of the curves were dependent on the size of the particles and the size of the samples used. The different nature of the polymeric materials (Fickian-based diffusion) and other materials (surface-based diffusion) showed differences in curve shapes, indicating dissimilarities in the drying kinetics between Fickian-based models and surface diffusion processes.

Before the commencement of this work, it was not possible to use existing equipment to investigate the drying kinetics at these low-moisture levels. A new apparatus was designed and built to determine desorption phenomena with particulate materials at low moisture levels ($< 1\%$). The unit incorporates an electronic microbalance for gravimetric analysis, with a mass spectrometer and a frost point meter for evolved gas analysis. Samples ranging from 35 to 2500 mg may be dried by through-circulation, cross-circulation or under vacuum. The sensitivity of the microbalance permits the drying of single isolated particles, single particle agglomerates or particles in layers. A second chamber enables larger samples (5-200 g) to be dried under vacuum. The unit was used to follow the drying of fine pharmaceuticals and polymers, silica gel and alumina at dry-bulb temperatures between 80 $degC$ and 140 $degC$ and dew points of -5 $degC$ and +5 $degC$, with through-circulating air flowrates of 0.00158 and 0.00709 kg m^2 s^{-1} or vacua to $4 * 10^{-4}$ $mbar$.

Traditionally, the heats of wetting used to estimate drying loads are assumed to rise exponentially with falling moisture content. For the most part, this was shown to be an adequate assumption, but to be not entirely correct. Curves of heat of wetting

against moisture content indicated less variation with moisture content while drying a monolayer. This indicates that there are less strongly sorbed sites on the pore surface. The surface chemistry of the pores "on paper" does indicate a more even surface activity but, in the real cases, heats of wetting calculated from equilibrium sorption isotherms most often show that this is not the case. Only when the pores are of uneven thickness or pore necking is present do strongly sorbed sites appear to be due to sorbed molecules being trapped and an exponential heat of wetting curve results.

Various empirical and traditional model sorption equations were tested to observe which of these fitting equations should be used at low-moisture contents. The modified BET equation appeared to be the best correlation for fitting a wide range of sorption isotherms for multilayered sorption. At monolayer loadings of moisture, a Henry-type or linear fitting correlation alone was found to be the most suitable.

The validity of various drying models was tested to see which models fit the low-moisture content drying processes. The drying stoichiometry yields the order of the drying kinetics through a knowledge of the chemistry. A transition from first-order drying to second order drying can often be uneven, as indicated for the drying of silica gel, because the silica gel surface dries in a "patchy" manner under sudden extreme drying conditions. For most materials tested, except the polymeric solids, the surface diffusion model appears to fit the experimental drying rates. For thicker samples, a greater error was introduced by not including a gas-phase mass transfer coefficient through the particulate bed. For these materials dried as isolated particles, single particle agglomerates and thin-layers, the surface diffusion model gave a better fit than other models. However, Fickian diffusion gave a good fit for the drying of the polymeric-based materials. This indicated that, in this instance, the drying kinetics of polymeric materials at higher moisture contents can be extrapolated to the drying of these materials at lower moisture contents. This is possible because the mechanisms for moisture transport at higher moisture contents are the same as the mechanisms responsible for moisture movement at lower moisture levels. At lower moisture contents, the "water clusters" just reduce in size. A receding evaporative interface model appeared to be an unsuitable assumption for low-moisture content drying, although it was difficult to prove that the drying of polymeric materials did not favour this type of drying model.

At low moisture contents, surface diffusive forces are assumed to dominate the drying behaviour. The results from this work indicated that this is indeed the case for the drying of non-swelling isolated particles, isolated particle agglomerates and very thin-layer particle beds. However, for thin-layers greater than $1mm$ in depth, a surface diffusion model is not the only driving force for drying. Interparticle gas/bulk flow diffusive elements and/or heat transfer coefficients through the layer would have to be considered, and incorporated with surface diffusion coefficients, to calculate the effective bed diffusion coefficient, D_{eff}, from a sum of the reciprocal diffusion coefficients. Modelling diffusion at low moisture contents depends very much on the strengths of the

sorbate-sorbent interactions. Information about the heat transfer through the drying sample would also influence the size of the effective diffusion of water vapour through the sample.

For swelling materials, other diffusive mechanisms become apparent. There is a significant amount of literature on the drying of polymer-based materials, which considers the effects of polymer relaxation and other structural effects on the drying behaviour.

Schlünder's heat transfer drying model gives a simplified approach to resolving drying mechanism at low-moisture levels while incorporating heat of wetting information. Calculations indicated that the only instance where this model is applicable at low-moisture contents is the drying of small ($d_p < 0.5\ mm$) isolated particles where there is little resistance to heat transfer. His model is more applicable at higher moisture contents.

Selectivity of drying at low-moisture contents was briefly investigated in this work. Selectivity in drying at higher moisture contents with liquid water and liquid solvent/s is most often observed. At lower moisture contents, say when drying is performed in an equivalent monolayer arrangement, selectivity becomes a function of the associated heats of wetting of the individual sorbed species, and therefore their ability to surface diffuse along the pores. Extrapolating the selective drying concepts adopted at higher moisture contents to lower moisture levels is not possible. The drying mechanisms are different. At these moisture levels, Krishna (1990a) showed that the drying fluxes of the sorbents of a binary mixture at low-moisture contents by surface diffusion are independent of each other, and can be modelled as separate entities.

In summary, the drying kinetics of particulate material at higher moisture contents ($> 1\%$) cannot always be extrapolated to drying to low-moisture levels. Surface diffusive mechanisms usual prevail at these low-moisture contents. Thus, temperature-driven mechanisms are the driving force behind the kinetics. In some cases, for the drying of hydrophobic materials below $< 1\%$ moisture contents, such as the copolymers investigated in this work, Fickian diffusive resistances become the driving force behind the kinetics because the moisture is held in water clusters rather than bound directly to the surface. Comment: very often particulate material contains both hydrophilic and hydrophobic surfaces, such as in many food ingredients, e.g. milk caseinates, so drying would be driven both by heat and mass transfer models.

Appendix A

PRELIMINARY DRYING KINETICS STUDIES AT HARWELL

A.1 SMOOTHING RAW DATA DRYING CURVES

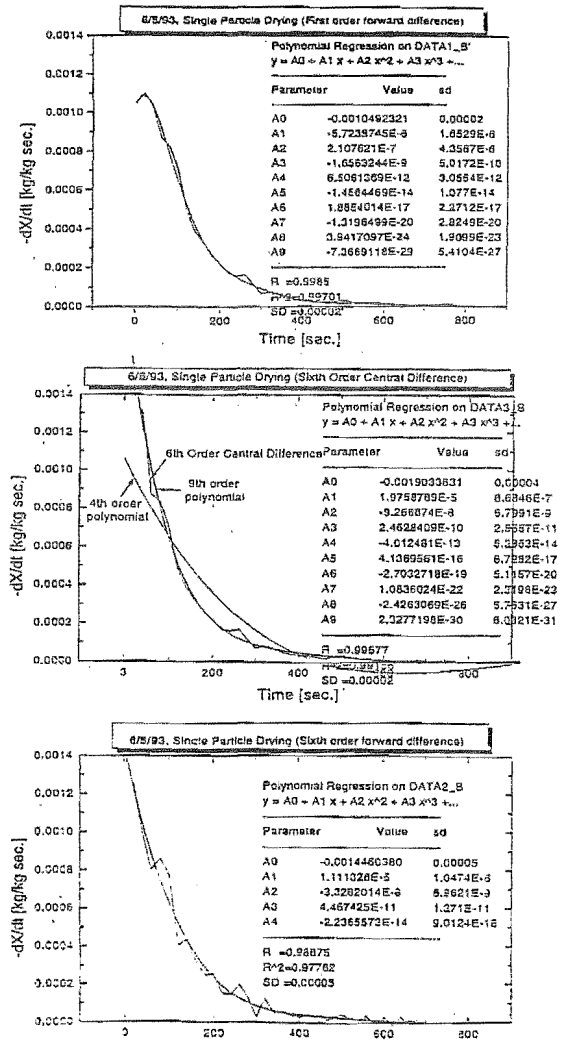

Figure A.1 Comparing different first-derivative methods to determine drying rates, as well as investigating the effects of fitting the data

A.2 RAW DATA OF OUTLET GAS HUMIDITY VS. TIME USING AN INFRARED GAS ANALYSER FROM KEECH (1992)

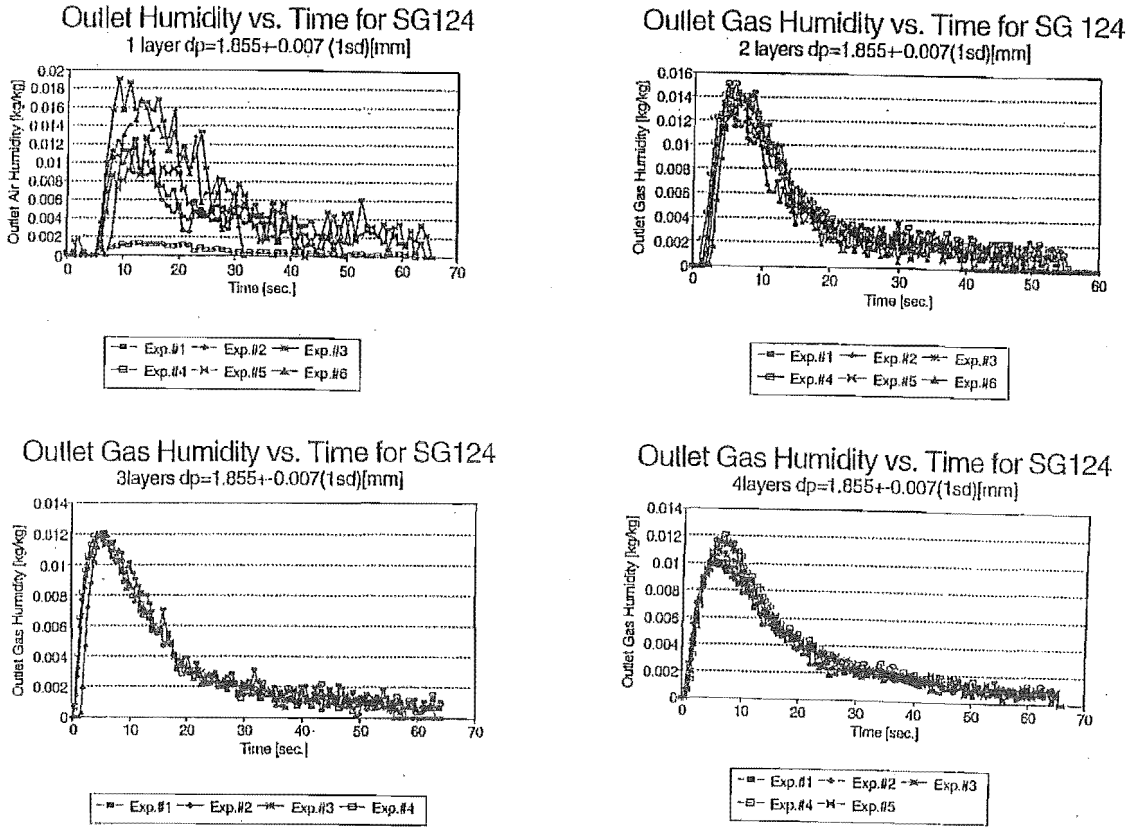

Figure A.2 Evolved gas profiles

A.3 MOISTURE CONTENT VS. TIME EXPERIMENTS

- Group A experiments

  1. A single particle dried at the centre of the crucible.
  2. A single particle dried at the edge of the crucible.

3. Two particles dried separated by two particle diameters.
4. Two particles dried at the centre.

- Group B experiments

1. One layer drying.
2. Two layer drying.
3. Three layer drying
4. Four layer drying.

A.3.1 Group A moisture content with time profiles

(see Figure A.3)

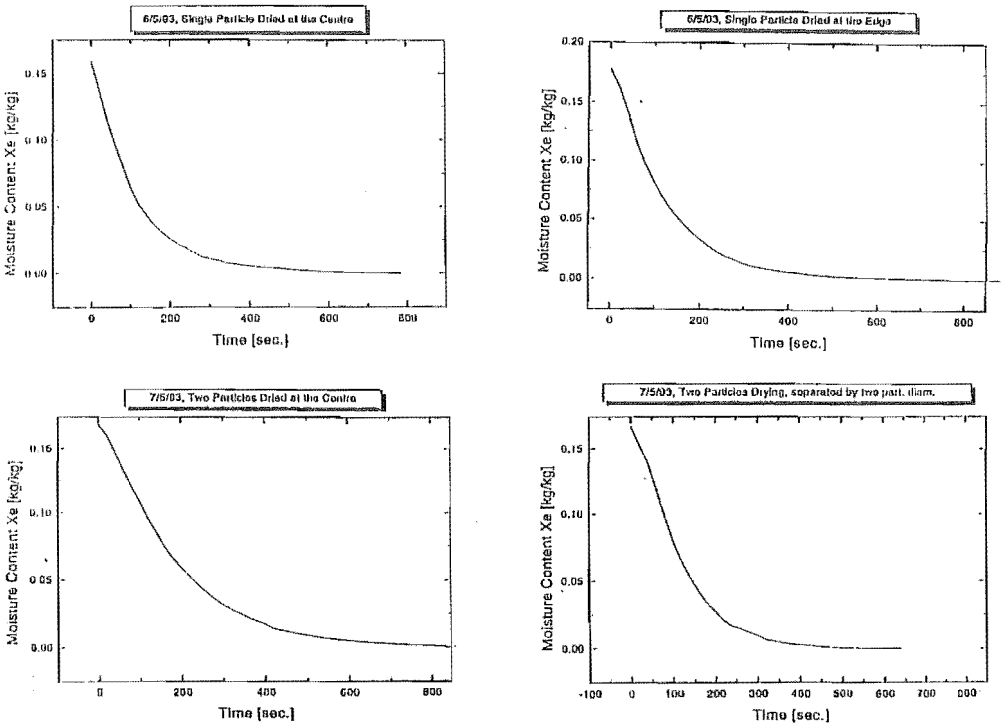

Figure A.3 Single and double isolated particle drying

A.3.2 Group B moisture content with time profiles

(see Figure A.4)

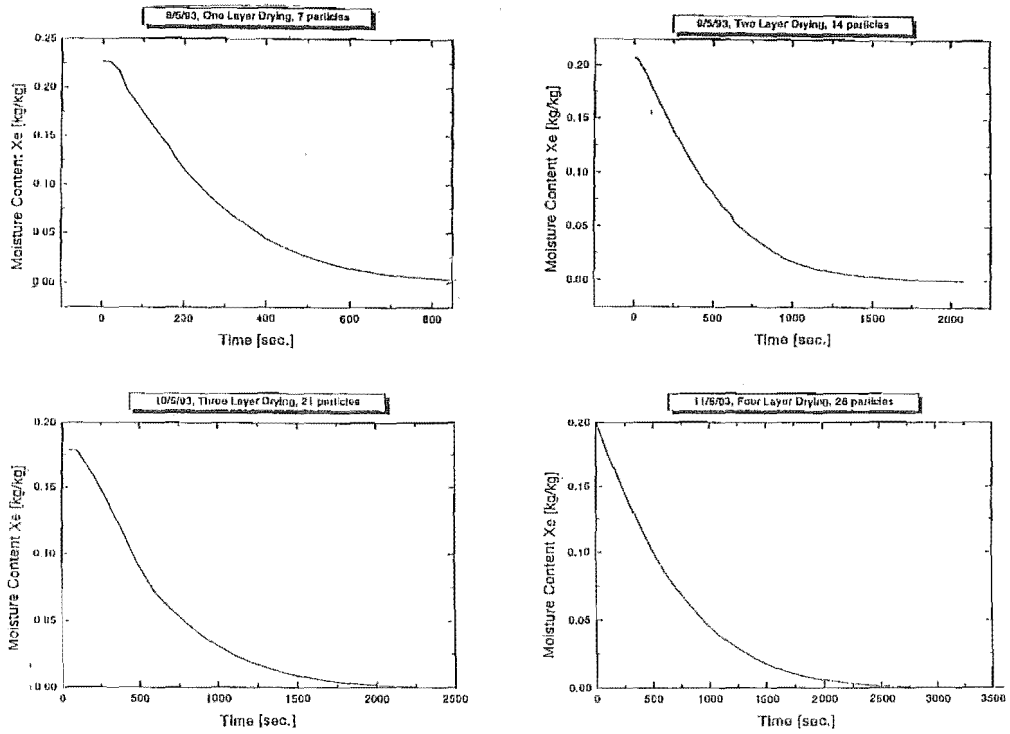

Figure A.4 Layer drying

A.4 FITTING DRYING RATE CURVES WITH TIME

A.4.1 Group A experiments

(see Figure A.5)

A.4.2 Group B experiments

(see Figure A.6)

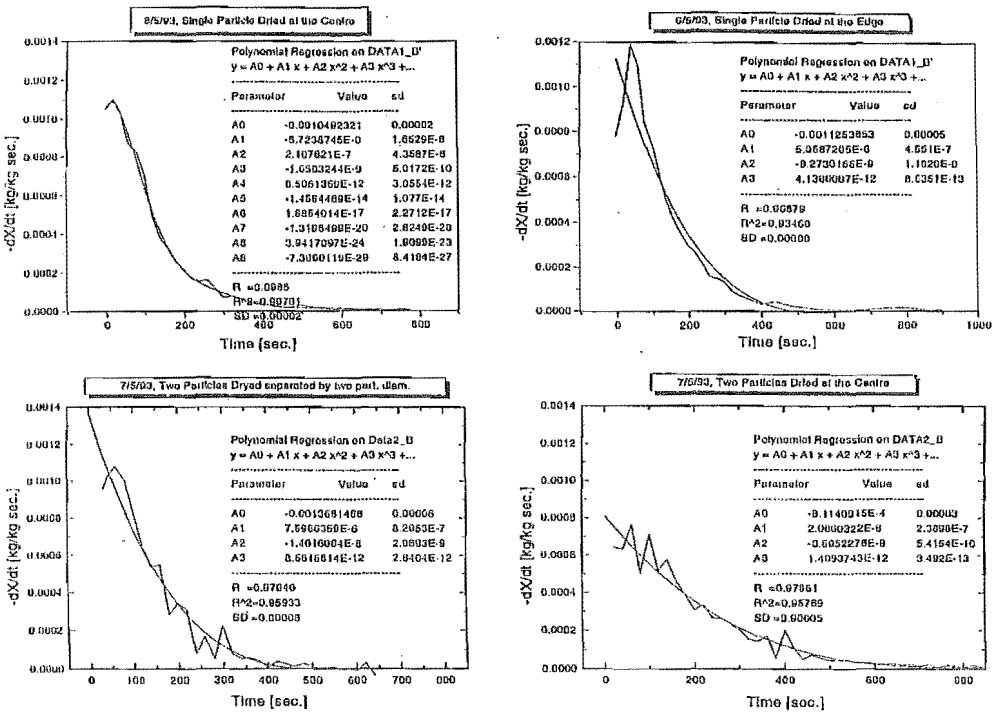

Figure A.5 $-dX/dt$ (1st order difference) vs. time for group A experiments

A.5 FITTING DRYING RATE CURVES WITH NORMALISED DRYING RATE

A.5.1 Group A experiments

(see Figure A.7)

A.5.2 Group B experiments

(see Figure A.8)

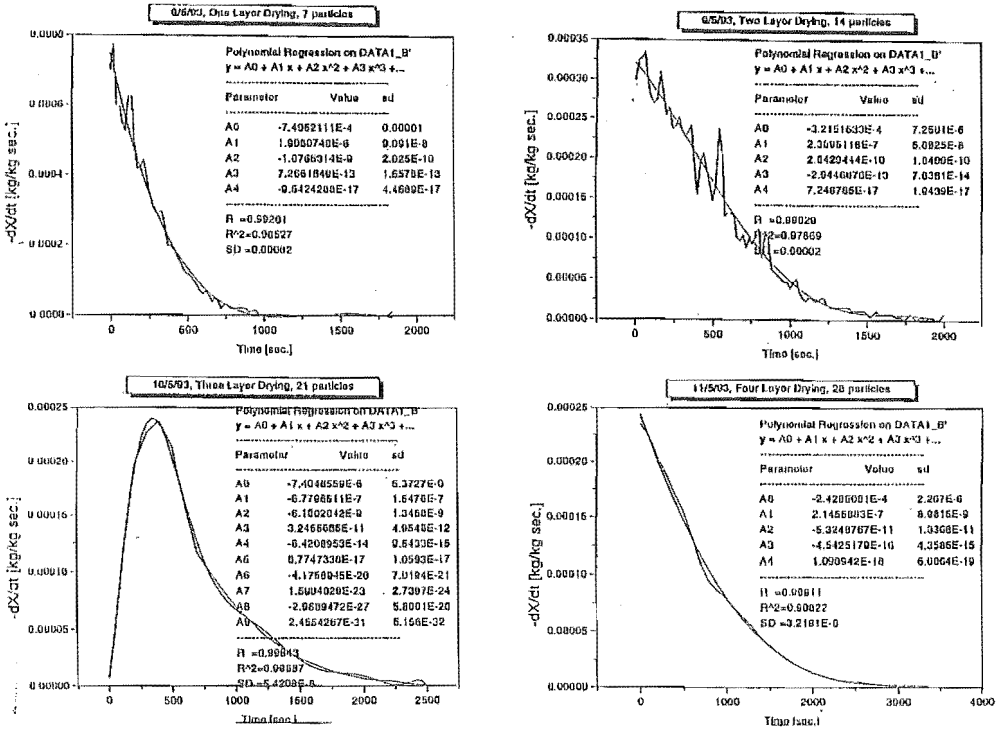

Figure A.6 $-dX/dt$ (1st order difference) vs. time for group B experiments

A.6 CHARACTERISTIC DRYING RATE CURVES WITH NORMALISED DRYING RATE

A.6.1 Group A experiments

(see Figure A.9)

A.6.2 Group B experiments

(see Figure A.10)

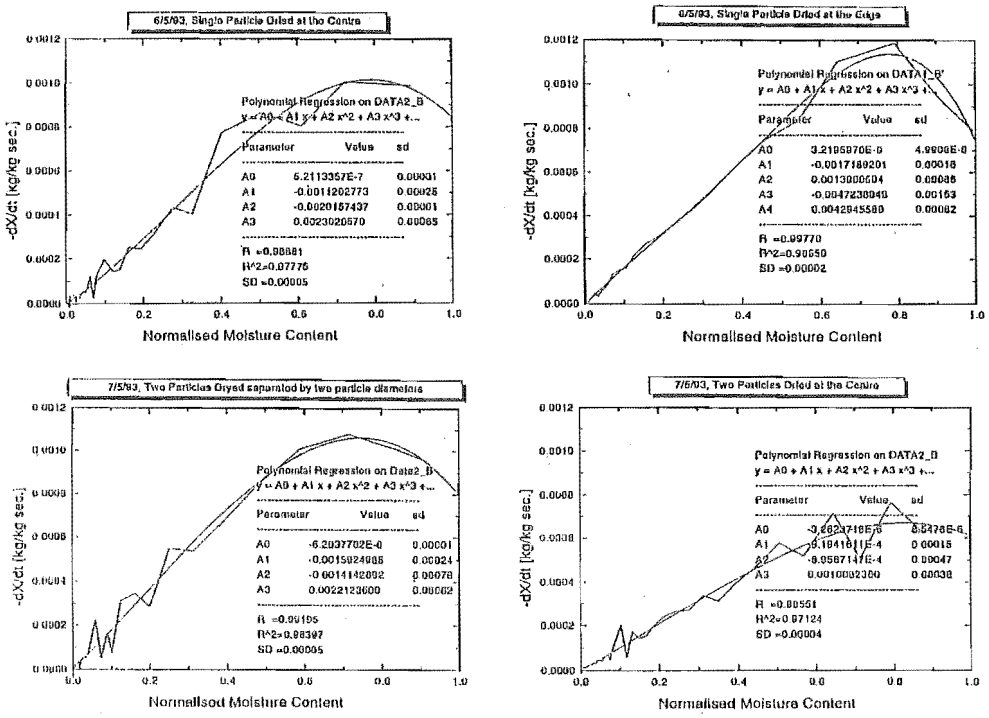

Figure A.7 $-dX/dt$ (1st order difference) vs. normalised moisture content for group A experiments

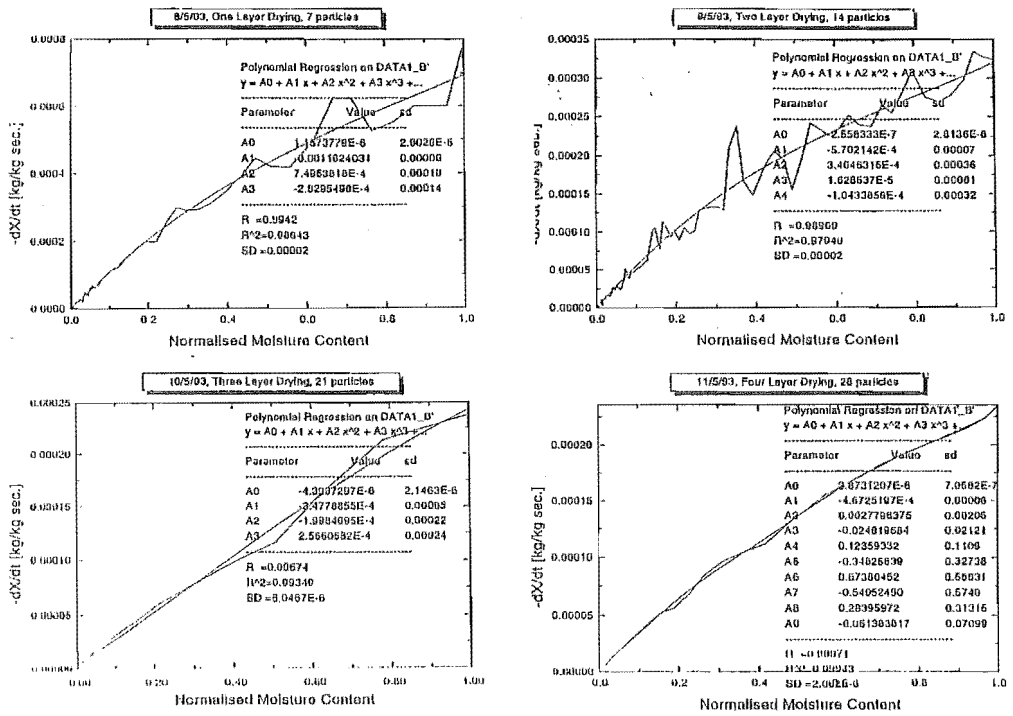

Figure A.8 $-dX/dt$ (1st order difference) vs. normalised moisture content for group B experiments

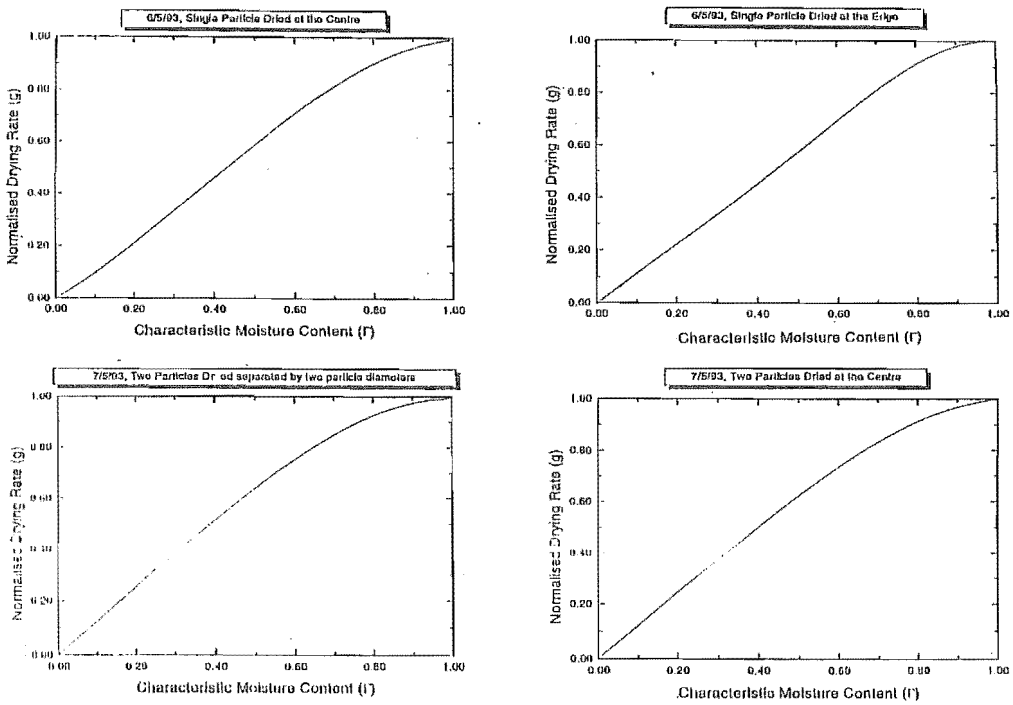

Figure A.9 Characteristic drying rate with normalised moisture content for group A experiments

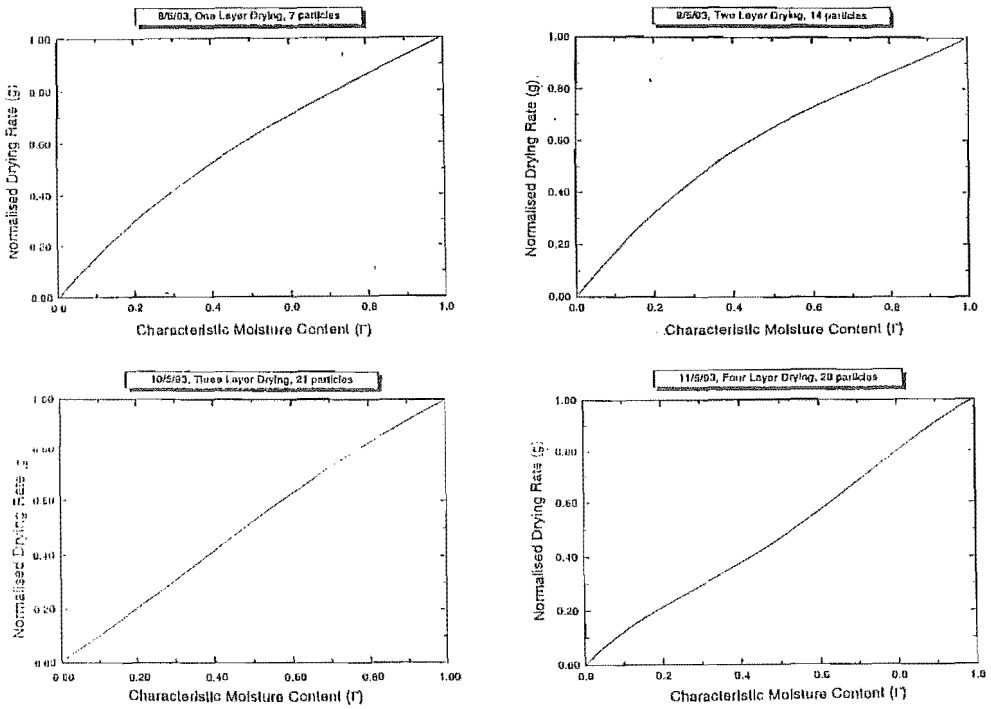

Figure A.10· Characteristic drying rate with normalised moisture content for group B experiments

Appendix B

THE NTH ORDER FORWARD DIFFERENCE DERIVATION

Testing the response of a forward difference operator on higher order differences.

Consider a function f(x).

Let h be a fixed real number and let f be a given function. The function D_f defined by the equation

$$\Delta f(x) = f(x+h) - f(x) \tag{B.1}$$

is called the forward difference of f. It is defined at those points x for which both x and $x + h$ are in the domain of f.

Suppose $f_p = (1+D)pf_o$ where D represents a finite difference.

The binomial theorem gives

$$f_p = \left(1 + p\Delta + \frac{p(p-1)}{1*2}\Delta^2 + \frac{p(p-1)(p-2)}{1*2*3}\Delta^3 + ...\right) f_o \tag{B.2}$$

Then

$$hf_p^1 = \frac{df_p}{dp} = \left(\Delta + \frac{2p-1}{2!}\Delta^2 + \frac{3p^2}{3!}\Delta^3 + ...\right) f_o \tag{B.3}$$

When p=1, we can get a forward difference formula:

$$hf_p^1 = \left(\Delta + 1/2\Delta^2 - 1/6\Delta^3 + 1/12\Delta^4 - 1/20\Delta^5 + 1/33\Delta^6 - ...\right) f_o \tag{B.4}$$

Comment on Notation

$$\frac{d}{DX}f(x) = \frac{df_p}{dp}\cdot\frac{dp}{dx} = \frac{df_p}{dp}\cdot\frac{1}{dx/dp} = \frac{df_p}{dp}\cdot\frac{1}{h} \tag{B.5}$$

where h is in the interval x.

Let

$$\frac{df_p}{dp} = f_p^I \tag{B.6}$$

The first difference is given by

$$\Delta f_o = f_1 - f_o \tag{B.7}$$

and other differences (of higher order) are given by the formula

$$\Delta^r f_n = \Delta^{r-1} f_{n+1} - \Delta^{r-1} f_n \tag{B.8}$$

i.e. when r=2, n=0;

$$\begin{aligned} \Delta^2 f_o &= \Delta f_1 - \Delta f_o \\ &= (f_2 - f_1) - (f_1 - f_0) \\ &= f_2 - 2f_1 + f_0 \end{aligned} \tag{B.9}$$

i.e. when r=3, n=0;

$$\begin{aligned} \Delta^3 f_o &= \Delta^2 f_1 - \Delta^2 f_o \\ &= (\Delta f(x_2) - \Delta f(x_1)) - (\Delta f(x_1) - \Delta f(x_0)) \\ &= ((f_3 - f_2) - (f_2 - f_1)) - ((f_2 - f_1) - (f_1 - f_0)) \\ &= (f_3 - 2f_2 + f_1) - (f_2 - 2f_1 + f_0) \\ &= f_3 - 3f_2 + 3f_1 - f_0 \end{aligned} \tag{B.10}$$

and

$$\Delta^3 f(x_1) = f_4 - 3f_3 + 3f_2 - f_1 \tag{B.11}$$

Continuing on this process, we can establish higher order differences.

Appendix C

RAW DATA OF DRYING KINETICS WORK AT LOW-MOISTURE CONTENTS

C.1 COMPARISON OF HARWELL DRYING KINETICS RESULTS WITH NEW APPARATUS

Tabulated results of single particle trials using new apparatus

Table C.1 Tabulated results of single particle trials using new apparatus.

	Single particles				Layers	
	Exp. # 1b	Exp. # 2b	Exp. # 3b	Exp. # 4b	Exp. # 5b	Exp. # 6b
Initial moisture content [kg/kg]	0.16	0.17	0.15	0.17	0.21	0.19
Diffusion coefficient, $(D)^*[m^2/s]$	3.47E-7	3.33E-7	3.36E-7	2.31E-7	2.32E-7	1.03E-7
Reynolds number, (Re_p)	73.3	73.3	73.3	73.3	73.3	73.3
Schmidt number, (Sc)	0.58	0.58	0.58	0.58	0.58	0.56
Sherwood number, (Sh)	6.38	6.38	6.38	10.52	10.52	10.52
Mass transfer coefficient, [1] (ko) $[kg/m^{-2}s^{-1}]$	2.76E-08	2.73E-06	3.11E-06	3.00E-06	2.08E-06	1.24E-06
Mass transfer coefficient, [2] (ko) $[kg/m^{-2}s^{-1}]$	3.69E-03	3.65E-03	3.7E-03	4.74E-03	4.79E-03	3.06E-03
Mass transfer coefficient, [3] (ko) $[kg/m^{-2}s^{-1}]$	7.82E-03	7.82E-03	7.81E-03	4.98E-03	4.98E-03	2.31E-03
fi $[kg/m^{-2}s^{-1}]$	0.379	0.381	0.335	0.379	0.333	0.295
Surface/Volume ratio, a $[m^2/m^3]$	7032	7032	7032	7032	7032	9801
Specific mass flow rate of air, G $[kg/m^{-2}s^{-1}]$	0.016	0.016	0.016	0.016	0.016	0.016
NTU	6.97E-01	0.693E-01	6.99E-01	7.91E-01	7.95E-01	8.96E-01

The mass transfer coefficient is defined as the bed-averaged interparticle resistance of water vapour in air.

Testing the concept of the characteristic drying curve for silica gel 124 at low air flows

(see Tables C.2 and C.3)

C.2 LOW-MOISTURE CONTENT DRYING KINETICS EXPERIMENTS

Determining the critical moisture content of the copolymer (I)

(see Table C.4)

Using the characteristic drying curve concept for the materials at low moisture contents

Table C.2 Tabulated experimental conditions and results of drying SG124 under laminar air flows.

	Exp. # 7	Exp. # 8	Exp. # 9	Exp. # 10	Exp. # 11	Exp. # 12	Exp. # 13	Exp. # 14	Exp. # 15
Initial moisture content, X_i [kg/kg]	0.118	0.191	0.116	0.304	0.158	0.177	0.203	0.183	0.168
Reynolds number, (Re)	4 [4]	4	4	4	73.3 [5]	73.3	73.3	73.3	73.3
Specific mass flow rate of air, G [$kgm^{-2}s^{-1}$]	0.0008	0.0008	0.0008	0.0008	0.016	0.016	0.016	0.016	0.016
T_{dry}, [K]	373	373	373	373	373	373	353	353	353
Y_{GI}, [kg/kg]	0.004	0.004	0.004	0.004	0.004	0.004	0.004	0.004	0.004
Dry bed weight, W_{GO} [kg]	0.00011	0.00011	0.00011	0.00011	0.00011	0.00011	0.00011	0.00011	0.00011
No. of data points in drying curve	1876	1800	1998	1976	1876	1876	967	995	999
Area of batch bed, A_b [m^2]	0.00196	0.00196	0.00196	0.00196	0.00196	0.00196	0.00196	0.00196	0.00196
Bed weight/area, W_{GO}/A_b	0.0566	0.0566	0.0566	0.0566	0.0566	0.0566	0.0584	0.0584	0.0584
Initial drying rate, -dX/dt, [kg/kgs]	0.000688	0.00119	0.00089	0.00214	0.000537	0.000425	0.000496	0.000667	0.000839
fi [$kgkg^{-1}s^{-1}$]	0.301	0.504	0.305	0.801	0.415	0.464	0.534	0.481	0.442
Surface/Volume ratio, a [m^2/m^3]	403	403	403	403	403	403	403	403	403
Mass transfer coefficient at fi (koi) [6] [$kg/m^{-2}s^{-1}$]	0.294	0.314	0.387	0.353	0.171	0.121	0.123	0.184	0.252
NTU	error	error	error	error	0.874	0.762	0.615	0.719	0.805
Drying kinetics exponent, C_1	1	1	1.164	1	1	0.976	1	1	1
Drying kinetics exponent, C_2	0.3103	0.4919	0.2814	0.7515	0.4017	0.06773	0.1634	0.4570	0.4293
Drying kinetics exponent, C_3	1.368	1.346	1.281	1.331	1.370	1.050	0.8068	1.152	1.311

Table C.3 Extension of above table

	Exp. # 16	Exp. # 17	Exp. # 18	Exp. # 19	Exp. # 20	Exp. # 21	Exp. # 22	Exp. # 23
Initial moisture content, X_i [kg/kg]	0.154	0.177	0.209	0.206	0.106	0.0727	0.167	0.150
Reynolds number, (Re)	73.3	73.3	73.3	73.3	73.3	73.3	73.	73.3
Specific mass flow rate of air, G [$kgm^{-2}s^{-1}$]	0.016	0.016	0.016	0.016	0.016	0.016	0.016	0.016
T_{dry}, [K]	393	393	413	413	373	373	373	373
Y_{OI}, [kg/kg]	0.004	0.004	0.004	0.004	0.004	0.004	0.004	0.004
Dry bed weight, W_b [kg]	0.0002	0.0002	0.0002	0.0002	0.0002	0.0002	0.0002	0.0002
No. of data points in drying curve	1543	1500	1500	1500	1717	1643	2000	4000
Area of batch bed, A_b [m_2]	0.00196	0.00196	0.00196	0.00196	0.000314	0.000314	0.000314	0.000314
Bed weight/area, W_b/A_b	0.102	0.102	0.102	0.102	0.637	0.6367	0.637	0.637
Initial drying rate, -dX/dt, [kg/kgs]	0.00116	0.00144	0.00209	0.00231	0.000270	0.000518	0.000694	0.000240
fi [$kgkg^{-1}s^{-1}$]	0.406	0.467	0.549	0.543	0.280	0.191	0.440	0.395
Surface/Volume ratio, a [m^2/m^3]	403	403	403	403	3180	3180	3180	3180
Mass transfer coefficient at fi (k_{oi}) [$kg/m^{-2}s^{-1}$]	0.379	0.411	0.507	0.566	0.0162	0.0457	0.0266	0.0102
NTU	0.831	0.662	0.429	0.425	1.260	1.860	0.775	0.913
Drying kinetics exponent, C_1	1	1	1	1.008	1	1	1	1.005
Drying kinetics exponent, C_2	0.3914	0.4506	0.5379	0.5060	0.04000	0.1811	0.4279	0.2298
Drying kinetics exponent, C_3	1.3748	1.4618	1.2848	1.2572	0.8192	1.2924	1.1251	1.0243

(see Tables C.5, C.6, C.7, C.8, C.9)

Vacuum single particle tests

(see Table C.10)

Vacuum drying tests of silica gel 124 and alumina

(see Tables C.11 and C.12)

where SPA-single particle agglometerates, OL-one layer and UL-uneven layer.

Drying kinetics at low-moisture contents of alumina containing a binary solution of water and isopropyl a

(see Table C.13)

Table C.4 Determining the critical moisture content of the copolymer I

	Exp. # 54	Exp. # 55	Exp. # 56
Initial moisture content, X_i [kg/kg]	0.0095	0.0091	0.0092
Specific mass flow rate of air, G [$kgm^{-2}s^{-1}$]	0.016	0.016	0.016
T_{dry}, [K]	100	100	100
Y_{GI}, [kg/kg]	0.004	0.004	0.004
Dry bed weight, W_b [kg]	0.003	0.003	0.003
No. of data points in drying curve	800	800	800
Drying kinetics exponent, C_1	0.260	0.603	0.806
Drying kinetics exponent, C_2	0.80	0.50	0.79
Drying kinetics exponent, C_3	1	0.40	0.77

Table C.5 Testing the characteristic drying curve concept for the materials at low moisture contents - alumina

	Exp. # 24	Exp. # 25	Exp. # 26	Exp. # 27	Exp. # 28
X_i [kg/kg]	0.004	0.004	0.004	0.004	0.004
G [$kgm^{-2}s^{-1}$]	0.016	0.0036	0.016	0.016	0.016
T_{dry}, [K]	100	100	120	100	100
Y_{GI}, [kg/kg]	0.004	0.004	0.004	0.02	0.004
Dry bed weight, W_b [kg]	0.003	0.003	0.003	0.003	0.001
No. of data points	400	400	400	400	400
Drying kinetics exponent, C_1	0.760	0.885	0.752	0.8027	0.880
Drying kinetics exponent, C_2	0.313	0.411	0.554	0.273	0.311
Drying kinetics exponent, C_3	1.225	1.209	1.089	1.162	1.021

Table C.6 Testing the characteristic drying curve concept for the materials at low moisture contents - iron sand

	Exp. # 30	Exp. # 31	Exp. # 32	Exp. # 33	Exp. # 34
X_i [kg/kg]	0.004	0.004	0.004	0.004	0.004
G [$kgm^{-2}s^{-1}$]	0.016	0.0036	0.016	0.016	0.016
T_{dry}, [K]	100	100	120	100	100
Y_{GI}, [kg/kg]	0.004	0.004	0.004	0.02	0.004
Dry bed weight, W_b [kg]	0.003	0.003	0.003	0.003	0.001
No. of data points	400	400	400	400	400
Drying kinetics exponent, C_1	0.740	0.592	1.00	0.580	0.837
Drying kinetics exponent, C_2	0.402	0.008	0.306	0.192	0.292
Drying kinetics exponent, C_3	1.290	1.079	0.772	0.273	0.221

Table C.7 Testing the characteristic drying curve concept for the materials at low moisture contents - pure terephthalic acid

	Exp. # 36	Exp. # 37	Exp. # 38	Exp. # 39	Exp. # 40
X_i [kg/kg]	0.004	0.004	0.004	0.004	0.004
G [$kgm^{-2}s^{-1}$]	0.016	0.0036	0.016	0.016	0.016
T_{dry}, [K]	100	100	120	100	100
Y_{GI}, [kg/kg]	0.004	0.004	0.004	0.02	0.004
Dry bed weight, W_b [kg]	0.003	0.003	0.003	0.003	0.001
No. of data points	400	400	400	400	400
Drying kinetics exponent, C_1	0.759	0.611	1.00	0.760	0.733
Drying kinetics exponent, C_2	0.264	0.343	0.314	0.402	0.477
Drying kinetics exponent, C_3	0.487	1.435	0.724	1.290	1.144

Table C.8 Testing the characteristic drying curve concept for the materials at low moisture contents - pre-dried terephthalic acid

	Exp. # 42	Exp. # 43	Exp. # 44	Exp. # 45	Exp. # 46
X_i [kg/kg]	0.004	0.004	0.004	0.004	0.004
G [$kgm^{-2}s^{-1}$]	0.016	0.0036	0.016	0.016	0.016
T_{dry}, [K]	100	100	120	100	100
Y_{GI}, [kg/kg]	0.004	0.004	0.004	0.02	0.004
Dry bed weight, W_b [kg]	0.003	0.003	0.003	0.003	0.001
No. of data points	400	400	400	400	400
Drying kinetics exponent, C_1	1	1	1	1	0.803
Drying kinetics exponent, C_2	0.327	0.321	0.221	0.286	0.273
Drying kinetics exponent, C_3	0.656	0.989	0.694	0.876	1.162

Table C.9 Testing the characteristic drying curve concept for the materials at low moisture contents - copolymer (II)

	Exp. # 48	Exp. # 49	Exp. # 50	Exp. # 51	Exp. # 52	Exp. # 53
X_i [kg/kg]	0.004	0.004	0.004	0.004	0.004	0.004
G [$kgm^{-2}s^{-1}$]	0.016	0.0036	0.016	0.016	0.016	0.036
T_{dry}, [K]	100	100	120	100	100	100
Y_{GI}, [kg/kg]	0.004	0.004	0.004	0.02	0.004	0.004
Dry bed weight, W_b [kg]	0.003	0.003	0.003	0.003	0.001	0.003
No. of data points	400	400	400	400	400	400
Drying kinetics exponent, C_1	0.872	0.931	0.810	0.569	1.09	0.954
Drying kinetics exponent, C_2	0.09	0.01	0.02	0.01	0.2	0.02
Drying kinetics exponent, C_3	1.17	1.1	1.07	1.1	1.2	1.05

Table C.10 Testing the characteristic drying curve concept for isolated particles at low moisture contents

	Exp. # 57 (alumina)	Exp. # 58 (sand)	Exp. # 59 (pre-dried TA)	Exp. # 60 (copolymer I)
X_i [kg/kg]	0.004	0.003	0.006	0.011
G [$kgm^{-2}s^{-1}$]	0.0	0.0	0.0	0.0
T_{dry}, [K]	100	100	100	100
Y_{GI}, [kg/kg]	0.0	0.0	0.0	0.0
Dry bed weight, W_b [kg]	0.001	0.001	0.001	0.001
No. of data points	800	800	800	800
Drying kinetics exponent, C_1	1	1	1.026	1
Drying kinetics exponent, C_2	0.11	0.09	0.31	0.55
Drying kinetics exponent, C_3	0.29	0.81	1.03	2.07

Table C.11 Testing the characteristic drying curve concept for single isolated particles of silica gel 124 under varying vacuum conditions

	Exp. # 61	Exp. # 62	Exp. # 63	Exp. # 64	Exp. # 65	Exp. # 66
X_i [kg/kg]	0.017	0.017	0.017	0.017	0.017	0.017
G [$kgm^{-2}s^{-1}$]	0.0	0.0	0.0	0.0	0.0	0.0
T_{dry}, [K]	100	100	80	80	120	120
Y_{GI}, [kg/kg]	0.0	0.0	0.0	0.0	0.0	0.0
Dry bed weight, W_b [kg]	0.001	0.001	0.001	0.001	0.001	0.001
No. of data points	1100	1100	1100	1100	1100	1100
Vacuum level	3.3e-02	4.0e-04	3.3e-02	4.0e-04	3.3e-02	4.0e-04
Drying kinetics exponent, C_1	1	1.1	1.05	1.1	1	1.
Drying kinetics exponent, C_2	0.75	0.77	0.77	0.61	0.52	0.55
Drying kinetics exponent, C_3	2.14	2.25	2.21	2.09	1.99	2.12
	Exp. # 67	Exp. # 68	Exp. # 69	Exp. # 70	Exp. # 71	
X_i [kg/kg]	0.017	0.017	0.017	0.017	0.017	
G [$kgm^{-2}s^{-1}$]	0.0	0.0	0.0	0.0	0.0	
T_{dry}, [K]	100	100	100	100	100	
Y_{GI}, [kg/kg]	0.0	0.0	0.0	0.0	0.0	
Dry bed weight, W_b [kg]	0.001	0.008	0.008	0.008	0.008	
No. of data points	1100	1100	1100	1100	1100	
Bed configuration	SPA	SPA	OL	OL	UL	
Vacuum level	3.3e-02	4.0e-04	3.3e-02	4.0e-04	3.3e-02	
Drying kinetics exponent, C_1	0.99	1	0.94	1.1	0.93	
Drying kinetics exponent, C_2	0.32	0.41	0.52	0.66	0.41	
Drying kinetics exponent, C_3	2.0	2.04	2.2	2.18	2.0	

Table C.12 Testing the characteristic drying curve concept for single isolated particles of alumina under varying vacuum conditions

	Exp. # 73	Exp. # 74	Exp. # 75	Exp. # 76	Exp. # 77	Exp. #78
Initial moisture content, X_i [kg/kg]	0.004	0.004	0.004	0.004	0.004	0.004
G [$kgm^{-2}s^{-1}$]	0.0	0.0	0.0	0.0	0.0	0.0
T_{dry}, [K]	100	100	80	80	120	120
Y_{GI}, [kg/kg]	0.0	0.0	0.0	0.0	0.0	0.0
Dry bed weight, W_b [kg]	0.0005	0.0005	0.0005	0.0005	0.0005	0.
No. of data points in drying curve	200	200	200	200	200	200
Vacuum level	3.3e-02	4.0e-04	3.3e-02	4.0e-04	3.3e-02	4.0e-04
Drying kinetics exponent, C_1	1	1.1	1.05	1.0	0.97	0.95
Drying kinetics exponent, C_2	0.62	0.64	0.70	0.73	0.30	0.40
Drying kinetics exponent, C_3	2.2	2.4	2.1	2.1	2.0	2.4
	Exp. # 79	Exp. # 80	Exp. # 81	Exp. # 82	Exp. # 83	
Initial moisture content, X_i [kg/kg]	0.004	0.004	0.004	0.004	0.004	
G [$kgm^{-2}s^{-1}$]	0.0	0.0	0.0	0.0	0.0	
T_{dry}, [K]	100	100	100	100	100	
Y_{GI}, [kg/kg]	0.0	0.0	0.0	0.0	0.0	
Dry bed weight, W_b [kg]	0.0005	0.003	0.003	0.003	0.003	
No. of data points in drying curve	200	200	200	200	200	
Bed configuration	SPA	SPA	OL	OL	UL	
Vacuum level	3.3e-02	4.0e-04	3.3e-02	4.0e-04	3.3e-02	
Drying kinetics exponent, C_1	0.96	1.11	1.2	1.0	1.0	
Drying kinetics exponent, C_2	0.01	0.2	0.09	0.14	0.12	
Drying kinetics exponent, C_3	2.3	2.2	2.4	2.6	2.0	

Table C.13 Testing the shape of the characteristic drying curve concept for alumina containing a binary solution of water and isopropyl alcohol

	Exp. # 100	Exp. # 101	Exp. # 102	Exp. #103
X_i [kg/kg]	0.059	0.055	0.056	0.004
Dry bed weight, W_b [kg]	0.001	0.001	0.001	0.001
No. of data points	800	800	800	800
Bed configuration	thin-layer	thin-layer	thin-layer	thin-layer
Vacuum level	4.0e-04	4.0e-04	4.0e-04	4.0e-04
Isopropyl alcohol, %,	100	66	33	0
Drying kinetics exponent, C_1	1.2	1.3	1.1	0.95
Drying kinetics exponent, C_2	0.56	0.57	0.57	0.60
Drying kinetics exponent, C_3	2.1	2.4	2.2	2.0
	Exp. # 89	Exp. # 90	Exp. # 91	Exp. #.92
X_i [kg/kg]	0.059	0.055	0.056	0.004
Dry bed weight, W_b [kg]	0.003	0.003	0.003	0.003
No. of data points	800	800	800	800
Bed configuration	thicker-layer	thicker-layer	thicker-layer	thicker-layer
Vacuum level	4.0e-04	4.0e-04	4.0e-04	4.0e-04
Isopropyl alcohol, %,	100	66	33	0
Drying kinetics exponent, C_1	1.0	1.2	1.0	0.94
Drying kinetics exponent, C_2	0.95	0.40	0.20	0.55
Drying kinetics exponent, C_3	2.1	2.2	2.0	1.9

Appendix D

OPERATING INSTRUCTIONS FOR NEW DRYING KINETICS APPARATUS

D.1 OPERATING INSTRUCTIONS

Proper guidelines are imperative for correct operation of this apparatus and **must be fully understood before start-up procedures begin.** As a number of operations are possible for this apparatus, each operating procedure is dealt with separately. The modes of operation are given in Table D.1.

Table D.1 Types of sample sizes and geometries that can be dried in the new apparatus

Conditions	Sample section	Sample size (g)	Operating method
Through-flow	1	Single particle	1
	1	1-4 layers, d_p=50 mm	2
	1	1-4 layers , d_p=100 mm	3
Vacua	1	Single particle	4
	1	1-4 layers , d_p=50	5
	2	1- 4 layers	6
	2	Particle bed (> 4 layers)	7

D.1.1 Important points to note before proceeding to respective operating method

- The room was originally built to provide a safe radiochemical enclosure at ground floor level. It has windowless concrete lined walls and contains a permanently operating extraction fan in the opposite corner of the room. Thus, a safe stable environment is provided for this apparatus.
- The important sections of the apparatus are powered through a main trip switch so that, in the event of power failure, these sections will not return back on line. The remaining sections not powered through this switch are:
  1. computer terminals,
  2. coolant to condensers and dew point cell,

3. glycol recycle,
4. back-out jackets for mass spectrometer (back-out normally performed before experiment) (Temp=90-100 *degC* controlled),
5. section #2 heater (100-120 *degC* controlled), and
6. dew point meter.

- All cables should be in the cable trays provided, and be tied and neatly aligned together. Electrical devices should be in their respective locations.
- Check line diagram and get to know where the respective valves, gauges, heaters, instruments, and the directions of air/liquid flow sections are located.
- Ensure that tables and benches are clean, clear and dry.
- Check to see if the extraction fan is on; if not, turn on.

D.1.2 Sample preparation

A sample needs to be exposed to an air-saturated environment for about 3 weeks in the humidification box with water trays provided: physical measurement laboratory 5, level 2, Denhem block. This should be done at a dry-bulb temperature of about 25-30*degC*(cool enough to prevent weakly physisorbed moisture from desorbing desorb from most solids).

D.1.3 Operating microbalance

Read this procedure carefully and understand the sequence of events.

- **Do not bump the sample housing #1 or the glassware associated with the microbalance.** This glassware is very vulnerable to any movement.
- Using the main sample holder, **no more than 2 grams of sample can be placed on this sample holder** or you will break the hooks on the balance arms (5 gram capacity including sample holder on balance arms).
- Changing the calibration weights on the small balance arm must be done with extreme care. To remove glassware around the small balance arm:
  1. remove rubber band from the hook on the glassware;
  2. carefully heat the joint (with the hair drier for about 20 seconds) between the microbalance and the housing on the small balance arm;
  3. turn the glassware carefully with an unscrewing motion until the glassware is removed. Again calibration weights must be placed on removed from the calibration pan with extreme care.

- Practice placing the sample holder (with or without sample) on the microbalance arm. **Note: this is a very sensitive piece of equipment, you must be extremely careful.** Touch only the bottom of the handle on the base of the sample holder with the tweezers; do not let the tweezers touch the base of the mesh. Once the hook is in the balance arm ring, release the tweezers slowly. Practice putting the holder on-and-off the balance arm until you are comfortable with the operation.

- After the sample holder is on the balance arm replace the bottom section of the glassware (condenser) by bending up the flexible metal tubing connected to it. Carefully slide (**do not put pressure on the upper section of the glassware**) from the side the glassware bottom section until it is aligned with the top glassware section. Check to see that there is enough sealant in the join and that no air bubbles are trapped between the glass surfaces. Get the flexible metal clip specifically designed for this joint and clip the two sections together. Secure each end of the clip together using the nut and bolt provided.

- You will need to put about 2.4 grams of calibration weights on the calibration holder to balance the sample arms for most single particle tests (d_p=2 mm or less). There is 200mg of deviation on the microbalance. For example, if you dry a 2 g sample, then a weight loss of only 10% moisture content is permissible (200 mg is 10% of 2 g).

D.1.4 Operating mass spectrometer

- Through-flow operation of section #1. - **Carefully** connect capillary tubes to base of sample section #1 (Note: you will be using only the smallest capillary from V11). To provide a free flow path for nitrogen gas:

  1. open valves V1, V5, V6, V11, V14, V16, V17.
  2. close valves V2, V3, V4, V7, V8, V9, V10, V12, V13, V15, V18, V19, V20, V21.

  Operating mass spectrometer module for through-flow operation.

  1. Ensure that all electrical devices are in the off position.
  2. Turn on main power trip switch.
  3. Turn on main power controller.
  4. Turn on Penning 8 controller (next to electronic frequency converter).
  5. Turn on E2M2, E2M1.5 and then (not before) turn on DIFF1.

6. Press START on the electronic frequency converter, and wait 2 minutes for the turbomolecular pump to obtain full speed. If the Penning 8 controller does not show vacua formation after 1 minute from turning on the frequency converter, turn off all pumps and make sure that a seal on the mass spectrometer section is made. If a vacuum is shown to be produced, proceed to next step.
7. Wait until the vacuum is below $5*10^{-5}$ *mbar* on the Penning 8 (this may take a while). Open V11 (smallest capillary) and V12. Observe the pressure on the Penning 8. If the pressure remains above $1*10^{-5}$ *mbar*, proceed to next step. If not, there may be a large leak on the capillary extension set; then close V12 and fix the leak before progressing to next step.
8. Turn on power supply to mass spectrometer (and close associated switch).
9. Turn on PC1. The mass spectrometer software will automatically boot up. Note that the mass spectrometer is not yet working. Turn on the power supply unit for the Transpector. For operation of software refer to operation manual #3 (Transpector gas analysis system - operation manual, section 7.3.2.)

- Vacuum operation of section #1. Carefully connect capillary tubes to base of sample section #1. To provide a vacuum at sample section #1:

  1. open valves V11, V12, V14, V16.
  2. close valves V1, V2, V3, V4, V5, V6, V7, V8, V9, V10, V13, V15, V17, V18, V19, V20, V21.

  GO TO operating mass spectrometer module for vacuum operation below.

- Vacuum operation of sample section #2. Carefully connect capillary tubes to base of sample section #2. To provide a vacuum at sample section #2:

  1. open valves V14, V16.
  2. close valves V1, V2, V3, V4, V5, V6, V7, V8, V9, V10, V11, V12, V13, V15, V17, V18, V19, V20, V21.

  GO TO operating mass spectrometer module for vacuum operation below.

- Operating mass spectrometer module for vacuum operation: - carefully place sample in respective sample section and seal section.

  1. Ensure that all electrical devices are in the off position.
  2. Turn on main power trip switch.
  3. Turn on main power controller.

4. Turn on Penning 8 controller (next to electronic frequency converter).
5. Turn on E2M2, E2M1.5 and then (not before) turn on DIFF1.
6. Press START on the electronic frequency converter, and wait 2 minutes for the turbomolecular pump to obtain full speed. If the Penning 8 controller does not show vacua formation after 1 minute from turning on the frequency converter, turn off all pumps and make sure that a seal on the mass spectrometer section is made. If a vacuum is shown to be produced, proceed to next step.
7. Wait until the vacuum is below $5*10^{-5}$ *mbar* on the Penning 8 (this may take a while). Open V12, then proceed to open either V9, V10 or V11 depending on system vacuum. Open V11 (smallest capillary) if the pressure on Pirani Penning 1005 is between 100 and 1000 *mbar* or open V9 if pressure is between 10 and 100 *mbar* or open V10 if pressure is between 1-10 mbar. As a greater vacuum is produced, you may need to open and close V9, V10 or V11. Observe the pressure on the Penning 8. If the pressure remains above $1*10^{-5}$ *mbar*, proceed to next step. If not, there may be a large leak on the capillary extension set; then close V12 and fix the leak before progressing to next step.
8. Turn on power supply to mass spectrometer (and close associated switch).
9. Turn on PC1. The mass spectrometer software will automatically boot up. Note that the mass spectrometer is not yet working. Turn on the power supply unit for the Transpector. For operation of software refer to operation manual #3 (Transpector gas analysis system - operation manual, section 7.3.2.)

D.1.5 Operating Dew-All 911

1. Set up auxiliary cooling to dew cell if determination of low humidities is required.
2. Turn power on.
3. Press dew point button.
4. Let dew point stabilise.
5. Record dew point (in Celsius) in thermocouple software program.

D.1.6 Thermocouple data acquisition program

The program will automatically boot up when the computer is switched on. Alternatively, the program can be restarted from DOS by loading CONTROL.BAS in the QBASIC environment. You will be asked to load a saved thermocouple configuration:

type $< N >$ to input new parameters or $< Y >$ to retrieve old settings (i.e. type "config1.cfg") and go to step 8. To customise new settings, type $< N >$.

1. Enter channel to be read: type $< 1 >, < 2 >$, ...,or$< 15 >< ENTER >$.
2. Input gain values: type $< 0.5 >, < 1 >, ..., < 1000 >$. Normal value is a gain of "50" $< ENTER >$.
3. Enter further channels: if you want to record other channels from 1-15, type $< Y >< ENTER >$ and go to step 1. Repeat until no further channels are required, type $< N >$ if you do not want to record further channels.
4. Enter number of readings to be taken: type $< 1 >, ..., < 9999 >< ENTER >$. For long drying tests, you will need a large number.
5. Enter timer interval between readings in seconds: type $< 1 >, ..., < 100 >< ENTER >$. Again for long drying times, choose a longer interval. Remember that there are 86400 seconds in a day.
6. Save data to disk file?: type $< N >$ for test runs or $< Y >$ for actual experiments (save as *.dat files).
7. Save this configuration to disk: type $< N >$ to use existing configurations or $< Y >$ to save settings made in steps 1-5 (save as *.cfg files).
8. Any alterations to be made?: type $< N >$ to accept input data from steps 1-5 or $< Y >$ to alter some settings from steps 1-5.

D.1.7 Microbalance initialisation routine

Check zero and calibrate?: Type $< Y >$ to check balance position.

1. Microbalance zero offset adjustment sequence. Ensure that the balance is stable and then press any key: type <> (any key).
2. Balance zero offset = -864000 to 864000 (given)
3. You want the balance zero offset to be slightly more positive (heavier on sample balance arm) than negative, because the sample to be dried will lose weight on drying. Make the balance zero offset more negative if the particle is large or if it has a high critical moisture content.
4. Do you wish to adjust the balance: type $< Y >$ to make adjustment (place or remove some calibration weights depending on what is required from part (3). Make adjustment then press any key. Continue to make adjustments and until you are happy with the balance offset. Enter calibration weight in grams:

$< 1 >, ..., < 10 >< ENTER >$. Enter value for running mean (1-255): type $< 1 >, ..., < 255 >$ $(normal 50)$ $< ENTER >$. Save data to disk file: type $< Y >$or$< N >$. Calibrate again?: type $< N >$ to accept calibration or $< Y >$ to change calibration and return.

Type $< N >$ if satisfied with balance position. Save data to disk file?: type $< N >$ for test runs or $< Y >$ for actual experiments (save as *.dat files). Table D.2 shows the outputs to the computer screen.

Table D.2 Description of outputs from QBASIC programme

Reading	Channel	Temp. *degC* channel 0-7	Pressure mbar channel 8-11	Microbal. channel 12
1	0 (dew-point cell)			
2	1 (thermocouple)			
...	... (thermocouple)			
8	7 (thermocouple)			
9	8 (pressure gauge)			
...	...(pressure gauge)			
12	11 (pressure gauge)			
13	12 (microbalance)			
14	13 (spare channel)			
...				
16	15 (spare channel)			

The reading indicates the number of progressive readings taken during experimental runs.

When you are comfortable with the above methods, start-up may begin.

D.2 OPERATING PROCEDURES FOR DRYING SAMPLES

D.2.1 Operating procedure number 1 for drying of a single particle under a through-flow in sample section #1

D.2.1.1 Hardware configuration

To provide a free flow path for nitrogen gas:

1. open valves V1, V5, V6, V11, V16, V17.
2. close valves V2, V4, V7, V8, V9, V10, V18, V19.

D.2.1.2 Software, instrumentation configuration

1. Ensure that all electrical devices are in the off position.
2. Turn on main power trip switch.

3. Turn on main power controller.
4. Turn on microprocessor & power supply unit (for microbalance).
5. Turn on PC#1 (refer mass spectrometer hardware and software operation) and PC#2.
6. The thermocouple/microbalance data acquisition program should be displayed, if not, reboot the computer.
7. Follow operating instructions, sections D and E.

D.2.1.3 Sample insertion

1. When the apparatus is stable and the software is running smoothly, remove base of sample section #1 and place particle at the centre of the sample pan.
2. Quickly but carefully replace base glass section.

D.2.2 Operating procedure number 2 for drying of layer/s (d_p) under a through-flow in sample section #1

D.2.2.1 Hardware configuration

To provide a free flow path for nitrogen gas:

1. pen valves V1, V5, V6, V11, V16, V17
2. close valves V2, V4, V7, V8, V9, V10, V18, V19.

D.2.2.2 Software, instrumentation configuration

1. Ensure that all electrical devices are in the off position.
2. Turn on main power trip switch.
3. Turn on main power controller.
4. Turn on microprocessor and power supply unit (for microbalance).
5. Turn on PC#1 (refer mass spectrometer hardware and software operation) and PC#2.
6. The thermocouple/microbalance data acquisition program should be displayed, if not, reboot the computer. Follow operating instructions, sections D and E.

D.2.2.3 Sample insertion

When the apparatus is stable and the software is running smoothly, remove base of sample section #1 and sample pan. Place particle layer/s over the sample pan. Quickly but carefully replace sample pan with sample layers and replace base glass section.

D.2.3 Operating procedure number 3 for drying of layer/s (d_p=100) under a through-flow in sample section #1

D.2.3.1 Hardware configuration

To provide a free flow path for nitrogen gas:

1. open valves V1, V5, V6, V11, V16, V17.
2. close valves V2, V4, V7, V8, V9, V10, V18, V19.

D.2.3.2 Software, instrumentation configuration

1. Ensure that all electrical devices are in the off position.
2. Turn on main power trip switch.
3. Turn on main power controller.
4. Turn on microprocessor and power supply unit (for microbalance, although it will not be used here).
5. Turn on PC#1 (refer mass spectrometer hardware and software operation) and PC#2.
6. The thermocouple/microbalance data acquisition program should be displayed, if not, reboot the computer. Follow operating instructions, sections D and E.

D.2.3.3 Sample insertion

1. When the apparatus is stable and the software is running smoothly, remove base of sample section #1 and sample pan. Place particle layer/s over the larger sample mesh pan provided.
2. Quickly but carefully replace large sample pan with sample layers inside the base sample section and close the flow path.

D.2.4 Operating procedure number 4 for drying of a single particle under a vacuum in sample section #1

D.2.4.1 Hardware configuration

To provide a vacuum chamber in sample section #1:

1. open valves V11, V12, V14, V16.

2. close valves V1, V2, V3, V4, V5, V6, V7, V8, V9, V10, V13, V15, V17, V18, V19, V20, V21.

D.2.4.2 Software, instrumentation configuration

1. Ensure that all electrical devices are in the off position.

2. Turn on main power trip switch.

3. Turn on main power controller.

4. Turn on microprocessor and power supply unit (for microbalance, although it will not be used here).

5. Turn on PC#1 (refer mass spectrometer hardware and software operation) and PC#2

6. The thermocouple/microbalance data acquisition program should be displayed, if not, reboot the computer. Follow operating instructions, sections D and E.

D.2.4.3 Sample insertion

1. When the apparatus is vacuum tight (can achieve $< 10^{-5}$ vacuum) and the software is running smoothly, release nitrogen gas into the chamber through V22 (then close V22), remove base of sample section #1 and sample pan. Place particle in the sample pan provided.

2. Quickly but carefully replace large sample pan with sample inside the base sample section and close the flow path.

3. Turn on vacuum.

4. Follow vacuum operation procedure for sample section #1.

D.2.5 Operating procedure number 5 for drying of a particle layer under a vacuum in sample section #1

D.2.5.1 Hardware configuration

To provide a vacuum chamber in sample section #1:

1. open valves V11, V12, V14, V16.
2. close valves V1, V2, V3, V4, V5, V6, V7, V8, V9, V10, V13, V15, V17, V18, V19, V20, V21

D.2.5.2 Software, instrumentation configuration

1. Ensure that all electrical devices are in the off position.
2. Turn on main power trip switch.
3. Turn on main power controller.
4. Turn on microprocessor and power supply unit (for microbalance, although it will not be used here).
5. Turn on PC#1 (refer mass spectrometer hardware and software operation) and PC#2.
6. The thermocouple/microbalance data acquisition program should be displayed; if not, reboot the computer. Follow operating instructions, sections D and E.

D.2.5.3 Sample insertion

1. When the apparatus is vacuum tight (can achieve $< 10^{-5}$ vacuum) and the software is running smoothly, release nitrogen gas into the chamber through V22 (then close V22),, remove base of sample section #1 and sample pan. Place particle layer in the sample pan provided.
2. Quickly but carefully replace large sample pan with sample layers inside the base sample section and close the flow path.
3. Turn on vacua.
4. Follow vacuum operation procedure for sample section #1.

D.2.6 Operating procedure number 6 for drying of particle layer/s (1-4 layers) under a vacuum in sample section #2

D.2.6.1 Hardware configuration

To provide a vacuum chamber in sample section # 2:

1. open valves V8, V14, V16;
2. close valves V1, V2, V3, V4, V5, V6, V7, V9, V10, V11, V12, V13, V15, V17, V18, V19, V20, V21.

D.2.6.2 Software, instrumentation configuration

1. Ensure that all electrical devices are in the off position
2. Turn on main power trip switch
3. Turn on main power controller
4. Turn on microprocessor and power supply unit (for microbalance, although it will not be used here)
5. Turn on PC#1 (refer mass spectrometer hardware and software operation) and PC#2
6. The thermocouple/microbalance data acquisition program should be displayed; if not, reboot the computer.
7. Follow operating instructions, sections D and E.

D.2.6.3 Sample insertion

1. When the apparatus (sample section #2) is vacuum tight (can achieve $< 10^{-5}$ vacuum) and the software is running smoothly, release nitrogen gas into the chamber through V22 (then close V22), remove lid off sample section #2. Place particle layers in the sample section #2.
2. Quickly but carefully replace section #2 lid and close the flow path.
3. Turn on vacuum.
4. Follow vacuum operation procedure for sample section #1.

D.2.7 Operating procedure number 7 for drying of particle bed (<4 layers) under a vacuum in sample section #2

D.2.7.1 Hardware configuration

To provide a vacuum chamber in sample section #2:

1. open valves V8, V14, V16;
2. close valves V1, V2, V3, V4, V5, V6, V7, V9, V10, V11, V12, V13, V15, V17, V18, V19, V20, V21.

D.2.7.2 Software, instrumentation configuration

1. Ensure that all electrical devices are in the off position.
2. Turn on main power trip switch.
3. Turn on main power controller.
4. Turn on microprocessor and power supply unit (for microbalance, although it will not be used here).
5. Turn on PC#1 (refer mass spectrometer hardware and software operation) and PC#2.
6. The thermocouple/microbalance data acquisition program should be displayed; if not, reboot the computer.
7. Follow operating instructions, sections D and E.

D.2.7.3 Sample insertion

1. When the apparatus (sample section #2) is vacuum tight (can achieve $< 10^{-5}$ vacuum) and the software is running smoothly, release nitrogen gas into the chamber through V22 (then close V22), remove lid off sample section #2. Place particle bed evenly in the sample section #2.
2. Quickly but carefully replace section #2 lid and close the flow path.
3. Turn on vacuum.
4. Follow vacuum operation procedure for sample section #1.

Appendix E

MOISTURE EQUILIBRIUM CHARACTERISTICS OF MATERIALS

E.1 SILICA GEL

Maximum hygroscopic moisture content=0.3 *kg water/kg wet solid.* Monolayer saturation, X_m = 0.11-0.135 *kg water/kg wet solid.*

The estimation of the condition for the apparently complete covering by a monolayer is difficult because a material dries in a "patchy" manner at the pore surface, except in those cases where the structure is highly ordered (e.g. zeolites, some activated carbons).

Because isotherms were performed at temperatures well below the temperature required to condense the active silica gel surface (100*degC*-120*degC*), it was assumed that most of the loss in weight during the desorption process was physisorbed water. Isotherms of silica gel indicate Henry-type behaviour (linear desorption) in the lower regions of monolayer loading. In this monolayer region, ten experimental points were plotted and fitted using a least sum of squares method. Fitting this linear region to Freundlich and Radke/Prausnitz correlations indicated a more homogeneous active pore surface than that predicted by the Langmuir-fitting calculations. However, there is some non-uniformity in active sites on the silica gel surface which may be a result of its microporous topology; for example, microporous obstructions (pore necking) in the solid may disable some low-moisture desorption.

Isotherms were fitted with known isotherm equations and correlations over higher moisture content ranges. A modified BET equation gave the best fit to the multilayer loading of moisture between relative humidities of 20-80% (1-r^2, 0.0065 (45*degC*), 0.0045 (65*degC*), 0.0032 (80*degC*)). The best empirical fits to this multilayer region were: SPS (1-r^2, 0.0048 (45*degC*), 0.0049 (65*degC*), 0.0048 (80*degC*)), Henderson (1-r^2, 0.0062 (45*degC*), 0.0067 (65*degC*), 0.0059 (80*degC*)), and Luikov (1-r^2, 0.011 (45*degC*), 0.010 (65*degC*), 0.0094 (80*degC*)). The general adsorption/desorption isotherms showed that the silica gel sample had an IUPAC type H2 hysteresis loop which is typical of a *type B* silica gel material. This made the fitting of the isotherm equations difficult over

20-80% relative humidity. Other empirical-based correlations indicate that silica gel has a restriction on the number of sorbed layers, which is understandable given the non-swelling nature of the material. Also, at these sorptive temperatures, there is not an increase in the number of active sites during sorption of moisture.

Surface area calculations from using single point BET (nitrogen sorption), geometries of particles, sorptive activity and cross-sectional areas of water compared with nitrogen showed that there is 170 000 times the internal surface area in the silica gel particles when compared with the external surface area. Results from nitrogen sorption tests gave the internal surface area to equal $450 m^2 g^{-1}$. This helped determine that 2.7 times the adsorbed moisture in the particle was not directly bound to the pores. Thus the average pore size would allow 5 water molecules to span them.

Most of the desorption of the water is performed below 40-50% relative humidity at dry-bulb temperatures of below $65 degC$. Drying between the relative humidities of 10-40% indicates a linear desorption profile of approximately 43% of the total moisture. This is consistent with a linear progression in heat of wetting over this region of between 0 and $1500 kJ\, kg^{-1}$ *dry solid*. Below 10% moisture content, a steeper desorption profile was evident for all the isotherm temperatures that were investigated. This gave a steeper heat of wetting range of between 1500 and $5000 kJ\, kg^{-1}$ *dry solid* below 10% moisture content

It has been shown that the transition of drying between physisorbed and chemisorbed moisture on the silica gel surface is non-ideal; for example, the surface dries in a "patchy" manner. This non-ideality may help describe the gradual change of slope in the isotherms around the 10% moisture content level. Active silica gel surface "modifies" or creates an ordered alignment of the generally irregular layered moisture held above the pore surface (Anderson and Wickersheim, 1964). Condensing all of the silica gel's surface by heating it to $1000 degC$ resulted in removing a further 0.057 *kg water/kg dry solid*, indicating an overall moisture content of physisorbed and chemisorbed moisture of 0.39 *kg water/kg "dry solid"*.

E.2 ALUMINA

Maximum hygroscopic moisture content = 0.004-0.005 *kg water/kg wet solid*. Monolayer saturation, X_m = 0.002-0.0022 *kg water/kg wet solid*.

No evidence of hysteresis was apparent during the progression of plotting the adsorption and desorption isotherms for alumina. This isotherm shows a typical shape of a microporous solid with a non-active surface. For example, the maximum hygroscopic moisture content is below 1%, a characteristic linear isotherm is present for multilayer loading, which can be described by unstructured water clustering, and, at low relative humidity regions, a steeper sorption isotherm is observed, indicating the sorption of a monolayer.

Moisture is physisorbed to the microporous structure in non-active alumina, with no chemical evidence of any condensed moisture being present. These very low monolayer loadings (0-0.2% moisture content) gave a high heat of wetting of 2300-2600$kJ\ kg^{-1}$. Isotherms of non-active alumina indicated Henry-type behaviour (linear desorption) in the lower regions of monolayer loading. In this monolayer region, nine experimental points were plotted and fitted using a least sum of squares method. Fitting this linear region to a Freundlich correlation appeared to fit well, but including a Henry-type parameter to the Freundlich equation did not improve the fitting. Thus, the alumina microporous surface is heterogeneous without any interactions evident between adsorbed water.

Multilayer loading equations and correlations were used to fit sorption isotherms for alumina over the entire moisture content range. A modified BET equation again gave the best fit to the multilayer loading of moisture between relative humidities of 20-80% (1-r^2, 8.6E-07 (45$degC$), 7E-07 (65$degC$), 7.3E-07 (80$degC$)). The best empirical fits to this multilayer region were: SPS (1-r^2, 9.9E-07 (45$degC$), 1.1E-06 (65$degC$), 5.3E-07 (80$degC$)), Henderson (1-r^2, 2.3E-06 (45$degC$), 1.1E-06 (65$degC$), 9.2 E-07 (80$degC$)), and Luikov (1-r^2, 2.4E-06 (45$degC$), 1.7E-06 (65$degC$), 1.7E-06 (80$degC$)). Other empirical-based correlations indicate that alumina has a restriction on the number of sorbed layers, which is understandable given the non-swelling nature of the material. Also, at these sorptive temperatures, there is not an increase in the number of active sites during sorption of moisture.

Surface area calculations showed that there is 240 times the internal surface area in the non-active alumina particles when compared with the external surface area. Results from nitrogen sorption tests gave the internal surface area to equal $75 m^2 g^{-1}$. This helped determine that 0.3 times the adsorbed moisture in the particle was not directly bound to the pore surface, which is consistent with the monolayer loading from the water sorption isotherms. The rigidity of the alumina matrix prevents particle swelling.

Exactly half of the desorbed moisture in the isotherm can be attributed to the directly bound physisorbed moisture in a monolayer. The desorption of this bound moisture is performed below 10% relative humidity at 45$degC$ and below 40% relative humidity at 80 $degC$. Below this moisture content range, a stable desorption profile is shown form all the isotherm temperatures that were investigated. This gave a stable heat of wetting of between 2300-2600 $kJ\ kg^{-1}$. A steeper progression in heat of wetting over higher moisture contents (between 0.2% and 0.4%) was observed at 0-2300 $kJ\ kg^{-1}$ wet solid.

E.3 IRON SAND

Maximum hygroscopic moisture content = 0.0028-0.003 *kg water/kg wet solid.* Monolayer saturation, X_m = 0.0023-0.0025*kg water/kg wet solid.*

This isotherm is similar to that of non-active alumina and shows a typical shape of a microporous solid with a non-active surface. For example, the maximum hygroscopic moisture content is below 1%, a characteristic linear isotherm is present for multilayer loading, which can be described by unstructured water clustering, and, at low relative humidity regions, a steeper sorption isotherm is observed, indicating the sorption of a monolayer.

Moisture is physisorbed to the microporous structure in non-active iron sand, with no chemical evidence of any condensed moisture being present. These very low monolayer loadings (0-0.2% moisture content) gave a high heat of wetting of 2300-2600$kJ\ kg^{-1}$. Isotherms of non-active iron sand indicated Henry-type behaviour (linear desorption) in the lower regions of monolayer loading. In this monolayer region, nine experimental points were plotted and fitted using a least sum of squares method. Fitting this linear region to a Freundlich correlation appeared to fit well, but including a Henry-type parameter to the Freundlich equation did not improve the fitting. Thus, the iron sand microporous surface is heterogeneous without any interactions evident between adsorbed water.

Multilayer loading equations and correlations were used to fit sorption isotherms were fitted for *degC* over the entire moisture content range. A modified BET equation again gave the best fit to the multilayer loading of moisture between relative humidities of 20-80% (1-r^2, 8.6E-07 (45*degC*), 7E-07 (65*degC*), 7.3E-07 (80*degC*)). The best empirical fits to this multilayer region were: SPS (1-r^2, 9.9E-07 (45*degC*), 1.1E-06 (65*degC*), 5.3E-07 (80*degC*)), Henderson (1-r^2, 2.3E-06 (45*degC*), 1.1E-06 (65*degC*), 9.2E-07 (80*degC*)), and Luikov (1-r^2, 2.4E-06 (45*degC*), 1.7E-06 (65*degC*), 1.7E-06 (80*degC*)). Other empirical-based correlations indicate that iron sand has a restriction on the number of sorbed layers, which is understandable given the non-swelling nature of the material. Also, at these sorptive temperatures, there is not an increase in the number of active sites during sorption of moisture.

Results from nitrogen sorption tests gave the internal surface area to equal 29 m^2g^{-1}. From sorption and surface area calculations, there is 7 times the internal surface area in the sand particles when compared with to the external surface area. This helped determine that 0.8 times the adsorbed moisture in the particle was not directly bound to the pore surface, which is consistent with the monolayer loading from the water sorption isotherms. Note with the rigidity of the iron sand matrix prevents particle swelling.

Exactly half of the desorbed moisture in the isotherm can be attributed to the directly bound physisorbed moisture in a monolayer. The desorption of this bound

moisture is performed below 10% relative humidity at $45 degC$ and below 40% relative humidity at $80 degC$. Below this moisture content range, a stable desorption profile is shown form all the isotherm temperatures that were investigated. This gave a stable heat of wetting of between 2300-2600kJ/kg. A steeper progression in heat of wetting over higher moisture contents (between 0.2% and 0.4%) was observed at 0-2300$kJ\ kg^{-1}$ *wet solid.*

E.4 ADIPIC ACID

Maximum hygroscopic moisture content = 0.07-0.08 *kg water/kg wet solid.* Monolayer saturation, X_m = 0.06-0.065 *kg water/kg wet solid.*

Hysteresis again was not apparent during the progression of plotting the adsorption and desorption isotherms for adipic acid. The shape of this isotherm is a variation of a *type I* isotherm. However, the extreme convex-upward shape indicates the strong affinity between the sorbed water and the active carboxyl end groups of the adipic acid molecules. The chemistry of the rehydration of the adipic acid end groups is described in the Chapter 6, and is the reason for this strong affinity of dry adipic acid for water. This isotherm shows a typical shape of a microporous solid with a hydrating surface. Condensing the adipic acid monomers to polymer forms takes place at low relative humidities regions. The steeper sorption isotherm at low humidities is observed indicates the sorption of a monolayer. The linear sorption behaviour at relative humidities above 20% shows further swelling of the lattice due to free water clustering on the existing water monolayer in the adipic acid particles.

At these monolayer loadings (0-6.3% moisture content) a high heat of wetting of 2200-3200 $kJ\ kg^{-1}$ was observed. Monolayer loading appears to fit a Langmuir correlation well, indicating that desorption in this region can assume first-order kinetics. The results also indicate that the adipic acid surface is uniform without any interactions between adsorbed water molecules. In this monolayer region, 15 experimental points were plotted and fitted using a least sum of squares method. Fitting this linear region to a Freundlich correlation appeared to fit well, and including a Henry-type parameter to the Freundlich equation did improve the fitting. Thus, the adipic acid surface is uniform without any interactions evident between adsorbed water molecules.

Multilayer loading equations and correlations were used to fit sorption isotherms for adipic acid over the entire moisture content range. A modified BET equation again gave the best fit to the multilayer loading of moisture between relative humidities of 0-80% (1-r^2, 0.00063 ($45 degC$), 0.00081 ($65 degC$), 0.00104 ($80 degC$). The best empirical fist to this multilayer region were: Schuchmann et al. (1-r^2, 0.00063 ($45 degC$), 0.00081 ($65 degC$), 0.00102 ($80 degC$)), SPS (1-r^2, 0.0051 ($45 degC$), 0.0040 ($65 degC$), 0.0032 ($80 degC$)), and Henderson (1-r^2, 0.0062 ($45 degC$), 0.0056 ($65 degC$), 0.0038 ($80 degC$)). Other empirical-based correlations indicate that adipic acid has a

restriction on the number of sorbed layers limiting the swelling nature of the material. Mainly there are uniform surface forces throughout the particles at $45 degC$ and $65 degC$, but, at higher temperatures, $80 degC$, a non-uniform surface is apparent. Also at these sorptive temperatures, there is not an increase in the number of active sites during sorption of moisture.

Surface area calculations showed that there is 13 times the internal surface area in the adipic acid particles when compared with the external surface area. Results from nitrogen sorption tests gave the internal surface area to equal $1.02 m^2 g^{-1}$. This helped determine that 281 times the adsorbed moisture in the particle was not directly bound to the pore surface, which is inconsistent with the monolayer loading from the water sorption isotherms. For non-swelling solids, 281 times the adsorption would take place above the monolayer. However, from sorption isotherms, 90-95% of adsorbed moisture was bound. Thus there should be 5-10% of sorbed moisture held above the monolayer. This inconsistency indicates that the adipic acid particles swell during the adsorption of water, exposing more polymer sections to be hydrated during adsorption.

Ninety-five percent of the desorbed moisture in the isotherm can be attributed to the directly bound chemisorbed moisture in an equivalent monolayer. The desorption of this bound moisture is performed below 10% relative humidity at $45 degC$ and below 40% relative humidity at $80 degC$. Below this moisture content range, a stable desorption profile was shown for all the isotherm temperatures that were investigated. This gave a changing heat of wetting of between 2200-3200 $kJ\ kg^{-1}$. A steeper initial progression in the heat of wetting over higher moisture contents (between 6.3% and 6.5%) was observed at 0-2200 $kJ\ kg^{-1}$ *wet solid*.

Fine organic chemicals similar to adipic acid have a high vapour pressure compared with other drying solids. This frustrates many attempts to dry these materials while minimising the breakdown of the drying solid. As a result of this problem, there is an active research interest into drying these types of fine chemicals. This work attempted to provide first empirical-based drying data on materials such as adipic acid, for example drying kinetics data, and then an understanding of the kinetics that would result in optimising drier performance.

Obviously the time to establish equilibrium for adipic acid and hydroquinone is significantly longer than for liquids such as water, which has been used to compare the vapour pressures.

In the drying rate curves of adipic acid, the weight loss of solid was shown by a final linear line (Figure E.1) after the moisture had been removed.

As the drying experiments were performed under constant temperature conditions, the linear appearance of the solid weight loss curve was extracted back to zero drying time. This was checked by monitoring the fragmentation of adipic acid using a mass spectrometer. The degree of dehydration of the lattice of the monomer units to the

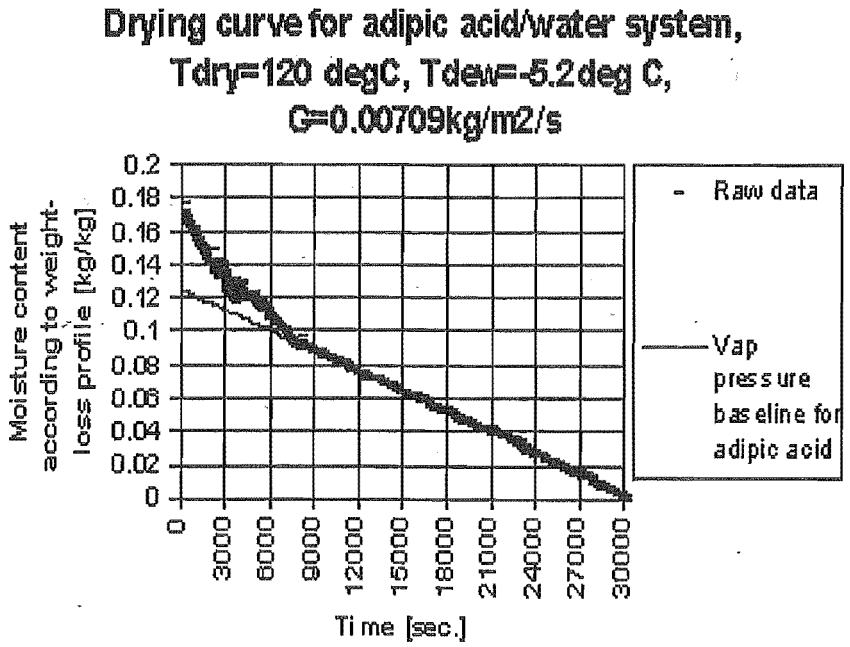

Figure E.1 Drying of a 1% adipic acid sample

polymorphic units was constant over the drying period. This made it then accurate to calculate the drying profile of water in adipic acid. Recalculation of the drying rate profile of water in adipic acid showed an initial moisture content of 1%. This initial moisture content was lower than that normally expected from monolayer saturation (7-15%); however, adipic acid can fully resist hydration of its monolayer in its stable polymorphic state. The degree of rehydration of this polymorphic state, over a period of 24 hours, showed a maximum hygroscopic moisture content of only 1% because the adipic acid sample was hydrated at a relative humidity of only 30%. The moisture isotherm of adipic acid showed a maximum hygroscopic moisture content of 7% after a four-week period of getting data to plot the adsorption isotherm over the entire relative humidity scale.

The final appearance of the dried adipic acid differed between the 1% and 7% initial moisture contents. The 1% sample first appeared as a white powder before drying and still resembled a white powder after drying. However, the final appearance of the 7% initial moisture content powder was transparent/white crystals. This is indicative of a change in chemistry during drying of the 7% sample. Dehydration of the 7% sample forced a polymorphic state from the condensed monomer units of adipic acid.

The drying rate curve of 1% initial moisture content adipic acid showed that constant drying rate period was observed over the first 1000 seconds of the 6000 second drying period. The falling-rate period began at a moisture content of 0.4%. The

characteristic drying curve of adipic acid appeared to be linear under these conditions (Figure E.1).

Adipic acid was a very difficult material to dry, which is typical of most dicarboxylic acids. The material itself has a high relative vapour pressure compared with most other particulates. The removal of physisorbed moisture from this material is relatively easy. However, the removal of chemisorbed moisture poses problems because the material also evaporates. This was evident from the increase in the 42 *amu* signal on the mass spectrometer, which is part of the fragmentation pattern emitted from the volatile adipic acid material. Fortunately, the required dried product does not require the removal of the chemisorbed moisture so the drying of adipic acid should have short residence times in an industrial drier to minimise solid losses. I found that drying adipic acid at T_{dry}=120 *degC* was sufficient and that the particle residence time could be determined from the type of drier, heat transfer and different bed configurations. Typically adipic acid is required in very large quantities for the production of nylon-6-6, so vacuum or batch drying is impractical; therefore I worked mainly on through-flow drying experiments. Removing the chemisorbed moisture from adipic acid resulted in a polymorphic adipic acid. Long needle shaped crystals were formed after extreme drying. However, a significant loss of adipic acid monomer was recorded during this extreme drying process.

E.5 PURE TEREPHTHALIC ACID

Maximum hygroscopic moisture content = 0.006-0.007*kg water/kg wet solid.* Monolayer saturation, X_m = 0.004 *kg water/kg wet solid.*

Pure terephthalic acid sorption isotherm has *type II* characteristics by showing a typical shape of a microporous solid with an active surface. For example, the maximum hygroscopic moisture content is below 1%, a characteristic linear isotherm is present for multilayer loading, which can be described by unstructured water clustering, and at low relative humidity regions, a steeper sorption isotherm is observed, indicating the sorption of a monolayer.

During an adsorption process from a dry solid, water diffuses into the particle and individual water molecules are physisorbed to the hydrophilic hydroxyl end groups of the monomer units, thus forcing an initial swelling of the particles as more hygroscopic end groups become exposed by the swelling. Around 55-60% of sorbed moisture is directly bound to the active hydroxyl end groups, with the remaining moisture held as free water in clusters surrounding this physisorbed moisture. No chemical evidence of any condensed moisture is possible in pure terephthalic acid. These very low monolayer loadings (0-0.4% moisture content) gave a high heat of wetting of 1800-2000 $kJ\ kg^{-1}$, and was stable for most sorption in the monolayer. Isotherms of pure terephthalic acid indicated Henry-type behaviour (linear desorption) in the lower regions of monolayer

loading. In this monolayer region, 11 experimental points were plotted and fitted using a least sum of squares method. Fitting this linear region to a Freundlich correlation appeared to fit well, but including a Henry-type parameter to the Freundlich equation improved the fitting. Thus, the alumina microporous surface is heterogeneous without any interactions evident between physisorbed water in the monolayer.

Multilayer loading equations and correlations were used to fit sorption isotherms for terephthalic acid over the entire moisture content range. A modified BET equation again gave the best fit to the multilayer loading of moisture between relative humidities of 0-85% (1-r^2, 3E-06 (45*degC*), 3.6E-06 (65*degC*), 2.9E-06 (80*degC*)). The best empirical fit to this multilayer region were: Schuchmann et al. (1-r^2, 3.1E-06 (45*degC*), 3.2E-06 (65*degC*), 3E-06 (80*degC*)), SPS (1-r^2, 1.3E-05 (45*degC*), 1.3E-05 (65*degC*), 1.1E-05 (80*degC*)), and Henderson (1-r^2, 1.5E-05 (45*degC*), 1.8E-05 (65*degC*), 1.5E-05 (80*degC*)). Other empirical-based correlations indicate that pure terephthalic acid has a restriction on the number of sorbed layers limiting the swelling nature of the material. Mainly there are uniform surface forces throughout the particles at 45*degC* and 65*degC*, but, at higher temperatures, 80*degC*, a non-uniform surface is apparent.

Surface area calculations showed that there is 6 times the internal surface area in the pure terephthalic acid particles when compared with the external surface area. Results from nitrogen sorption tests gave the internal surface area to equal $0.21 m^2 g^{-1}$. This helped determine that 109 times the adsorbed moisture in the particle was not directly bound to the pore surface, which is inconsistent with the monolayer loading from the water sorption isotherms. For non-swelling solids, 109 times the adsorption would take place above the monolayer. However, from sorption isotherms, 55-60% of adsorbed moisture was bound. Thus there should be 40-45% of sorbed moisture held above the monolayer. This inconsistency indicates that the pure terephthalic acid particles swell during the adsorption of water, exposing more polymer sections to be hydrated during adsorption.

Fifty-five to sixty percent of the desorbed moisture in the isotherm can be attributed to the directly bound physisorbed moisture in a monolayer. The desorption of this bound moisture is performed below 10% relative humidity at 45*degC* and below 30% relative humidity at 80*degC*. Below this moisture content range, a stable desorption profile was shown for all the isotherm temperatures that were investigated. This gave a stable heat of wetting of between 1800 and $2000 kJ\ kg^{-1}$. A steeper progression in the heat of wetting over higher moisture contents (between 0.4% and 0.6%) was observed at 0-1800 $kJ\ kg^{-1}$ *wet solid*.

E.6 NON-DRIED TEREPHTHALIC ACID

Maximum hygroscopic moisture content = 0.013 *kg water/kg wet solid*. Monolayer saturation, X_m = 0.004-0.005 *kg water/kg wet solid*.

Non-dried terephthalic acid gave the same sort of sorption isotherm as the pure form. Again this shows type II characteristics by showing a typical shape of a microporous solid with an active surface. However, the only exception to the pure form was during the initial desorption isotherm at $45 deg C$; a higher hygroscopic moisture content was observed due to the organic solvents present in this pre-dried form. Favourable sorption of non-aqueous polar solvents was evident and resulted in swelling of the terephthalic matrix.

The same characteristics of sorption were found for the pre-dried form of terephthalic acid.

E.7 POLYSTYRENE-BUTADIENE COPOLYMER I

Maximum hygroscopic moisture content = 0.012-0.0013 *kg water/kg wet solid.* Monolayer saturation, X_m = 0.007-0.008 *kg water/kg wet solid.*

Copolymer I shows a sorption isotherm of *type II* characteristics. The highly non-spherical shape of the particle with a large shape factor causes excessive sorption of water around the exposed nucleophilic sections on the copolymer chains. The increase in surface area as a result of the small particle diameters observed made large monolayer sorption at the surface possible. Of the three copolymer I investigated experienced the highest attainable moisture content as a result of the larger external surface area. Long exposure of copolyjmer I to 50-80% relative humidity at $45 deg C$ gave evidence of water diffusing partially into the external surfaces of the particles. This partial diffusion resulted in the water molecules forming water clusters around existing adsorbed water molecules, increasing the moisture content from 0.7% to 0.11%. Partial swelling of the external surface regions may result from the appearance of water clustering. No chemical evidence of any condensed moisture is possible in copolymer I, only individual water molecules are physisorbed to nucleophilic sites along the exposed section of polymer chains. These very low monolayer loadings (0-0.7% moisture content) gave a gradual increase in heat of wetting of between 500 and $1500 kJ\ kg^{-1}$. The water clustering showed a much lower heat of wetting of between 0 and $500 kJ\ kg^{-1}$.

The general adsorption/desorption isotherms showed that the copolymer I sample had a linear isotherm region between relative humidities of 50-90%. Below 20% relative humidity, Langmiur sorption was indicated.

Monolayer loading appears to fit a Langmuir correlation quite well, indicating that desorption in this region can assume first-order kinetics behaviour with the desorption rate given as $k_d\theta$. Including a Henry-type parameter to a Freundlich equation improved the fitting, thus indicating (at low concentrations) that assumed Henry-type behaviour is prevalent. The results also indicated that the copolymer I surface is uniform without any interactions between adsorbed water molecules

Multilayer loading equations and correlations were used to fit sorption isotherms for copolymer I over the entire moisture content range. A modified BET equation again gave the best fit to the multilayer loading of moisture between relative humidities of 0-85% ($45 deg C$:1-r^2 = 7.1E-06, $65 deg C$:1-r^2 = 9.9E-06, $80 deg C$:1-r^2 = 1.2E-05). The best empirical fit to this multilayer region was observed by Schuchmann *et al.* (1985) at relative humidity< 60% ($45 deg C$:1-r^2 = 4.3E-06, $65 deg C$:1-r^2 = 6.5E-06, $80 deg C$:1-r^2 = 8E-06), and Henderson ($45 deg C$:1-r^2 = 4E-05, $65 deg C$:1-r^2 = 4.7E-05, $80 deg C$:1-r^2 = 4.7E-05). Other empirical-based correlations indicate that copolymer I has a poor restriction on the number of sorbed layers limiting possible swelling of the material.

Surface area calculations showed that there is 27 times the internal surface area in the copolymer I particles when compared with the external surface area. Results from nitrogen sorption tests gave the internal surface area to equal $0.51 m^2 g^{-1}$. This helped determine that 98 times the adsorbed moisture in the particle was not directly bound to the pore surface.

Strongly hydrophilic polymers such as wool, silk and cellulose material typically show typical *type III* isotherms in the BET classification. The less hydrophilic rubbers, plastics and synthetic fibres show *type II* behaviour. Hydrophobic polymers with very low critical moisture contents have linear isotherms, due to the presence of water clusters, which can approximately be rewritten as Fick's second law resembling the solution of the "ordinary" diffusion equation.

E.8 POLYSTYRENE-BUTADIENE COPOLYMER II

Maximum hygroscopic moisture content = 0.0019-0.0021 *kg water/kg wet solid.* Monolayer saturation, X_m = 0.0003 *kg water/kg wet solid.*

Copolymer II shows a sorption isotherm with linear characteristics. The large gelatinous nature of the material combined with the large particle sizes showed that water sorption was not favourable, with a maximum hygroscopic moisture content of 0.2%. Of the three copolymers investigated, copolymer II experienced the lowest attainable moisture content as a result of the smallest external surface area. Long exposure of copolymer II to 50-80% relative humidity at $45 deg C$, $65 deg C$ and $80 deg C$ gave evidence of water diffusing partially into the external surfaces of the particles. This partial diffusion resulted in the water molecules forming water clusters around existing adsorbed water molecules. Partial swelling of the external surface regions may result from the appearance of water clustering. No chemical evidence of any condensed moisture is possible in copolymer II, only individual water molecules are physisorbed to nucleophilic sites along the exposed section of polymer chains. At these very low loadings (0.04-0.2% moisture content) the water clustering showed a lower heat of wetting of between 0 and $2000 kJ\ kg^{-1}$.

The general adsorption/desorption isotherms showed that the copolymer II sample had a linear isotherm region between relative humilities of 5-90%. Monolayer sorption was limited to relative humidities below 10% and accounted for 20% of the total sorption recorded. From the linear appearance of sorption above the monolayer above 50% relative humidity, we can deduce that the copolymer II surface does not influence the bond strengths of the unbound water. As a result, "water clustering" occurs between the polymer chains over the entire range of sorption. The copolymer II material is more hydrophobic than the other two polystyrene-butadiene copolymers. Heat of sorption calculations indicated a gradual increase in heats of sorption while drying the copolymer II sample.

Because the copolymer II particles are large (4 *mm*) and because of the gelatinous nature of the material, there appeared to be an insignificant monolayer loading. Because the calculated monolayer loading was small compared with that of other solids, fitting monolayer correlations to this region would be of no benefit. Results of minimising the least sum of squares are listed.

A BET correlation gave a poor fit for copolymer II for all relative humidities ($45 deg C$:1-r^2 = 3.1E-06, $65 deg C$:1-r^2 = 2.5E-06,$80 deg C$:1-r^2 = 1.2E-06). A modified BET correlation gave a very good fit through the entire range of relative humidities, compared with other monolayer loading correlations. Calculations indicated that a finite hygroscopic moisture content exists, and the enthalpy difference between the first and second successive layers of water molecules was between 1000 and 2000$kJ\ kg^{-1}$. ($45 deg C$:1-r^2 = 7E-08, $65 deg C$:1-r^2 = 2E-08, $80 deg C$:1-r^2 = 2.6E-08). The GAB equation gave a similar result to the modified BET correlation. ($45 deg C$:1-r^2 = 1.9E-07, $65 deg C$:1-r^2 = 3.8E-07, $80 deg C$:1-r^2 = 2.8E-08).

The Henderson correlation gave the best fit for the large linear desorption region of the isotherm ($45 deg C$:1-r^2 = 2.9E-08, $65 deg C$:1-r^2 = 1.7E-08, $80 deg C$:1-r^2 = 2.4E-09). Other good fits were recorded by the Luikov and modified b correlations ($45 deg C$:1-r^2 = 4.2E-08, $65 deg C$:1-r^2 = 2.6E-08, $80 deg C$:1-r^2 = 2.8E-09). Another good fit was recorded by the SPS correlation ($45 deg C$:1-r^2 = 1.2E-07, $65 deg C$:1-r^2 = 3.9E-08, $80 deg C$:1-r^2 = 2.2E-09).

Surface area calculations showed that there is 19 times the internal surface area in the copolymer II particles when compared with the external surface area. Results from nitrogen sorption tests gave the internal surface area to equal $0.05 m^2 g^{-1}$. This helped determine that 167 times the adsorbed moisture in the particle was not directly bound to the pore surface.

E.9 POLYSTYRENE-BUTADIENE COPOLYMER III

Maximum hygroscopic moisture content = 0.009-0.011 *kg water/kg wet solid.* Monolayer saturation, X_m = 0.002-0.0022 *kg water/kg wet solid.*

Copolymer III shows a sorption isotherm characteristic of *types I* and *II*. The highly non-spherical shape of the particle with a large shape factor causes excessive sorption of water around the exposed nucleophilic sections on the copolymer chains. The increase in surface area as a result of the small particle diameters observed made large monolayer sorption at the surface possible. Copolymer III experienced a slightly less maximum attainable moisture content than copolymer I, probably due to slightly less external surface area. Long exposure of copolymer III to 50-80% relative humidity at 45 $degC$ gave evidence of water diffusing partially into the external surfaces of the particles. This partial diffusion resulted in the water molecules forming water clusters around existing adsorbed water molecules, increasing the moisture content from 0.3% to 0.8%. Partial swelling of the external surface regions may result from the appearance of water clustering. No chemical evidence of any condensed moisture is possible in copolymer III; only individual water molecules are physisorbed to nucleophilic sites along the exposed section of polymer chains. These very low monolayer loadings (0-0.3% moisture content) gave a gradual increase in the heat of wetting of between 2400 and 2600 $kJ\,kg^{-1}$. The water clustering showed a comparable heat of wetting of between 0 and 2400 $kJ\,kg^{-1}$ for the higher moisture contents.

The monolayer loading in copolymer III is about 25% of the total water adsorption. From the linear appearance of sorption above the monolayer above 10% relative humidity, we can deduce that the copolymer III surface does not influence the bond strengths of the unbound water held above the monolayer. As a result "water clustering" occurs between the polymer chains. The monolayer region consists of individual water molecules bound to the electrophilic aromatic rings of the styrene and the electrophilic double bonds of butadiene. Heat of sorption calculations indicated a gradual increase in heats of sorption while drying into the monolayer.

The general adsorption/desorption isotherms showed that the copolymer III sample had a linear isotherm region between relative humidities of 10-90%. Below 10% relative humidity, Langmiur sorption was indicated.

Monolayer loading appears to fit a Langmuir correlation quite well, indicating that desorption in this region can assume first-order kinetic behaviour with the desorption rate given as $k_d\theta$. Including a Henry-type parameter to a Freundlich equation improved the fitting, thus indicating (at low concentrations) that assumed Henry-type behaviour is prevalent. The results also indicated that the copolymer III surface is uniform without any interactions between adsorbed water molecules.

A modified BET correlation gave a much better fit through the entire range of relative humidities. Calculations indicated that a finite hygroscopic moisture content exists (45$degC$,1-r^2=0.00011, 65$degC$,1-r^2=8.9E-05, 80$degC$,1-r^2=1.4E-05). The GAB equation gave the same result as the modified BET (45$degC$:1-r^2=0.00011, 65$degC$:1-r^2=8.9E-05, 80$degC$:1-r^2=1.4E-05). The best fitting empirical correlations are given in

order: Schuchmann, SPS, Henderson. The Schuchmann correlation gave the best fit for relative humidity < 60% ($45 degC$ 1-r^2=0.00537, $65 degC$ 1-r^2 =0.00017, $80 degC$ 1-r^2=1.4E-05). Another good fit was recorded by the SPS correlation ($45 degC$ 1-r^2 =0.00154, $65 degC$ 1-r^2=0.00071, $80 degC$ 1-r^2=0.00028). Another good fit was recorded by the Henderson correlation ($45 degC$ 1-r^2=0.001, $65 degC$ 1-r^2=0.00123, $80 degC$ 1-r^2 = 0.00028). Other empirical based correlations indicate that copolymer III has a poor restriction on the number of sorbed layers limiting possible swelling of the material.

Surface area calculations showed that there is 59 times the internal surface area in the copolymer III particles when compared with the external surface area. Results from nitrogen sorption tests gave the internal surface area to equal $0.58 m^2 g^{-1}$. This helped determine that 72 times the adsorbed moisture in the particle was not directly bound to the pore surface

E.10 HEAT-TREATED SILICA GEL

Maximum hygroscopic moisture content=0.15-0.17 $kgwater/kgwetsolid$. Monolayer saturation, X_m =0.06-0.08 $kgwater/kgwetsolid$.

Silica gel type 124 was heated to $1000 degC$, so that all the condensable water was removed and prevented from regenerating. This is called silica gel (heat treated). No evidence of hysteresis was apparent during the progression of plotting the adsorption and desorption isotherms for silica gel (heat treated). Thus, here only the desorption isotherms are shown in Figure 6.37. This isotherm shows a typical shape of a microporous or mesoporous solid with a non-active surface. For example, a characteristic linear isotherm is present for multilayer loading, which can be described by unstructured water clustering, and, at low relative humidity regions, a steeper sorption isotherm is observed, indicating the sorption of a monolayer.

Moisture is physisorbed to the porous structure in the heat-treated silica gel, with no chemical evidence of any condensed moisture being possible. The low monolayer loadings (0-8% moisture content) gave an unusually high but stable heat of wetting of 3000 $kJ\ kg^{-1}$. Isotherms of the silica gel indicated Henry-type behaviour (linear desorption) in the lower regions of monolayer loading. In this monolayer region, ten experimental points were plotted and fitted using a least sum of squares method. Fitting this linear region to a Freundlich correlation appeared to fit well, but including a Henry-type parameter to the Freundlich equation did not improve the fitting. Thus, the silica gel porous surface is heterogeneous without any interactions evident between adsorbed water.

Multilayer loading equations and correlations were used to fit sorption isotherms for the silica gel over the entire moisture content for all relative humidities. A modified BET equation again gave the best fit to the multilayer loading of moisture between

relative humidities of 10-90% (45*degC*,1-r^2=0.00011, 65*degC*,1-r^2=8.9E-05, 80*degC*,1-r^2=1.4E-05). The best empirical fits to this multilayer region were: Schuchmann for relative humidity < 60% fit (45*degC*:1-r^2=0.00537, 65*degC*:1-r^2=0.00017, 80*degC*:1-r^2=1.4E-05), SPS (45*degC*:1-r^2=0.00154, 65*degC*:1-r^2=0.00071, 80*degC*: 1-r^2 =0.00028), and Henderson (45*degC*:1-r^2=0.001, 65*degC*:1-r^2=0.00123, 80*degC*:1-r^2=0.00028). Other empirical-based correlations indicate that the silica gel has a restriction on the number of sorbed layers, which is understandable given the non-swelling nature of the material. Also, at these sorptive temperatures, there is not an increase in the number of active sites during sorption of moisture.

From the above calculations, the silica gel particles are not ideally spherical but have 170 000 times more surface area than spherical particles. This increase in surface area would be a result of irregularities in the external surface. Thus there appears to be 2.7 times the adsorption of water into the silica gel particle than adsorbed on to the surface. So adsorption on to the external silica gel surface is negligible. With heat treatment of the silica gel, micropores may be blocked off by the formation of peroxo groups. A reduction in surface area from 450 m^2g^{-1} to 250m^2g^{-1} showed the significance of peroxo group formation. This may help indicate the proportion of micropores in the silica gel 124 material. If one assumes that all the micropores are blocked off by the formation of peroxo groups, which has been proven (Young, 1958) especially when heating it to 1000*degC*, then in this case the ratio of micropores to mesopores is 25:45 or 5:8. From the shapes of both silica gel isotherms, this could be highly probable. This would help decipher the kinetics behaviour of drying silica gel to low moisture contents.

Exactly half of the desorbed moisture in the isotherm can be attributed to the directly bound physisorbed moisture in a monolayer. The desorption of this bound moisture is performed below 10% relative humidity at 45*degC* and below 20% relative humidity at 80*degC*. Below this moisture content range, a stable desorption profile was shown for all the isotherm temperatures that were investigated.

Appendix F

RAW DATA FOR CHARACTERISTIC DRYING RATE CURVES

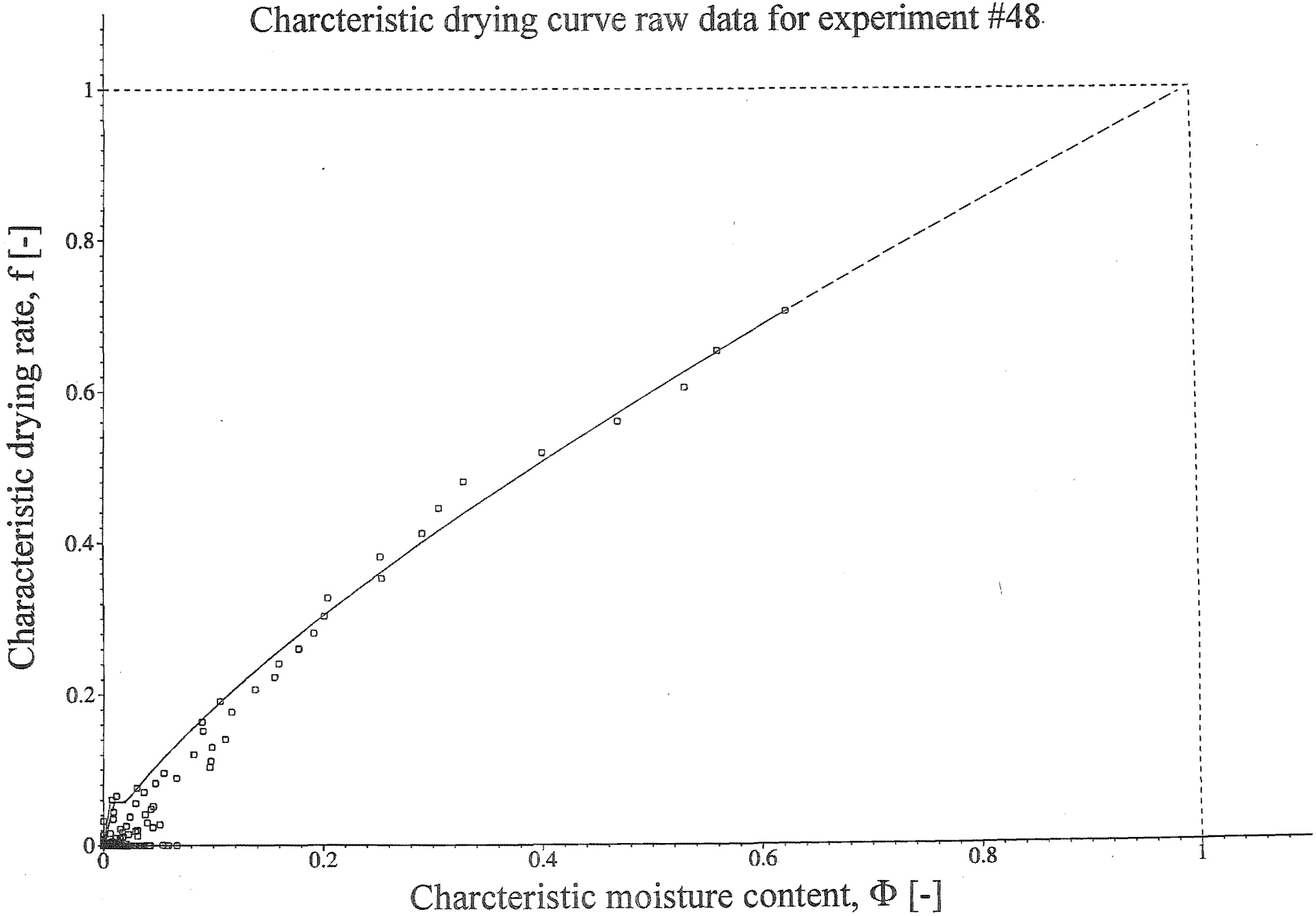
Charcteristic drying curve raw data for experiment #48
Characteristic drying rate, f [-]
Charcteristic moisture content, Φ [-]
0
0.2
0.4
0.6
0.8
1

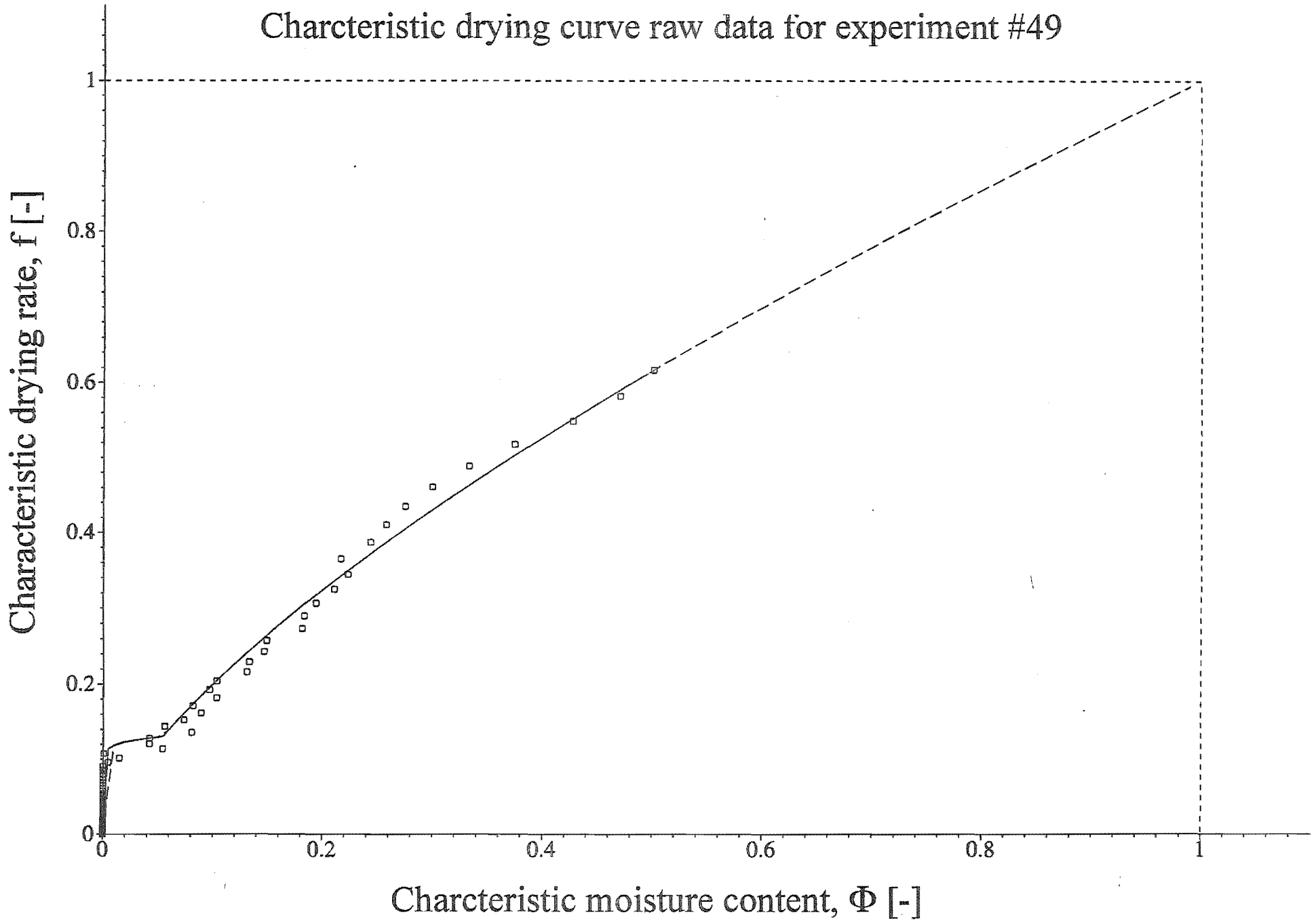
Charcteristic drying curve raw data for experiment #49
Characteristic drying rate, f [-]
Charcteristic moisture content, Φ [-]
0
0.2
0.4
0.6
0.8
1

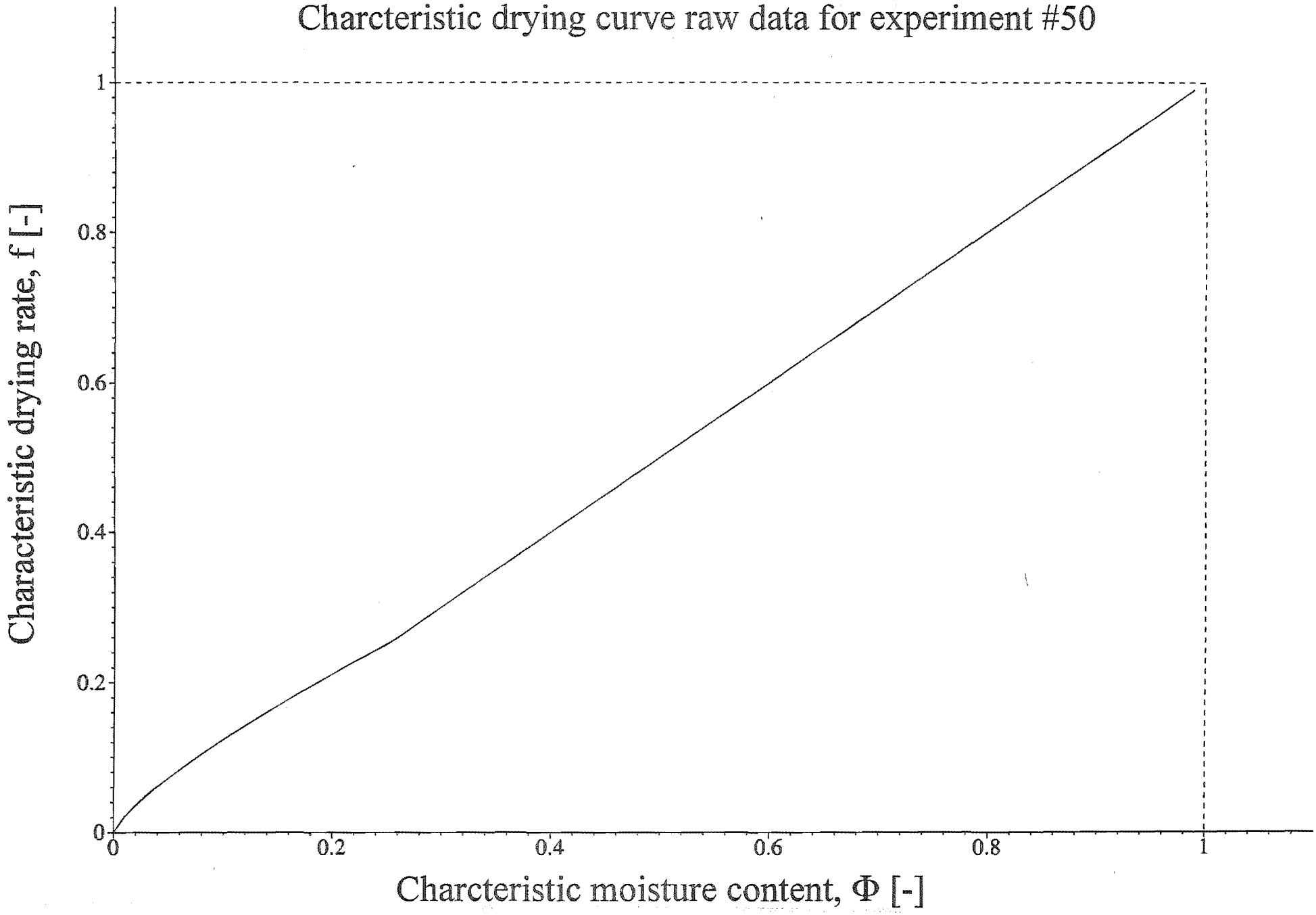
Charcteristic drying curve raw data for experiment #50
Characteristic drying rate, f [-]
Charcteristic moisture content, Φ [-]
0
0.2
0.4
0.6
0.8
1

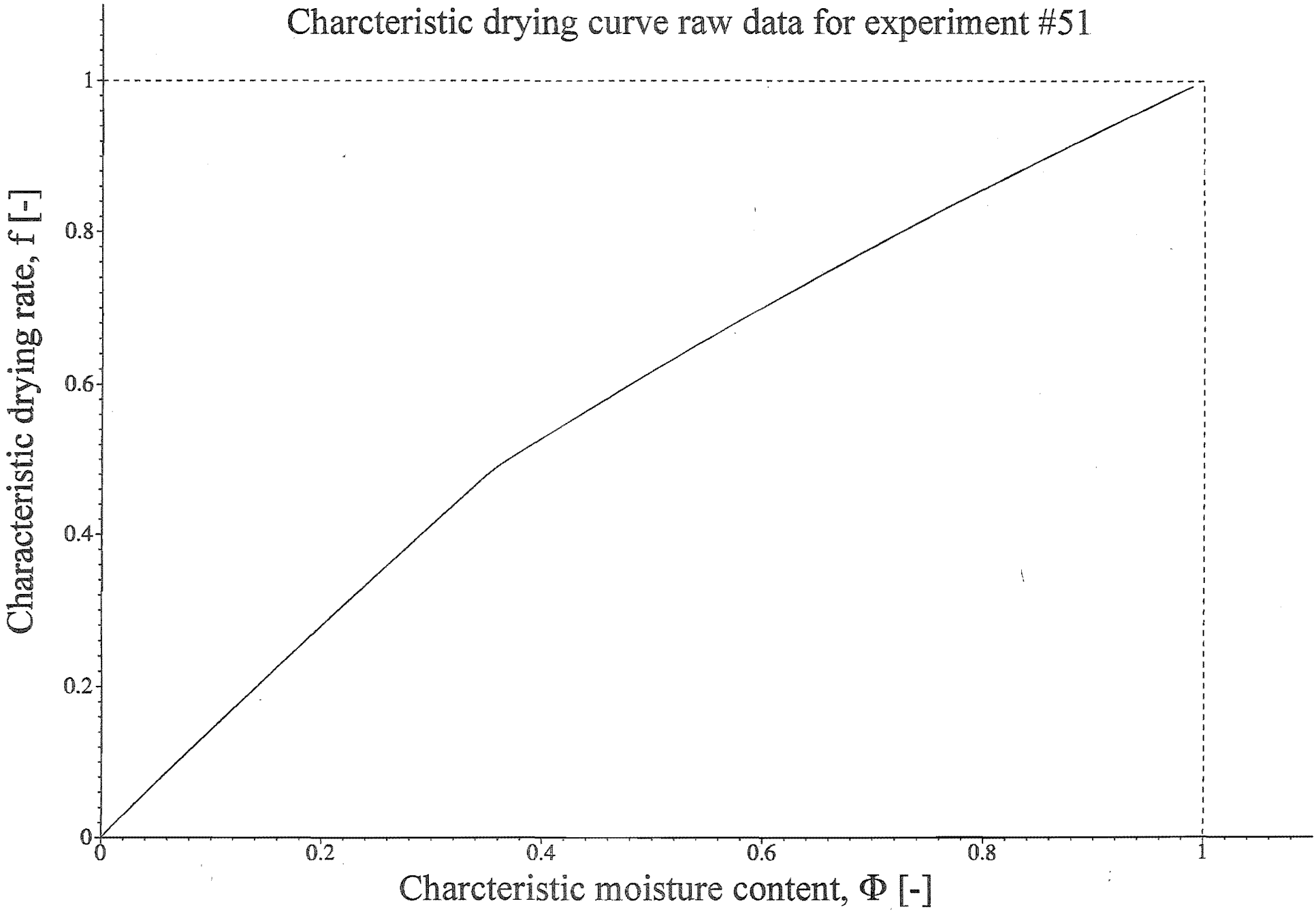
Charcteristic drying curve raw data for experiment #51
Characteristic drying rate, f [-]
Charcteristic moisture content, Φ [-]
0
0.2
0.4
0.6
0.8
1

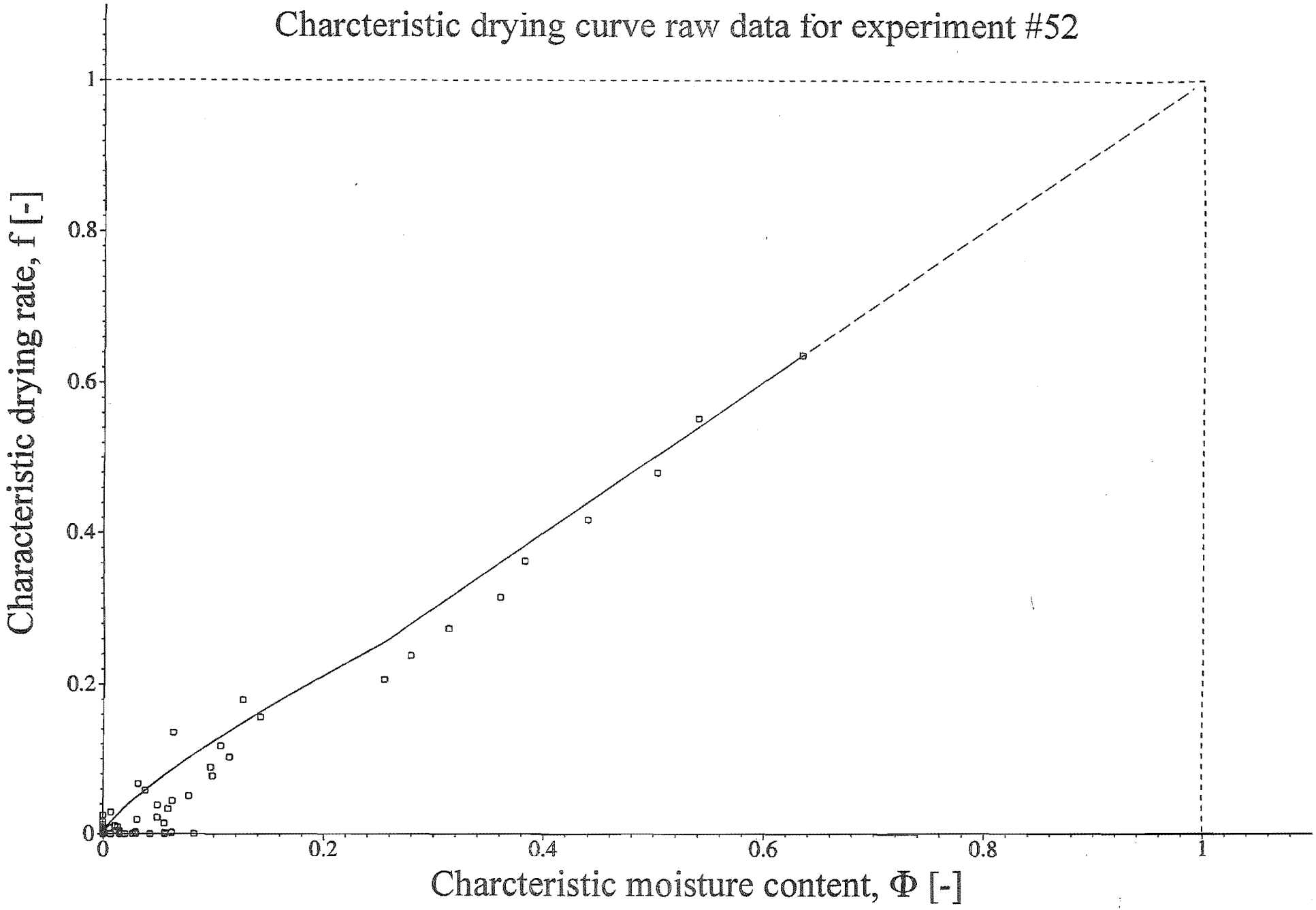
Charcteristic drying curve raw data for experiment #52
Characteristic drying rate, f [-]
Charcteristic moisture content, Φ [-]
0
0.2
0.4
0.6
0.8
1

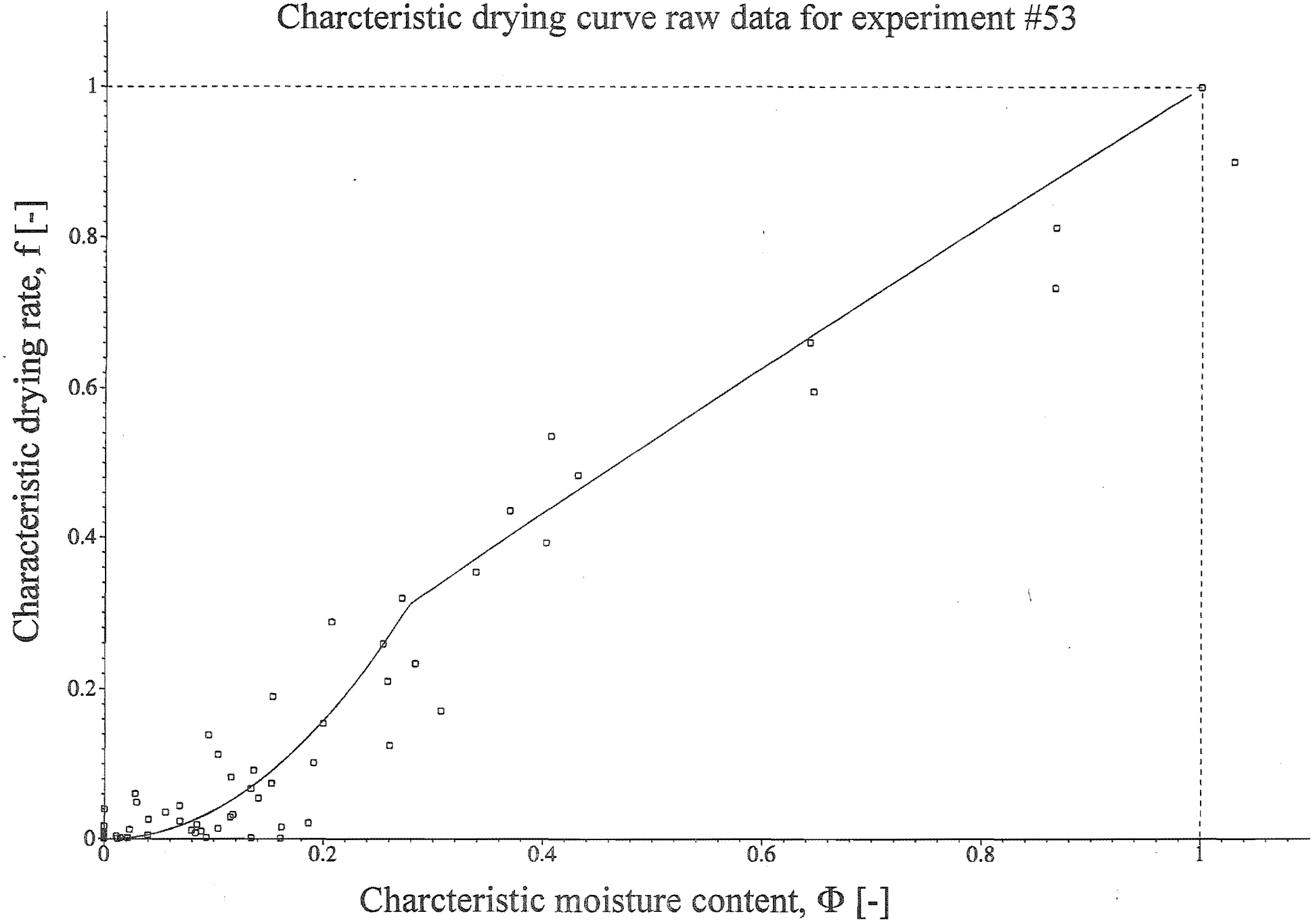
Charcteristic drying curve raw data for experiment #53
Characteristic drying rate, f [-]
Charcteristic moisture content, Φ [-]
0
0.2
0.4
0.6
0.8
1

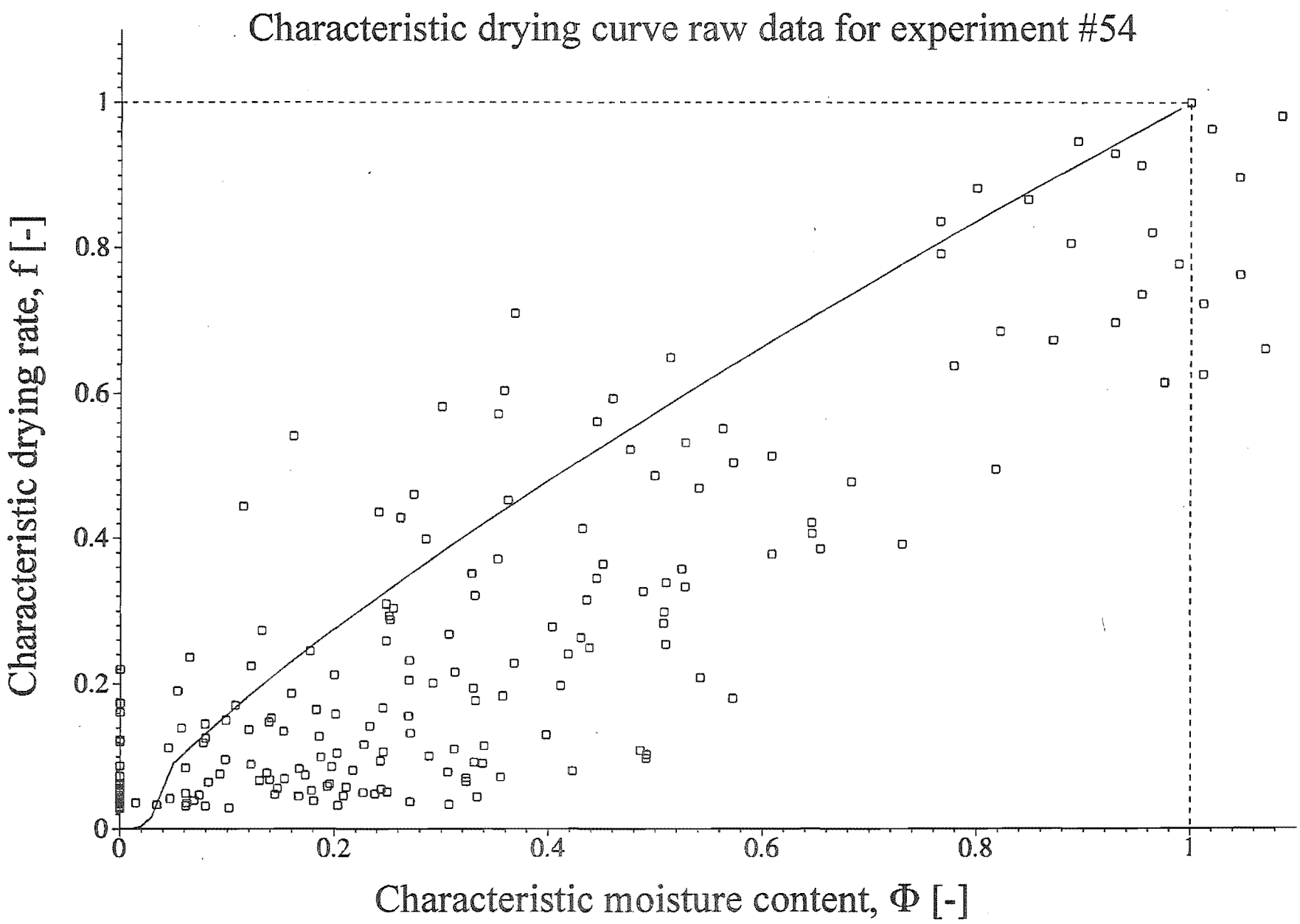
Characteristic drying curve raw data for experiment #54
Characteristic drying rate, f [-]
Characteristic moisture content, Φ [-]
0
0.2
0.4
0.6
0.8
1

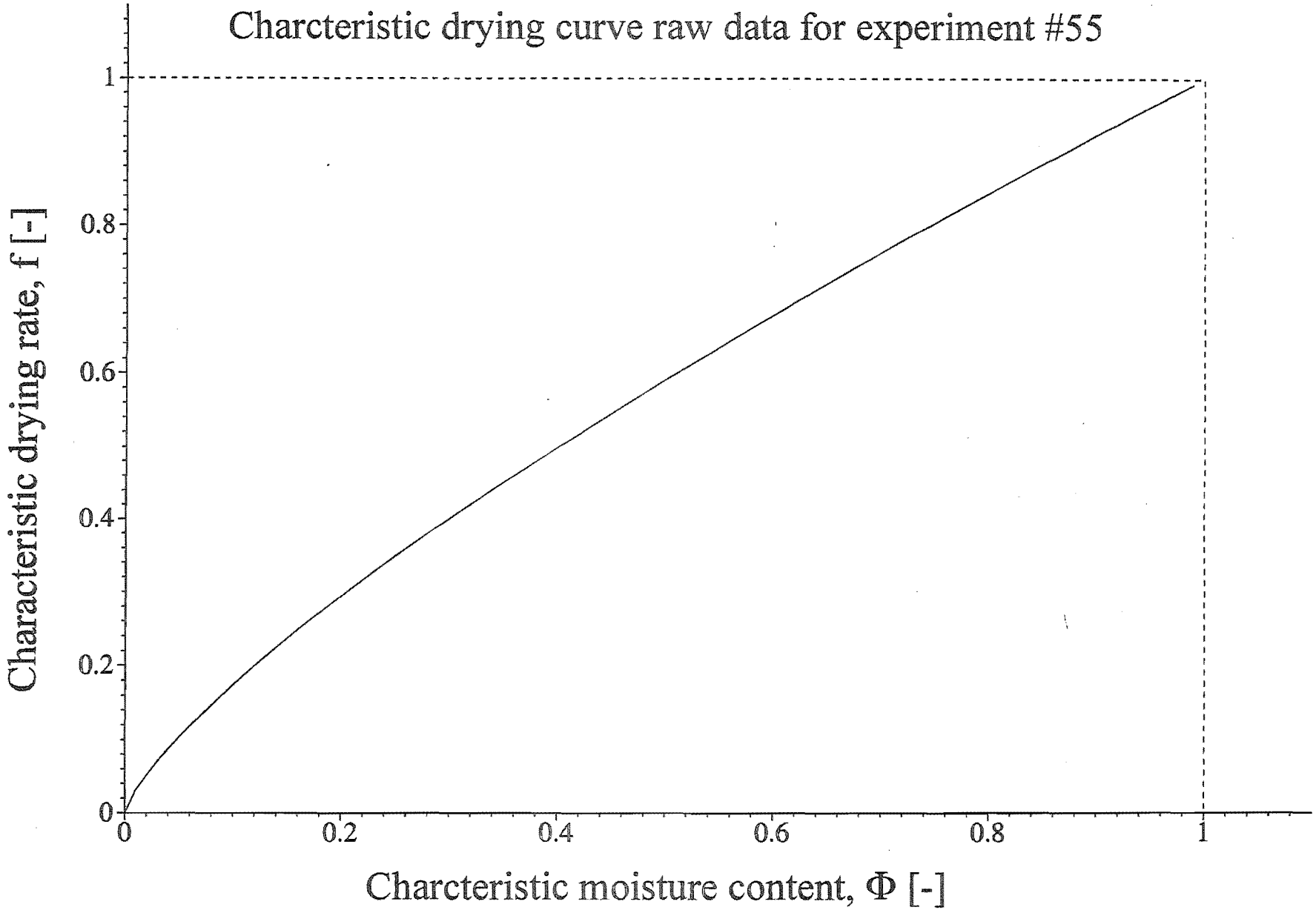
Charcteristic drying curve raw data for experiment #55
Characteristic drying rate, f [-]
Charcteristic moisture content, Φ [-]
0
0.2
0.4
0.6
0.8
1

Appendix G

SOFTWARE PROGRAM FOR OPERATION OF NEW DRYING KINETICS APPARATUS

This program CONTROL.BAS is the thermocouple/microbalance initialisation program. It is written in QBASIC language. Its function is to: retrieve and control operation of the A/D eurocard provided with the microbalance; receive and convert information about the various thermocouples and pressure gauges in the apparatus through the multiplexer; store weight loss data as a function of time, pressure data as a function of time, temperature profile information as a function of time.

```
' Pcl812 / Pcld889 Data Acquisition system
 ' arrays and variables
        CLS
        OPTION BASE 0
        DIM SHARED c(36) AS INTEGER
        DIM SHARED chan(32) AS INTEGER
        DIM SHARED gain(32) AS INTEGER
        DIM SHARED ptr(32) AS INTEGER
        DIM SHARED dat1(32) AS SINGLE
        DIM SHARED g(32) AS INTEGER
        DIM SHARED status(32) AS INTEGER
        DIM typ$(60)
        DIM tpe(16) AS INTEGER
        DIM v1(16)
        DIM v2(16)
        DIM SHARED stat$(32)
        DEFINT I
        SAVED = 0
        DIM hi(16)
        DIM lo(16)
        datfil = 1
        confil = 1
        typ$(1) = "TC"
        typ$(2) = "mV"
        typ$(3) = "Pirani1005"
        typ$(4) = "PiraniII"
        typ$(5) = "Penning8"
        typ$(51) = "Penning8(1)"
        typ$(52) = "Penning8(2)"
        typ$(53) = "Penning8(3)"
        GOSUB tcvars
        CLS
        LOCATE 1, 1
        PRINT "      Thermocouple/Microbalance Data Acquisition Program"
        LOCATE set, 1: PRINT "Load saved TC configuration Y/N?"
        GOSUB yesno'Get answer
        IF ANS$ = "n" THEN SAVED = 0: GOTO configtemp
        SAVED = 1
        GOSUB loadconf'load saved configuration
        GOSUB confdisp'display configuration
        GOTO alterconf
configtemp:
        'Configuration data entry
        c = 1
        IF SAVED = 1 THEN c = c + 1
        GOSUB clrtxt' clear text lines
        LOCATE set, 1: PRINT "Enter channel number to be read:0-15"
        GOSUB getkbd'Get keyboard input
        a = VAL(kbdin$)
        IF a >= 16 GOTO badval 'value out of range range
        GOTO goodval: 'value in range
badval:
        GOSUB clrtxt 'clear text lines
        LOCATE set, 1
```

```
        PRINT "Value out of range, 0-15 allowable"
        PRINT "Press any key to continue"
        GOSUB idle
        GOTO configtemp
goodval:
        status(a) = 1
        chan(a) = a' save channel number
        ptr(c) = a
reenter:
        GOSUB clrtxt
        LOCATE set, 1: PRINT "Enter the gain setting for channel "; chan(a)
        PRINT "Values allowed are: 0.5,1,2,10,50,100,200,1000"
        GOSUB getkbd: 'get input
        gain(a) = VAL(kbdin$)
        GOSUB convgain: 'convert gain value
        GOSUB gettype'channel type
        GOTO goodgain'gain value ok
badgain: 'bad gain value
        GOSUB clrtxt
        LOCATE set, 1
        PRINT "Value out of range: Press any key to continue."
        GOSUB idle
        GOTO reenter: 're-enter gain value
goodgain:
        g(a) = g ' save chan. converted gain setting
        GOSUB confdisp'display chan/gain setting
        GOSUB clrtxt' clear text lines '
        LOCATE set, 1: PRINT "Enter further channels? :Y/N"
        GOSUB yesno: 'get answer
        IF ANS$ = "y" GOTO morechans
        GOTO conf2
morechans:
        c = c + 1
        GOSUB clrtxt' clear text lines
        GOTO configtemp
gettype:
        GOSUB clrtxt
        LOCATE set, 1: PRINT "Enter input type for chan "; a
        LOCATE set + 1, 1: PRINT "Thermocouple=<TC>"
        LOCATE set + 2, 1: PRINT "mV=<V>"
        LOCATE set + 3, 1: PRINT "Pirani1005=<PIR1005>"
        LOCATE set + 4, 1: PRINT "PiraniII=<PIRII>"
        LOCATE set + 5, 1: PRINT "Penning8=<PEN8>"

        GOSUB getkbd
        tpe(a) = 0
        IF kbdin$ = "TC" OR kbdin$ = "tc" THEN tpe(a) = 1: GOTO typend
        IF kbdin$ = "V" OR kbdin$ = "v" THEN tpe(a) = 2: GOTO typend
        IF kbdin$ = "pir1005" OR kbdin$ = "PIR1005" THEN tpe(a) = 3: GOTO typend
        IF kbdin$ = "pirii" OR kbdin$ = "PIRII" THEN tpe(a) = 4: GOTO typend
        IF kbdin$ = "pen8" OR kbdin$ = "PEN8" THEN tpe(a) = 5: GOTO penrange
        IF tpe(a) < 1 GOTO gettype
        GOTO typend
penrange:
```

```
        GOSUB clrtxt
        LOCATE set, 1: PRINT "Enter range for Penning Gauge <1,2,3>"
        GOSUB getkbd
        IF kbdin$ = "1" THEN tpe(a) = 51
        IF kbdin$ = "2" THEN tpe(a) = 52
        IF kbdin$ = "3" THEN tpe(a) = 53
        IF kbdin$ < "1" GOTO penrange
        IF kbdin$ > "3" GOTO penrange
typend:
        RETURN

alterconf:
        'make alterations to configuration
        GOSUB clrtxt' clear text lines
        LOCATE set, 1: PRINT "Any alterations to be made? Y/N?"
        GOSUB yesno: 'get answer
        IF ANS$ = "y" THEN GOTO reconf
        GOTO confin'continue with data acquisition
reconf:
        tcdatfil = 1: tcconfil = 1
        GOTO configtemp' re-enter all settings

conf2:
        GOSUB clrtxt' clear text lines
        LOCATE set, 1: PRINT "Enter number of readings to be taken"
        GOSUB getkbd
        rdg = VAL(kbdin$)
        GOSUB confdisp
        GOSUB clrtxt'clear text lines
        LOCATE set, 1: PRINT "Enter time interval between readings in seconds"
        GOSUB getkbd
        delay = VAL(kbdin$)
        GOSUB confdisp
rerun:
        GOSUB clrtxt' clear text lines
        LOCATE set, 1: PRINT "Save data to disk file? Y/N"
        GOSUB yesno
        IF ANS$ = "n" THEN datfil = 0: GOTO nodatfil
        GOSUB clrtxt' clear text lines
        LOCATE set, 1: PRINT "Enter a data file name for this session"
        GOSUB getkbd
        datfil$ = kbdin$
        GOSUB savform
        GOTO nodatfil
savform:
        CLS
        PRINT "   Choose format to save data to disk"
        PRINT
        PRINT " 1  Microbalance data only"
        PRINT " 2  Microbalance and pressure data only"
        PRINT " 3  All data"
        PRINT
        PRINT "Enter number, 1,2 or 3"
        GOSUB getkbd
```

```
        datpr = VAL(kbdin$)
        IF datpr < 0 OR datpr > 3 THEN GOTO savform
        GOSUB confdisp
        RETURN
nodatfil:
        GOSUB clrtxt' clear text lines
        LOCATE set, 1: PRINT "Save this configuration to disk? Y/N"
        GOSUB yesno
        IF ANS$ = "n" THEN confil = 0: GOTO noconfil
        GOSUB clrtxt' clear text lines
        LOCATE set, 1: PRINT "Enter config. file name. <filename.cfg>"
        GOSUB getkbd
        confil$ = kbdin$
        GOSUB confdisp
noconfil:
        GOSUB clrtxt' clear text lines
        LOCATE set, 1: PRINT "Any alterations to be made? Y/N"
        GOSUB yesno
        IF ANS$ = "y" THEN GOSUB confdisp: GOTO configtemp
        IF confil = 0 THEN GOTO confin
        GOSUB savconf' save config file
        GOTO confin

confdisp:
        'display current configuration
        CLS
        LOCATE 1, 1
        PRINT "                Data capture configuration"
        i = 0
        'display chan/gain setup
        LOCATE (set), 50: PRINT "Channel"
        LOCATE (set), 58: PRINT "Gain"
        LOCATE (set), 65: PRINT "Type"
chkstat:
        'display channel configurations
        IF status(i) = 0 THEN GOTO nextch
        LOCATE (set1 + i), 52: PRINT chan(i)
        LOCATE (set1 + i), 58: PRINT gain(i)
        LOCATE (set1 + i), 65: PRINT typ$(tpe(i))
nextch:
        i = i + 1
        IF i = 16 THEN GOTO capmode
        GOTO chkstat
capmode:
        'display tc data capture mode settings
        LOCATE (set1 + 5), 1: PRINT "Taking "; rdg; " readings"
        LOCATE (set1 + 7), 1: PRINT "Interval="; delay; " seconds"
        LOCATE (set1 + 9), 1: PRINT "Data file name is "; datfil$; "     "
        LOCATE (set1 + 11), 1: PRINT "TC Configuration file name is "; confil$; "    "
        RETURN
clrtxt:
        'clear text entry lines
        LOCATE set, 1: PRINT "                                    "
        LOCATE (set + 1), 1: PRINT "                                        "
```

```
        LOCATE (set + 2), 1: PRINT "                                    "
        RETURN

chanstat:
        'count number of channels to be read/set channel status flag
        num = 16' max possible number of channels
        FOR i = 0 TO 15
        IF gain(i) > 1000 THEN num = num - 1: status(i) = 0
        NEXT i
        RETURN
confin:
        IF datfil = 1 THEN GOSUB savform
        CLS
        GOSUB microbal
        ' enter data acquisition routine
        IF datfil = 0 THEN GOTO skipfil
        ' open disk data file
        'OPEN datfil$ FOR OUTPUT AS #2
skipfil:
        GOSUB getdata: 'get data
endrdg:
        CLOSE #2
        CLOSE #3
        CLS : TIMER OFF
        LOCATE 2, 10: PRINT "End of data acquisition"
        LOCATE 4, 5: PRINT "Re-run with same settings? Y/N"
        GOSUB yesno
        IF ANS$ = "y" THEN GOTO rerun
endrun:
        PRINT "Program terminated"
        END


getdata:
        'data acquisition routine
        CLS : PRINT "Starting data acquisition"
        GOSUB chanstat' get number of channels to be read
        CLS
        count = 0' set readings counter to zero
        'LINE (0, 0)-(0, 400)
        'LINE (0, 350)-(400, 350)
        'LINE (0, 0)-(0, 350)
        'LINE (400, 0)-(400, 350)
        LOCATE 1, 1: PRINT "Reading"
        LOCATE 1, 15: PRINT "Channel"
        LOCATE 1, 30: PRINT "Data"
        LOCATE 1, 50: PRINT "Type"
' data acquisition routine
timer1:
        ON TIMER(delay) GOSUB timeout
        TIMER ON
idle1:
        GOTO idle1
timeout:
```

```
        count = count + 1: 'increment readings counter
        IF count = rdg + 1 THEN RETURN endrdg:  'test for end of readings count

        'start data acquisition
        OUT ioport% + 11, 1: ' ENABLE TRIGGER
        i = 0' set channel counter to zero
chkstatus:
        IF status(i) = 1 THEN GOTO flagged
        IF i = 16 THEN GOTO chanend
        i = i + 1: GOTO chkstatus
flagged:
        DUMMY = INP(ioport% + 4): 'CLEAR STATUS FLAG
        GOSUB readcjc: 'read cjc channel
        GOSUB readchan: 'read a/d channel
        IF tpe(i) = 1 THEN GOSUB lintc: 'linearize reading
        IF tpe(i) = 3 THEN GOSUB pir100
        IF tpe(i) = 4 THEN GOSUB pirII
        IF tpe(i) = 51 THEN GOSUB pen1
        IF tpe(i) = 52 THEN GOSUB pen2
        IF tpe(i) = 53 THEN GOSUB pen3
        i = i + 1
        IF i = 16 THEN GOTO chanend' end of channels
        GOTO chkstatus: 'take next reading

chanend:
readmbal:
        GOSUB mbsample' read microbalance
        GOSUB readdewall'read Dew-All meter
        GOSUB display: 'display readings
        GOSUB savdat: 'save readings to disk file
        RETURN idle1 'read channels again

readcjc:
        ' READ CJC CHANNEL
        OUT (ioport% + 10), 9'select pcl 812 a/d chan 9 (cjc)
        GOSUB readad        'read a/d converter
        GOSUB convcjc 'convert cjc volts to temp
        RETURN

readchan:
        ' READ SELECTED CHANNEL
        OUT (ioport% + 10), 0'SELECT PCL812 MUX A/D CHANNEL 0
        OUT (ioport% + 13), (chan(i) + g(i)): 'set pcl 889 mux selected chan+gain
        GOSUB readad' read a/d converter
        ' CONVERT A/D READING TO VOLTS
        v1(i) = (hi(i) * 256 + lo(i) - 2048) * 1 / 2048 / gain(i)
        RETURN

readdewall:
        OUT (ioport% + 10), 1'select Dew-All dew point reading
        GOSUB readad' read a/d converter
        'convert reading to volts
        dewpoint = (hi(i) * 256 + lo(i) - 2048) * 1 / 2048
        RETURN
```

```
convcjc:
        ' CONVERT CJC VOLTS TO TEMP
        CJC = (hi(i) * 256 + lo(i) - 2048) * 1 / 2048
        CJC = CJC * 1000 / 24.4
        RETURN

readad:
        ' read pcl 812 A/D converter
        OUT (ioport% + 12), 0'initiate a/d conversion
        hi(i) = INP(ioport% + 5)
chkadflag:
        IF hi(i) > 15 THEN GOTO chkadflag'check a/d status
        lo(i) = INP(ioport% + 4)
        RETURN

lintc:
        ' linearize t/c
        v = R0 + CJC * (R1 + CJC * R2)
        v2 = v + v1(i)
        ' T1=P0+V2*(P1+V2*(P2+V2*(P3+V2*(P4+V2*(P5+V2*(P6+V2*(P7+V2*(P8+V2*P9)))))))
        T1 = v2 * (P5 + v2 * (P6 + v2 * (P7 + v2 * (P8 + v2 * P9))))
        T2 = P0 + v2 * (P1 + v2 * (P2 + v2 * (P3 + v2 * (P4 + T1))))
        dat1(i) = INT(T2 * 100 + .5) / 100
        RETURN

getkbd:
        ' get keyboard input routine
        LINE INPUT " "; kbdin$
        RETURN

yesno:
        ' yesno routine
        ANS$ = INKEY$: IF ANS$ = "" GOTO yesno
        IF ANS$ = "Y" OR ANS$ = "y" THEN ANS$ = "y": GOTO good
        IF ANS$ = "N" OR ANS$ = "n" THEN ANS$ = "n": GOTO good
        GOTO yesno
good:
        RETURN

idle:
        T$ = INKEY$: IF T$ = "" GOTO idle
        RETURN

display:
        ' display routine
        i = 0' set channel counter to zero
chkchan:
        IF status(i) = 0 THEN GOTO nextch2
        LOCATE i + 2, 1: PRINT count' Nth reading
        LOCATE i + 2, 15: PRINT chan(i)'channel number
        LOCATE i + 2, 30: PRINT dat1(i)'data value
        LOCATE i + 2, 50: PRINT typ$(tpe(i))'data type
nextch2:
```

```
        i = i + 1
        IF i = 16 THEN GOTO endch
        GOTO chkchan

endch:

        LOCATE set1 + 16, 1: PRINT "Dew-All dew point= "; dewpoint
        LOCATE set1 + 17, 1: PRINT "Microbalance weight= "; mbal$
        RETURN

savdat:
        ' save data to disk file
        IF datfil = 0 THEN GOTO savexit
        OPEN datfil$ FOR APPEND AS #2
        'PRINT #2, "Reading"; count: 'identify reading
        IF datpr = 1 THEN GOTO data1
        IF datpr = 2 THEN GOTO data2
        IF datpr = 3 THEN GOTO data3

data1:
        PRINT #2, mbal$
        GOTO savexit
data2:
        PRINT #2, mbal$; dat1(8); dat1(9); dat1(12)
        GOTO savexit
data3:
        ' save to disk only required data

        i = 0' set channel counter to zero
chkstat1:
        IF status(i) = 0 THEN GOTO nextch1
        PRINT #2, "ch"; chan(i); "type"; tpe(i); " gain"; gain(i); " "; " data "; dat1(i)
nextch1:
        IF i = 16 THEN GOTO savebal
        i = i + 1
        GOTO chkstat1

savebal:
        PRINT #2, "mbal  "; mbal$' write microbalance data to disk
savedew:
        PRINT #2, "dew  "; dewpoint' write dewpoint data to disk
        CLOSE #2
savexit:
        CLOSE #2
        RETURN

cvars:
        'Thermocouple variables
        ""J" TYPE TC
        R0 = -7.500001E-07
        R1 = 5.053E-05
        R2 = 2.3E-08
        P0 = -.36
        P1 = 19750.9
```

```
        P2 = -175117!
        P3 = 18212970#
        P4 = -2831128000#
        P5 = 271508380000#
        P6 = -13801412100000#
        P7 = 379243843000000#
        P8 = -5371925500000000#
        P9 = 3.0840254D+16
        set = 3: set1 = 5
        ioport% = &H220
        FOR i = 0 TO 15
        status(i) = 0
        NEXT i
        RETURN

convgain:
        ' convert gain value
        g = 7
        IF gain(a) = .5 THEN g = 0
        IF gain(a) = 1 THEN g = 16
        IF gain(a) = 2 THEN g = 32
        IF gain(a) = 10 THEN g = 48
        IF gain(a) = 50 THEN g = 64
        IF gain(a) = 100 THEN g = 80
        IF gain(a) = 200 THEN g = 96
        IF gain(a) = 1000 THEN g = 112
        IF SAVED = 1 THEN GOTO convgainend
        IF g = 7 THEN RETURN badgain
convgainend:
        RETURN
savconf:
        ' save tc configuration
        OPEN confil$ FOR RANDOM AS #1 LEN = 52
        FOR i = 1 TO 16
        FIELD #1, 2 AS ch1$, 2 AS gn1$, 2 AS tp1$, 2 AS del$, 2 AS rdg$, 20 AS dat$, 20 AS con$, 2
AS stat$
        LSET ch1$ = MKI$(chan(i))
        LSET gn1$ = MKI$(gain(i))
        LSET tp1$ = MKI$(tpe(i))
        LSET del$ = MKI$(delay)
        LSET rdg$ = MKI$(rdg)
        LSET dat$ = datfil$
        LSET con$ = confil$
        LSET stat$ = MKI$(status(i))
        PUT #1, i
        NEXT i
        CLOSE #1
        RETURN

loadconf:
        ' load saved tc configuration
        GOSUB clrtxt' clear text lines
        'FILES "*.cfg"
        LOCATE set, 1
```

```
        PRINT "Enter name of config file to load. <filename.cfg>"
        GOSUB getkbd
        OPEN kbdin$ FOR RANDOM AS #1 LEN = 52
        FIELD #1, 2 AS ch1$, 2 AS gn1$, 2 AS tp1$, 2 AS del$, 2 AS rdg$, 20 AS dat$, 20 AS con$, 2
AS stat$
        GET #1, 1'get first settings record
        rdg = CVI(rdg$)
        delay = CVI(del$)
        datfil$ = dat$
        confil$ = con$
        FOR i = 1 TO 16' get the rest of the settings
        GET #1, i
        chan(i) = CVI(ch1$)
        gain(i) = CVI(gn1$): gain(a) = gain(i)
        GOSUB convgain' convert gain setting
        g(i) = g
        tpe(i) = CVI(tp1$)
        delay = CVI(del$)
        status(i) = CVI(stat$)
        NEXT i
        CLOSE #1
        IF datfil$ = "" THEN datfil = 0
        IF confil$ = "" THEN confil = 0
        RETURN


microbal:
        CLS
        'CI Microbalance Initialisation Routine
        ' set up com port
        OPEN "com2:9600,n,8,1,ds,cs,cd" FOR RANDOM AS #3
        PRINT #3, "e0" 'set controller to interactive mode 0
        LOCATE 5, 10
init:
        CLS
        LOCATE 1, 1
        PRINT "          Microbalance Initialisation routine"
        LOCATE 8, 5
        PRINT "Check Zero and calibrate? key Y(yes) or N(no)"
        GOSUB yesno
        IF ANS$ = "n" THEN c = 0: GOTO endcal
        GOSUB zeroadj
        GOSUB calib

        CLS
        LOCATE 1, 1
        PRINT "          Microbalance Initialisation routine"
        LOCATE 3, 1
        PRINT "Calibrate again? key Y(yes) or N(no)"
        GOSUB yesno
        IF ANS$ = "y" THEN GOTO init
        RETURN
mbsample:
        Y = 13' ascii value of <cr-lf>
```

```
        n = count
        PRINT #3, "p"
        c = 0: GOSUB comread
        p = 1' set start pointer for string search routine
        GOSUB getpos
        GOSUB getstr
        RETURN

zeroadj:
        ' ROUTINE TO ADJUST ZERO OFFSET
        GOSUB comread
        n = 1
        Y = 13 'set balance input string stop pointer to <cr-lf>

        CLS
        LOCATE 5, 10
        PRINT "Microbalance zero offset adjustment sequence"
        PRINT "Ensure balance is stable then press any key"
        GOSUB idle
        PRINT "Please wait..."

        PRINT #3, "z"
        c = 0
        GOSUB comread
        p = 1'set start pointer for string search routine
        GOSUB getpos
        GOSUB getstr
        PRINT "Balance zero offset= "; mbal$
        LOCATE 10, 4: PRINT "Do you wish to adjust the balance? key Y(yes) or N(no)"
        GOSUB yesno
        IF ANS$ = "n" THEN RETURN
adj:
        CLS
        PRINT "Make adjustment then press any key"

        GOSUB idle
        PRINT "Please wait..."
        n = n + 1
        PRINT #3, "z"

        c = 0: GOSUB comread
        'mbal$(n) = r$
        p = 1'set start pointer for string search routine
        GOSUB getpos
        GOSUB getstr
        LOCATE 12, 2: PRINT "This reading= "; mbal$
        LOCATE 14, 2: PRINT "Previous reading= "; mbal1$
        LOCATE 16, 2: PRINT "Make further adjustments? key Y(yes) or N(no)"
        GOSUB yesno
        IF ANS$ = "n" THEN RETURN
        mbal1$ = mbal$
        p = 1
        GOTO adj
        RETURN
```

```
calib:
        'Routine to calibrate balance
        n = 1
        p = 1: Y = 13'set stop pointer for balance input string
        CLS
        PRINT "Calibration Routine"
        LOCATE 5, 5
        'PRINT #3, "c" ' calibrate command to balance

        'c = 0: GOSUB comread' read returned value

        'GOSUB getstr
        'PRINT "Cal.WT="; mbal$(n); "  :type <CR> to continue or new value <CR>"
        PRINT "Enter calibration weight in mGrams"
        LINE INPUT v$ 'enter new calibration weight
        IF VAL(v$) = 0 THEN GOTO calib
        PRINT "New calibration value entered= "; VAL(v$); "mG"; " Is this correct? Y/N"
        GOSUB yesno
        IF ANS$ = "n" THEN GOTO calib
        PRINT "Place"; VAL(v$); "mG "; "weight on balance then press any key"
        GOSUB pause
        'PRINT #3, "c"'calibrate command to balance
        PRINT #3, "c "; v$; CHR$(13)'send calib. weight to balance
        c = 0: GOSUB comread'read returned value
        p = 1'set start pointer for string search routine
        GOSUB getpos
        GOSUB getstr 'retrieve value from input string
        LOCATE 10, 5: PRINT "New calib.Val = "; mbal$
        LOCATE 12, 2: PRINT "Press any key to continue"
        GOSUB pause
rmean:
        'Set running mean value
        CLS
        LOCATE 4, 5
        PRINT "Routine to set running mean value"
        n = 1
        p = 1: Y = 13'set start/stop pointers for balance input string
        LOCATE 6, 10
        PRINT "Set number of conversions for running mean"
        'LOCATE 9, 1: PRINT "Retreiving current value-Please wait..."
        'PRINT #3, "m" 'command to balance
        'c = 0: GOSUB comread'read balance response

        'GOSUB getstr
        'LOCATE 11, 6
        'PRINT "Running mean value= "; mbal$; " : type <CR> or new value"
        PRINT "Enter Value for running mean (1-255)"
        LINE INPUT v$ ' enter new value from keyboard
        IF VAL(v$) = 0 THEN GOTO endcal
        PRINT "New running mean value entered= "; v$; " Is this correct? Y/N"
        GOSUB yesno
        IF ANS$ = "n" THEN GOTO rmean
        PRINT #3, m; v$; CHR$(13)'send to balance with <cr>
```

```
endcal:
        CLS
        mbaldatfil = 1' default save data flag on
        GOTO mbalend
        LOCATE 1, 1
        PRINT "          Microbalance Initialisation routine"
        LOCATE 3, 1
        PRINT "Save Data to disk file? Y/N"
        GOSUB yesno
        GOTO mbalend
        IF ANS$ = "n" THEN mbaldatfil = 0: GOTO mbalend
        LOCATE 5, 1: PRINT "Enter a file data file name"
        GOSUB getkbd
        LOCATE 7, 1: PRINT "Data file name is "; kbdin$; " is this correct? Y/N"
        GOSUB yesno
        IF ANS$ = "n" THEN GOTO endcal
        mbalfil$ = kbdin$
        mbaldatfil = 1
        'OPEN mbalfil$ FOR OUTPUT ACCESS READ WRITE AS #4
mbalend:

        RETURN

comread:
        'get data from comm. port buffer
        FOR d = 1 TO 300: NEXT d' delay
        T = c'point to start of latest buffer entry
        c = LOC(3)' check for characters in buffer
        IF c = 0 OR c > T THEN GOTO comread' buffer empty-check again
        r$ = INPUT$(LOC(3), #3)'read buffer into variable
        RETURN

getpos:
        ' routine to find position of first data value in report string
        cr$ = MID$(r$, p, 1)'read first character in report string
        IF ASC(cr$) = 32 THEN sp = sp + 1: GOTO nextsp' check for <space>
        IF ASC(cr$) = 45 THEN GOTO getposfin' check for <->
        IF ASC(cr$) > 47 AND ASC(cr$) < 58 THEN GOTO getposfin' check for numeral
        p = p + 1: GOTO getpos' get next character

nextsp:
        p = p + 1' increment pointer
        GOTO getpos 'check for another space character
getposfin:
        RETURN

getstr:
        'extract data from microbalance report string
        st = p' start at first data value pointed to by variable <p>
        se = INSTR(st, r$, CHR$(Y))'get end position
        sl = se + 1 - st'  string length
        mbal$ = MID$(r$, st, sl - 1)'point to relevant part of string
        RETURN
```

```
pause:
        p$ = INKEY$: IF p$ = "" GOTO pause
        RETURN

pir100:
        'convert mV to mBar for Pirani100s gauge
        x = dat1(i)
        IF x <= .206 GOTO eqn1
        IF (x > .206) AND (x <= .376) GOTO eqn2
        IF (x > .376) AND (x <= .94) GOTO eqn3
        IF (x > .94) AND (x <= 1.49) GOTO eqn4
        IF (x > 1.49) AND (x <= 2.12) GOTO eqn5
        IF (x > 2.12) AND (x <= 3.07) GOTO eqn6
        IF (x > 3.07) AND (x <= 5) GOTO eqn7
        IF (x > 5) AND (x <= 7.02) GOTO eqn8
        IF (x > 7.02) AND (x <= 8.5) GOTO eqn9
        IF (x > 8.5) AND (x <= 8.96) GOTO eqn10
        IF (x > 8.96) AND (x <= 9.23) GOTO eqn11
eqn1:
        dat1(i) = .001 - .00556 * x + .03559 * x ^ 2 - .03559
        RETURN
eqn2:
        dat1(i) = .022551 + .030629 * x + .063071 * x ^ 2 - .030228
        RETURN
eqn3:
        dat1(i) = -.35628 + .063177 * x + .03783 * x ^ 2 + .34158
        RETURN
eqn4:
        dat1(i) = .222639 - .58422 * x + .360359 * x ^ 2 + .0797
        RETURN
eqn5:
        dat1(i) = .082896 - .23109 * x + .136098 * x ^ 2 + .10152
        RETURN
eqn6:
        dat1(i) = -.02938 + .077832 * x + .05422 * x ^ 2 - .066877
        RETURN
eqn7:
        dat1(i) = .312846 - 1.16054 * x + .236063 * x ^ 2 + 1.70608
        RETURN
eqn8:
        dat1(i) = 1.012837 - 8.91428 * x + .934193 * x ^ 2 + 22.5237
        RETURN
eqn9:
        dat1(i) = 44.92934 - 148.026 * x + 10.32395 * x ^ 2 + 493.373
        RETURN
eqn10:
        dat1(i) = 2096.366 - 5268.68 * x + 308.5062 * x ^ 2 + 20430.3
        RETURN
eqn11:
        dat1(i) = 4.93E-09 ^ (-2.93901 * x + .623121 * x ^ 2) - .01736 * x ^ 2
        RETURN
pirII:
        'convert mV to mBar for PiraniII gauge
        x = dat1(i)
```

```
        IF x <= 5 GOTO eqn12
        IF x > 5 GOTO eqn13
eqn12:
        dat1(i) = .740722 - .5306 * x + .064919 * x ^ 2 + .43191 + 4.491884 ^ (-14.9797 * x ^ 2)
        RETURN
eqn13:
        dat1(i) = .128543 - .05847 * x + .002129 * x ^ 2 + .24434 + 4.491884 ^ (-14.9797 * x ^ 2)
        RETURN

pen1:
        x = dat1(i)
        IF x <= 8.6 GOTO eqn14
        IF x > 8.6 GOTO eqn15
eqn14:
        dat1(i) = -.000084 + .000153 * x - .000045 * x ^ 2 + 5010000! * x ^ 3
        RETURN
eqn15:
        dat1(i) = -.00015 - .26823 * x + .054649 * x ^ 2 + .001907 * x ^ 3 - .00098 * x ^ 4 + .0000513 * x
^ 5
        RETURN
pen2:
        x = dat1(i)
        dat1(i) = .49062 + 2.56E-06 * x + 1.4E-08 * x ^ 2 - .491
        RETURN
pen3:
        x = dat1(i)
        dat1(i) = .133334 + 4.19E-07 * x - .0000064 * x ^ 2 - .26 + .127 ^ (.00005 * x ^ 2)
        RETURN
```

REFERENCES

ADAMSOM, W. (1972), *Investigation into the characteristic drying curve for the continuous drying of glass spheres*, BEReport, Dept. Chem. Proc. Eng., Univ. of Canterbury, New Zealand.

ANDERSON, R. (1946), *J. Am. Chem. Soc.*, Vol. 68, p. 686.

ANDERSON, J.J. AND WICKERSHEIM, K. (1964), *Surf. Sci.*, Vol. 2, pp. 252–260.

ASHWORTH, J. (1972), *The mathematical simulation of the batch-drying behaviour of softwood timber*, PhD thesis, Univ. of Canterbury, New Zealand.

ASHWORTH, J. (1979), *Interpretation of small-scale drying tests, in Handbook of Solids Drying*, Dept. Chem. Eng., Univ. of Birmingham, U.K., 1 ed., pp. 229–246.

ASHWORTH, J. AND CARTER, J. (1980), *Examination of the drying behaviour of silica gel granules by continuous weighing in an airstream, Drying '80*, Hemisphere, Washington, D.C., 1 ed., pp. 151–159.

ATKINS, P. (1988), *Physical Chemistry*, Oxford University Press, Oxford, U.K.

AUDU, T. AND JEFFREYS, G. (1975), 'The drying of drops of particulate slurries', *Trans. Inst. Chem. Eng.*, Vol. 53, p. 165.

BABBITT, J. (1950), 'On the differential equations of diffusion', *Can. J. Res.*, Vol. 28, Sec. A, pp. 449–473.

BAKER, F. AND SING, K. (1976), *J. Colloid Interface Sci.*, Vol. 55, p. 605.

BARRER, R. AND BARRIE, J. (1958), *J. Poly. Sci.*, Vol. 28, p. 377.

BASSETT, D., BOUCHER, E. AND ZETTLEMOYER, A. (1968), 'Adsorption studies on hydrated and dehydrated silicas', *J. Colloid Interface Sci.*, Vol. 27, Sec. 4, pp. 649–658.

BAUER, R. AND SCHLUNDER, E. (1978), 'Effective radial thermal conductivity of packing in gas flow. part ii. thermal conductivity of the packing fraction without gas flow', *Int. Chem. Eng.*, Vol. 18, No. 2, pp. 189–204.

Bering et al. (1971), On the thermodynamics of adsorption in micropores Institute of Physical Chemistry, Academy of Sciences of the USSR, Moscow (1971). V-71.

BETTLEHEIM, F. AND VOLMAN, D. (1957), *J. Polym. Sci.*, Vol. 24, p. 445.

BIRD, R., STEWART, W. AND LIGHTFOOT, E. (1960), *Transport Phenomena*, John Wiley and Sons, New York,. Chapter 1.5.

BOEHM, H. (1966), *Adv. Catal.*, Vol. 16, p. 179.

BRUNAUER, S. (1943), *The Adsorption of Gases and Vapors*, Princeton Univ. Press, Oxford Univ. Press, Oxford, U.K.

BRUNAUER, S., EMMETT, P. AND TELLER, E. (1938), *J. Am. Chem. Soc.*, Vol. 60, p. 309.

BUCKINGHAM, E. (1907), *Studies on the movement of soil moisture*, US Dept. Agr. Bull, US Dept. Agr., Washington, D.C. Vol. 38.

Chen, P. and Schmidt, P.S. (1988), An integral model for convective drying of hygroscopic and non-hygroscopic materials, Proc. 6th Int. Drying Symp., Versailles. Vol. 1., OP.287.

CHEN, S. AND WHITAKER, S. (1986), *Moisture distribution during constant rate drying period for unconsolidated porous media: Failure of the diffusion theory, Drying '86*, Hemisphere, Washington, D.C., 1 ed., pp. 39–48.

COBBINAH, S. (1984), PhD thesis, Toulose.

Compton, D.A.C and Powell, J.R and Crocombe, A. (1991), TGA/FT-IR and DSC/FT-IR: Combined approaches to solving problems, SPIE 8th International Conference on Fourier Transform Spectroscopy.

COULSON, J. AND RICHARDSON, J. (1955), *Chemical Engineering, Volume One - Fluid Flow, Heat Transfer and Mass Transfer*, Pergamon Press, London, U.K. p. 259.

CRANK, J. (1970), *The Mathematics of Diffusion*, Clarendon Press, Oxford, U.K.

DAY, A. (1963), *Trans. Faraday Soc.*, Vol. 59, p. 1218.

DE BOER, J. (1953), *The Dynamic Character of Adsorption*, Clarendon Press, Oxford, U.K.

DUBININ, M. (1968), *Adv. Colloid Interface Sci.*, Vol. 2, p. 217.

DUBININ, M. (1972), *Adsorption-Desorption Phenomena*, Academic Press, New York, p. 3.

Dubinin, M.M. and Astakhov, V.A. (1970), 2nd Int. Conf. on Molecular- Sieve Zeolite, Worcester, Mass (1970).

ECKERT, E. (1950), *Introduction to the Transfer of Heat and Mass*, McGraw-Hill, Inc., New York.

ETZLER, F. AND CONNERS, J. (1991), 'A dsc/tga method for determination of the heat of vaporisation', *Thermochim. Acta.*, Vol. 189, pp. 185–192.

EUCKEN, A. (1914), 'Verhandlungen d.', *D. Phys. Ges.*, Vol. 16, p. 345.

EVANS, A. AND KEEY, R. (1975), 'Definition and variation of diffusion coefficients when drying capillary-porous material', *Chem. Eng. J.*, Vol. 10, pp. 135–144.

EVANS III, R. (1961), 'Gaseous diffusion in porous media at uniform pressure', *J. Chem. Phys.*, Vol. 35, p. 2076.

EVANS III, R. (1962), 'Gaseous diffusion in porous media ii. effect of pressure gradients', *J. Chem. Phys.*, Vol. 36, p. 1894.

EVERETT, D. AND POWL, P. (1976), *J. Chem. Soc. Faraday I*, Vol. 72, p. 619.

FEDOROV, N., IVAKHNYUK, G. AND BABKIN, O. (1990), 'Factors that determine the sorption properties of impregnated desiccants', *J. Appl. Chem.*, Vol. 63, Sec. 6, pp. 1165–1168.

FICK, A. (1855), 'Uebar diffusion', *Ann. Phys.*, Vol. 94, p. 59.

FIESER, J. (1961), *Advanced Organic Chemistry*, Renhold Publishing Corporation, New York, pp. 217–261.

FOURIER, J. (1755), *The Analytical Theory of Heat*, trans. by A. Freeman, Dover, New York.

FOWLER, R. AND GUGGENHEIM, E. (1939), *Statistical Thermodynamics*, Cambridge University Press, Cambridge, U.K.

FRANKS, F. (1972), *Water: A Comprehensive Treatise v2. Water in Crystalline Hydrates, Aqueous Solutions of Single Non-electrolytes*, Wiley, New York.

FREUNDLICH, H. (1926), *Colloid and Capillary Chemistry*, Metheun, London, U.K. pp. 110–134.

GIRON-FOREST, D., GOLDBRONN, C. AND PIECHON, P. (1989), 'Thermal analysis methods for pharamacopoeial materials', *J. Pharm. Biomed. Anal.*, Vol. 7, Sec. 12, pp. 1421–1433.

GOLDMANN, F. AND POLANYI, M. (1928), *Z. Phys. Chem. A*, Vol. 132, p. 321.

GUGGENHEIM, E. (1966), *Applications of Statistical Mechanics*, Clarendon Press, Oxford, U.K.

GURFEIN, N., DOBYCHIN, D. AND KOPLIENKO, L. (1970), 'Factors that determine the sorption properties of impregnated desiccants', *Zh. Fiz. Khim.*, Vol. 44, p. 741.

HAERTLING, M. AND SCHLUNDER, E. (1980), 'Prediction of drying rates', *J. Separ. Proc. Technol.*, Vol. 1, pp. 47–50.

HALLSTROM, A. AND WIMMERSTEDT, R. (1983), 'Drying of porous granular materials', *Chem. Eng. Sci.*, Vol. 38, pp. 1507–1516.

HALSEY, G. (1948), *J. Chem. Phys.*, Vol. 16, p. 931.

HATAKEYAMA, T. AND HATAKEYAMA, H. (1992), 'Molecular relaxation of cellulose polyelectrolytes with water', *ACS Symp. Ser*, Vol. 489 (Viscoelasticity Biomater), pp. 329–340.

HILL, J. (1940), PhD thesis, Mass. Inst. Technol. (T.L.Davis).

HIRAI, Y. AND NAKAJIMA, T. (1988), 'Moisture sorption of polyelectrlyte complex between poly(acrlic acid) and poly(4- vinylpyridine)', *J. Appl. Polym. Sci.*, Vol. 35, pp. 1325–1332.

HOBSON, J. AND CHAPMAN, R. (1972), *Adsorption-Desorption Phenomena*, ed. Ricca, F., Academic Press, London, U.K. pp.33–47.

HOFMANN, U., ENDELL, K. AND WILM, D. (1934), *Angew. Chem.*, Vol. 47, p. 539.

HOUGEN, O., MCCAULEY, H. AND MARSHALL, W. (1940), 'Limitations of diffusion equations in drying', *Trans. AIChE.*, Vol. 36, pp. 183–210.

JAAFAR, F. AND MICHALOWSKI, S. (1990), 'The modified bet equation', *J. Drying Technol.*, Vol. 8, No. 4, pp. 811–827.

KAPOOR AND YANG, R. (1989), *AIChE J.*, Vol. 35, Sec. 10, pp. 1735–1738.

KAST, W. AND JOKISCH, F. (1972, 8), 'Shapes of isotherms and sorption kinetics on porous solids', *Chem. Ing. Tech.*, Vol. 44, pp. 556–563.

KEECH, A. (1992), *The use of thin layer methods to measure drying kinetics (effects of varying bed geometry)*, BEReport, Dept. Chem. Proc. Eng., Univ. of Canterbury, New Zealand.

KEEY, R. (1972), *Drying: Principles and Practice*, Pergamon Press, Oxford, U.K. pp. 178.

KEEY, R. (1978), *An Introduction to Industrial Drying Operations*, Pergamon Press, Oxford, U.K. pp. 173.

KEEY, R. (1992), *Drying of Loose and Particulate Materials*, Hemisphere Publishing Corporation, New York. pp. 215-254.

KEEY, R. AND SUZUKI, M. (1974), 'On the characteristic drying curve', *Int. J. Heat Mass Transfer*, Vol. 17, pp. 1455–1464.

Keey, R.B. and Wu, Y. (1989), An analysis of the suction-drum drying of wool, Proc. 4th Australasian Conf. Heat Mass Transfer (1989), Melbourne. 217–225.

Keey, R.B. and Langrish, T.A.G. and Reay, D. (1985), The application of the characteristic drying curve to the drying of porous material, Proc. 3rd Australasian Conf. Heat Mass Transfer (1985), Melbourne. 103–110.

KISELEV, A. AND LYGIN, V. (1959), *Kolloidn. Zh.*, Vol. 21, p. 561.

Kravichik, T. and Korin, E. and Borde, I. (1988), Studies of the drying kinetics of air flow through thin layers of silica gel, Proc. 6th Int. Drying Symp. (1988), Versailles. pp.OP.625-OP.632.

KRISCHER, O. (1938), 'Grundsetze der feuchtigskeitsbewegung in trocknungsgutern: Kapillarwwasserbewegung und wasserdampfdiffusion (basic laws of moisture movement in drying materials: capillary-water movement and water-vapour diffusion)', *VDI Z.*, Vol. 82, pp. 373–378.

KRISCHER, O. (1942), 'Die warme- und stoffaustausch im trocknungsgut (heat and mass transfer in a drying material)', *VDI Forschungsh.*, Vol. 415, pp. 1–22.

KRISHNA, R. (1990a), 'Multicomponent surface diffusion of adsorbed species; a description based on the generalised maxwell-stefan equations', *Chem. Eng. Sci.*, Vol. 45, pp. 1779–1791.

KRISHNA, R. (1990b), 'Problems and pitfalls in the use of ficks formulation for intraparticle diffusion', *Chem. Eng. Sci.*, Vol. 48, pp. 845–861.

KRISHNA, R. (1990c), 'A unified approach to the modelling of intraparticle diffusion in adsorption processes, part b', *Gas Separ. Purif.*, Vol. 7, pp. 91–104.

KRISHNA, R. (1992), 'Problems and pitfalls in the use of the fick formulation for intraparticle diffusion', *Chem. Eng. Sci.*, Vol. 48, No. 5, pp. 846–848.

Krishna, R. (1993a), The generalized Maxwell-Stefan approach to diffusion in porous solids, Proc. 5th Conf. New Directions in Separation Technology, Noordwijkerhout, Holland (1993).

KUNII, D. AND LEVENSPIEL, O. (1969), *Fluidisation Engineering*, John Wiley and Sons, New York.

LANGMUIR, I.J. (1918), *J. Chem. Soc.*, Vol. 40, p. 1361.

LANGRISH, T. (1984), *An investigation into the characteristic drying curve concept*, BEReport, Dept. Chem. Proc. Eng., Univ. of Canterbury, New Zealand.

LANGRISH, T. (1988), *The mathematical modelling of cascade rotary dryers*, PhD thesis, Balliol College, University of Oxford, U.K.

LANGRISH, T., BAHU, R. AND REAY, D. (1991), 'Drying kinetics of particles from thin-layer drying experiments', *Trans. I. ChemE.*, Vol. 69, Part A.

LEWIS, W. (1921), 'The rate of drying of solid materials', *J. Ind. Eng. Chem.*, Vol. 13, pp. 427–433.

LIOU, J. AND BRUIN, S. (1982), 'An approximate method for the nonlinear diffusion problem with a power relation between the diffusion coefficient and concentration. i. computation of desorption times', *Int. J. Heat Mass Transfer*, Vol. 25, pp. 1209–1229.

LUI, H., ZHANG, L. AND SEATON, N. (1992), *Chem. Eng. Sci.*, Vol. 47, No. 17/18, pp. 4393–4404.

LUIKOV, A. (1935), 'The drying of peat', *Ind. Eng. Chem.*, Vol. 27, pp. 40–69.

LUIKOV, A. (1966), *Heat and Mass Transfer in Capillary Porous Bodies*, Pergamon Press, Oxford. pp. 199.

MacElroy, J.M.D. and Kelly, J.J. (1978), The kinetics of drying of microporous materials, First international symposia on drying, ed. A.S. Mujumdar. Science Press (1978), Versailles. pp. 10–23.

MANLEY, T. (1989), 'Thermal analysis of polymers', *Pure Appl. Chem.*, Vol. 61, Sec. 8, pp. 1353–1360.

MARTIN, H. (1989), 'Low peclet number particle-to-fluid heat and mass transfer in packed beds', *Chem. Eng. Sci.*, Vol. 33, pp. 913–919.

MASON, E. (1963), 'Gaseous diffusion in porous media iii. thermal transpiration', *J. Chem. Phys.*, Vol. 38, p. 1808.

MASON, G. (1988), 'Determination of pore-size distributions and pore-size interconnectivity of vycor porous glass from adsorption-desorption', *Proc. R. Soc. Lond.*, Vol. 415, pp. 453–486.

MASON, E. AND MALINAUSHAS, A. (1983), *Gas Transport in Porous Media; the Dusty Gas Model*, Technical Report, Elsevier, Amsterdam.

MASON, E., MALINAUSKAS, A. AND EVANS III, R. (1967), 'Flow and diffusion of gases in porous media', *J. Chem. Phys.*, Vol. 46, Sec. 8, p. 3199.

MAXWELL, J.C. (1867), 'On the dynamical theory of gases', *Philos. Trans. R. Soc.*, Vol. 157, p. 49.

MIKHAIL, R. AND SHEBL, F. (1970), *J. Colloid Interface Sci.*, Vol. 34, p. 66.

MOLLEKOPF, N. AND SCHLUNDER, E.U. (1986), *Contact drying of granulated product under vacuum, Drying '86*, Hemisphere, London, 1 ed., pp. 502–513.

MORIMOTO, T., NAGAO, M. AND IMAN, J. (1971), 'Flow and diffusion of gases in porous media', *Bull. Chem. Soc. Japan*, Vol. 44, p. 1282.

NAONO, H., FUJIWARA, R. AND YAGI, M. (1980), 'Determination of physisorbed and chemisorbed waters on silica gel and porous silica glass by means of desorption isotherms of water vapour', *J. Colloid Interface Sci.*, Vol. 26, Sec 1, pp. 74–82.

NEWMAN, A. (1931), *Trans. AIChE.*, Vol. 27, pp. 310–333.

NOSSAR, M., CHANTEIN, M. AND DUTYRER, A. (1974), 'High-intensity drying of textile fibres - 5. the time of drying of beds of loose scoured wool', *J. Text. Inst.*, Vol. 65, pp. 581–587.

OHNO, H., SHIBAYAMA, M. AND TSUCHIDA, E. (1983), 'Dsc analysis of bound water in the microdomains of interpolymer complexes', *Makromol. Chem.*, Vol. 184, pp. 1017–1024.

Okazaki, M. (1989), Transport phenomena in the drying of porous material, Proc. 4th Australasian Heat Mass Transfer Conf., Christchurch, New Zealand (1989). p. 45–56.

Okazaki, M. and Yamasaki, T. and Toei, R. (1978), Conductive heat drying of a granular bed with low water content, Proc. 1st Internal Symp. Drying, Montreal (1978).

OKAZAKI, M., TAMON, H. AND TOEI, R. (1981), *AIChE Journal*, Vol. 27, p. 262.

ONSAGER, L. (1931), 'Reciprocal relations in irreversible processes', *Phys. Rev.*, Vol. 37, pp. 405–426.

PAPADAKIS, S. (1992), *Correlations for the equilibrium moisture content of solids*, Research Report, SPS, Harwell Laboratories, Oxfordshire, U.K.

PECK, R. AND KAUH, J. (1969), 'Evaluation of drying schedules', *AIChE. J.*, Vol. 15, pp. 85–88.

PENDLETON, P. AND ZETTLEMOYER, A. (1984), 'A study of the mechanisms of micropore filling', *J. Colloid Interface Sci.*, Vol. 98, Sec. 2, pp. 439–446.

PICKETT, G. (1946), *J. Am. Chem. Soc.*, Vol. 40, p. 1361.

POLANYI, M. (1916), 'Verhandlungen d.', *D. Phys. Ges.*, Vol. 18, p. 55.

Polanyi, M. (1932), The adsorption of gases by solids, Discussion held by the Faraday Society (1932). 316.

PRESS, W., TEUKOLSKY, S., VETTERLING, W. AND FLANNERY, B. (1992), *Numerical Recipes in C - The Art of Scientific Computing*, Cambridge University Press, Cambridge, U.K.

QUENARD, D. AND BENTZ, D. (1992), *Capillary Condensation, Hysteresis and Image Analysis, Drying '92*, Hemisphere Publishing Corporation, pp. 253–262.

Quenard, D. and Sallee, H. (1988), The transport of condensable water vapour through microporous building materials, Proc. 6th Int. Drying Symp., Noordwijkerhout, Versailles (1988).

RADJY, F. (1974), *J. of Mat. Sc.*, Vol. 9.

RADKE, C. AND PRAUSNITZ, J. (1972), *Ind. Eng. Chem. Fundam.*, Vol. 11, p. 445.

REAY, D. AND ALLEN, R. (1982), 'The effect of bed temperature on fluid-bed batch drying curves', *J. Separ. Process. Tech.*, Vol. 3,4, pp. 11–13.

REES, L. AND RICHARDS, R. (1986), *Zeolites*, Vol. 6, pp. 17–25.

Riede, Th. and Schlunder, E.U., Selective evaporation of a ternary mixture containing one non-volatile component, Proc. 6th Int. Drying Symp., Noordwijkerhout, Versailles (1988).

ROUSE, P. (1947), *J. Am. Chem. Soc.*, Vol. 69, p. 1068.

ROUSLEY, R. (1961), *AIChE. J.*, Vol. 7, p. 308.

SAZANOV, E. (1989), 'Mass spectrometric thermal analysis of polymers based on furyl alcohol', *J. Therm. Anal.*, Vol. 35, pp. 1365–1371.

SCHICKETANZ, W. (1971), 'Vergleigh des trocknungsverhaltens von sch ttungen kapill rpor ser materialen (comparison of the drying process of beds of capillary-porous materials)', *Chem. Ing. Tech.*, Vol. 43, pp. 245–251.

SCHLUNDER, E. (1976), 'Fortschritte und entwicklungsten den zen bei der auslegung von trocknern f r vorgeformte trocknungsg ter (advances and development trends in the design of dryers for preformed drying goods)', *Chem. Ing. Tech.*, Vol. 48, pp. 190–198.

SCHLUNDER, E. (1978), *Chem. Ing. Tech.*, Vol. 50, p. pp.749.

SCHLUNDER, E. (1980), *Drying '86*, Hemisphere, London, 1 ed., pp. 157–182.

SCHLUNDER, E. (1984), *Einfuhrung in die Stoff bergang (Introduction to Mass Transfer)*, Georg Thieme, Stuttgart, Germany,. pp. 56–62.

SCHUCHMANN H., ROY, I. AND PELEG, M. (1988), 'Empirical models for moisture sorption isotherms at very high water activities', *J. Food Science*, Vol. 55, No. 3, pp. 759–762.

SEATON, N. (1991), 'Determination of the connectivity of porous solids form nitrogen sorption measurements', *Chem. Eng. Sci.*, Vol. 46, No. 8, pp. 1895–1909.

SHERWOOD, T. (1929a), 'The air drying of solids i.', *Ind. Eng. Chem.*, Vol. 21, pp. 12–16.

SHERWOOD, T. (1929b), 'The air drying of solids ii.', *Ind. Eng. Chem.*, Vol. 21, pp. 976–980.

SHERWOOD, T. (1936), 'The air drying of solids', *Trans AIChE*, Vol. 32, pp. 150–168.

SHOLAKOV, A., KEL'TSEV, N., TOROCHESHNIHOV, N. AND SHUMYAKSKII, Y. (1970), *Teckhnol. Inst.*, Vol. 65, pp. 76–78.

SLADEK, K., GILLILAND, E. AND BADDOUR, R. (1974), *Ind. Eng. Chem. Fundam.*, Vol. 13, p. 100.

STANISH, M., SCHAJER, G. AND KAYIHAN, F. (1986), 'A mathematical model of drying for hygroscopic porous media', *AIChE. J.*, Vol. 32, pp. 1301–1311.

STASZCZUK, P. (1986), 'Determination of liquid vapour adsorption and desorption on and from solids by means of the derivatograph ii, determination of kinetics and isotherms of adsorption and desorption of water vapour on silica gel', *J. Therm. Anal.*, Vol. 31, pp. 911–916.

STEELE, W. (1956), *J. Chem. Phys.*, Vol. 25, p. 819.

STEFAN, J. (1871), ' ber das gleichgewicht und die bewegung insbesondere die diffusion von gasgemengen.', *Sitzber. Akad. Wiss. Wein*, Vol. 63, p. 63.

Steinmetz, D and Baxerres, J.L and Hemati, M and Laquerie (1991), Drying of alumina porous particles under isothermal conditions, Proc. 6th Int. Drying Symp., Noordwijkerhout, Versailles (1991).

STOECKI, H, F., LAVANCHY, A. AND KRAEHENBUEL, F. (1982), *Adsorption at the Gas-Solid and Liquid-Solid Interface*, Rouquel, J., Sing, K.S.W., eds., Oxford. p. 201.

SUZUKI, M. (1988), *Adsorption Engineering*, Chemical Engineering Monographs 25.

Thijssen, H.A.C and Coumans, W.J. (1984), Short-cut calculation of non- isothermal drying rates of shrinking and non-shrinking particles containing an expanding gas phase, Proc. 4th Int. Drying Symp., IDS'84 Kyoto (1984).

THURNER, F. AND SCHLUNDER, E. (1986), 'Fortschritte zum besseren verst ndnis der trocknung por ser g ter die mit bin ren gemischen beladen sind (progress towards understanding the drying of porous materials wetted with binary mixtures)', *Chem. Eng. Process.*, Vol. 20, pp. 9–25.

TSOTSAS, E. (1992), *Measurement and modelling of intraparticle drying kinetics: A review, Drying '92*, Elsevier Science Publishers, B.V., pp. 217–261.

TUBBS, J. (1976), *Drying characteristics of loose scoured wool*, BEReport, Dept. Chem. Eng., Univ. of Canterbury, New Zealand.

VAN BRAKEL, J. (1980), *Mass transfer in convective drying, Advances in Drying*, Hemisphere, Washington, D.C., 1 ed., pp. 217–261.

VAN DEN BERG, C. (1985), *Development of BET - like models for sorption of water on Foods, Theory and Relevance, Properties of water in Foods*, Martinus Nijhoff Publishers, Dordrecht.

VAN DEN BROEKE, L. AND KRISHNA, R. (1995), 'Experimental verification of the maxwell-stefan theory for micropore diffusion', *Chem. Eng. Sci.*, Vol. 50, pp. 2507–2522.

VANEEK, V., MARKVART, M. AND DRBOHLOV, R. (1966), *Fluidised-Bed Drying*, Pergamon Press, Oxford, U.K. 73-76.

VANMEEL, D. (1958), 'Adiabatic convection batch drying with recirculation of air', *Chem. Eng. Sci.*, Vol. 9, pp. 36–44.

WARREN, N. (1983), *A mathematical model of simultaneous heat and mass transfer in a rigid porous material during the falling rate period of drying*, PhD thesis, Dept. Chem. Eng., Univ. of Surrey, Guildford, U.K.

WEIDERHOLD, P. (1982), *Humidity Measurements, Selecting Humidity Sensors for Industrial Processes Handbook*, General Eastern Instruments Corp., Watertown, Massachusetts, pp. 502–513.

WHITAKER, S. (1977), 'Simultaneous, heat, mass, and momentum transfer in porous media', *Adv. Heat Transfer*, Vol. 13, pp. 119–203.

WHITAKER, S. (1980), *Heat and mass transfer in porous media, Advances in Drying*, Hemisphere, Washington, D.C., 1 ed., pp. 23–61.

Whitaker, S. (1984), Moisture transport mechanism during the drying of granular porous media, Proc. 4th Int. Symp. Drying IDS'84, Kyoto (1984).

YANG, R., FENN, J. AND HALLER, G. (1973), *AIChE J.*, Vol. 19, p. 1052.

YOSHIYUKI, H. AND NAKAJIMA, T. (1988), *J. Appl. Polymer Sci.*, Vol. 35, pp. 1325–1332.

YOUNG, G. (1958), *J. Colloid Interface Sci.*, Vol. 13, p. 75.

ZHANG, Q., LANGRISH, T. AND KEEY, R. (1992), *The use of thin layer methods to measure drying kinetics (effects of varying gas conditions)*, ResearchReport, Dept. Chem. Proc. Eng., Univ. of Canterbury, New Zealand.